FEBRUARY 2023

Ph.D. in Civil Engineering

ISRAA SABBAR ABBAS

REPUBLIC OF TURKEY

GAZİANTEP UNIVERSITY

GRADUATE SCHOOL OF NATURAL & APPLIED SCIENCES

RHEOLOGICAL, FRESH, MECHANICAL, AND DURABILITY PROPERTIES OF MECHANOCHEMICALLY ACTIVATED RICE HUSK ASH AND GLASS POWDER/ SLAG-BASED GEOPOLYMER FOR GROUTING AND DEEP MIXING

Ph.D. THESIS

IN

CIVIL ENGINEERING

BY

ISRAA SABBAR ABBAS

FEBRUARY 2023

RHEOLOGICAL, FRESH, MECHANICAL, AND DURABILITY PROPERTIES OF MECHANOCHEMICALLY ACTIVATED RICE HUSK ASH AND GLASS POWDER/ SLAG- BASED GEOPOLYMER FOR GROUTING AND DEEP MIXING

Ph.D. Thesis

in

Civil Engineering

Gaziantep University

Supervisor

Prof. Dr. Hanifi ÇANAKCI

by

Israa Sabbar ABBAS

February 2023

RHEOLOGICAL, FRESH, MECHANICAL, AND DURABILITY PROPERTIES OF MECHANOCHEMICALLY ACTIVATED RICE HUSK ASH AND GLASS POWDER/SLAG-BASED GEOPOLYMER FOR GROUTING AND DEEP MIXING

submitted by **Israa Sabbar ABBAS** in partial fulfillment of the requirements for the degree of Doctor of Philosophy in **Civil Engineering, Gaziantep University** is approved by,

Prof. Dr. Mehmet İshak YÜCE
Director of the Graduate School of Natural and Applied Sciences …….....

Prof. Dr. Aytaç GÜVEN
Head of the Department of Civil Engineering …….....

Prof. Dr. Hanifi ÇANAKCI
Supervisor, Civil Engineering
Gaziantep University …….....

Exam Date: 28 February 2023

Examining Committee Members:

Prof. Dr. Hanifi ÇANAKCI
Thesis Supervisor, Civil Engineering
Gaziantep University …….....

Prof. Dr. Hamza GÜLLÜ
Civil Engineering
Gaziantep University …….....

Assoc. Prof. Dr. Nihat ATMACA
Civil Engineering
Gaziantep University …….....

Asst. Prof. Dr. Muhammet ÇINAR
Civil Engineering
Kahramanmaraş Sütçü İmam University …….....

Asst. Prof. Dr. Eyyüb KARAKAN
Civil Engineering
Kilis 7 Aralik University …….....

I hereby declare that all information in this document has been obtained and presented in accordance with academic rules and ethical conduct. I also declare that, as required by these rules and conduct, I have fully cited and referenced all material and results that are not original to this work.

Israa Sabbar ABBAS

ABSTRACT

RHEOLOGICAL, FRESH, MECHANICAL, AND DURABILITY PROPERTIES OF MECHANOCHEMICALLY ACTIVATED RICE HUSK ASH AND GLASS POWDER/ SLAG- BASED GEOPOLYMER FOR GROUTING AND DEEP MIXING

ABBAS, Israa Sabbar
Ph.D. Thesis in Civil Engineering
Supervisor: Prof. Dr. Hanifi ÇANAKCI
February 2023
222 pages

This research investigates the use of mechanochemical activation as an alternative activation technique to overcome the difficulties associated with conventional two-part geopolymers and increase the reactivity of a one-part geopolymer during ambient curing. The study synthesizes ready-to-use geopolymeric precursors through the mechanochemical grinding of raw materials in a solid state, resulting in an eco- and user-friendly geopolymer binder that requires only the addition of water. The binder is then used to prepare geopolymer grouts and deep soil mixes, with properties evaluated and compared to those of slag-based conventionally activated geopolymer (CSG) and ordinary Portland cement (OPC). Four rice husk ash (RHA) and glass powder (GP) replacement ratios are used to investigate the feasibility of using RHA and GP as partial precursors in slag-based mechanochemically activated geopolymer (MSG) binder. Various tests are performed to examine the properties of the resulting grouts and deep soil mixes, including rheological behavior, fresh properties, mechanical characteristics, and microstructure analysis. The results showed that the rheological characteristics and fresh properties of MSG grouts were considerably enhanced in terms of groutability when slag was replaced with 0–30% RHA and GP. In addition, the mechanical characteristics increased with the increased partial replacement of slag with RHA and GP up to 20% and decreased beyond that. In terms of activation mechanism, the mechanochemical activation technique reduced the rheological and fresh properties while the strength increased by 18% compared to the conventional activation method. Microstructural analysis revealed the existence of more unreactive particles in both conventionally activated geopolymer and MSG grout containing 30% RHA and GP. The results also confirmed that MSG grouts had a shorter setting time and more stable bleeding capacity than OPC grout. this study investigates the mechanical and durability properties of soil specimens stabilized with OPC, MSG, and CSG exposed to magnesium sulfate solutions for 60 and 120 days. The results show that MSG-stabilized soil attained the highest UCS, followed by CSG and OPC stabilizers. In addition, the UCS trend of MSG-stabilized soil increased with increasing partial substitution of slag with RHA up to 20% and afterward declined. Meanwhile, the UCS reached the highest when the amount of GP was 10% of the geopolymer stabilizer. The MSG samples with 20% RHA and GP exhibit less visual deterioration, discoloration, expansion, and cracking than other DSM samples. Partial replacement of slag with RHA and GP up to 20% was recorded as the highest residual UCS.

Key Words: Grouting, Deep Soil Mixing, Mechanochemical Activation, Geopolymer, Rheological, Strength, Durability, Rice Husk Ash, Glass Powder.

ÖZET

ÇAMURCULUK VE DERİN KARIŞTIRMA İÇİN MEKANOKİMYASAL OLARAK AKTİVASYON EDİLMİŞ PİRİNÇ KAVUĞU KÜLÜ VE CAM TOZU/SLAG TABANLI GEOPOLİMERİN REOLOJİK, TAZE, MEKANİK VE DAYANIKLILIK ÖZELLİKLERİ

ABBAS, Israa Sabbar
Doktora Tezi, İnşaat Mühendisliği
Tez Danışmanı: Prof. Dr. Hanifi ÇANAKCI
Şubat 2023
222 sayfa

Bu çalışmada, geleneksel iki parçalı geopolimerin kullanımındaki zorluklarını aşmak ve oda sıcaklığında sertleşen alternatif bir aktivasyon tekniği olarak mekanokimyasal aktivasyonun kullanıldığı tek parça geopolimer bağlayıcı elde edilmesi araştırılmıştır. Çalışma, katı hâldeki atık maddelerin mekanokimyasal öğütme yöntemiyle hazırlanmasını içerir, böylece sadece su ilavesi gerektiren çevre dostu ve kullanımı kolay bir geopolimer bağlayıcı oluşturuldu. Geliştirilen bu yeni bağlayıcının özellikleri, geleneksel olarak aktive edilen geopolimer (CSG) ve normal portland çimentosu (OPC) ile karşılaştırıldır. Araştırmada, dört farklı pirinç kabuğu külü (RHA) ve cam tozu (GP) oranı kullanıldı. Elde edilen enjeksiyon harcı ve bu harç kullanılarak derin karıştırma yöntemi ile iyileştirilen zemin numunelerinin çeşitli özellikleri; reolojik davranış, taze özellikler, mekanik dayanım ve mikroyapı incelendi. Test sonuçları, cüruf yerine %30 oranına kadar pirinç kabuğu külü veya cam tozu eklenmesi durumunda, mekanokimyasal aktive dilene geopolimer (MSG) harcının reolojik ve taze özelliklerinin önemli ölçüde iyileştiğini göstermiştir. Ayrıca, grout harcının mekanik özelliğinin, piriç kabuğu külü veya cam tozonun %20 oranında cüruf ile kısmi değiştirilmesiyle arttığı fakat %20'den sonra basınç dayanımının azaldığı gözlendi. Sonuçlar ayrıca, MSG harçlarının OPC harçlarına göre daha kısa sertleşme süresine ve daha iyi su kusma özelliğine sahip olduğunu gösterdi. Bu çalışma ayrıca, 60 ve 120 gün boyunca magnezyum sülfat çözeltilerine maruz bırakılan OPC, MSG ve CSG ile iyileştirilmiş zemin örneklerinin mekanik dayanımları incelendi. Test sonuçlar, MSG ile stabilize edilmiş zeminin serbest basınç dayanımının CSG ve OPC ile stabilite edilmiş zeminde daha iyi olduğunu gösterdi. Cürufun pirinç kabuğu külü ve cam tozu ile %20'ye kadar kısmen yer değiştirmesi ile en yüksek serbest basınç dayanım değeri kaydedilmiştir.

Anahtar Kelimeler: Geopolimer, Mekanokimyasal Aktivasyon, Enjeksiyon, Derin Zemin Karıştırma, Reoloji, Mukavemet, Pirinç kabuğu külü, Cam tozu, Durabilite.

"Dedicated to my family"

ACKNOWLEDGEMENTS

I thank **ALLAH** almighty for bestowing me with enough courage and strength to pursue my studies.

In reality, It is with a heavy heart that I begin this acknowledgment section of my Ph.D. thesis. While **my parents** (rest in peace) are not here to witness this milestone in my life, their unwavering support and love have been a constant source of inspiration and motivation throughout my academic journey. I cannot express how much I miss you and how much I wish you were here to witness this momentous occasion in my life. Your love, guidance, and support were the driving force behind my academic pursuits, and I am forever grateful for everything you did for me.

To the planets that walk in my skies and give me light, warmth and happiness, who shared my life, my **brother and sisters**.

Also, I would like to express my deepest appreciation and gratitude to my uncle **Abdulkerim AHMED** for his unwavering support, encouragement, and guidance.

To my advisor and mentor, **Prof. Dr. Hanifi ÇANAKCI**, thank you for your guidance, patience, and expertise throughout my Ph.D. study. Your unwavering support has been invaluable to me, and I am grateful for everything you have done to help me reach this point.

In particular, I would like to express my heartfelt gratitude to my dear friend and companion **Dr. Mukhtar Hamid ABED** for his unwavering support and encouragement for seven years, from the beginning of the Master's degree until the completion of the Ph.D. I'd like to thank you for being there during the tough times when I felt like giving up. You are truly a gift in my life, and I am forever grateful for your friendship.

Thank you for being my friend and companion and for sharing this special moment with me. Your friendship means the world to me.

TABLE OF CONTENTS

Page

LIST OF TABLES

Page

LIST OF FIGURES

Page

LIST OF ABBREVIATIONS

DM	Deep mixing
DSM	Deep soil mixing
DMM	Deep mixing method
OPC	Ordinary Portland cement
AAMs	Alkali-activated materials
SG	Raw slag-based geopolymer
CSG	Conventionally activated slag-based geopolymer
MSG	Mechanochemically activated slag-based geopolymer
OPG	One-part geopolymer
MC-OPG	Mechanochemical activation one-part geopolymer
GGBFS	Ground granulated blast furnace slag
FA	Fly ash
Al	Aluminum
Al_2O_3	Alumina
Si	Silicon
SiO_2	Silica
C-S-H	Calcium silicate hydrate
C-A-S-H	Calcium aluminate silicate hydrate
N-A-S-H	Sodium aluminate silicate hydrate
CaO	Calcium oxide
$Ca(OH)_2$	Calcium hydroxide
Fe_2O_3	Iron
NaOH	Sodium hydroxide

Na_2SiO_3	Sodium silicate
$MgSO_4$	Magnesium sulfate
UCS	Unconfined compressive strength
UPV	Ultrasonic Pulse Velocity
SEM	Scanning electron microscope
XRD	X-ray diffraction
FTIR	Fourier transform infrared
XRF	X-ray fluorescence
EDS	Energy-dispersive spectroscopy
w/b	Water binder
s/b	Soil- binder
Wc	Water content

CHAPTER I

INTRODUCTION

1.1 General

The grouting and deep soil mixing are widely utilized for ground improvement in geotechnical applications such as water barriers, tunnels, mines, and building foundations to maintain ground integrity by filling voids and fractures. Grouting and deep mixing could be employed in challenging site circumstances, cause less noise, vibration, and surface settlements, and deliver more cost- and time-effective solutions than alternative ground improvement methods, including conventionally drilled piles (Coduto et al., 1999; Kitazume & Terashi, 2013). The grouting system employs pipelines with high-pressure grouts that are injected into the ground and mixed with the in-situ soil, whereas the deep mixing method involves drilling to soft clay utilizing mechanical mixers or augers. These techniques depend on chemical processes triggered by binders that generate cementitious links to enhance the soil's mechanical characteristics, such as bearing capacity, settlement and shrinkage, liquefaction susceptibility, and hydraulic conductivity (Boehm, 2004; Shen et al., 2013). The deep mixing process does not include compaction; hence, grouts often have large wet fractions to produce the required fluidity for a homogenous and uniform binder-soil combination throughout the injection depth. However, it is essential to emphasize that the characteristics of grout slurry in its fresh state are a highly complex problem in terms of rheology, which governs the soil-grout mixture after the hardening phase of the grout column begins (Nikbakhtan & Osanloo, 2009). The grout mixes ought to possess sufficient enough fluidity and fresh characteristics to facilitate the pumping process (Nguyen et al., 2011), provide convenient service for the nozzles (Güllü, 2016), and provide effective penetration into soil voids (Cristelo et al., 2013), as well as high mechanical strength, low cost, and environmental friendliness (Z. Li et al., 2021). These goals are often achieved and controlled by rheological testing, mechanical characteristics monitoring, and chemical investigations.

Cement-based grouts are currently the most widely utilized grouting material; nevertheless, it has several drawbacks, such as high bleeding, long setting time, limited strength performance at higher water-to-binder ratios and high cost owing to widespread use (Aboulayt et al., 2018; Güllü & Ali Agha, 2021). Furthermore, the rising consumption of ordinary Portland cement has had adverse environmental effects such as significant carbon-dioxide emissions, resource depletion, dust generation, etc. (Bilondi et al., 2018; John L Provis et al., 2010; John L Provis & Bernal, 2014).

During the manufacturing process, a considerable quantity of CO_2 is emitted into the atmosphere at a rate of around one ton of CO_2 per ton of Portland cement, which accounts for 7% of worldwide carbon-dioxide emissions (Du et al., 2017; M. Zhang et al., 2013). Therefore, researchers are currently researching alternate binders that might minimize the carbon footprint of grouting and deep soil mixing works (Arulrajah et al., 2018; J. Zhang et al., 2019). On the other hand, the disposal of industrial by-products and agricultural wastes in landfills has become another severe environmental concern (Scharff, 2014). All these issues together have contributed to the formation of ecologically friendly construction materials that promote the concept of sustainability.

One of the alternatives is alkali-activated materials (AAMs), which emits 60–80 % less carbon dioxide and consume 60% less energy during manufacture than ordinary Portland cement (Rios et al., 2019). Davidovits, (1994) introduced the concept of "geopolymers," which are binders made from solid silicoaluminate precursors and an alkali activator produced from agro-waste or industrial materials that contain high levels of amorphous silicon and aluminum, such as metakaolin, silica fume, fly ash, bottom ash, slag, volcanic ash, rice husk, and glass powder (Bai et al., 2020; Canakci et al., 2019; Kurtoğlu et al., 2018). Geopolymer materials are a potential future alternative to traditional Portland cement as a sustainable building material because of many benefits such as improved durability and strength properties, rapid hardness, low creep and shrinkage, low permeability, automated humidity and temperature, high resistance to fire and chemical corrosion, and lower greenhouse gas emissions during production. In addition, geopolymers can be made using industrial by-products or agro-waste materials, reducing the reliance on natural resources and contributing to a more sustainable building industry (Arulrajah et al., 2018; Humur & Çevik, 2022; A. Mehta & Siddique, 2017a; M. Zhang et al., 2013).

Several recent studies have been conducted on using geopolymers as soil stabilizers (Ghadir & Ranjbar, 2018a; Rios et al., 2019; Yaghoubi et al., 2019). Geopolymer binders can improve the density and microstructure of soil particles, resulting in enhanced soil volume stability and mechanical characteristics (M. Zhang et al., 2013). Therefore, it is feasible to utilize the geopolymer in applications involving the stabilization of soil at shallow depths(e.g., shallow foundation, base or subbase in the pavement, embankment, airport building, etc.) as well as deep soil mixing (Arulrajah et al., 2018; Teerawattanasuk & Voottipruex, 2019).

The durability of stabilized soils is a crucial design consideration for deep soil mixing, particularly in harsh environments (chemical attacks, carbonation, Ca^{+}, freezing/thawing, and wetting/drying cycles) (Bellato et al., 2012; Denies et al., 2015; Ikegami et al., 2003). Sulfate and acid attack is one of the most significant elements affecting the long-term endurance of geotechnical engineering projects (Goncalves et al., 2019; Zhu, Liang, et al., 2021). In practice, underground constructions may be subjected to sulfates when groundwater is contaminated (agricultural, industrial, or air pollution) or gypsum is present in the soil. Therefore, in DSM, water and sulfated soils may constitute the soil-cement material, thereby enhancing their negative influence. It is well known that the various types of sulfate assaults produce mechanical and chemical deterioration in clayey soils in particular (Helson et al., 2018). Industrial plants can release liquid, solid, and gaseous emissions that contribute to environmental pollution, which can reach the ground and groundwater. The problem is aggravated by pollution's impact on the bearing foundations of industrial buildings, which weaken them and occasionally result in their collapse due to cavities.

1.2 Problem Statement

Currently, the application of geopolymer binders is mainly restricted to small-scale applications. Despite their remarkable eco-friendliness, which promotes their use as a possible alternative to OPC. To maximize the remarkable environmental friendliness of geopolymer materials, emphasis should be given to large-scale geopolymer applications to optimize utilization in the construction sector. Conventionally, geopolymer is a two-part mixture of a liquid alkali solution and solid silicoaluminate source materials. The synthesis of conventional geopolymers involves using an

alkaline solution, typically made by dissolving sodium hydroxide (NaOH) flakes in a sodium silicate solution. This results in an exothermic reaction that generates heat and elevates the temperature of the solution; the alkaline solution is often prepared in advance and cooled to room temperature before being added to the solid silicoaluminate precursor (H. Y. Zhang et al., 2016). Hostile activator solutions, which are user-unfriendly, are commonly utilized to dissolve silicoaluminate source materials and regulate the mechanical and microstructure characteristics of the resultant geopolymer binder. (W. K. W. Lee & J, 2002; W. K. W. Lee & Van Deventer, 2003). The two-component mixture that produces "conventional" geopolymers has several deficiencies (Peter Duxson & Provis, 2008). These restrictions may involve issues with the handling and mixing high amounts of highly corrosive and usually viscous alkali activator solutions would be difficult for mass and commercial production of geopolymer materials and would hinder the widespread use of conventionally geopolymer binder. In addition, the reaction between the aluminosilicate source and the alkaline solution creates a sticky and thick paste, thereby making it difficult and complex to control the geopolymer's rheology (J. L. Provis, 2009). Another constraint of the two-part geopolymer system is its susceptibility to the ratio of alkali to accessible silicate, which can be challenging to regulate when waste materials are utilized as a silica source, as these materials may contain different amounts of accessible silicate (Criado et al., 2007). Improper control of water and alkali content in the geopolymer mixture during curing or service can result in the transfer of alkalis and water to the surface of the geopolymer, which may cause issues such as efflorescence, excessive permeability, and water absorption (Kani et al., 2012; John L Provis et al., 2010). Hence, developing a one-part, "just add water" geopolymer combination as an alternative way more analogous to the usage of typical Portland cement-based materials is one of the most important stages toward large-scale geopolymer deployment in the construction sector. One-part geopolymers binder combines solid alkaline activators with solid aluminosilicate precursors (Ke et al., 2015; Masi et al., 2021; Muthukrishnan et al., 2021). Using solid activators to produce geopolymer can improve its commercial viability by facilitating the fabrication of a one-part "just add water" combination, similar to traditional cement-based (Nematollahi, Sanjayan, & Shaikh, 2015).

However, the drawbacks of using this technique were once again revealed, as only strength performances were achieved after curing at ambient temperature. Also, the one-part system resulted in more porosity and water absorption, leading to pores that were more detrimental to the durability of these binders (Ren et al., 2021). Furthermore, one-part geopolymers binders are mostly addressed in terms of heat curing, hence restricting the possible application areas of these systems in environments where heating is prohibited (e.g., grouting, deep soil mixing building materials for in situ applications, materials for rendering, restoration, etc.) (Masi et al., 2021). Therefore, this investigation employed a mechanochemical activation approach as an alternative activation mechanism to overcome the challenges associated with conventional two-part geopolymers and used mechanochemical activation to improve the reactivity of one-part geopolymers during ambient curing. Furthermore, incorporating full slag as a primary constituent in geopolymer grout results in a significant increase in viscosity and a decrease in setting time, presenting a challenge in the pumping process and potentially resulting in mechanical damage to grouting machinery, premature grout shrinkage, and diminished long-term chemical resistance. Thus, the aforementioned issues are addressed in this research.

1.3 Mechanochemical Processing

Mechanochemistry refers to the physical and chemical transformation generated by mechanical energy in a material (Guo et al., 2010). A simple grinding process typically induces this phenomenon at ambient temperature and atmospheric pressure (in ball mills, planetary mills, etc) (Baláž et al., 2006). Mainly, mechanochemistry concerns the Physiochemical alterations and chemical reactions that occur when substances are subjected to mechanical energy. Grinding and co-grinding are common methods used to induce mechanochemical responses in mills. In these processes, mechanical energy is applied to the material by the milling equipment, which can include ball mills, planetary mills, attritor mills, or other types of mills. The mechanical energy from the mill causes physical and chemical transformations in the material, such as breaking down the particle size, creating new surfaces, and promoting chemical reactions.

Grinding, which reduces the particle size of a material by subjecting it to mechanical forces such as impact, compression, or shearing, can be used to enhance the reactivity

of the precursor and activator of the geopolymer. This can increase the surface area of the material, promoting faster and more complete reactions between the precursor and activator.

Co-grinding, the process of grinding two or more materials together, can also induce mechanochemical reactions in mills. Co-grinding can promote responses between the different components of the mixture, such as the precursor and activator, by increasing the surface area of the materials and promoting more intimate contact between them. Both grinding and co-grinding are common and efficient techniques that can induce mechanochemical reactions in mills, making them suitable for applications such as the manufacturing of solid geopolymers (Boldyrev, 2004). Therefore, this research employs mechanochemical processing to transform raw materials into geopolymer binders. The raw materials consisted of silicoaluminate precursors and sources of solid alkaline cations; mechanochemical synthesis of these raw materials was achieved by ball-milling of their mixtures. The co-grinding action incorporates alkali cations into the aluminosilicate structure by breaking the aluminosilicate linkages.

Figure 1.1 depicts the mechanochemical activation mechanism schematically. Incorporating readily available network-breaking cations (Na^+, K^+, Mg^{2+}, and Ca^{2+}) throughout mechanochemical synthesis can be tuned to govern the dissolving rates of the glassy phases prominent in fly ash-based aluminosilicate (Matalkah et al., 2017). Where the presence of alkali cations in a glassy phase enhances the potential for framework disordering and the formation of Al–O–Al bonds (Hadi et al., 2016). Furthermore, divalent alkaline cations accelerate dissolution relative to monovalent alkaline cations, allowing glasses to exhibit variable dissolution rates based on their composition (Peter Duxson & Provis, 2008).

The transformation of an aluminosilicate-based geopolymer cement typically involves four initial steps: (i) ion exchange; (ii) hydrolysis; (iii) network breakdown; and (iv) release of silicon and aluminum. The dissolution and breakdown mechanisms that occur during the synthesis of a geopolymer binder involve the simple addition of water, which leads to the prompt speciation, gelation, reorganization, and polymerization of the silicoaluminate precursors; these processes result in the formation of a solid alkali aluminosilicate hydrate-based binder (solid geopolymer) (Van Jaarsveld et al., 2003).

The solid geopolymer particle possesses an amorphous silicoaluminate structure with monovalent and divalent network-modifying cations. The glassy structure of geopolymers dissolves when the pH is moderately high, and it is caused by the partial release of alkali cations, such as sodium (Na^+) or calcium (Ca^{2+}), into the solution. This process is comparable to the dissolution of the glassy structure that occurs under acidic circumstances, which is initiated by the ion exchange of hydrogen ions (H^+) for alkali cations such as Na^+ or Ca^{2+}. The difference between using Ca^{2+} or Na^+ ions in synthesizing a geopolymer is that the chemical reactions that occur are different. Sodium ions (Na^+) have a smaller ionic radius and a higher charge density, which allows them to react faster and more extensively with the aluminosilicate precursors to form a geopolymer. Calcium ions (Ca^{2+}) have a larger ionic radius and a lower charge density, which leads to a slower reaction rate and less extensive crosslinking between the precursors. The dissolution process of the glassy structure is an important step in forming geopolymers, as it leads to forming of a network of silicate and aluminate chains that give the final material its strength and durability (Matalkah et al., 2017). The behavior of surface charging substantially governs the network breakdown process during glass transition. The release of Si and Al ions while synthesizing a geopolymer binder is controlled by the specific glassy phase utilized and the leaching environment; in some instances, both Si and Al ions are released synchronously, but in others, only one component is preferentially leached. The influence of alkaline earth cations in glass increases the tendency for framework disorder, including forming a tiny concentration of Al–O–Al bonds and a higher-than-strictly-required non-bridging oxygen atom content (Matalkah et al., 2017). The specific glassy phase or combination of glassy phases used in synthesizing a geopolymer binder can significantly impact the properties of the resulting binder. An optimal glassy phase would allow for the customization of key characteristics such as workability, setting time, strength development, and durability (Peter Duxson & Provis, 2008).

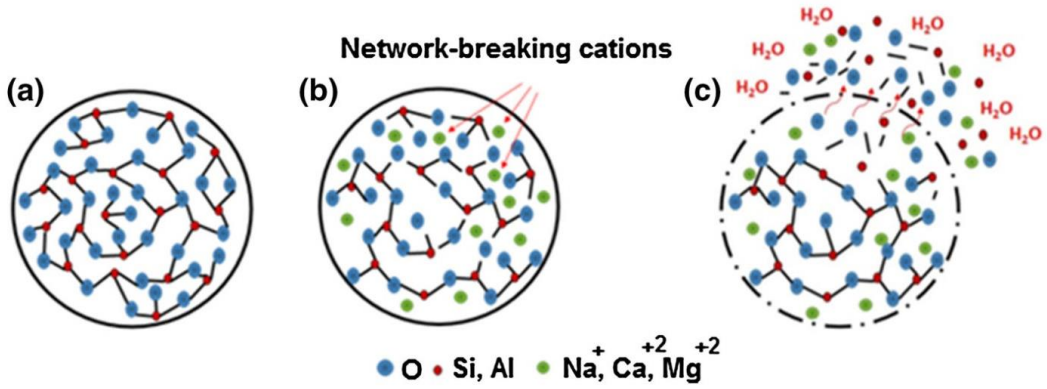

Figure 1.1 Schematics illustrating the mechanochemical transformation of alkaline activators and aluminosilicate precursors into geopolymer binders (Matalkah et al., 2017).

1.4 Significance of the Study

This study developed an innovative solid-state chemical approach to produce commercially viable and environmentally sustainable geopolymer binders. This approach utilized mechanochemical activation at ambient temperature to transform the raw materials into solid geopolymeric binders. Mechanochemical processing involves co-grinding raw materials such as silicoaluminate precursors (such as slag or fly ash) and sources of alkaline earth and alkaline metal cations (such as sodium silicate sodium hydroxide) using a ball mill. The co-grinding action incorporates alkali cations into the structure of silicoaluminate by breaking the silicoaluminate linkages, where alkalis facilitate mechanochemical activation of the silicoaluminate precursor. The resultant mechanochemically activated geopolymer binder can be applied in geotechnical applications, the concrete industry, and any other application that uses equipment and processes frequently utilized in Portland cement is a significant benefit for a large-scale transition of the technology to the construction markets.

In addition, geopolymerization via mechanochemical activation provides numerous benefits over conventional activation. The most crucial advantage of geopolymerization via mechanochemical activation is that it avoids handling aggressive alkali solutions since the mechanochemical activation process includes reactions in a dry state, and only water is added to the geopolymeric precursor mixture, making it a nonhazardous method. In contrast, the alkaline solution used in

conventional activation (pH range: 10–14) is hazardous and may cause skin irritation if it accidentally touches those handling it.

Furthermore, one of the main advantages of using mechanochemically synthesized geopolymer cement is that it can be easily transported and stored in a dry form, similar to traditional cement. This makes it convenient for use on construction sites, where the addition of water can be easily controlled to produce the desired consistency for the intended application. Additionally, the mechanochemically geopolymeric mix composition eliminates the need for separate storage and handling of alkaline activator solutions, which can be hazardous to handle and negatively influence the environment if not handled properly. The mechanochemically activated geopolymeric precursor is well-suited for cementitious material use and for prefabricated or pre-engineered geopolymeric end products, hence enhancing its commercialization. In addition, it is possible to alter properties at the precursor stage by changing essential formulations before the mechanochemical grinding process. In other words, mechanochemical geopolymerization enables the user to customize the characteristics of the geopolymeric end product in order to acquire the desired properties, which is not feasible with conventional geopolymerization. Moreover, mechanochemical activation geopolymers may overcome the significant issues posed by high cost, transportation, and long-term storage for building and construction materials. Overall, mechanochemically synthesized geopolymer cement can provide a more sustainable and design convenient alternative to traditional OPC.

1.5 Research Objectives

The main objective of the study is to develop a mechanism for preparing a new environmentally friendly and easy-to-use geopolymer with good rheological, fresh, and mechanical properties that can be used as an alternative to cement in various engineering applications; the most important of which are grouting and deep soil mixing, as well as an alternative mechanism to the traditional activation mechanism, which is dangerous to the user and difficult to market commercially, its application is limited to the difficulty of work With him on the sites. Overall, the goal is to demonstrate the potential of mechanochemically activated geopolymer binders as a viable and sustainable alternative to conventionally activated geopolymer for grouting

and deep soil mixing applications. In addition, Overcome the challenges associated with using full slag in geopolymer grout, such as high viscosity and short setting time. Moreover, explore the use of other waste materials containing aluminosilicate to increase the maximum benefit from the mechanochemical activation technique. To achieve these aims, this study has been conducted in several stages:

1. Determine the most optimal combination of RHA and GP replacements and NaOH molarity that can result in the highest-quality MSG grout with desirable properties for various engineering applications. A conventionally activated geopolymer grout and an ordinary Portland cement (OPC) grout were also investigated for comparison. A series of tests was examined in this stage such as:
    - The rheological characteristics of geopolymer grout were studied in order to understand its flow behavior and suitability for injection into soil or rock by measuring the rheological flow curves (i.e., viscosity versus shear rate curves and, shear stress versus shear rate curves) and rheological parameters (i.e., plastic viscosity and, yield stress) and of the geopolymer grout mixtures.
    - The fresh characteristics of geopolymer grout, such as setting time and bleeding, were studied to understand its stability and workability.
    - The mechanical performance of geopolymer grout, such as ultrasonic pulse velocity (UPV) and unconfined compressive strength (UCS), were studied in order to understand its performance in engineering applications.
    - Microstructural analysis: to examine the microstructure of the cured geopolymer grout specimens using techniques such as X-ray diffraction (XRD), scanning electron microscopy (SEM) and Fourier transform infrared (FTIR).
2. Application of geopolymer grout in deep soil mixing: potential application of mechanochemically activated geopolymer (MSG) stabilizers for deep soil mixing (DSM). A conventionally activated geopolymer (CSG) stabilizer was also evaluated for comparison purposes. Four rice husk ash (RHA) and glass powder (GP) replacement ratios were used (0%, 10%, 20%, and 30% by the total precursor weight) to investigate the feasibility of using RHA and GP as a

partial precursor in mechanochemically activated slag-based geopolymer (MSG) stabilized soil. The samples of deep soil mixing (OPC, MSG and CSG) were immersed in a 1% magnesium sulfate ($MgSO_4$) solution for 60 and 120 days. The appearance, mass changes, ultrasonic pulse velocity (UPV), unconfined compressive strength (UCS), and FTIR spectra of the DSM specimens were tested to evaluate their sulfate erosion resistance.

1.6 Organization of Dissertation

This dissertation represents the culmination of this study's research and is divided into seven chapters. This section offers an overview of the structure and substance of the dissertation.

Chapter 1 introduces the background, research motivation, problem statement, mechanochemical process, and study objectives.

Chapter 2 presents an extensive review of the existing literature pertaining to conventional soil stabilization methodologies and their associated limitations. Additionally, the chapter introduces the concept of geopolymers, a class of materials utilized as grouting and soil stabilizers, and elaborates on their properties. The chapter examines the historical applications of geopolymers as soil stabilizers and highlights the advantages of these materials compared to traditional stabilization methods.

Chapter 3 provides a detailed description of the various procedures used to synthesize a geopolymer. This involves an in-depth discussion of the raw material selection process and the mix proportioning methods utilized to optimise the geopolymer mix for this research study. Also describes the experimental methods and testing processes used to achieve the study's research goals.

Chapters 4 describes the development and characterization of eco- and user-friendly grout production via mechanochemical activation of slag/rice husk ash geopolymer.

Chapter 5 presents the effect of glass powder on the rheological and mechanical properties of slag-based mechanochemical activation geopolymer grout.

Chapters 6 and 7 discuss the mechanical and durability characteristics of clayey soil stabilization using eco- and user-friendly mechanochemical activation of slag/RHA and GP geopolymer compared with conventionally activated geopolymer stabilizer

Chapter 8 presents a summary of the significant findings and conclusions derived from the research study. The chapter highlights the key results obtained from the laboratory experiments and discusses their implications in the context of the study's objectives. Additionally, it offers recommendations for future research to build on the current study's findings and address any knowledge gaps identified.

CHAPTER II

LITERATURE REVIEW

2.1 Introduction

This chapter reviews the available literature on soil stabilization methods and discusses difficulties in stabilizing weak soils. The first section of the chapter provides an in-depth analysis of conventional soil stabilization techniques, including mechanical and chemical approaches. Physical methods involve adding materials to the soil to modify its properties, such as compaction and densification. In contrast, chemical techniques involve utilizing chemical additives such as bitumen, lime, and cement to enhance the soil's mechanical properties.

The second and third sections of the chapter investigate the potential of geopolymers as a green class of soil stabilization materials and detail prior research on stabilizing soils with geopolymers.

2.2 Conventional Soil Stabilization Techniques

Problematic soils pose significant challenges for construction or engineering projects due to their properties. Some common problematic soils include:

- Expansive soils: These soils contain minerals that can absorb water and cause significant swelling and shrinkage, leading to foundation damage and structural issues.
- Collapsible soils: These soils are loose and prone to collapsing under the weight of structures, leading to settling and subsidence.
- Soft soils: These soils have the low bearing capacity and can cause settlements and deformation of structures.
- Organic soils: These soils are high in organic matter and are usually weak and compressible, making them unsuitable for construction.

- Saline soils: These soils contain high levels of salts, which can cause corrosion and damage to concrete and steel structures. Acid sulfate soils: These soils are high in sulfuric acid and can cause corrosion and damage to concrete and steel structures and release toxic gases.

Effective soil stabilization techniques are necessary to overcome the challenges posed by problematic soils in construction and engineering projects. Stabilizing problematic soils involves improving their physical and chemical properties to increase their strength, load-bearing capacity, and durability.

2.2.1 Mechanical Stabilization

Mechanical stabilization techniques involve physical modifications to the soil without altering its inherent properties. This is accomplished through the use of various materials and methods. Mechanical stabilization aims to improve the soil's physical characteristics, such as shear strength and permeability, to prevent damage to structures built on top of them (F. Bell, 1993; Nazarian et al., 2015). Deep densification, precompression, and reinforcement are among the techniques used in the mechanical stabilization of soil. Deep densification increases the soil's bulk density by rapidly expelling air from soil pores, resulting in higher shear strength and lower permeability, hence decreasing the soil's probability of settling. Vibro-compaction and dynamic compaction are the two most common deep densification processes to stabilize soil(Kirsch & Bell, 2012).

Vibro-compaction methods involve vibratory techniques that decrease extra pore water pressure, permeability, boosting shear strength and permitting consolidation. In addition, it increases the soil's bearing capacity, mitigates liquefaction risk, and reduces settlement (Banerjee et al., 2018; Nicholson, 2014). This approach uses vibratory methods to reduce extra pore water pressure, hence facilitating consolidation and boosting shear strength. Additionally, it has been shown to mitigate liquefaction potential and decrease settlement (Banerjee et al., 2018; Nicholson, 2014). Despite its effectiveness in stabilizing soils, vibro-compaction was much more effective on cohesionless soil (Nicholson, 2014).

It is worth noting that low-density compaction of soil might be utilized to reduce the heave of problematic soils; meanwhile, it is vital to guarantee that the soil retains

sufficient strength at low density. Nonetheless, it is essential to highlight that particle interlocking and rearrangement by compaction in cohesive soils can be challenging. Densification of soils employing vibro-compaction and dynamic compaction methods is particularly successful in cohesionless soils, but particle rearrangement and interlocking in cohesive soils are more challenging to achieve (Nicholson, 2014). Therefore, the effectiveness of these techniques in cohesive soils may be limited.

Dynamic compaction applies high-energy impact to densify loose, granular soils. On the basis of the tamper's weight, the number of drops, and the drop height into a grid that covers the majority of the soil to be compacted, the required density is attained. Dynamic compaction enhances the soil's engineering characteristics by boosting its bearing capacity and strength and reducing its void ratio. According to Nicholson (2014), dynamic compaction is considered undesirable for clayey soils since it is most effective on cohesionless soils.

Reinforcement is another method of stabilizing soil, and geosynthetics are used to create reinforcement. Geosynthetics, such as geogrids, geocells, and geotextiles, are synthetic materials with high tensile strength, durability, and resistance to environmental degradation, making them ideal for soil reinforcement. Several studies have investigated the effectiveness of geosynthetics in soil reinforcement. Biswas and Ghosh (2018, 2019) conducted research to evaluate the performance of geotextile-reinforced soil retaining walls and found that the geotextile reinforcement significantly increased the stability of the walls. Similarly, George et al. (2019a; 2019b; 2019c) studied the effectiveness of geocell reinforcement in enhancing the load-bearing capacity of soft clay and found that the geocells improved the soil's strength and stiffness significantly. The use of geosynthetics for soil reinforcement has become increasingly popular in recent years, and they have been utilized to reinforce various types of structures, including pavements, slopes, and earth-retaining walls, among others. Geosynthetics offer several advantages over traditional soil reinforcement methods, such as ease of installation, cost-effectiveness, and resistance to environmental degradation.

2.2.2 Chemical Stabilization

Chemical stabilization is a soil stabilization method that involves adding chemicals to the soil to improve its physical and mechanical properties. The chemicals used in chemical stabilization react with the soil particles, causing changes in their chemical and physical characteristics. Chemical stabilization offers several advantages over other soil stabilization methods. It is cost-effective, requires less time for construction, and can be used on a wide range of soils. Additionally, chemical stabilization can improve the soil's bearing capacity, strength, and durability, reduce settlement, and increase resistance to erosion and deformation, making it suitable for construction purposes (Khoury et al., 2013; Puppala et al., 2003) The chemical stabilization process involves mixing the chemicals with the soil using various techniques such as grouting, and mixing (deep mixing) methods. The application method depends on the type of chemical used, soil type, and site conditions. The kind of soil to be stabilized determines the type of stabilizer used and its clay content, plasticity, and mineralogy (Firoozi et al., 2017; Raja et al., 2014). Chemical stabilizers are generally categorized as traditional and non-traditional stabilizers. The upcoming subsection provides a detailed account of both the grouting and deep mixing methods employed for stabilization and an overview of the types of stabilizers used, including both traditional and non-traditional varieties.

2.2.2.1 Grout

Grouting is a process that involves filling small voids, cracks, or defects in materials such as rock, soil, concrete, and masonry using a pressurized material. Grouting may be used in soil to fill void spaces or compact soil through densification, whereas it can be used in construction to repair cracks in concrete or masonry. Specialized geotechnical techniques, such as jet grouting and deep soil mixing with grout, use pressure grouting as a critical component. Grouting can also be used to improve the installation and capacity of soil anchors, rock bolts, and foundation piles (Barrdahl, 2022). Grout is a material that can be made from a variety of ingredients, including cement, liquids, solid chemicals such as hot bitumen, and different types of resins. Grout is typically caused by combining two or more components to achieve the desired properties. Grout can have a consistency ranging from a fluid to a stiff, mortar-like

state. It is typically injected in a fluid form to fill cavities but hardens once it has filled all necessary voids and becomes stationary. According to Warner, (2004) grout is widely utilized in construction and has a wide range of applications, including:

- Strengthen soil, rock or the affected medium: Grouting can be used to strengthen weak soils, fractured rock, or other affected media by injecting a grout material under pressure. This process can improve the load-bearing capacity of the soil or rock and prevent the settlement or collapse of structures built on top of them.
- Reduce water flow and seepage: Grouting can also be used to reduce water flow and seepage through soil or rock. This is typically achieved by injecting a waterproof grout material into the affected area, which forms a barrier that prevents water from passing through.
- Correct settlement damages to structures: Settlement of structures can cause damage over time, but grouting can be used to correct this problem. By injecting grout under a foundation or other structure, the voids that have formed due to settlement can be filled, which helps to stabilize the structure and prevent further damage.
- Immobilize hazardous materials and fluids: Grouting can be used to immobilize hazardous materials and fluids, such as radioactive waste or contaminated soil. The grout material helps to encapsulate the hazardous material, preventing it from spreading and causing harm to the environment or human health.
- Create bearing piles: Grouting can also be used to create bearing piles, which are typically used to support heavy structures such as bridges or high-rise buildings. This is achieved by drilling a hole into the ground and filling it with grout, which hardens to form a solid column that can support the structure's weight.
- Support soil and create secant-pile walls: Grouting can be used to support soil and create secant-pile walls, which are typically used in foundation construction. This is achieved by drilling a series of overlapping holes into the ground and filling them with grout, which hardens to form a solid wall that can support the weight of the structure.

- Fill massive voids/sinkholes in soil or rock: Grouting can also be used to fill massive voids or sinkholes in soil or rock. This is typically achieved by injecting a grout material into the void or sinkhole, which fills the space and provides additional support to the surrounding soil or rock.
- Install and increase the capacity of anchors and tiebacks: Grouting can be used to install and increase the capacity of anchors and tiebacks, which are typically used to stabilize slopes or retain walls. This is achieved by drilling a hole into the soil or rock and installing an anchor or tieback, which is then grouted in place to provide additional support.

Several studies have investigated the effectiveness of grout in construction and repair applications. One study by Warner, (2004) found that grout can be used to strengthen soil, rock, or other affected media, reduce water flow and seepage, correct settlement damages to structures, immobilize hazardous materials and fluids, create bearing piles, support soil, and fill massive voids and sinkholes in soil or rock. Another study by Wang et al. (2021) and Fangtian et al. (2016) examined the performance of grouted anchor bolts in underground mines. The authors found that grout can provide significant reinforcement to the surrounding rock mass and increase the load-bearing capacity of the bolts. Other studies have focused on the properties of grout itself, such as its tensile strength, compressive strength, and durability. For example, a study by Soroushian et al. (2003) evaluated the impact of various additives on the compressive strength of grout. The authors found that adding silica-fume and fly ash improved the strength performance of the grout. There are four mechanisms for achieving this result: compaction, permeation, fracture, and chemical exchange (Warner, 2004). Figure 2.1 depicts the visual representation of these methods.

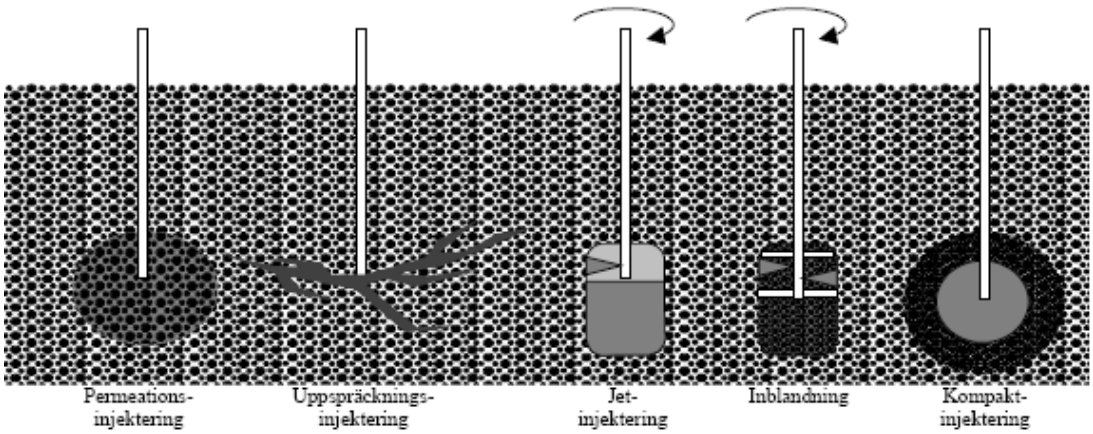

Figure 2.1 Different methods of grouting in soils (Lagerlund, 2009).

2.2.2.1.1 Compaction Grouting

Compaction grouting is a method of grouting that involves injecting low-slump, low-mobility grout into the soil at high pressures to compact and densify it. The grout is injected into the soil through a probe, which is typically drilled into the soil to the desired depth. The grout then displaces the soil particles and fills the voids between them, resulting in densification and compaction of the soil. Compaction grouting is often used to improve the load-bearing capacity of the soil, settlement, mitigate and stabilize structures. It is particularly effective in loose or poorly compacted soils, where it can increase the density of the soil and improve its shear strength. Compaction grouting can also be used to fill voids or sinkholes in the soil and provide support for structures experiencing settlement (Brown & Warner, 1973). One of the benefits of compaction grouting is that it can be performed without excavation, which reduces the disturbance to the surrounding soil and minimizes the risk of damage to existing structures. Additionally, it can be used in a a vast array of soil types, including sand, gravel, and silt, except clay. However, there are also some limitations to compaction grouting. For example, it may not be effective in soils with high plasticity or high-water content, as the grout may not be able to penetrate the soil properly. It can also be difficult to control the spread of the grout in heterogeneous soil conditions, which can lead to unpredictable results (El-Kelesh et al., 2002). Additionally, compaction grouting can be relatively expensive compared to other grouting methods, due to the equipment and labor required for the high-pressure injection process.

Compaction grouting is commonly used at new construction sites and can mitigate the liquefaction potential during earthquakes. It can even be used to correct buildings exposed to settlement damage, making it very flexible and useful in restricted or isolated spaces (Warner, 2004).

2.2.2.1.2 Permeation Grouting (Granular Soils)

Permeation grouting involves injecting a low-viscosity, fluid-like grout into the soil at low pressures to permeate and fill the voids within the soil. The grout is injected into the soil through a probe or injection pipe, which is inserted into the soil to the desired depth. The grout then flows through the soil, filling the voids and gaps between soil particles, and eventually solidifies to form a stable mass (Warner, 2004).

Permeation grouting is often used to improve soil stability, mitigate settlement, and control water seepage in soil. It can also be used to create an impermeable barrier to prevent the flow of hazardous substances or groundwater. This technique is particularly effective in soils that are cohesive or have low permeability, such as clay or silty soils. One of the benefits of permeation grouting is its ability to penetrate deeply into the soil, filling small voids and gaps that are difficult to reach using other grouting methods. It can also be used to treat large areas of soil, providing a uniform improvement in soil strength and stability. Additionally, the low-pressure injection process reduces the risk of damage to existing structures and minimizes the disturbance to the surrounding soil. However, permeation grouting does have some limitations. The low-viscosity grout used in permeation grouting may not be suitable for soils with high permeability, as the grout may flow through the soil too quickly to achieve the desired results. The process can also be slow, as the grout needs time to penetrate and fill the soil voids. Additionally, Permeation grouting may be ineffective in highly plastic soils, as the grout may not be able to permeate the soil effectively (Warner, 2004).

2.2.2.1.3 Fracture Grouting

Fracture grouting is a commonly utilized technique in geotechnical engineering to enhance soil-bearing capacity and reduce permeability. Studies on hydraulic fracture have been conducted through field excavation and laboratory testing, as reported by

(Murdoch, 1990) and (Kleinlugtenbelt et al., 2006). This approach has been applied in various projects, including mitigating subgrade landslides on highways and reinforcing pile foundations. Moreover, fracture grouting is a widely utilized method for groundwater control, whereby the injection of grout into fractures and other openings in rock formations reduces the hydraulic conductivity of the rock mass and controls the flow of groundwater. This technique is especially relevant for tunneling and underground construction projects, where the effective management of water infiltration is of paramount importance. In line with this, Feng et al. (2023) have demonstrated the efficacy of fracture grouting in mitigating groundwater ingress and controlling pore water pressure in underground projects. Furthermore, fracture grouting is commonly utilized to enhance the support of foundations. Through the improvement of the soil or rock mass surrounding the foundation, fracture grouting can increase the load-bearing capacity of the foundation and mitigate settlement. Several studies have demonstrated the efficacy of this technique in increasing the bearing capacity of shallow foundations. For example, Zhang et al., (2013) conducted laboratory tests and reported that the use of cement-based grout for fracture grouting can increase the bearing capacity of a shallow foundation by up to 100%. Choo et al. (2018) similarly found that fracture grouting led to significant improvements in the bearing capacity of shallow foundations, highlighting its utility in foundation support.

This technique involves injecting a grout mixture into fractures and voids in the soil or rock to fill the spaces and create a stronger, more stable mass. Several studies have shown that fracture grouting can enhance soil shear strength and reduce the risk of slope instability (Ng and Menzies, 1994; Ng et al., 2002; Ni and Wang, 2019). Ng et al. (2002) conducted laboratory tests on clayey soil samples and found that fracture grouting with cement-based grout improved the soil strength and reduced deformation. Ni and Wang (2019) conducted numerical simulations and showed that fracture grouting can reduce the stress concentration around the cracks in the soil and improve the overall stability of the slope.

Despite the benefits of fracture grouting, there are also potential drawbacks that must be considered. For example, excessive grouting can lead to forming a rigid mass that can transmit stress and induce fractures in adjacent rock or soil layers (Huang et al., 2018). In addition, the effectiveness of fracture grouting depends on several variables,

including the characteristics of the grout mixture, the geometry of the cracks, and the permeability of the surrounding rock or soil (Li et al., 2018).

2.2.2.2 Deep Mixing Method

Deep mixing is a practical technique that can be used in most soft soil applications. The mechanized mixing technique employs the use of a revolving mixing instrument drilled into the soil. The mechanism is then reversed, withdrawn, and concurrently injected with a dry binder that is blended into the soil. An immediate reaction occurs between the binder and soil during the rotating process. The resultant enhanced soil is in the shape of a column with diameters between 0.5 and 1 meter and lengths up to 25 meters. These columns may connect to form the cellular structure of an in-situ wall, or the whole mass may be stabilized (Kazemain & Barghchi, 2012; Kazemian & Huat, 2010). According to Arulrajah et al.(2018), the DSM method involves drilling a predetermined depth with auger-mixing equipment and injecting and mixing a binder into the in-situ soil. The engineering features of the in-situ soil are improved due to chemical interactions between the in-situ soil and the binder. These chemical interactions result in the formation of circular columns of stabilized clay beneath the ground's surface.

Dry mixing is a highly efficient method for enhancing the load-bearing capacity of soft soils. The composition of cement, lime, and admixtures can be altered to produce a wide range of strength gains. The most significant benefits are observed in low-moisture inorganic soils (R Hashim & Islam, 2008). In the mid-1970s, the deep mixing method (DMM) was independently developed in Japan and Sweden and has since become a widely used and valued soil improvement approach worldwide (Mitchell & Jardine, 2002). DMM is specifically designed to treat soft soils and is subdivided into three categories:), deep soil mixing (DSM), and shallow soil mixing (SSM and jet grouting systems (JGS) (Kazemain & Barghchi, 2012). The DMM is an in-situ soil treatment method that improves the soil's characteristics by mixing it with cementitious and/or other materials. Often, the method is categorized as dry and wet, depending on the kind of binder utilized, the blending process (rotary or jet-assisted), and the vertical depth blended. According to Bruce and Geosystems (2000) the dry method employs a dry powdered binder, while the wet method employs a water-binder

slurry. Although the execution machines used for the two methods may differ, the properties of the treated soil remain largely similar. Differences in design and application procedures stem from the intended purpose of improvement, which impacts installation patterns and strength requirements (Bredenberg et al., 1999) . Additionally, DMM promotes column-type procedures employing lime/cement. It is a method to enhance strength, deformation characteristics, and hydraulic conductivity of soil. The DMM is a soil treatment technique that involves the use of various binders, including fly ash, cement, lime, and other additives, mixed with soil using rotating mixing tools to create hardened columns. These columns are formed through pozzolanic reactions between the soil grains and binder . Anagnostopoulos and Chatziangelou, (2008) reported that the key advantage of this method is its ability to achieve long-term strength improvement, especially with certain types of binders. The pozzolanic reaction might continue for a prolonged duration, resulting in a continuous rise in the strength of cement-stabilized soil as cure time increases (Roslan Hashim & Islam, 2008).

2.2.2.3 Traditional Stabilizers

Lime, ordinary Portland cement, and fly ash are chemical soil stabilizers traditionally used and widely recognized for their effectiveness and economic feasibility in treating weak soils. These stabilizers utilize pozzolanic reactions and cation exchange with soil minerals, providing the necessary strength and stability to the soil (R Hashim & Islam, 2008). These traditional stabilizers have been proven to be reliable and cost-effective solutions for soil improvement.

2.2.2.3.1 Lime

The Chinese, Romans, and inhabitants of the Indian subcontinent have employed lime for building purposes since ancient times. Lime can be used to stabilize weak soils by improving the soil's strength and increasing its resistance to erosion. Lime works by reacting with the clay particles in the soil, forming stable compounds that help to bind the soil together.

Calcium hydroxide ($Ca(OH)_2$), commonly referred as hydrated lime, or calcium oxide (CaO), also known as quicklime, is utilized for stabilization purposes. As demonstrated

by Equation 2.1, quicklime is produced by evaporating the carbon dioxide created during the calcining of high-quality limestone at high temperatures.

$$\underset{\text{Limestone}}{CaCO_3} \xrightarrow[\text{Heat} \geq 1000\,^{\circ}C]{} \underset{\text{quick lime}}{CaO} + \underset{\text{Carbon Dioxide}}{CO_2} \qquad (2.1)$$

Then, quicklime is dissolved with water to create hydrated lime. Equation 2.2 depicts the hydration process:

$$\underset{\text{quick lime}}{CaO} + \underset{\text{water}}{H_2O} \rightarrow \underset{\text{calcium hydroxide}}{Ca(OH)2} + \text{heat} \qquad (2.2)$$

While hydrated lime and quicklime are generally stable chemicals, they undergo a reversible reaction with carbon dioxide to generate calcium carbonate (Boynton 1980). Quicklime (calcium oxide) is high chemically reactive with water, and when exposed to moisture, it rapidly reacts with water to form hydrated lime (calcium hydroxide).

Lime treatment is a commonly established, successful, and economically viable approach for stabilizing weak soils. Lime may be utilized in a two-step, complex technique to achieve the desired purpose of stabilizing soils. The initial stage of soil stabilization with lime involves two interrelated processes: flocculation-agglomeration reactions and cation exchange, which create an instantaneous change in the soil's texture and plasticity (Dallas N Little, 1995). Flocculation or agglomeration, in particular, is a phenomenon wherein clay particles undergo reorganization to form loosely bound micro-clusters or flocs, affected by the soil-water chemistry and mineralogy of the soil. The resulting creation of larger clay clusters renders the soil friable, compatible, and workable, providing a foundation for long-term soil stabilization.

The second stage of lime soil stabilization involves a pozzolanic reaction, which occurs over a more extended period and contributes to the increased strength performance of soil. Pozzolans are finely divided materials containing high amounts of alumina or silica that can react with calcium hydroxide and water, forming a strong cementitious binder (Dallas N Little, 1995). The pozzolanic phases consist of minerals rich in aluminate and silicate, which are present in the clay. The reaction between the pozzolans and calcium hydroxide results in the forms of either calcium-aluminate hydrate (CAH) or calcium-silicate hydrate (CSH), both of which are strong

cementitious compounds, as reported by Duxson et al. (2007). The duration of the pozzolanic reactions can vary considerably, ranging from months to years, based on several factors, such as the solubility reactivity of the pozzolans reactivity and the soil's pH.

The utilization of lime for treating weak soils induces multiple beneficial impacts that enhance soil characteristics, including improved workability, California Bearing Ratio (CBR), resilient modulus, UCS, shear strength, and durability, while simultaneously reducing plasticity index and swelling potential (Holtz, 1969; D N Little, 1996; Dallas N Little, 1995; Puppala et al., 1996; M R Thompson, 1970; Marshall R Thompson, 1966, 1969). Although lime treatment is effective in improving the characteristics of weak soils, it has certain limitations. Lime treatment is ineffective on granular soils and is associated with long-term leaching and durability problems. In sulfate-rich soils, applying lime can result in excessive heaving and distress, leading to infrastructure damage (Puppala et al., 2019). Another drawback of lime treatment is its significant negative impact on the environment. The production of lime requires substantial amounts of energy and emits tens of millions of metric tons of carbon dioxide annually, contributing to greenhouse gas emissions and climate change. Therefore, alternative solutions need to be explored to address these limitations and reduce the environmental impact of soil improvement techniques.

2.2.2.3.2 Ordinary Portland Cement (OPC)

OPC is another frequently used binder in stabilizing problematic soil for decades, and it is known to enhance the mechanical performance of soils by increasing their strength, stiffness, and durability. The addition of cement to soil can also reduce their compressibility, permeability, and susceptibility to erosion.

Cement production typically involves using three primary raw materials: limestone, gypsum, and clay. Limestone is the primary source of lime (CaO), while the clay provides silica (SiO_2), alumina (Al_2O_3), and iron (Fe_2O_3). The primary reaction that occurs during cement manufacture is the calcination of clay and limestone, which occurs at high temperatures ≥1.300°C. This reaction leads to the formation of calcium silicates and aluminates, which are the primary cementitious compounds responsible for the binding properties of cement (P. K. Mehta & Monteiro, 2014). The clinker

obtained from the calcination process is then ground to a fine powder and mixed with gypsum, which serves as a retarding agent, delaying the setting time of the cement. As demonstrated in Equation 2.3, the process may be reduced to its elementary manner:

$$\text{Limestone} + \text{Clay} + \text{Gypsum} \xrightarrow[\text{Heat} \geq 1300\ ^{\circ}\text{C}]{} \text{Cement} \qquad (2.3)$$

Cement stabilization is a process that involves mixing soil, cement, and water in appropriate proportions to achieve desired soil properties. The method of cement stabilization is similar to that of lime stabilization, involving various physico-chemical processes, such as cation exchange, agglomeration, flocculation, cementitious hydration, and pozzolanic reactions. During the cement stabilization process, the cement reacts with the soil particles to form a dense and solid mass. The cementitious hydration process creates C-S-H gel, which binds the soil particles together, leading to improved soil strength and stiffness. Cation exchange occurs between the cement and soil particles, replacing weakly held cations with calcium ions. This process contributes to improving soil plasticity and reducing its swelling potential. Agglomeration and flocculation involve the formation of larger soil particles or flocs, which improve the soil's workability and reduce its plasticity. The formation of larger particles also contributes to improved soil strength and stiffness.

Pozzolanic reactions occur when cement reacts with pozzolanic materials in the soil, such as clay minerals, producing more cementitious compounds, such as C-S-H and C-A-H. These compounds contribute to the overall strength and durability of the stabilized soil. During hydration, the two calcium-silicate phases release calcium hydroxide-hydrate to initiate the stabilizing process (Prusinski & Bhattacharja, 1999). Equations 2.4 and 2.5 depict the hydration processes that lead to the creation of calcium hydroxide and calcium silicate hydrate:

$$2(3\text{CaO}.\text{SO}_2) + 6\,\text{H}_2\text{O} \rightarrow \text{CSH} + 3\text{Ca(OH)2} \qquad (2.4)$$

$$2(2\text{CaO}.\text{SO}_2) + 4\,\text{H}_2\text{O} \rightarrow \text{CSH} + \text{Ca(OH)2} \qquad (2.5)$$

Numerous studies have demonstrated that cement as a soil stabilizer can effectively decrease the plasticity index and volume change potential while increasing the CBR, shear strength and UCS of soils (F. H. Chen, 2012; Christensen, 1969; Kézdi, 1979; Petry & Wohlgemuth, 1988). The effectiveness and economic viability of cement

stabilization are superior in granular soil because of the reduced amount of Portland cement required and the decreased workability of cohesive soils.

The utilization of cement for soil stabilization encounters comparable limitations to those associated with lime, primarily stemming from the energy-intensive nature of its production process, which harms the environment. Additionally, the use of cement may lead to potential issues such as cracking, brittle failures, and susceptibility to sulfate attacks. During the manufacturing process, a significant amount of CO_2 is released into the atmosphere at a rate of around one ton of CO_2 per ton of Portland cement, which accounts for 7% of global carbon-dioxide emissions (Du et al., 2017; M. Zhang et al., 2013). Thus, researchers are actively looking for alternate binders that might reduce the carbon footprint of grouting and DSM works (Arulrajah et al., 2018; J. Zhang et al., 2019).

2.2.2.3.3 Fly ash

Fly ash is a pozzolanic material that is produced as a byproduct of coal combustion, characterized by its fine, grey, dust-like particles composed of microspheres of alumina and silica glass (Mateos & Davidson, 1962). Unlike the produced products, lime, and cement, fly ash has a chemical composition that varies greatly depending on its source and process of manufacture. Fly ash is usually categorized as Class F (non-self-cementing) or Class C (self-cementing) according to ASTM and AASHTO standards. Class (C) fly ash has a high proportion of lime (CaO), allowing it to be used as the sole binder in the proper amounts. In contrast, Class F fly ash contains little to no lime, necessitating an activator, such as lime or cement, to activate the stabilizing processes.

Stabilizing soils using fly ash involves two key steps: immediate and long-term pozzolanic reactions. The immediate reaction consists of the agglomeration of soil particles, resulting in increased workability of the soil. Furthermore, a long-term pozzolanic reaction takes place over time, forming a cementitious binder that improves the soil's engineering characteristics. The efficiency of fly ash as a stabilizing agent and the kinetics of its reactions are significantly influenced by a range of factors, including its chemical composition, the amount of fly ash utilized, temperature, the sort of soil being treated, and the water content of the mixture (Usmen & Bowders Jr,

1990). According to Zulkifley et al. (2014), applying fly ash in soil stabilization decreases the soil's plasticity index while enhancing its UCS and CBR values. However, Parsons (2002) has noted that the impact of Class C fly ash on the swell potential of high plasticity index soils (PI = 30) may be minimal.

The utilized of fly ash as a sole effective binder in reasonable amounts remains a matter of concern. Additionally, the setting time and reaction times of fly ash can vary. Furthermore, using fly ash for soil stabilization raises air-quality concerns in the immediate application area and may lead to respiratory problems in workers. On the other hand, the disposal of industrial by-products and agricultural wastes in landfills has become another severe environmental concern (Scharff, 2014). All of these factors have contributed to the development eco-friendly building materials that support the notion of sustainability.

2.2.2.4 Non-traditional Stabilizers

Traditional soil stabilizers are widely utilized worldwide to efficiently stabilize problematic soils. Nonetheless, non-soil stabilizers were employed when traditional stabilizers are unavailable or of inferior quality. Moreover, worries about rising costs, prolonged curing times, undesirable chemical reactions rate in high-sulfate soils, and negative effects on the environment associated with traditional stabilizers have prompted researchers to consider non-traditional stabilizers as an alternate stabilizing approach.

Non-traditional stabilizers represent a broad category of materials that can be employed as binders to stabilize soils, rocks, and other geotechnical materials. This category comprises a diverse range of substances, including but not limited to slag, polymers, mine tailings, enzymes, salts, kiln dust, sulfonated oils, glass powder, resins, rice husk, rubber tires, fibers, etc. These materials are employed as stabilizers in situations where traditional stabilizers are either unavailable or fail to meet the desired quality criteria (Caballero et al., 2016; Diniz et al., 2017; S. He et al., 2018; Karatai et al., 2017; P. Kumar & Singh, 2008; Dallas N Little & Nair, 2009; Petry & Little, 2002; Tingle & Santoni, 2003). The application of non-traditional stabilizers in soil stabilization has been gaining attention due to their derivation from by-products of various industries or waste materials requiring appropriate disposal techniques.

However, their soil stabilization efficiency is lower than traditional stabilizers. Combining non-traditional stabilizers with complimentary additives or activating chemicals can boost their effectiveness (Sharma & Sivapullaiah, 2016; Tingle et al., 2007). Despite the increasing research on non-traditional stabilizers, the current literature remains limited and primarily focused on their performance, with little attention paid to the underlying stabilization mechanisms. Furthermore, the assessment of their performance is inadequate, with most studies concentrating only on unconfined compressive strength and swelling reduction, with little investigation into other essential engineering properties.

2.2.2.4.1 Geopolymers

Geopolymers represent a promising class of binding material that utilizes the alkali aluminosilicate precursor reactions to achieve binding. These materials are characterized by possessing mechanical and physical properties comparable to those of OPC, while also exhibiting reduced environmental impact.

Geopolymers are synthesized through the alkali activation of aluminosilicate precursors. This process results in the formation of large three-dimensional (3D) networks of covalently bonded alumina-silicates that are distinguished by their excellent strength performance, low shrinkage, and superior durability characteristics (P. Duxson et al., 2007). Geopolymers are generated from relatively inexpensive silicoaluminate precursors such as slag, clay, fly ash, and metakaolin (Cheng & Chiu, 2003; J. Davidovits, 1991; Gordon et al., 2005; Van Jaarsveld et al., 2002). Geopolymers can be produced within a relatively short period and harden at ambient temperatures. This feature makes them an environmentally friendly and sustainable alternative to traditional building materials. The synthesis of geopolymers from waste materials like fly ash and slag has the added advantage of providing an effective means of recycling such materials (Lizcano et al., 2012).

2.2.2.4.1.1 Historical Background

The development of alkaline-activated materials (AAMs) can be traced back to 1908, when Kuhl, a German scientist, patented the creation of materials similar to Portland cement by combining an aluminosilicate precursor, such as vitreous fly ash or slag, with an alkali source, such as alkali sulfate or carbonate (John L Provis & Van

Deventer, 2013). Subsequently, Purdon, (1940) experimented with different blast furnace slags activated by calcium hydroxide and sodium hydroxide solutions, resulting in materials with strengths, flexural, and tensile properties comparable to those of OPC. In the 1950s, Glukhovsky discovered that low-calcium or calcium-free aluminosilicates, such as clay, could create alkali-activated binders similar to natural minerals and called them "soil cement" and "soil silicates." Glukhovsky's discovery is considered the first documented synthesis of geopolymers.

Geopolymers had garnered significant attention since the 1980s when Joseph Davidovits, a French material scientist , first developed them through the alkali activation of naturally occurring materials such as limestone, dolomite, and kaolinite (Davidovits, 1991). Later, Davidovits developed and produced various aluminosilicate blends as fire-resistant resins. Since then, geopolymer applications and utilization have been investigated in several sectors, including chemistry, mineralogy, material sciences, and engineering. Geopolymers have been used in several applications such as thermal insulation, containment of radioactive materials, fire-resistant materials, corrosion-resistant coatings, etc. (J. Davidovits, 1991; P. Duxson et al., 2007; Hussain et al., 2004; John L Provis & Van Deventer, 2009; Jadambaa Temuujin et al., 2009, 2011; Van Jaarsveld et al., 1999).

Terminology

Davidovits first introduced the concept of geopolymers in the 1980s. Geopolymers are defined as inorganic ceramics based on alumino-silicates, and their charge balance is achieved through a group I or II oxides, such as Na, K, or Ca. These materials can form rigid gels under pressure and ambient temperature conditions and can be shaped into near-net dimension bodies that transform into crystalline or amorphous structures. Geopolymers are classified as a type of alkali-activated material (AAM) and are considered a subset of this class of materials (J. L. Bell et al., 2009).

AAMs are manufactured by combining an alkaline activator with an aluminosilicate precursor, and their characteristics are comparable to those of ordinary cement binders. On the other hand, geopolymers are a type of AAM binder that typically contains little to no calcium and is often synthesized using aluminosilicate precursors such as metakaolin or fly ash (John L Provis & Van Deventer, 2013) It is noteworthy that

despite several decades of research on geopolymer binders, there remains a degree of ambiguity regarding the appropriate terminology for these materials, owing to the lack of an established nomenclature system. These innovative binders are frequently referred to as "alkali-activated materials," "inorganic polymers," or "geopolymers." However, the accurate classification and naming of each binder material would necessitate extensive investigation.

Figure 2.2 presents a well-recognized categorization of alkali-activated materials (AAMs). The darker shading in the Figure 2.2 represents higher Na and/or K concentrations, while the calcium and aluminum content is used to compare OPC and calcium sulfo-aluminate cement with AAMs. This categorization was proposed by van Deventer et al. (2010).

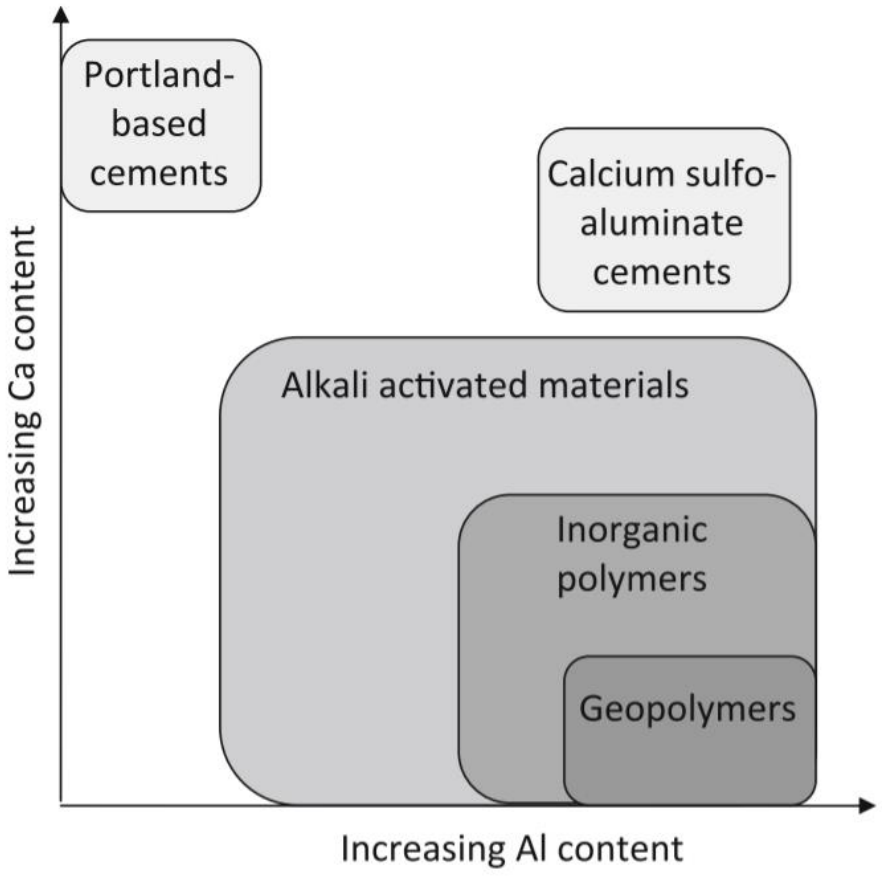

Figure 2.2 General classification of AAMs and its subsets (van Deventer et al., 2010).

2.2.2.4.1.2 Conceptual Structure of Geopolymers

Chemically, Geopolymer materials are classified as polycationic materials, with the term "sialate" derived from "silicon-oxo-aluminate." Polysialates are characterized as ring or chain polymers in which Si^{4+} and Al^{3+} ions are tetrahedrally coordinated with oxygen (as shown in Figure 2.3), and they can exhibit varying degrees of crystallinity, ranging from amorphous to semi-crystalline (J. Davidovits, 1991). Geopolymers can be described using the empirical formula of polysilanes, as presented in Equation 2.6:

$$M_n\{(-(SiO_2)_z) - AlO_2\}_n . wH_2O \quad (2.5)$$

Here, M denotes the alkali metal cation (e.g., K, Na, or Ca), n represents the degree of polycondensation, z denotes the silicon-to-aluminum (Si: Al) ratio, which is typically 1, 2, or 3, and w denotes the molar amount of water. Based on the Si: Al atomic ratio (z), oligomeric units of polysilanes can be classified as poly(sialate) (PS), poly(sialate-siloxy) (PSS), and poly(sialate-disclose) (PSDS), as illustrated in Figure 2.3.

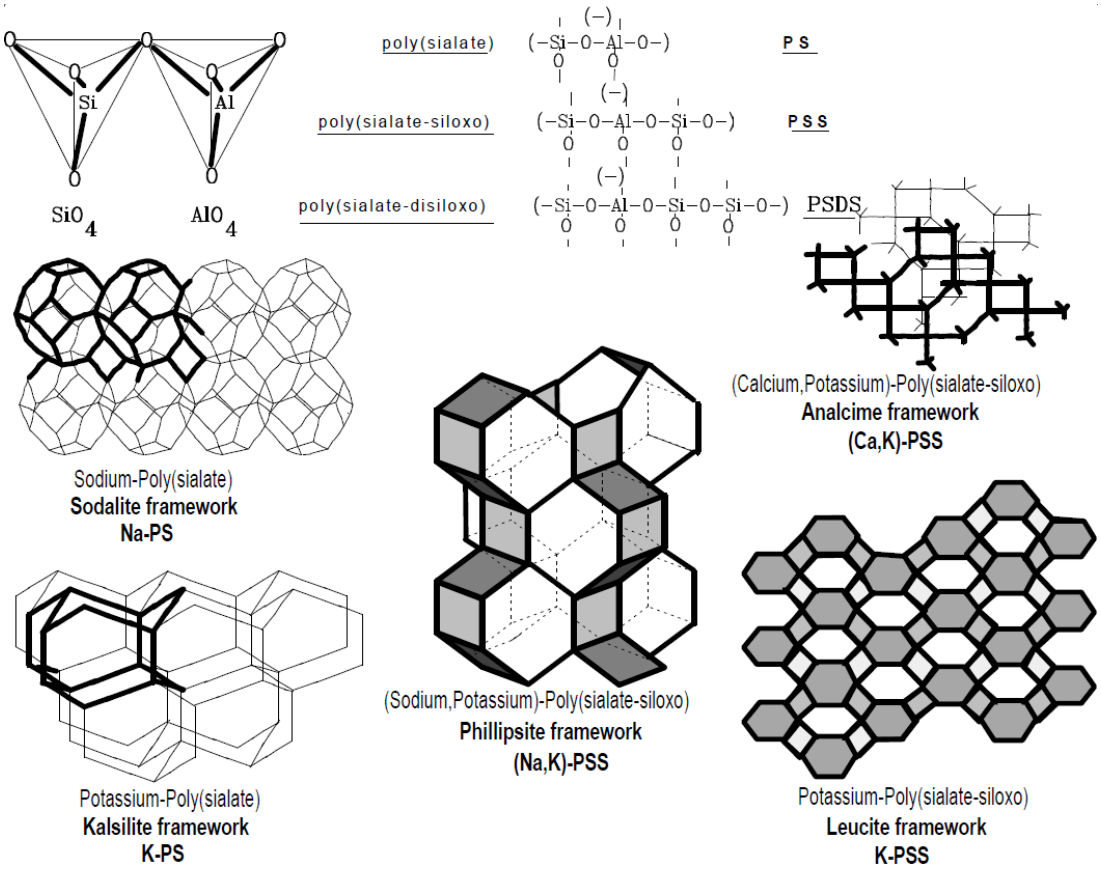

Figure 2.3 Geopolymer monomer system and associated crystal structures (J. Davidovits, 1991).

Geopolymers are generally considered to possess a non-crystalline structure and are characterized by a broad diffuse halo in their X-ray diffraction (XRD) patterns, as opposed to the sharp diffraction peaks observed for crystalline materials (J. Davidovits, 1991). The XRD patterns of geopolymers exhibiting this characteristic halo are illustrated in Figure 2.4. Typically, geopolymers cured at temperatures below 80°C are amorphous, but they can undergo crystallization at elevated temperatures (Barbosa & MacKenzie, 2003). These crystalline phases have atomic structural similarities to zeolitic minerals (John L Provis & Van Deventer, 2009).

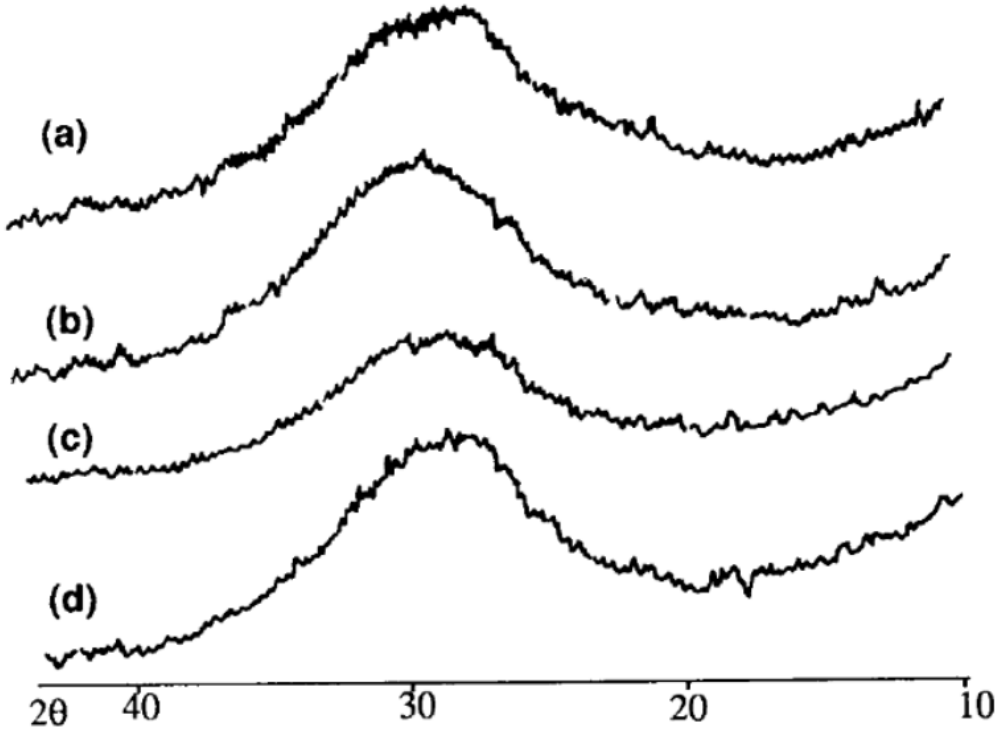

Figure 2.4 XRD diffractograms of (a, b) [Na, K]-PSS and (c, d) [K]-PSS (J Davidovits, 1988).

Davidovits states that most geopolymers are cured at lower temperatures, which results in a non-crystalline structure. In contrast, the crystalline forms seen in Figure 2.5 represent the final structures resulting from full crystallization processes at high temperatures. As depicted in Figure 2.5, geopolymers are distinguished by a dense network of aluminosilicate chain or ring polymers (J.Davidovits, 1991). If a geopolymer has not entirely reacted with its constituents, free silicate, and aluminate

groups will remain inside the partially formed ring or chain structures, eventually undergoing polycondensation to complete the connections.

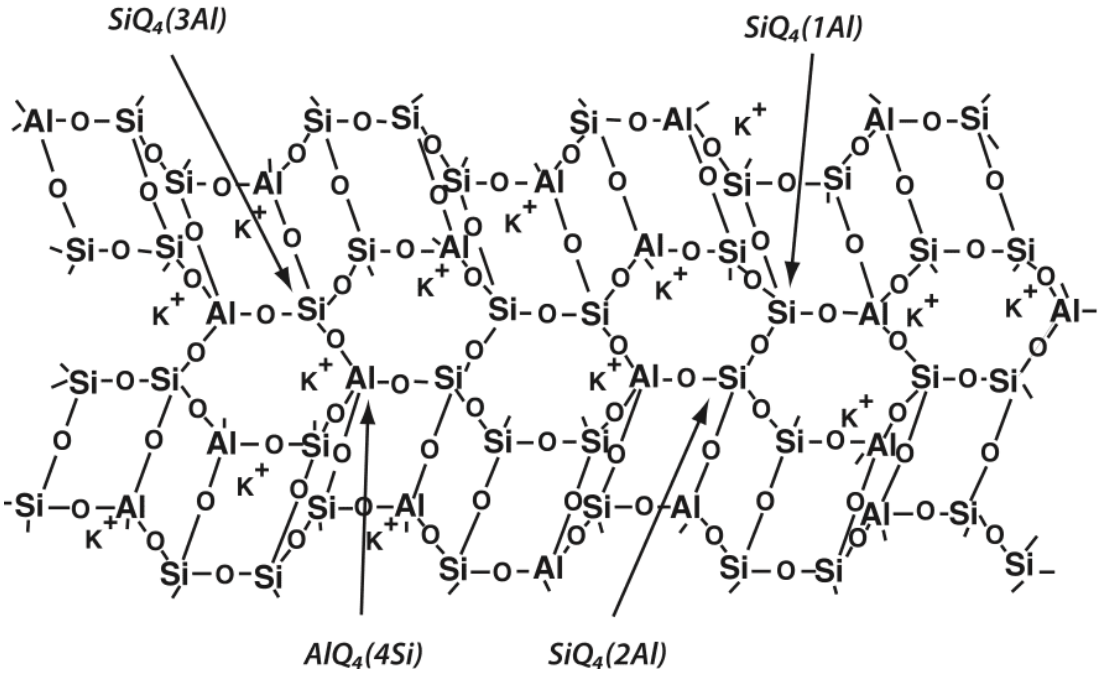

Figure 2.5 Three-dimensional network model of a completely reactive potassium-based geopolymer (J. Davidovits, 1991).

2.2.2.4.1.3 Conceptual Geopolymerization Process

Geopolymer synthesis is a complicated process involving alkali-activated polycondensation reactions. Polycondensation reactions are commonly used to form polymers by bonding monomers, and as a result, water or other condensed molecules are often released as a byproduct (Bhat & Kandagor, 2014). In the 1950s, Glukhovsky postulated a generic method for geopolymerization involving three essential steps: destruction-coagulation, coagulation-condensation, and condensation-crystallization. However, researchers have sought to describe the geopolymerization process as technology advances more comprehensively. This has led to an improved understanding of the process, building upon the foundation laid by earlier work (J. Davidovits, 1991; John L Provis & Van Deventer, 2009). Figure 2.6 presents a simplified schematic of the geopolymerization process, providing an overview of the major processes involved. Geopolymerization can be divided into five distinct stages:

dissolution, speciation equilibrium, gelation, reorganization, and polymerization and hardening, as described in previous studies (P. Duxson et al., 2007; Medri et al., 2010).

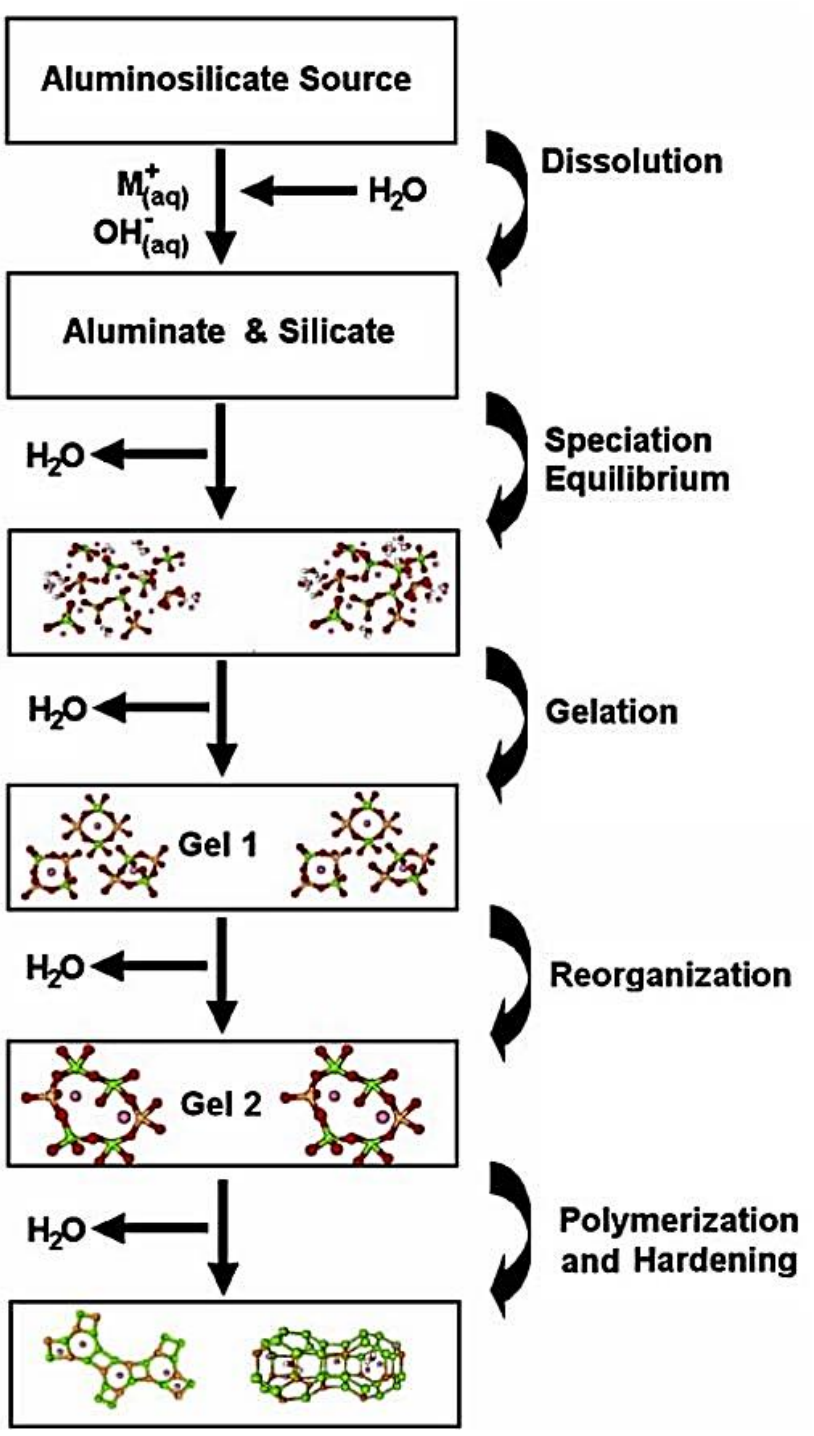

Figure 2.6 Process diagram of geopolymerization (Duxson et al., 2007).

The initial stage of geopolymerization, dissolution, involves the reaction between an aluminosilicate precursor and an alkali activator solution comprising water, metal

cations, and additional silica. The high pH of the critical causes hydrolysis of the precursor, resulting in the formation of monomeric silicate ($Si(OH)_4^{2-}$) and aluminate ($Al(OH)_4^{3-}$) species. During the dissolution stage of geopolymerization, a complex and supersaturated aluminosilicate solution is generated. This solution undergoes polycondensation reactions of monomeric or oligomeric units, leading to the formation of large networks or chains, which eventually result in gelation. As this process occurs, water is released and accumulates within the gel pores, but it is not chemically bound to the geopolymer structure (Duxson et al., 2007). As the geopolymerization process continues, the gel structure undergoes rearrangement and reorganization, forming a complex three-dimensional (3-D) network. This network is characterized by extensive networks of aluminosilicates, which are typical of geopolymers. Subsequent curing leads to solidifying and forming considerably more advanced polymeric networks that ultimately undergo crystallization.

The process of gelation, which involves the development of a three-dimensional network of aluminosilicates from dissolved species, is influenced by several factors, including the concentration of reactive species, the type, and quality of raw materials, processing conditions, and time. As a result, the gelation rate and subsequent hardening of different geopolymer formulations varies, depending on the specific raw materials employed in the geopolymer synthesis process.

2.2.2.4.1.4 Geopolymer Synthesis and Influencing Factors

The production of geopolymers involves integrating four key components: an alkali-metal cation source, an aluminosilicate precursor, an additional silica source, and water. The alkaline activator solution is the product of mixing the alkali-metal cation source, an additional silica source, and water in suitable quantities. The aluminosilicate materials are then combined with the alkaline activator solution to form a slurry, which is then cured to make the crystalline geopolymer.

Davidovits initially coined the term geopolymer to describe alkaline hydroxide/silicate-activated calcined clay (metakaolin) (John L Provis & Van Deventer, 2009). Typical raw materials employed in geopolymer production include fly ash, calcined clay, and slag (P Duxson, 2009). Several factors, such as presence of contaminants, mix design, and curing environment significantly influence the duration

for geopolymer gelation and subsequent solidification. It is worth noting that the properties of geopolymers are susceptible to seemingly minor factors, such as the quality of the precursor material, the amount of alkali activator used, the presence of reactive alumina, and the moisture content (Buchwald et al., 2007; Fletcher et al., 2005; Lizcano et al., 2012; Rowles & O'connor, 2003).These factors can significantly affect the gelation and solidification process and the ultimate strength and durability of the resulting geopolymer product. These contributing elements that determine geopolymer characteristics are elaborated in the following sections.

Aluminosilicate Precursor

The source materials should have a significant quantity of amorphous aluminum and silicon. The raw ingredients may be natural minerals, such as calcined kaolinite, or industrial by-products (e.g., slag, bottom ash, and fly ash) (J. Davidovits, 1991). Numerous factors should be considered in the selection of precursor type, including availability, cost, application type, and end-user demand, which influence the selection of source materials for producing geopolymer (Wallah et al., 2005). It has been discovered that two or more source materials can be used in the same mix as slag and fly ash (the most commonly used materials), where it has been reported that the use of slag with fly ash eliminates the need for heat curing or oven curing (Ismail et al., 2013). Additionally, it was discovered that the high alumina and silica content in fly ash and slag had a significant impact on the improvement of geopolymer strength performance and durability properties in general, as sodium-aluminum-silicate-hydrate gel and calcium-aluminum-silicate-hydrate gel was formed with a more favorable higher cross-linking degree, respectively (Marathe et al., 2016). There are several investigations available in the literature about the physical, chemical, mechanical, and thermal characteristics and application of geopolymer materials derived from metakaolin as the source materials (Kamseu et al., 2012; Khater, 2013; Rakhimova, 2020; Rashad, 2019; Tironi et al., 2012). Similarly, there are numerous studies on engineering characteristics and the field application of geopolymeric material made by utilizing industrial by-products materials, mainly slag and fly ash (Ahn et al., 2016; Çevik et al., 2018; Duan et al., 2017; El-Didamony et al., 2012; Emin et al., 2018; Kim et al., 2014; Sundar Kumar & Ash, 2013; N. K. Lee et al., 2016; Partha et al., 2013; Ushaa et al., 2015; Wallah et al., 2005; P. Zhang et al., 2018). The primary source

materials for this doctoral research are slag and fly ash. The next sections discuss the features and characteristics of the source aluminosilicate precursor materials for geopolymer production.

Slag is a non-metallic by-product of the iron manufacturing sector that is generally referred to as slag. It is a useful by-product used in aggregate and concrete production. In 1865, Germany began commercial manufacturing of lime-activated blast furnace slag. After approximately 15 years, slag was introduced to be utilized as a full or partial replacement in concrete production (Their & Özakça, 2018). Since then, slag has been employed in manufacturing concrete on a global scale. After iron ore, coke, and limestone, the slag floats over the molten iron at around 1500 to 1600 degrees Celsius in the furnace. The slag is molten and may comprise between 30% and 40% SiO_2 and approximately 40% CaO. This means that slag has a chemical composition comparable to that of cement. Upon extraction of the molten iron, the residual slag is composed of silica and alumina oxides. Through a rapid water-quenching process, the slag solidifies into a glassy granulate, which is subsequently dried and ground to the desired size (Higgins, 2007). ASTM C 989-99 classifies slag into three strength grades based on its activity index, with grade 120 having the highest activity index and displaying greater cementitious properties than Portland cement (ASTM C989-99, 1999). Compared to the manufacturing of OPC, which emits approximately one ton of carbon dioxide, the iron and steel sector's slag waste produces only 0.07 tons of CO_2 and consumes around 1300 MJ of energy per ton (Their & Özakça, 2018). The cooling conditions determine the development of mineral crystals and the number and size of gas bubbles that can escape before becoming trapped by the solidifying slag mass. Consequently, the slag's porosity and crystalline structure are attained through cooling. Three distinct forms of slag can be produced from the molten mass, depending on the cooling techniques employed. The quick cooling procedure produces a granular product comprising 85 and 95 % non-crystalline calcium aluminate silicates, which are more energetic than the crystalline material (Their & Özakça, 2018). Slag production can be achieved using two primary methods: granulation and palletization. In the granulation process, an intense water jet pressure is utilized to rapidly cool the molten slag, producing 5 mm slag pellets. In contrast, the slag is fed into a spinning drum with cold water during the pelletization process, resulting in rapid temperature

reduction. The slag particles produced through the pelletization process typically have a diameter of approximately 10 cm, and particles with a diameter of 0.6 cm are considered optimal to generate the slag in its most advantageous state (Newman & Choo, 2003).

Slag's physical and chemical properties vary depending on the raw materials used in the production process. The typical constituents of slag are shown in Table 2.1. Despite the addition of pozzolanic by-products during the blending process, slag has a chemical composition similar to that of OPC. Additionally, slag contains minor minerals such as Fe_2O_3, MgO, SO_3, Na_2O, and K_2O (Suresh & Nagaraju, 2015). As seen in Figure 2.7, SEM micrographs of slag typically show irregular flake-shaped particles with angular and sharp edges. Slag differs from fly ash in that the Si-O-Si link must be broken to become reactive with lime. If slag is exposed to water and chemical activators, it can begin to function chemically and generate new products related to its glassy structure. Generally, sulfates and/or alkaline solutions can perform as activators and chemically combine with slag. When these activators are utilized, their capacity to disturb the system's glassy structure as well as elevate the pH to a critical level indicates their action (Their & Özakça, 2018). Slag production is sufficient worldwide and exceeds 300 million tons per year. The pozzolanic reactivity of slag is high, making it sustainable for usage in the construction industry (S. K. Nath & Kumar, 2013). Slag utilization as a precursor for manufacturing geopolymer concrete minimizes greenhouse gas emissions, the use of cement, and the disposal of slag wastes (Sakir et al., 2020). Slag has been utilized as a cement alternative for a long time, and numerous researchers started employing it in creating cement in 1939. It had been claimed that 100 MPa compressive strength may be attained by employing slag in the manufacturing of self-compacted concrete (Islam et al., 2015).

Table 2.1 Physical and chemical properties of slag (Suresh & Nagaraju, 2015).

Characteristics	Values
Calcium oxide (%)	42
Silica (%)	35
Alumina (%)	13
Magnesia (%)	8
Color	Pale white
Specific gravity	2.7
Bulk density (kg/m^3)	1160
Fineness (m^2/kg)	350

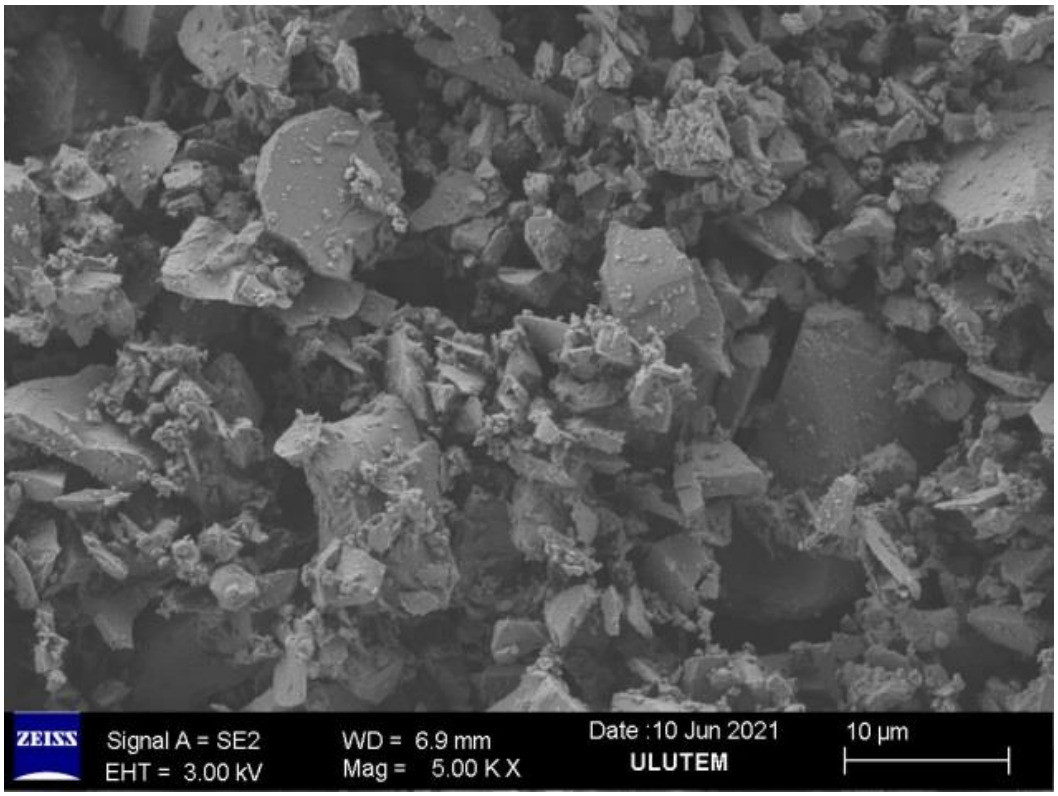

Figure 2.7 SEM image of slag (Hamid Abed, Sabbar Abbas, et al., 2022).

Fly ash (pulverized fuel ash) is a fine solid residue produced by coal-fired power plants (ASTM C618, 2015). Fly ash particles are collected using bag houses or electrostatic precipitators before releasing the gases coal burning creates into the atmosphere. Nowadays, most of the world's electricity is generated by coal-fired power stations; therefore, fly ash is widely available worldwide (Ng, 2011). Mehta (1999) estimated that about 300 MT of fly ash is collected annually from power plants in China and India; however, only about 20 MT of fly ash was used in 1998. According to Ng

(2011), approximately 64 MT of fly ash was produced from coal-fired power plants in the United States in 2004, with only 25 million tons being used. According to Heidrich et al. (2013), Australia and New Zealand produced approximately 12.5 MT of fly ash in 2002; however, only about 4.1 million fly ash were employed in diverse applications. The cement and concrete industries mostly consume utilized fly ash. Fly ash is also used in geotechnical/structural engineering, agriculture, and mining (Heidrich et al., 2013). Malhotra and Carino (1991) observed that excess fly ash is typically deposited in landfills or drained straight into the ocean, posing an environmental threat and squandering fly ash because it's a valuable material and can be utilized in other applications (Ng, 2011). Fly ash is a byproduct of the burning of coal and may be divided into two categories, class F and class C, based on their chemical composition. ASTM C618 (2015) defines class F fly ash as having a minimum of 70% SiO_2, Al_2O_3, and Fe_2O_3, and a maximum of 20% CaO. On the other hand, class C fly ash has a lower percentage of SiO_2, Al_2O_3, and Fe_2O_3 (50%) and a higher calcium content (20%) (ASTM C618, 2015). The chemical composition of fly ash is shown in Table 2.2. Class C fly ash has more complicated mineralogical characteristics than class F. and it is rich in magnesium oxide and sulfur trioxide (Tho-In et al., 2012). It contains crystalline compounds such as anhydrite, periclase, merwinite, sodalite, dicalcium silicate, alkali sulfates, free lime, and tricalcium aluminate, as well as quartz, magnetite, mullite, and hematite (J Temuujin et al., 2009). Unburned carbon, amorphous siliceous, and aluminous also form part of class C fly ash. The high calcium content in class C fly ash leads to a different geopolymer structure than class F, resulting in more substantial self-cementing properties that allow for setting and hardening at ambient temperature. The composition of fly ash is influenced by factors such as coal specifications, combustion systems, ash collection methods, and cooling rate (Tikalsky et al., 2001). Typically, fly ash particles are spherical and have a size range of less than 1 μm to 150 μm (Ng, 2011). However, there are also rounded, angular and irregular, particles, as well as pieces of coarser particles and fused particles as shown in Figure 2.8. The inclusion of spherical particles can modify the flow characteristics of fresh concrete, making it simpler to compress than concrete without fly ash (Their & Özakça, 2018).

The fineness of fly ash is an important physical property that affects its pozzolanic activity. The smaller the particle size, the greater the surface area, which leads to increased pozzolanic activity due to the increased reaction rate. The amount of ash retained on sieve No. 25 (0.44 mm) indicates the fineness of fly ash. This property is generally not affected by emission control and combustion methods (Tikalsky et al., 2001). Recent studies have suggested that the fineness of fly ash is a critical physical property that influences the performance and quality of concrete. The pozzolanic activity of fly ash is influenced by particle size, and finer particles have a greater surface area, resulting in an increased reaction rate. As such, particle size distribution can significantly impact the overall quality of concrete (Tikalsky et al., 2001). Another important physical feature of fly ash that affects its quality is the loss of ignition (LOI). The LOI of fly ash refers to the weight loss that occurs during ash ignition and is primarily due to the presence of unburned carbon following combustion. Fly ash with a higher LOI value can absorb air-entraining admixtures, leading to decreased pozzolanic activity and increased mixing water, ultimately minimizing the air entrainment of concrete. Thus, limiting the LOI of fly ash used in concrete production is crucial. According to the ASTM C618, (2015), the LOI for both classes of fly ash (C and F) utilized in concrete production should not exceed 5% and 6%, respectively.

Table 2.2 The chemical composition of fly ash (ASTM C618, 2015).

Item	Class C	Class F
(SiO_2+Al_2O_3+ Fe_2O_3) wt ≥	50.0%	70.0%
SO3 wt≥	5.0	5.0
(SiO_2+Al_2O_3+ Fe_2O_3) wt ≥	50.0%	70.0%
CaO	> 10%	< 10%
Moisture content wt≥	6.0	6.0
Loss on ignition (LoI) wt≥	3.0	3.0

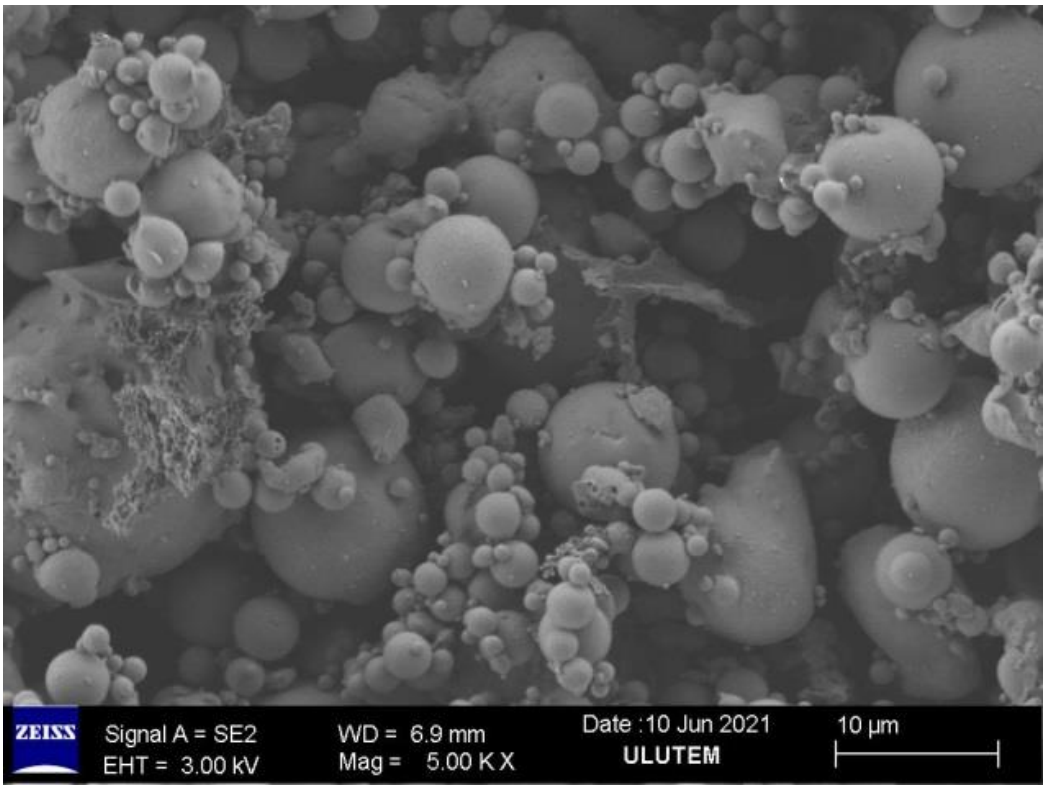

Figure 2.8 SEM image of fly ash (Hamid Abed, Sabbar Abbas, et al., 2022).

Rice is a highly-consumed staple food worldwide, with paddy grain production reaching approximately 497 million metric tons in the 2019/2020 period (S. S. Hossain et al., 2021). The milling of paddy grain typically generates 0.20-0.25 kg of rice husk (RH) per kilogram of paddy grain, which possesses low nutritional value but retains considerable calorific value (~15 MJ/kg) (Aghaeipour et al., 2017). Therefore, RH is commonly used as a fuel for combustion in boilers, producing a waste material known as rice husk ash (RHA) (Figure 2.9), which constitutes about 25 wt% of the original

husk. The improper disposal of RHA can lead to numerous ecological concerns, including the creation of ash lands, water contamination, and air pollution that can adversely affect human health. Thus, there is a pressing need to develop sustainable technologies to utilize RHA instead of resorting to landfilling. It is worth noting that RHA contains a significant amount of amorphous silica (~85-90 wt%) (S. K. S. Hossain et al., n.d.) and exhibits pozzolanic properties (Thiedeitz et al., 2020) , as shown in Table 2.3. In light of this, several investigations have been carried out over the past decade to explore the potential of RHA as a supplementary portion for ordinary Portland cement or sand in mortar or concrete, serving as a filler material, silica source, or synthesizing an alkaline activator solution (Na_2SiO_3) for geopolymerization. (Thiedeitz et al., 2020)].

Various factors, including the processing conditions and the source of the parent material, influence the properties of agro-waste. Agro-waste undergoes multiple processing steps during extraction from the parent material, which may alter its physicochemical characteristics depending on parameters such as temperature and the presence of other chemicals. The composition of rice husk ash (RHA) is primarily influenced by the ecological nature of its origin, including the soil chemistry of the parent material, as discussed in depth by Fapohunda et al. (2017)]. In addition, using fertilizers during paddy cultivation can also affect the composition of RHA (Jittin et al., 2020).

Numerous studies have identified that rice husk ash (RHA) exhibits pozzolanic activity, which is influenced by its processing conditions. Wansom et al. (2010) evaluated the pozzolanic activity index of RHA by measuring the change in electrical conductivity of RHA + Ca $(OH)_2$ paste through impedance spectroscopy. The addition of RHA in the solution resulted in decreased conductivity due to the absorption of Ca^{2+} ions by the amorphous silica present in RHA. Nair et al., 2008) correlated the pozzolanic activity of RHA with lime after analyzing the silanol sites on the surface of RHA silica via nuclear magnetic resonance (NMR) spectroscopy. Jittin et al. (2020) determined that RHA demonstrates a pozzolanic action index greater than 75% within 7 days, classifying it as a pozzolanic material according to ASTM C311 (2018).

Several researchers have studied the use of RHA in the synthesis of geopolymers. Kusbiantoro et al. (2012) investigated the strength performance of microwave-incinerated RHA and fly ash geopolymer, while He et al. (2013) described geopolymers derived from red mud/RHA husk ash. In both researches, alkaline solutions comprised sodium silicate and sodium hydroxide. Bouzón et al. (2014) found that a suspension of RHA/NaOH heated in a reflux system may be utilized as a substitute for commercial water glass (sodium silicate) for fluid catalytic cracking in geopolymer design. While Tchakouté et al. (2016) employed RHA to synthesize geopolymers from metakaolin and RHA. They concentrated on synthesizing sodium silicate utilizing RHA and paid little attention to the partial replacement of metakaolin by RHA in the solid mixture before reacting with the sodium hydroxide solution. Overall, RHA has shown great potential as a sustainable and cost-effective material for geopolymer synthesis.

Table 2.3 Chemical properties of RHA (Abbas et al., 2022).

Constituent (%)	Values
Cao	1.38
Al_2O_3	0.1
SiO_2	91.6
Fe_2O3	0.64
MSGO	-
SO_3	0.21
K_2O	5.14
Na_2O	-
Loss on ignition	5.43

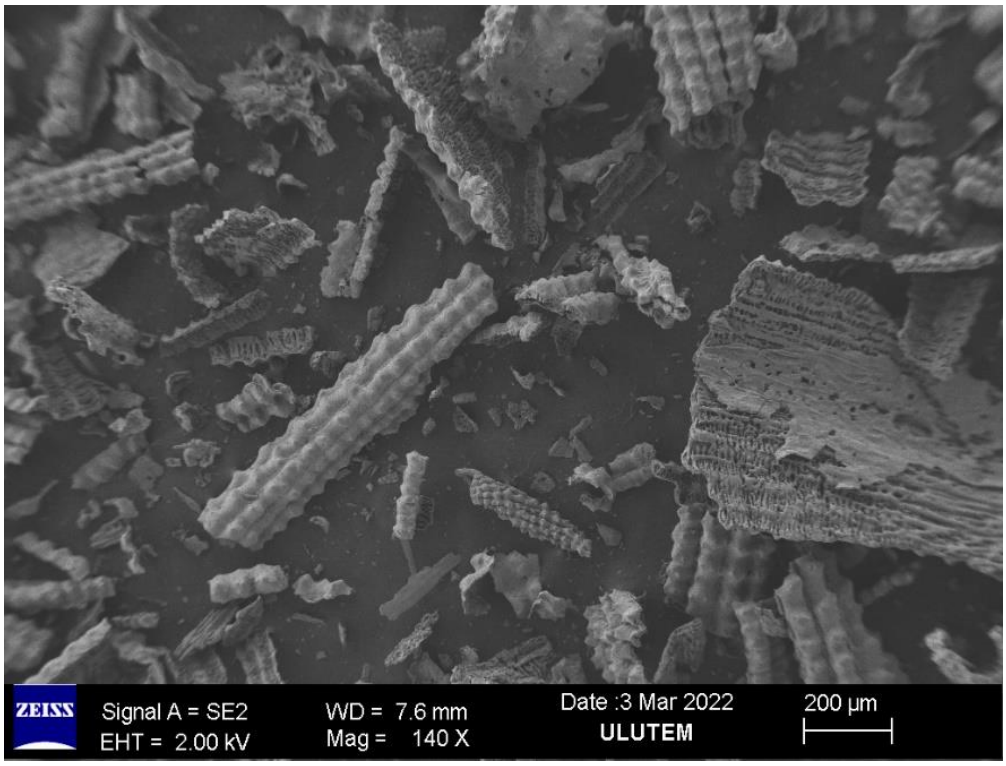

Figure 2.9 SEM image of rice husk ash (RHA) (Abbas et al., 2022).

Waste glass powder (GP) is a prevalent inorganic solid waste generated from both daily life and industrial production activities (Ling & Poon, 2017). The unique characteristics of glass, such as its fragility and limited lifetime, contribute to the significant production of GP during its use (Solanki et al., 2020). As indicated by (Siberian et al., 2019), large amounts of GP waste are generated and stockpiled annually in Australia, the United States, and the European Union, amounting to 1, 10, and 1.5 million tons, respectively. Despite the potential for recycling and utilization, only a fraction of GP waste is effectively managed, with recycling rates ranging from 34% to 73% (Siberian et al., 2019). Consequently, there remains a significant opportunity to enhance the efficient utilization of GP, which continues to be predominantly disposed of in landfills, occupying massive land resources and causing long-lasting environmental pressures (Ling & Poon, 2017). Hence, it is imperative to prioritize the development of eco-friendly and efficient approaches to recycling and utilizing GP. Waste glass has been found to contain more than 70% amorphous silica (see Table 2.4) and has a relatively stable chemical composition, which is essential because soda-lime glass constitutes the majority of the industrially manufactured glass (Si et al., 2020; Xiao, Ma, et al., 2020; Xiao, Polaczyk, et al., 2020). As seen in Figure

2.10, SEM micrographs of GP typically show irregular flake-shaped particles with angular and sharp edges.

In recent years, the potential of waste glass powder (GP) as a precursor binder in alkaline-activated composites has been highlighted due to its high solubility in alkali media (Canakci et al., 2019; Y. Liu et al., 2019; Samarakoon et al., 2020). Tho-In et al. (2016) found that replacing 10%–20% of fly ash with GP slightly enhanced the compressive strength by 4.2% at 7 days of pure fly ash geopolymer cured at 60 ◦C for the first 48 hr. Maraghechi et al. (2017) reported that incorporating 20% GP in alkali-activated mortars with 80% fly ash resulted in a 13% higher strength value at 56 days than the mixture without GP. The authors attributed this improvement to the steam curing process at 60 ◦C, which may have facilitated the dissolution of more silica from the glass. However, Bobiric\ua et al. (2015) reported that incorporating glass powder as a partial precursor material decreased the strength of fly ash-based geopolymers, even though the specimens were cured for 24 hours at 60 ◦C.

Several earlier studies have investigated the potential of glass powder as a partial precursor in a fly ash-slag binder matrix. For instance, Zhang et al. (2017) explored the effects of GP as a partial substitution for fly ash in an alkaline-activated FA-slag binder mix at ambient temperature. The authors concluded that there was a significant increase in compressive strength as the GP amount increased. Similarly, (Samarakoon et al. (2020) reported a similar trend for fly ash-slag binders with GP, ascribed to developing more calcium-dominant reaction products. However, these studies did not explore the effects of using GP above 30%, and the slag content was considerably higher, constituting 50% of the total binder. Due to the increased reactivity of slag in an alkaline media, this greater slag concentration may inhibit GP's actual reaction or performance in blended systems. Moreover, some earlier attempts have demonstrated that replacing slag with GP cannot improve the strength of alkali-activated mortar cured at room temperature, possibly due to the lower reactivity of glass powder compared to that of slag (Fernández-Jiménez et al., 2017; Maraghechi et al., 2017; Yuyou et al., 2016).

Table 2.4 Physicochemical characteristics of GP (Hamid Abed et al., 2022).

Constituent (%)	GP
Cao	8.21
Al_2O_3	1.0
SiO_2	78
Fe_2O3	0.52
MgO	0.14
SO_3	0.6
K_2O	0.09
Na_2O	12
Modulus ratio	
H_2O	
Specific gravity	2.54
Specific surface (m^2/kg)	382

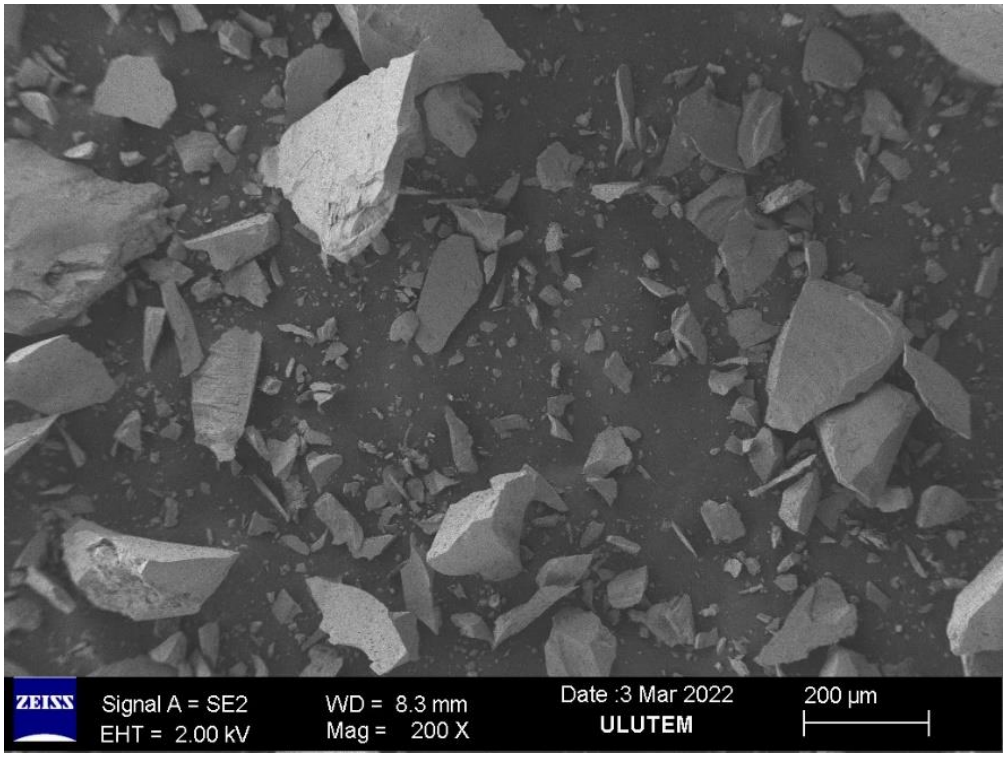

Figure 2.10 SEM image of glass powder (GP) (Hamid Abed et al., 2022).

Alkaline activators

Alkaline activators can refer to any strong alkaline solution that can be utilized to produce geopolymers. According to Davidovits, (1991a), in ancient times, calcium hydroxide was the alkaline activator, and volcanic ash was the source material to construct the pyramids. Alonso and Palomo (2001) investigated using calcium hydroxide as an alkali activator liquid to form geopolymers. Nowadays, potassium/sodium silicate liquids and potassium/sodium hydroxides are widely utilized as alkali activators liquids in the manufacture of geopolymers (Barbosa et al., 2000; Wallah et al., 2005; Kong et al., 2007; Oh et al., 2010; Nematollahi, Sanjayan, & Ahmed Shaikh, 2015; Yahya et al., 2015).

According to Palomo et al. (1999), adding a soluble silicate (potassium or sodium silicates solution) to an alkali hydroxide (potassium or sodium hydroxides solution) accelerates the geopolymerization reaction. Additionally, Xu and Van Deventer (2000) revealed that soluble silicate in an alkaline liquid enhances the synthesis of geopolymer precursors upon mineral-solution contact. Xie and Xi, (2001) examined the influence of activator amount on the strength of a geopolymer mix. They found that an alkali activator/fly ash ratio resulted in a stronger geopolymer. Fernández-Jiménez and Palomo (2005) studied the influences of alkaline activator sort on the geopolymer's characteristics. Their investigation employed sodium hydroxide, sodium carbonate (Na_2CO_3), and sodium silicate solutions to synthesize alkali-activated fly ash. They discovered that the alkaline activator considerably influenced the geopolymeric reaction. They found that the geopolymer prepared with NaOH liquid had the maximum compressive strength, followed by a mixture prepared with sodium silicate solution; however, the mechanical properties were decreased when Na_2CO_3 solution was used as an activator. They indicated that the amount of sodium oxide significantly affects the compressive strength of alkali-activated fly ash. Fernandez-Jimenez et al. (2006) reported a considerable increase in mechanical strength when an alkaline solution, including soluble silicate, was used activator rather than merely alkali hydroxide. This is owing to the increased density of the paste caused by the presence of soluble silica in the alkali liquid.

2.2.2.4.2 Geopolymer Grout

Cement-based grouting materials are commonly used for soil stabilization and anti-seepage purposes. However, in recent years, there has been increasing interest in using geopolymer grouting materials, particularly alkali-activated slag-fly ash cementitious materials, for soil stabilization applications.

Geopolymer grouting materials offer several advantages over traditional cement-based materials. For example, they are typically more environmentally friendly since they can be made from industrial byproducts like slag and fly ash. Geopolymer grouts can also have higher compressive strength and lower shrinkage than traditional cement-based grouts (Abbas et al., 2022). To ensure that geopolymer grouting materials can effectively penetrate the soil and provide the desired strength and anti-seepage properties, it is important to consider their rheological and fresh properties. Specifically, the grout should have a low viscosity to allow it to penetrate the soil easily and enough shear strength to prevent segregation and maintain stability. Additionally, the grout should have appropriate setting time and early strength development to ensure that it can achieve the desired strength properties in a timely manner.

The use of geopolymer grouting materials as an alternative to cement-based grouting materials has been explored in recent research. Cristelo et al. (2013) performed an experimental investigation on the rheology of geopolymer grouts composed of fly ash. The study aimed to investigate several properties of grouts, including fluidity, setting time, shrinkage, capillary absorption, and expansion behavior, density and, mass variation during the curing process. Results obtained from the study revealed a significant correlation between UCS and fluidity of the grouts, where an increase in fluidity resulted in a decrease in UCS. This relationship is particularly relevant in jet grouting applications, as grouts' fluidity determines the grout's velocity at the nozzle and the soil/grout mixing capability. Also, the research revealed that fly ash-geopolymer-based grout had a lower porosity than cement-based grout. In addition, Wang et al., (2018) developed a road grouting geopolymer utilizing slag and optimized the mixture ratio based on setting time, fluidity, and UCS. The results indicated that the geopolymer paste made with blast furnace slag had minimal bleeding and expansion, indicating excellent dimensional stability. In another work by Güllü et al.

(2019), the rheological characteristics of geopolymer grout were investigated and compared to those of OPC-based grouts using cold-bonded fly ash and fly ash at different dose rates and water/binder ratios. The results indicated that geopolymer grout exhibited notable advantages over fly ash and geopolymer aggregate in practical grouting applications as a viable alternative to traditional cement-based materials. In a research conducted by Aboulayt et al. (2018), the properties of geopolymer grouts were thoroughly examined using stabilizer mixes of metakaolin and fly ash. The study found that adding xanthan gum improved the stability of the grouts by acting on the activation solution without significantly affecting the geopolymerization reaction.

Zhang et al. (2019a) conducted a study investigating the characteristics of geopolymer-based grouting materials, including slag and fly ash. The researchers varied the ratios of slag to fly ash and the molarity of NaOH between the ranges of 0.2-1.0 and 0.5-4.0 M, respectively. The study's findings revealed that the addition of slag improved the flowability of the grouts, while fly ash and sodium hydroxide enhanced their stability. The setting time decreased as the ratios of slag to fly ash and NaOH molarity increased. Furthermore, it was observed that the concentration of sodium hydroxide had a more influence on the viscosity of the grouts over time in comparison to the slag to fly ash ratios. Adding fly ash and NaOH decreased the UCS of the hardened grouts, whereas the inclusion of slag enhanced their strength properties. By adjusting the slag to fly ash ratios and the sodium hydroxide molarity, the researchers could tailor the grouts' setting time from 0.5 to 5.5 hours, with a UCS of up to 7.48 MPa after 28 days and a bleeding capacity of less than 2.5%. The optimal slag to fly ash ratio and NaOH molarity were found to be 0.8 and 2.0 M, respectively. These geopolymer-based grouting materials with these optimum characteristics fulfill the grouting engineering performance criteria for grouting reinforcements.

Li et al. (2021) found that ultrafine red mud improved the properties of low-cost grouting material for underground engineering compared to coarse red mud. Ultrafine red mud prolonged the setting time, reduced viscosity and thixotropy, and improved slurry stability. It resulted in lower mechanical strength than coarse red mud, but still showed promise. The iron component in ultrafine red mud enhanced the geopolymerization process.

2.2.2.4.3 Geopolymer Stabilized Soil

Over the years, researchers have formulated various kinds of geopolymers intended for diverse construction and engineering applications, such as acid and fire -resistant materials, high-tech resins, composites for infrastructure repair and reinforcement, low-tech building materials, and 'green' cement and concrete. Geopolymers have received interest as potential replacements to cement because of their comparable characteristics, and the recent trend for utilizing more inventive and environmentally friendly construction materials. In recent years, researchers have investigated the efficiency of geopolymers in stabilizing problematic soils, and this premise has gained popularity since 2010. However, it is essential to note that despite the considerable body of literature on the creation of numerous forms of geopolymers for different applications, geopolymer research as soil stabilizers is restricted and mostly from other countries.

A number of studies have utilized fly ash-based geopolymers (single-precursor) to enhance the mechanical performance of silty and clayey sands ((Cristelo et al., 2012; Dungca & Codilla II, 2018; Rios et al., 2016), as well as high-plasticity clays (Phetchuay et al., 2014)and low-plasticity soils (Z. Liu et al., 2016). In the United States, researchers have utilized single-precursor metakaolin-based geopolymers to enhance the swell potential and strength characteristics of a synthetic lean clay (M. Zhang et al., 2013, 2015) and a high-plasticity clay (Khadka et al., 2018).Moreover, geopolymer research has extended to utilizing multiple precursors by combining fly ash (FA) with slag (H. H. Abdullah et al., 2017; Mohammadinia et al., 2016) or calcium carbide residue (CCR) (Phetchuay et al., 2016; Phummiphan et al., 2017) to enhance the properties of both coarse and fine-grained soils. Additionally, other single-precursor materials such as slag (Du et al., 2017), palm-oil fuel ash (Pourakbar et al., 2016), and volcanic ash (Miao et al., 2017) have been utilized for geopolymer development in the context of soil improvement.

The literature on geopolymer stabilization of soils is included in Table 2.5, indicating that a significant amount of research on this topic has been conducted in recent years. In most cases, the effectiveness of geopolymers in stabilizing soils has been evaluated

by measuring the improvement in UCS, while in some instances, CBR or swell, shrinkage testing has also been employed.

Geopolymer stabilization has demonstrated a significant increase in the UCS of soils. Nevertheless, the impact of geopolymer treatment on other engineering characteristics, such as volume change (i.e., shrinkage and swell) and durability properties, remains an area that requires additional investigation. Researchers have undertaken microstructural analyses through elemental and mineralogical characterization, as well as microscopic observations utilizing techniques such as, EDS XRF, XRD, and SEM to better understand the mechanisms by which geopolymers stabilize soils.

Table 2.5 Literature review of geopolymer stabilization of soils.

Geopolymer Precursor material	**Soil type (USCS)**	**Improvement observed**	**Author(s)&Publication Year**
Fly ash class (F)	SM	UCS	(Cristelo et al., 2012)
Metakaolin	CL	UCS, Shrinkage	(M. Zhang et al., 2013)
Fly ash	CH	LL, PL, UCS	(Phetchuay et al., 2014)
Metakaolin	CL	UCS,1-D Swell	(M. Zhang et al., 2015)
Palm-oil fuel ash	CH	UCS, Durability, UPV	(Pourakbar et al., 2016)
Fly ash class (F)	CL	UCS	(Z. Liu et al., 2016)
Fly ash class (F)and slag	GW	UCS, MR	(Mohammadinia et al., 2016)
Fly ash class (F) and CCR	CH	UCS	(Phetchuay et al., 2016)
Fly ash class (F)	SM	UCS, Durability, UPV	(Rios et al., 2016)
Slag	CL	UCS, Hydraulic Conductivity	(Du et al., 2017)
Fly ash class (C) and CCR	SC-SM	UCS	(Phummiphan et al., 2017)
Fly ash class (F) and slag	CH	LL, PL, UCS	(H. H. Abdullah et al., 2017)
Volcanic ash	CH	Swell, LL, PL, UCS	(Miao et al., 2017)

Table 2.5 Continued

Fly ash class (F)	SM	UCS, CBR	(Dungca & Codilla II, 2018)
Metakaolin	CH	Swell, UCS	(Khadka et al., 2018)
Fly ash class (F) and slag	Soft marine clay	UCS	(Arulrajah et al., 2018)
Fly ash class (F) and slag	Soft marine clay	UCS	(Yaghoubi et al., 2019)
Fly ash class (F) and slag	Kaolin (CH, CL)	UCS, CU	(H. H. Abdullah et al., 2019)
Metakaolin	Fine-grained soil	UCS	(S. Wang et al., 2021)
Fly ash and slag	Soft soil	UCS, Durability	(Luo, Zhang, et al., 2022)

The enhancement strength characteristics of geopolymer-treated soil are due to the geopolymer gel's development during the curing process, which physically binds adjacent soil particles together to create a solid bind (Z. Liu et al., 2016). Zhang et al. (2013) reported no direct chemical interaction between the soil minerals and geopolymer precursors since the microstructural investigation of geopolymer-treated soil reveals no new mineral production. Pourakbar et al. (2016) and Liu et al. (2016) examined the impact of the cation source in the alkali activator solution on the strength performance of geopolymer-treated soil. Specifically, they compared the effects of potassium hydroxide (KOH) and sodium hydroxide (NaOH) for mixtures with the same fly ash/soil ratio. Results showed that the KOH-activated geopolymer provided a higher UCS value than the NaOH-activated geopolymer. The smaller hydration sphere of K^+ ions facilitate the formation of more polymeric chains, resulting in a denser and stronger geopolymer structure. Na^+ ions, on the other hand, have a larger hydration sphere, which hinders the formation of strong polymeric chains, resulting in a weaker geopolymer structure. Therefore, using KOH as an activator in

geopolymerization processes can lead to higher strength performance of geopolymer-treated soil than using NaOH (Pourakbar et al., 2016).

Khadka et al. (2018) reported that MK-based geopolymers resulted in higher strength and lower swell reduction than FA-based ones. However, It is essential to ensure that geopolymer-treated soil specimens are cured under consistent and appropriate conditions, as differences in curing temperature and humidity can affect the resulting strength and durability properties. Higher curing temperatures and lower relative humidity conditions can result in dehydrated specimens, potentially providing misleading results for strength gain (Cristelo et al., 2012; Phetchuay et al., 2014; M. Zhang et al., 2013, 2015). Therefore, it is crucial to consider the appropriate curing conditions for geopolymer-treated soil specimens to evaluate their strength and durability properties accurately.

CHAPTER III

EXPERIMENTAL PROGRAM

3.1 General

This chapter presents detailed information about the experimental program of all studied samples, such as materials description, geopolymer binder preparation, specimen preparation, and casting procedures. Furthermore, the experimental tests (rheological, fresh, mechanical, and microstructural) of all the studied samples are presented. All the experimental program procedures were conducted in the labs of the civil engineering department at Gaziantep University.

3.2 Materials

3.2.1 Ordinary Portland Cement (OPC)

The present study employs an ordinary Portland cement (OPC) of type CEM I 42.5R as the binder material in the control group, which adheres to the (ASTM C150/C150M-17) standards. The chemical analysis and physical characteristics of the OPC are seen in Table 3.1.

Table 3.1 Chemical analysis and physical characteristics of OPC.

Constituent (%)	OPC
a) Chemical composition	
CaO	62.6
SiO_2	20.25
Al_2O_3	5.31
MgO	2.82
Fe_2O_3	4.04
K2O	0.92
SO_3	2.73
Na_2O	0.22
Loss on ignition	4.4
b) Physical characteristics	
Specific surface(m^2/kg)	326
Specific gravity	3.15
Fineness (Blaine) (m^2/Kg)	394

3.2.2 Rice Husk Ash (RHA)

Rice husk ash (RHA) was used as a partial precursor in slag-based mechanochemically activated geopolymer (MSG) grout. The RHA was acquired from a rice manufacturing plant in Edirne, Turkey. This factory produces and sells the RHA used in this study as a commercial waste material. The RHA that passes through the 150 μm sieve was adapted for mechanochemical activation. Table 3.2 depicts the chemical composition and physical characteristics of RHA.

Table 3.2 Physical and Chemical characteristics of RHA.

Constituent (%)	RHA
a) Chemical composition	
CaO	1.38
Al_2O_3	0.1
SiO_2	91.6
Fe_2O_3	0.64
MgO	0.5
SO_3	0.21
K_2O	5.14
Loss on ignition	5.43
b) Physical characteristics	
Specific surface(m^2/kg)	1060
Specific gravity	1.97
Cu (Coefficient of uniformity)	7.1
Cc (Coefficient of curvature)	1.15

3.2.3 Green Glass Powder (GP)

The GP is obtained from green soda-lime bottles collected primarily from shops in Gaziantep, Turkey. The waste green soda-lime bottles were first washed with tap water to remove labels from the exterior of the glass and then cleaned inside to remove impurities. The waste green soda-lime bottles were naturally dried in the laboratory for 24 hours and grounded to powder using a Los Angeles abrasion machine. Finally, the glass powder passed the No. 35 sieve with a particle size of less than 0.5 mm and was adapted for the mechanochemical activation process. Table 3.3 depicts the chemical composition and physical characteristics of GP.

Table 3.3 Physical and Chemical characteristics of GP.

Constituent (%)	GP
a) Chemical composition	
CaO	8.21
Al_2O_3	1.0
SiO_2	78
Fe_2O_3	0.52
MgO	0.14
SO_3	0.06
K_2O	0.09
Na_2O	12
b) Physical characteristics	
Specific surface(m^2/kg)	382
Specific gravity	2.54
Cu (Coefficient of uniformity)	13.9
Cc (Coefficient of curvature)	1.55

3.2.4 Ground Granulated Blast Furnace Slag

Ground granulated blast furnace slag (GGBFS), also known as SL in accordance with the ASTM C 989 standard, is a by-product resulting from the melting down of steel and iron during the manufacturing process. It primarily comprises calcium and aluminosilicates and is recognized for its cementitious properties, which are akin to those of Portland cement. Moreover, slag is widely accessible, making it a favorable aluminosilicate source for geopolymer production.

Slag is incorporated with the RHA or GP -based geopolymer grout because it possesses high mechanical strength and good durability in corrosive environments (Marjanović et al., 2015).. However, slag binder has some problematical properties such as poor workability, high viscosity, fast setting, and high shrinkage (Hojati & Radlińska, 2017; Lu et al., 2021; M. Palacios et al., 2021; Ye & Radlińska, 2016, 2017). Table 3.4 depicts the chemical composition and physical characteristics of slag.

Table 3.4 Physical and Chemical characteristics of Slag.

Constituent (%)	Slag
a) Chemical composition	
CaO	34.19
Al_2O_3	40.42
SiO_2	10.6
Fe_2O_3	1.28
MgO	7.63
SO_3	0.68
K_2O	0.0128
Na_2O	-
b) Physical characteristics	
Specific surface(m^2/kg)	565
Specific gravity	2.9
Cu (Coefficient of uniformity)	4.33
Cc (Coefficient of curvature)	0.47

3.2.5 Alkaline Activators

This research selected sodium hydroxide (NaOH) and sodium silicate (Na_2SiO_3) as alkaline activators. Sodium hydroxide solution was prepared one day before mixing with different molar concentrations (1.25, 2.5, and 3.75 M) using NaOH beads of 97-98% purity locally purchased and dissolved in faucet water. Sodium silicate was used in two forms, a powder form (metasilicate-Penta) for preparing mechanochemical geopolymer and a liquid solution for preparing the conventional geopolymer. Based on previously published works that adopted the mechanochemical activation approach, a ratio of Na_2SiO_3/NaOH = 0.5 was selected to prepare the alkaline activator (Bhardwaj et al., 2020; Gupta et al., 2020; Gupta, Bhardwaj, Mishra, Prasad, et al., 2017; Manish et al., 2016; Mudgal et al., 2019). Table 3.5 displays sodium silicate's chemical and physical properties in both liquid and powder forms.

Table 3.5 Physical and Chemical characteristics of sodium silicate and sodium hydroxide.

Constituent (%)	(Na_2SiO_3-Penta) Powder	(Na_2SiO_3) liquid	NaOH
a) Chemical composition			
Solid content, %	58.04		
SiO_2, %	28	29.4	
Na_2O, %	29	14.7	
Fe, ppm	6		
Cl-, ppm	3		
Weight Ratio	0.998		
Loss of ignition	41.96		
Modulus ratio	1	2	
H_2O	43		
b) Physical characteristics			
Melting point	73^0C		
Shape	Granular		
Odor	Odorless		
Water solubility	23.05 gm/100 ml		
Bulk Density, $Ib/m^3(gm/cm^3)$	55(0.88)		
pH (1% solution)	12.4		13-14
Partical Size Analysis	90-95% in 12-30 mesh		

NAOH

Na_2SiO_3 liquid

Na_2SiO_3 Powder

3.2.6 Water

Tap water from the laboratory was used to make the solution. Some amount of water was also added to source materials while mixing to increase the workability of the mix because super plasticizer was not used.

3.2.7 Soil

The soil (CL) utilized in this experiment for assessing DM is fine-grained soil with liquid and plastic limits of 41 and 24, respectively. According to the modified proctor test ASTM (D1557-12, 2009), the maximum dry unit weight and optimal moisture content of soil are 17.3 kN/m^3 and 18.1%, respectively, as shown in Table 3.6.

According to the unified soil classification system (USCS), the soil used in the experiments was categorized as a low plasticity clay (CL) (ASTM D2487-11) and also

falls under the category of clayey soil based on its quality grade (A-7-6) and group index (19) (AASHTO, 1993), as shown in Figure 3.1. Prior to use, the soil was passed through a sieve with a 0.42 mm opening and then oven-dried for a day until its moisture content reached zero. To prepare the soil-binder samples for the experiment, the protocol recommended by Bhadriraju et al. (2008) and Pakbaz & Farzi (2015) was followed, which involves treating weak soil with water content close to the liquid limit. The particle size distribution of the clay used in the experiment is shown in Figure 3.2, and Table 3.7 lists the chemical composition and physical characteristics of the soil.

Table 3.6 Characteristics of soil (clay).

Parameters	Value
Classification (USCS)	CL
Plastic limit (PL)	25
Liquid limit (LL)	41
Plasticity index (PI)	16
Specific gravity (Gs)	2.77
passing No.200	90
Optimum moisture content, OMC, (%)	19.2
Swelling (%)	3.58
Maximum dry unit weight (kN/m^3)	17.5
Clay (%)	58
Silt (%)	32

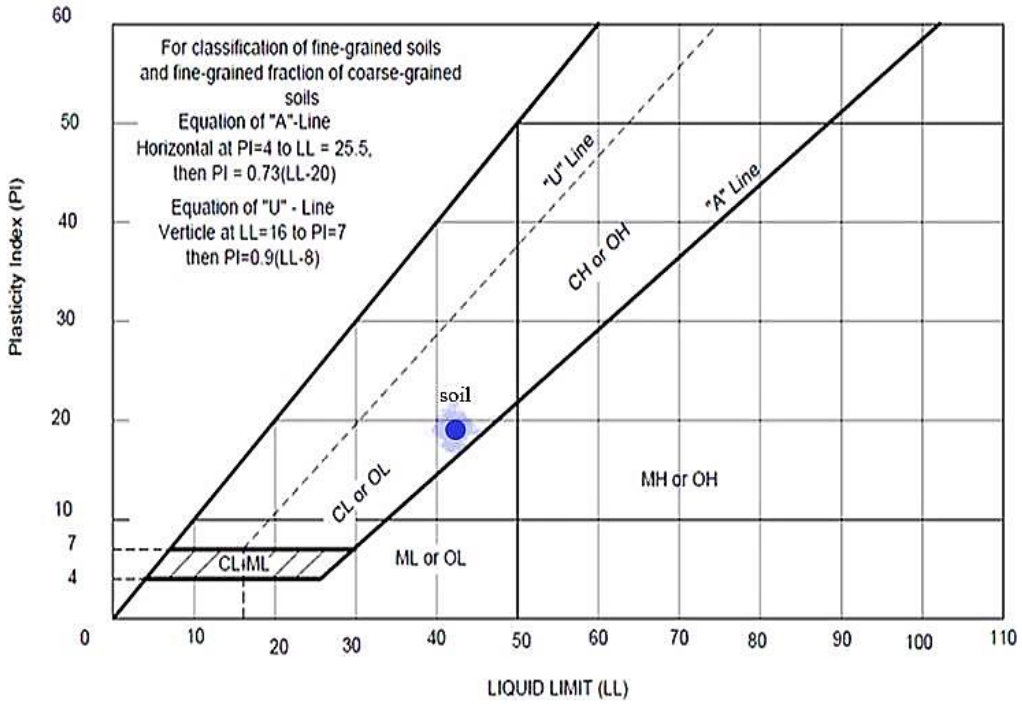

Figure 3.1 Plasticity chart for the soils.

Table 3.7 Chemical and physical characteristics of clay.

Constituent (%)	Soil
a) Chemical composition	
CaO	18.24
Al_2O_3	6.36
SiO_2	17.25
Fe_2O_3	10.7
MgO	0.44
SO_3	0.08
K_2O	1.49
b) Physical characteristics	
Specific gravity	2.7

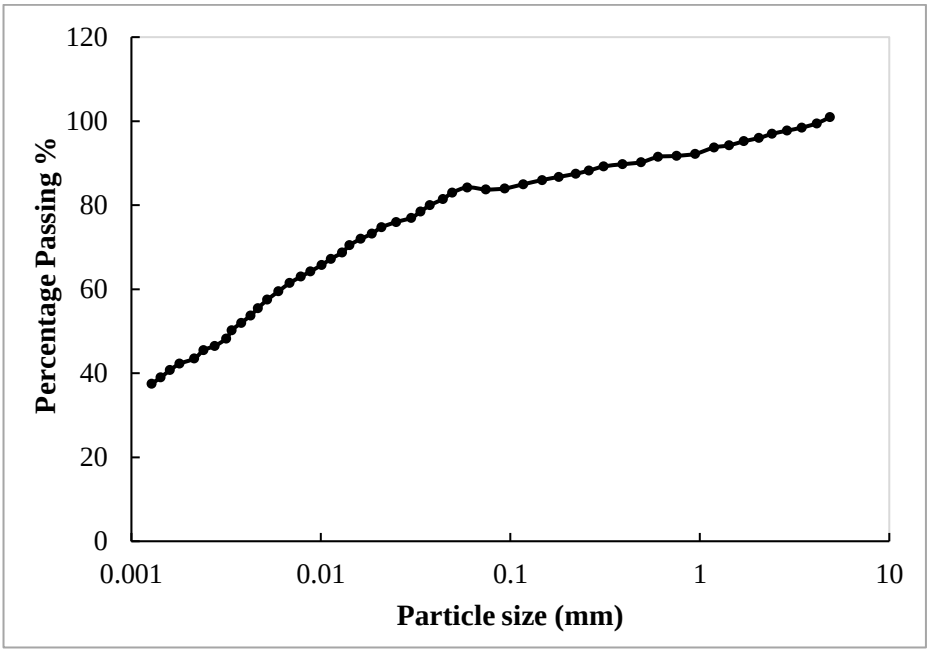

Figure 3.2 Soil grain size distribution (clay).

3.3 Geopolymer Binder Preparation

In this research, mechanochemical activation was employed to improve the reactivity of a one-part geopolymer during ambient curing and as a substitute activation strategy for overcoming the challenges associated with conventional two-part geopolymers, which is shown in Figure 3.3. Therefore, this study adopted mechanochemically activated slag-based geopolymer (MSG) and conventionally activated slag-based geopolymer (CSG) to prepare geopolymer grout. Regarding CSG preparations, sodium hydroxide beads were calculated, weighed with 3.75 molarity, and dissolved in tap

water. An exothermic reaction occurred during the mixing time, and the liquid became very hot. For that reason, the liquid was stored at ambient temperature before it was used till the chemical equilibrium was gained; then, after the NaOH solution was cooled down, the sodium silicate was added. In general, the alkali activator liquid was prepared at least one day before mixing the CSG ingredients.

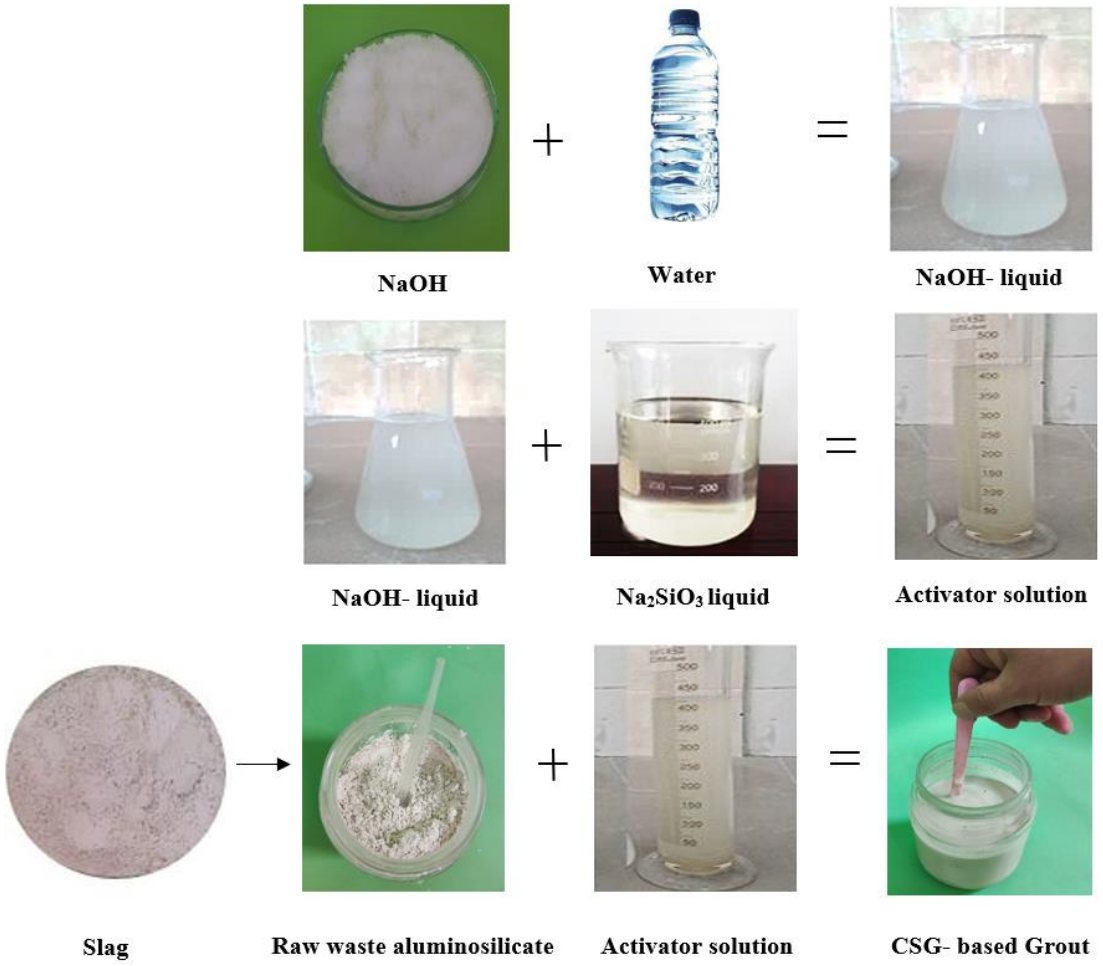

Figure 3.3 The production process of conventionally activated geopolymer grout.

For the preparation of MSG grout, all raw materials, such as chemical material (NaOH, Na_2SiO_3) and alumina-silica precursor (slag, GP or RHA), were grinded for 2 hours using a ball mill of 80 kg capacity using 12 balls, each with a mass of 400 g and a diameter of 45 mm. Through the ball milling process (grinding), the components (particles) of mixed raw materials are trapped between the balls and the container wall which was caused by the continuous impact of the particles and grinding. After that,

the obtained MSG powder was mixed with faucet water to manufacture MSG grout, as shown in Figure 3.4.

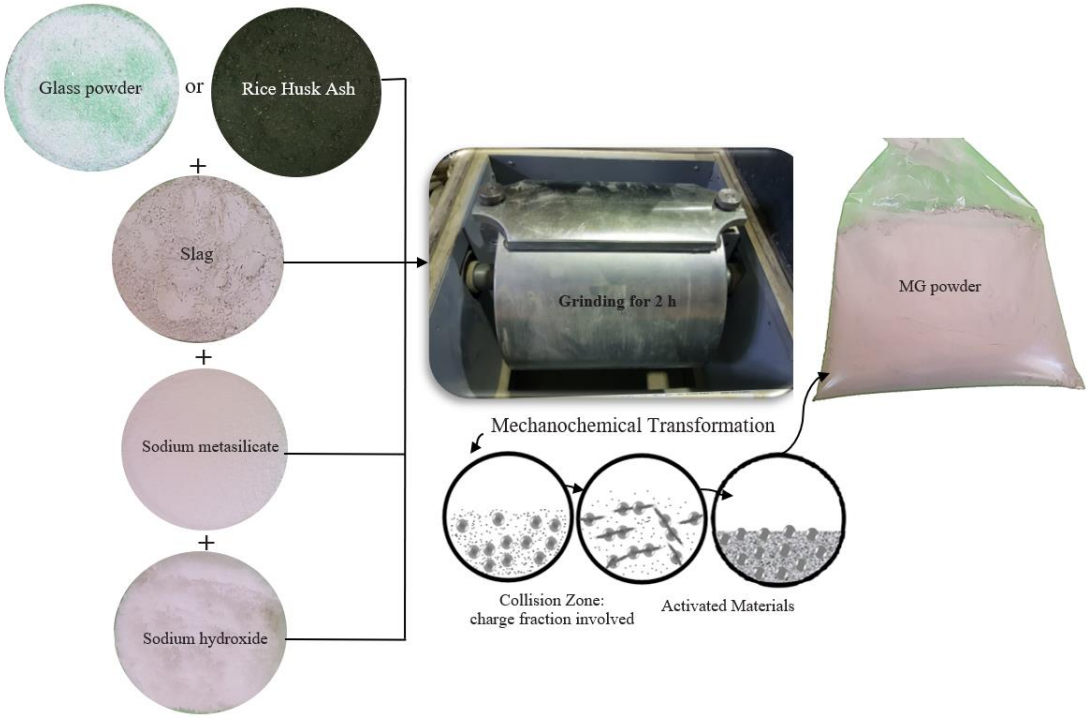

Figure 3.4 The production process of mechanochemically activated geopolymer powder

3.4 Specimens Preparation

All specimens for this research were prepared at ambient temperature (23±3°C and humidity of 50%±5) and in line with previous procedures (Güllü & Ali Agha, 2021; Hamid Abed, Sabbar Abbas, et al., 2022; Singhi et al., 2017) and standards (ASTM D4016- 14; ASTM D4320/D4320M-09).

In order to prepare all specimens for viscometer, fresh, and strength testing of geopolymer grout, the dry mixtures (stabilizer) were mixed for 1 minute at 100 rpm, and then the water (or alkali solution in the case of CSG grout) was added at a fixed temperature of 20 ± 3 °C and mixed at 150 rpm and for 2 minutes with 300 rpm. It should be noted that in preparing the soil-binder specimens for this experiment, the method employed was in accordance with previous efforts on deep mixing by Arulrajah et al. (2018), Canakci et al. (2018), Güllü et al. (2021) and Odeh & Al-Rkaby (2022). The mixing procedure was the same as preparing specimens for all the tests, as seen in Figure 3.5. First, the oven-dried soil and water were separately weighed and

mixed in a container to set the moisture content of the remoulded soil to 36% (LL-5); this moisture content was chosen to simulate soft soil. According to previous studies Bhadriraju et al. (2008), Güllü et al. (2017), and Pakbaz & Farzi (2015), deep mixing treatment is generally carried out on soils that have water content near the liquid limit. The remoulded soil was placed in the sealed bag for 24 hours to ensure sufficient interaction between the soil particles and moisture. According to previous research Chew et al. (2004) and (Arulrajah et al. (2018), the soil may be stabilized more efficiently when the dose of stabilization agent is 20–30% of the dry soil. Thus, 30% of the dry mass of the soil was allocated to the stabilizing agent. However, for the preparation of the mixture of the MSG-stabilized soil (mechanochemically activated geopolymer stabilized soil), MSG binder and water were mixed until a homogenous grout mixture was formed. Then, dry soil (clay) is mixed with water. The soil (clay+water) was then mixed with the grout mixture (Figure 3.5). Likewise, CSG grout is substituted for MSG-based grout in the preparation of CSG-stabilized soil. Meanwhile, the remolded soil and geopolymer (MSG and CSG) slurry were mixed by the mixer at 240 rpm speed for 3 min and stirred evenly to produce geopolymer-stabilized soil was then poured into cylindrical molds with a diameter of 50 mm and a height of 100 mm. Three parallel specimens were prepared for each group in order to minimize the possibility of mistakes during the experiment. The stabilized soil was vibrated after each filling for 10–20 seconds to remove any air bubbles that may have occurred during the specimen preparation procedure. Then, the geopolymer-stabilized soil specimens were cured (23 ± 3°C) in well-closed plastic bags until the target time (Figure 3.6).

Figure 3.5 Mixing procedure to preparation DSM specimen.

Figure 3.6 Geopolymer-stabilized soil samples.

3.5 Testing Methods

The experimental program of this research. Involves two primary efforts: i) investigate the characteristics and properties of geopolymer grout by performing experiments on rheological flow curves (i.e., viscosity versus shear rate curves and shear stress versus shear rate curves) and rheological parameters (i.e., yield stress, and plastic viscosity), fresh states (setting time, bleeding capacity), mechanical properties (compressive strength, ultrasonic pulse velocity), and microstructural behaviors (SEM and XRD and FITR analysis). ii) Assessing the strength performance and durability properties of deep soil mixing by testing the visual appearance, mass changes, and mechanical properties (UCS and UPV tests). Furthermore, SEM and FITR analysis describe microstructural behaviors of best-performed geopolymer silcrete specimens.

3.5.1 Rheological (Viscometer Test)

The viscometer (rheometer) test was conducted to determine the rheological properties of the geopolymer grout mixtures. This test was conducted using a ProRheo R180 Instrument (Coaxial rotating cylinder rheometer) from Germany, as shown in Figure 3.7. The rheological measurements were obtained under standard ambient conditions of temperature (23 ± 3 °C) and relative humidity (50 ± 5%), as recommended by Fluids, (2003). The test measures the shear stress and shear rate of the grout mixture, which helps to understand its rheological behavior and how it will flow and perform during application. The results of the rheometer test can be used to optimize the grout mixture for different applications, such as injection into joints or filling of voids in soil

or rock. To ensure a consistent and homogeneous grout mix, the rheological properties of the geopolymer grout mix were evaluated using the same procedure for all experiments (mixing speed, mixing, temperature).

Figure 3.7 Coaxial rotating cylinder Rheometer.

All geopolymer grout mixes evaluated by the rheometer were prepared for 300 gr by weight, then mixed at 150 rpm for 1 minute and 300 rpm for 2 minutes to achieve homogenous grout before testing. The grout mixture was then placed in the testing cup for viscometer (rheometer) testing to determine its shear stress and shear rate curve, from which the (plastic viscosity and yield stress) can be calculated. However, based on the viscometer trials, it was discovered that the grout mixtures were unable to present flow curves with shear rates less than 500 s^{-1}; thus, the shear rates applied in this research to calculate shear stress and apparent viscosity were 500 s^{-1}, 571.43 s^{-1}, 642.86 s^{-1}, 714.29 s^{-1}, 785.71 s^{-1}, 857.14 s^{-1}, 928.57 s^{-1}, and 1000 s^{-1}. (Figure 3.8)**.** The shear rate was maintained constant for a duration of 15 seconds to achieve an equilibrium state in a total of 2 min. The apparent viscosity and shear stress vs the shear rate depicted by the flow curves were determined for both segments (ascending

and descending); however, only the data acquired by the ascending portion were used in this study, as a similar procedure was followed in earlier work (Güllü et al., 2019; Güllü & Ali Agha, 2021; Park et al., 2005; Şahmaran, 2008; Widjaja & Lee, 2013; Ammar Yahia & Khayat, 2001). In nonlinear responses for the rheological curves, the dilatant (shear-thickening) performance occurs when both shear rate and viscosity increase, as presented in Figure 3.9. Nevertheless, the viscosity decreases with the increasing shear rate in a negative gradient, and the flow leads to a pseudoplastic (shear-thinning) performance (Ammar Yahia & Khayat, 2001).

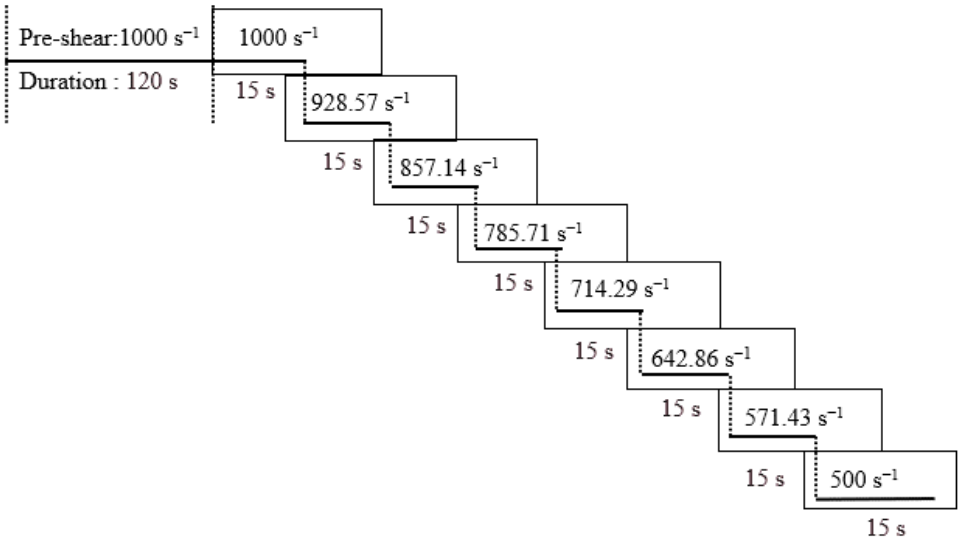

Figure 3.8 The shear rate protocol was used to draw the flow curves.

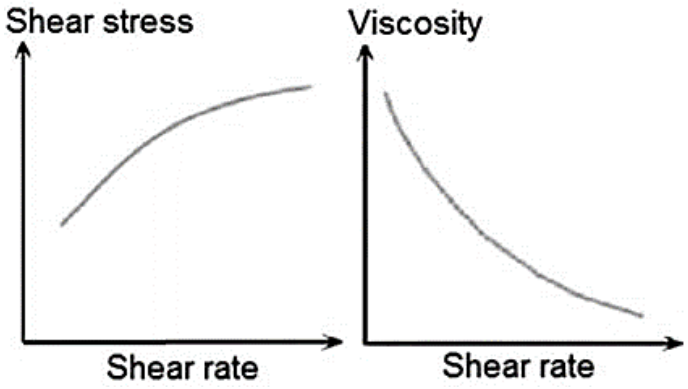

(a) Pseudoplastic (shear-thinning)

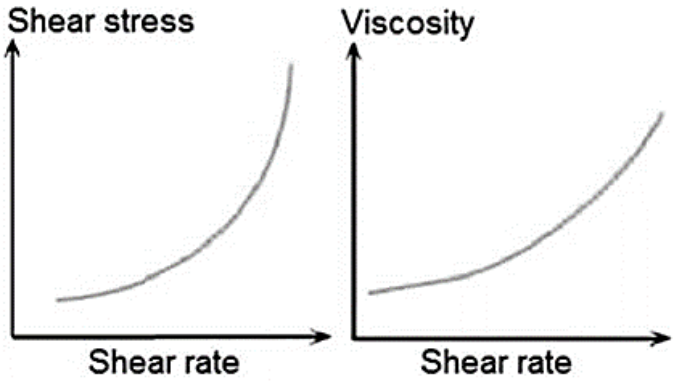

(b) Dilatant (shear-thickening)

Figure 3.9 Typical rheological behaviour (Kazemian et al., 2012).

The yield stress is related to cohesion in soil or slump in concrete corresponds to the least shear stress to create the flow grout, while the plastic viscosity can be related to stickiness, pumpability, finishability, placeability, and segregation (Park et al., 2005; A Yahia et al., 2016). In this study, a modified Bingham model has been adopted by the previous studies (Şahmaran, 2008; A Yahia et al., 2016; Ammar Yahia & Khayat, 2001), and the plastic viscosity and yield stress were obtained by Eq.(3.1)

$$\tau = \tau_0 + \mu_p \dot{\gamma} + c\dot{\gamma}^2 \quad (3.1)$$

Where τ_0 is the yield stress (Pa), τ is stress (Pa), $\dot{\gamma}$ is the shear rate (s^{-1}), μ_p is the plastic viscosity (Pa.s), and c is a constant). The nonlinear behavior of fluids, including shear thickening, shear thinning, and the Bingham model, can be characterized by the

ratio of the second-order term to the linear term (c/μ_p). Specifically, $c/\mu_p > 0$, $c/\mu_p < 0$, and $c/\mu_p = 0$ indicate the occurrence of shear thickening, shear thinning, and the Bingham model, respectively (Güneyisi et al., 2016).

3.5.2 Bleeding (Stability)

Bleeding can be a problem in grouting applications because it can reduce the effectiveness of the grout in achieving its intended purpose. When bleeding occurs, the water in the grout separates from the solid particles and can enter the surrounding ground, leading to a non-homogeneous quality of grouting. This can be particularly problematic in ground improvement applications, where the stratification of water and cementitious materials within the soil matrix or rock fractures can reduce the overall effectiveness of the grouting. Bleeding can also cause issues with the handling and transport of grout, as the loss of water can increase the viscosity of the grout and lead to problems with sedimentation in mixing tanks and pipes. To minimize bleeding in grouting applications, it is important to carefully control the water content and viscosity of the grout and to ensure that it is properly mixed and transported.(Khatami & O'Kelly, 2018).

The sedimentation ratio is an important parameter to consider when evaluating the stability of a suspension, as it can indicate the potential for separating the solid particles from the liquid phase. Suspensions with a high sedimentation ratio may be prone to settling and separation, which can affect the flow properties of the grout and potentially cause clogging of injection equipment or pipes. It is important to ensure that the suspension remains stable during handling and application in order to maintain the desired properties of the grout and achieve the intended geotechnical benefits. Factors that can influence the sedimentation ratio include the size and shape of the solid particles, the concentration of the solid phase, and the viscosity of the liquid phase.

The bleeding capacity was determined in accordance with (ASTM:C940-10a, 2010); a 1000 mL graduated cylinder was utilized for the grout mixture (Figure 3.10), and the fresh grout was allowed to settle in the cylinder for two hours to complete the sedimentation of the mixture suspension. The stability of a suspension can be evaluated through the sedimentation ratio (dV/V), which is defined as the volume of

clear water (dV) separated on top of the suspension divided by the initial grout volume (V = 1000 ml). A sedimentation ratio not exceeding 5% after two hours has been classified as a "stable suspension" by Deere et al. (1982), while (Kutzner, 2020) has reported a sedimentation ratio of less than 10%. It should be noted that a high sedimentation ratio is typical of pure cement grouts and can have significant practical implications. If sedimentation of solids occurs during grouting, the voids being treated and the grouting pipelines may become obstructed, rendering the grout unable to flow any further.

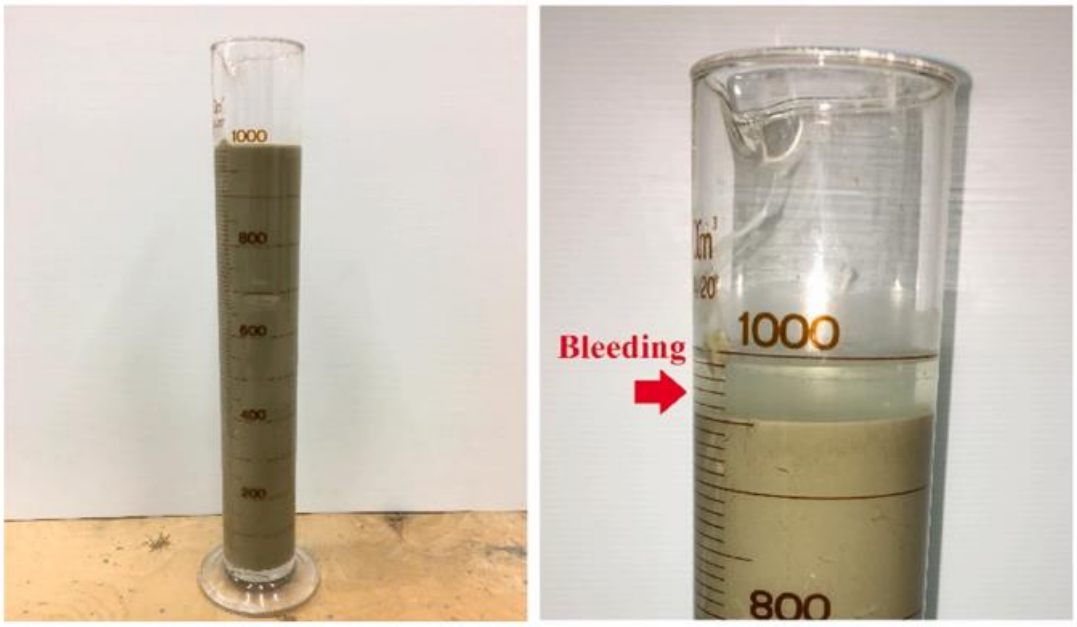

Figure 3.10 Bleeding test. Before to start the curing (on the left) and test ending (on the right). The arrow indicates the bleeding water.

3.5.3 Setting Time

The measurement of setting time was carried out through the Vicat needle test, as illustrated in Figure 3.11. American Society for Testing & Mater (1987) defines the initial setting time as the duration from the preparation of the grout when the penetration height of the Vicat needle in the specimen is 25 mm, while the final setting time is defined as the duration when the penetration height of the Vicat needle in the specimen is less than 1 mm. It is worth mentioning that the bleeding water was eliminated, and the mould was filled with grout after the cessation of bleeding.

Figure 3.11 Vicat Apparatus Test.

3.5.4 Unconfined Compressive Strength

Unconfined compressive strength tests were accomplished according to (ASTM C942-15; ASTM D2938-95; ASTM, 2009a; D. ASTM, 2006). the fresh grout was cast into cylindrical moulds with a height of 100 mm and a diameter of 50 mm. The geopolymer mixtures were poured into the sealed moulds, which were sealed with plastic membranes. The grout specimens were kept at room temperature for 7 days and 28 days. The UCS tests were conducted on the specimens by applying a uniaxial load under displacement control at a 1 mm/min rate, as depicted in Figure 3.12. The peak axial stress observed at the point of failure was considered as the UCS value for the respective specimen.

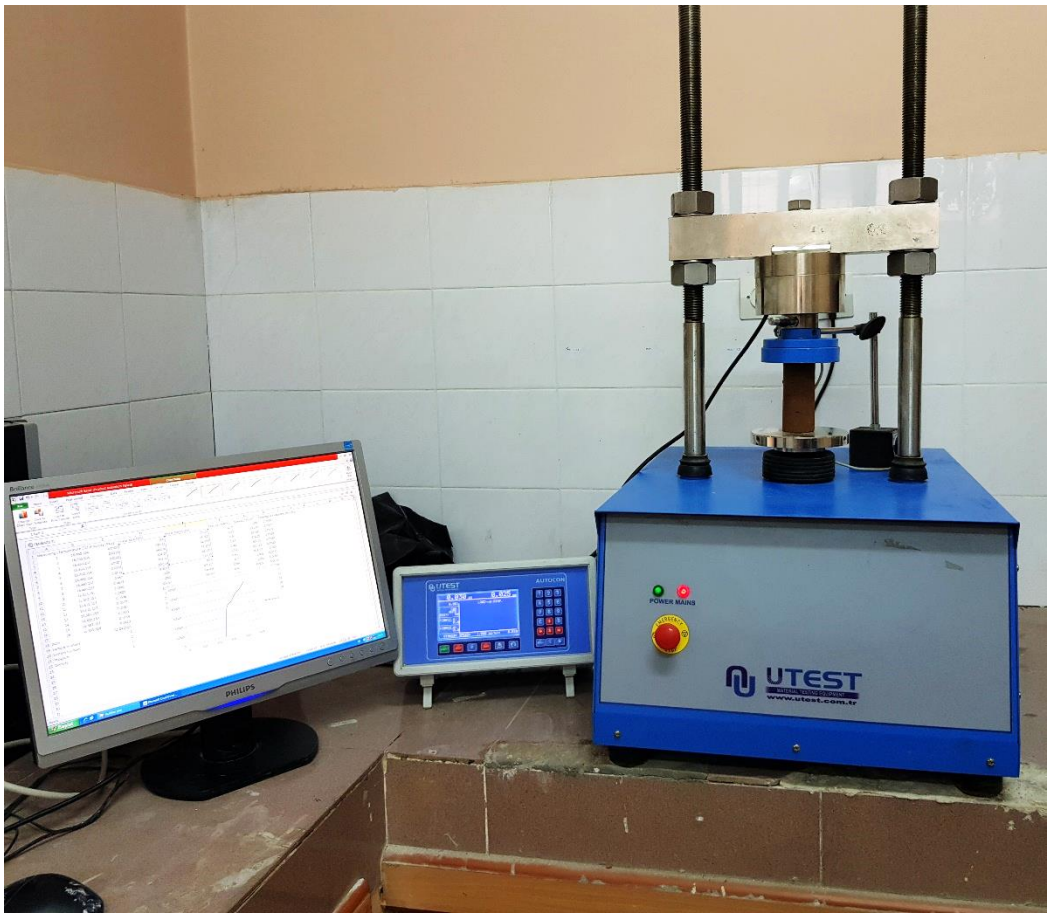

Figure 3.12 The Uni-axial unconfined compressive strength test machine.

The deep soil mixing strength test was conducted using specimens and moulding processes similar to those used for grouting. The grout mixture, with a water-to-binder ratio of 1 (equivalent to 2.5 molarity), and soil (clay) at the optimal moisture content of LL-5 were mixed at a binder-to-soil ratio of 30% to produce soil-binder (DSM) specimens. These specimens were cured for 28, 60, and 120 days in well-sealed plastic bags at 23 °C ± 3 before UCS testing. The UCS tests were conducted according to ASTM D5102-09, with a similar loading rate and UCS estimation as for the grouting specimens. To better understand the effectiveness of deep mixing, the UCS ranges of the improved soil based on soil type and binder quantity are presented in Figure 3.13.

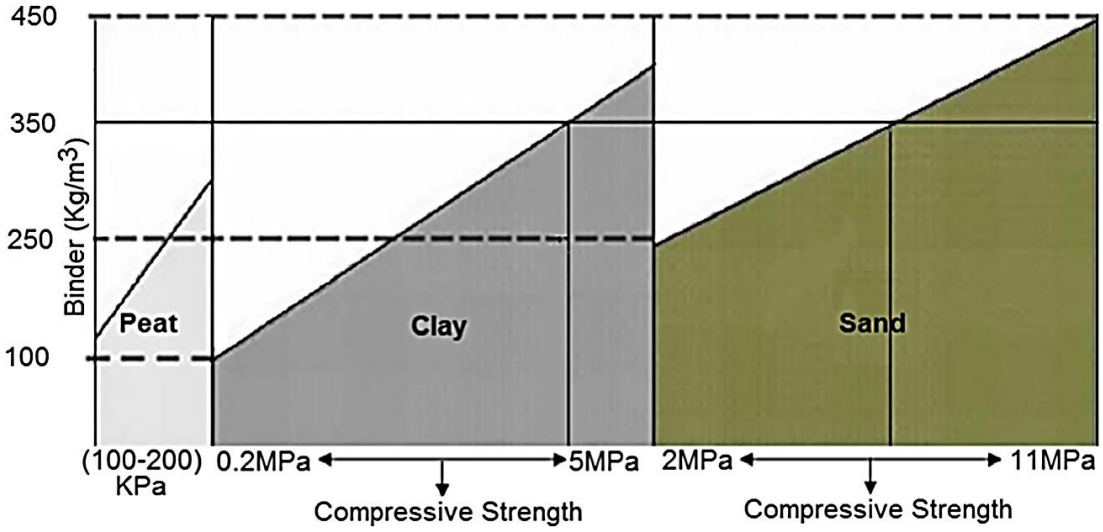

Figure 3.13 Some ranges of the strength of enhanced ground dependent upon the binder dosage (Abbey et al., 2015; Kitazume & Terashi, 2013).

3.5.5 Ultrasonic Pulse Velocity (UPV)

Ultrasonic pulse velocity (UPV) is a non-destructive test method that can reveal the strength performance of hardened samples and may also be used to evaluate the specimens' dynamic characteristics (Anon, 1979). Moreover, the UPV values assist in indicating the stiffness performances of samples of various qualities. UPV testing was performed for the grouting and DSM specimens just before UCS testing in accordance with ASTM C597–09 (C. ASTM, 2009). In this research, all samples (UCS, UPV) were tested by at least three replicates, and the average of their results was utilized to determine their performance. It is important to note that the homogeneity of the grout mixture can significantly influence the resulting UPV values, which are often correlated with the strength characteristics of the cured specimens. A more uniform and homogeneous grout mixture typically results in faster velocities and better overall strength enhancement. The UPV test procedure involves leveling both surfaces (bottom and top) of the hardened samples to ensure efficient wave transmission between the samples and the transducer (Figure 3.14). A thin gel layer is coated on the transducer's surface to measure samples' pulse wave velocity precisely. The reference bar is utilized to validate the precision of the UPV equipment. Then, the longitudinal vibrations pulse is applied to the surface of the specimens, and the pulse velocity is measured after it has travelled through the samples. The pulse is captured and

converted to energy, and the pulse velocity (m/s) is determined. The magnitude of the measurements can be interpreted using classifications provided in previous studies Anon (1979) (Table 3.8).

Table 3.8 UPV Classification (Anon, 1979).

Class	Definition	UPV (m/s)
1	Very high velocity	>5000
2	High velocity	5000-4000
3	Middle velocity	4000–3500
4	Low velocity	3500–2500
5	Very low velocity	<2500

Figure 3.14 Ultrasonic pulse velocity test instrument.

3.5.6 Microstructural Analysis

A scanning electron microscope (SEM) inspection was also performed on the raw materials, the geopolymer precursors produced due to the mechanochemical grinding process, the hardened geopolymer grout, and DSM samples utilizing a ZEISS Gemini SEM 300 (Figure 3.15). X-ray diffraction (XRD) was applied to qualitatively evaluate the crystalline structure of the geopolymeric powder before and after the mechanochemical activation procedure. A Fourier transform infrared (FTIR) study was performed between 450 and 2000 cm^{-1} to identify chemical bonds in the hardened geopolymer grout and DSM samples.

Figure 3.15 SEM device used in this study.

3.5.7 Durability Properties

The durability properties of the DSM samples exposed to chemical attacks followed as reported by Kamon et al. (1993). However, no specific test method exists to evaluate the durability of DSM exposed to chemical attack. In this study, magnesium sulfate ($MgSO_4$) with a concentration of 1% by weight was prepared, and the specimens were fully soaked in the chemical solution for 120 days (after 28 days of curing at room temperature). Prior to chemical exposure, the samples were submerged in water for 24 hours and then dried at 23 °C for 2 hours to measure their initial weight. Every 15 days during the exposure period, samples were collected from the magnesium sulfate solution tank and washed with water to eliminate any chemical reaction products that remained on the exposed samples' surface. The stabilized soil specimens were then dried for 2 hours at 23 ºC before being weighed. The magnesium sulfate is replenished every 15 days in all cases. Various tests, including visual inspection, mass change, UCS, and UPV loss, were conducted at regular intervals throughout the duration of exposure to determine the impact of a chemical solution on geopolymer-stabilized soil samples. The mass change was calculated in order to evaluate the deterioration of the specimens induced by the formation of a new phase after chemical exposure. The change in mass was estimated by calculating the change in mass of DSM samples evaluated before and after the chemical attack using according to equation (3.2) (Zhigang Zhang et al., 2020).

$$Mass\ loss(\%) = \frac{m_{0-}m_1}{m_0}100 \qquad (3.2)$$

Where m_0 and m_1 are the initial and final weight of DSM specimens before and after exposed to chemical environment, respectively. Before conducting strength tests, stabilized soil specimens were visually inspected for symptoms of deterioration, such as cracking, spalling, and delamination.

CHAPTER IV

DEVELOPMENT AND CHARACTERIZATION OF ECO- AND USER-FRIENDLY GROUT PRODUCTION VIA MECHANOCHEMICAL ACTIVATION OF SLAG/RICE HUSK ASH GEOPOLYMER

4.1 Overview

This chapter aimed to explore the potential of mechanochemical activation as an alternative activation technique to address the challenges associated with conventional two-part geopolymers and enhance the reactivity of a one-part geopolymer during ambient curing. The solid-state mechanochemical grinding of raw materials with varying compositions resulted in the synthesis of readily available geopolymeric precursors, which, upon the addition of water, facilitated the development of eco- and user-friendly geopolymer grout. Additionally, conventionally activated geopolymer grout and ordinary Portland cement (OPC) grout were analyzed for comparative purposes. The study investigated four rice husk ash (RHA) replacement ratios (0%, 10%, 20%, and 30% by the total precursor weight) to assess the feasibility of using RHA as a partial precursor in mechanochemically activated slag-based geopolymer (MSG) grout. A comprehensive range of tests were conducted, including rheological analysis (flow curve response, yield stress, and plastic viscosity), fresh properties (setting time and bleeding capacity), mechanical characteristics (unconfined compressive strength and ultrasonic pulse velocity), and microstructure examination (scanning electronic microscopy and X-ray Diffraction). Table 4.1 presents all the mixture proportions of both CSG and MSG grouts.

Table 4.1 Mix proportions of OPC, CSG and MSG-based grout.

		Weight %						
Molarity	Mix ID	Slag	RHA	NaOH	Na_2SiO_3	OPC	Grinding duration: h	w/b
3.75	MSG	85	0	10	5	-	2	0.75
	MSG-RH10	75	10	10	5	-	2	0.75
	MSG-RH20	65	20	10	5	-	2	0.75
	MSG-RH30	55	30	10	5	-	2	0.75
3.75	CSG	85	0	10	5	-	-	0.75
-	OPC	-	-	-	-	100	-	0.75

4.2 Analysis of Microstructure

The particle size is considered the primary factor controlling rheological and mechanical characteristics variance. The particle size distribution of RHA and slag before and after mechanochemical activation is shown in Figure 4.1. The d50 (mean size) of raw RHA and slag was 34 μm and 22 μm, respectively, whereas the mean size of RHA and slag diminished to 23 μm and 15 μm, respectively, after 2 h of grinding in a ball mill with sodium hydroxide and sodium metasilicate.

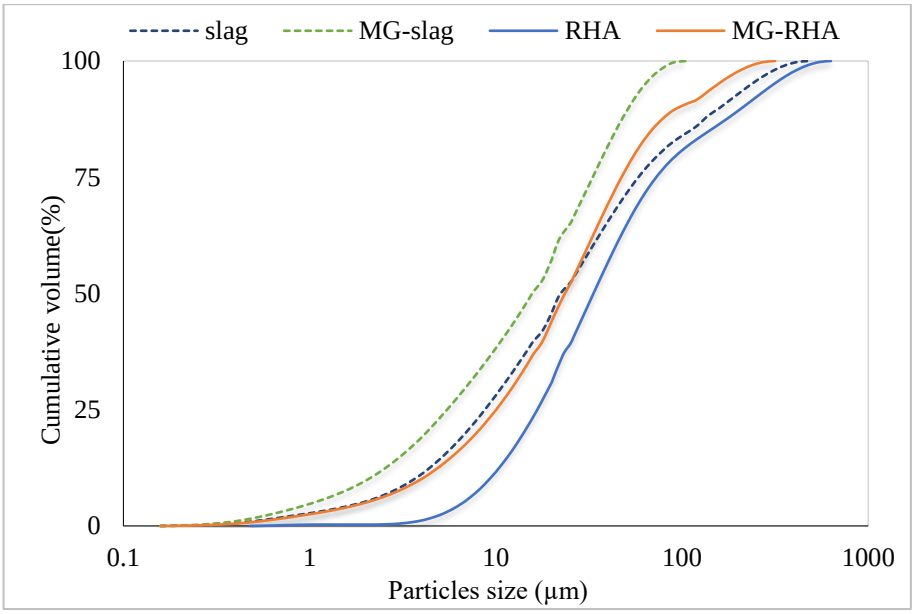

Figure 4.1 Particle size distribution of RHA and slag before and after mechanochemical activation.

Scanning electron microscopy analysis (SEM) shows the microstructural approximation of slag and RHA precursors before and after mechanochemical activation. As shown in Figure 4.2a, the raw slag particles are non-uniform and heterogeneous, with sub-rounded to angular forms for the material components. The roughness and edges were observed in both the angular and bulk particles (Baalamurugan et al., 2021). As shown in Figure 4.2b, most raw RHA particles have an irregular shape, are amorphous, and have high porosity.

Figures. 4.2c and 4.2d show the microstructural analysis of the mechanochemical activation of slag and RHA precursors obtained after 2h of co-grinding in the presence of chemical powder (NaOH and sodium metasilicate). After co-grinding, the slag and RHA particles were coated with solid chemical powder (NaOH and Na_2SiO_3), which also reduced the average size of the precursors and solid chemicals. Nonetheless, after mechanochemical grinding, the slag and RHA particles still develop angular and slightly deformed shapes. Furthermore, the surface area of the particles clearly increased during mechanochemical activation and resulted in a higher reaction rate of the geopolymeric precursors. Additionally, initial bonding between the particles was observed (Figure 4.2d) due to the addition of NaOH and sodium metasilicate, which

might reflect the MSG powder's adhesive nature. However, the influence of ball milling of all raw materials resulted in increased amorphousness and formation of the geopolymeric precursor (Gupta, Bhardwaj, Mishra, Mudgal, et al., 2017). (Hamid Abed, Sabbar Abbas, et al., 2022) reported that grinding of fly ash and slag with NaOH and sodium metasilicate for 2 h resulted in the formation of cracks and defects, which augmented the surface roughness of the surface the particles and conferred increased reactivity to the geopolymeric precursors.

The XRD patterns have been adopted to assess the effect of co-grinding of geopolymeric precursors before and after mechanochemical activation, as presented in Figure 4.3. Before co-grinding, the raw slag-based geopolymer (SG) precursor has a vitreous structure with an amorphous nature as eminent from a hump around 28° – 33° (2θ value) with a peak position at 30°. Also, crystalline phases are represented by sharp peaks composed primarily of akermanite, gehlenite, calcium silicate, and merwinite, as seen by the steep peaks reported between $2\theta = 15°$ and $2\theta = 90°$ (Yusuf et al., 2014; Y. J. Zhang et al., 2008). After co-grinding, the peak intensity of the co-grinded MSG precursor is more attenuated than the raw SG precursor, implying that the crystalline phases of the slag have amorphized as a result of the mechanochemical grinding with NaOH and sodium metasilicate. The mechanochemical activation increased the disorder and surface area and stimulated the reaction between the raw powders (Gupta, Bhardwaj, Mishra, Mudgal, et al., 2017).

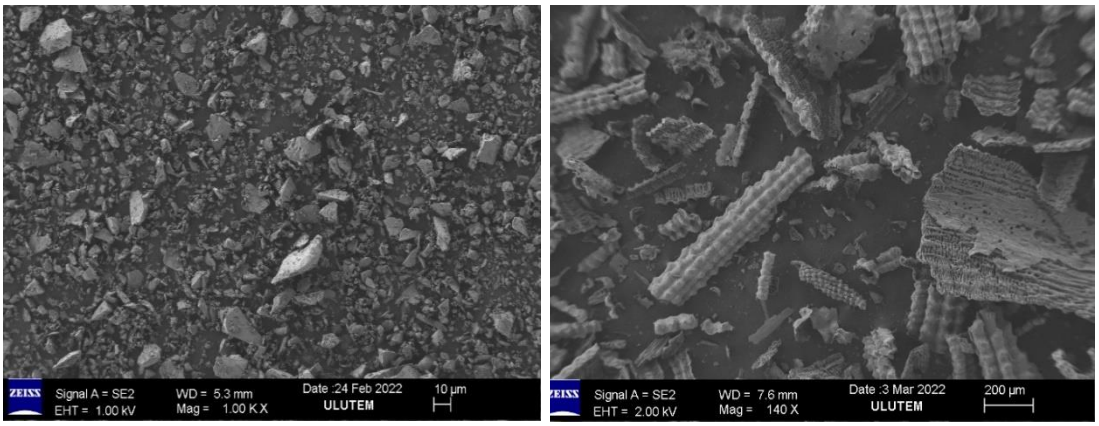

(a) raw slag (b) raw RHA

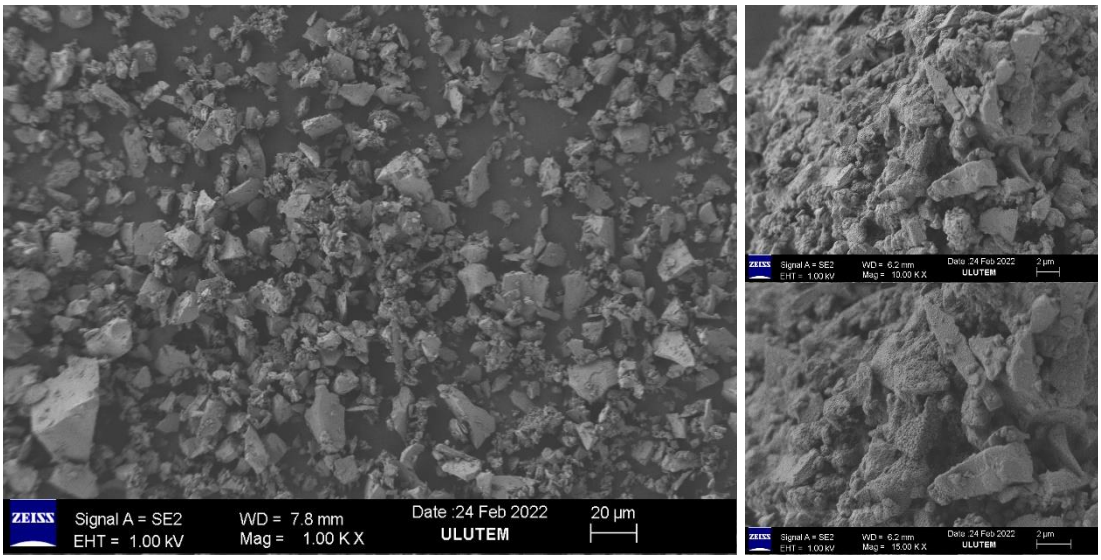

(c) slag- MSG

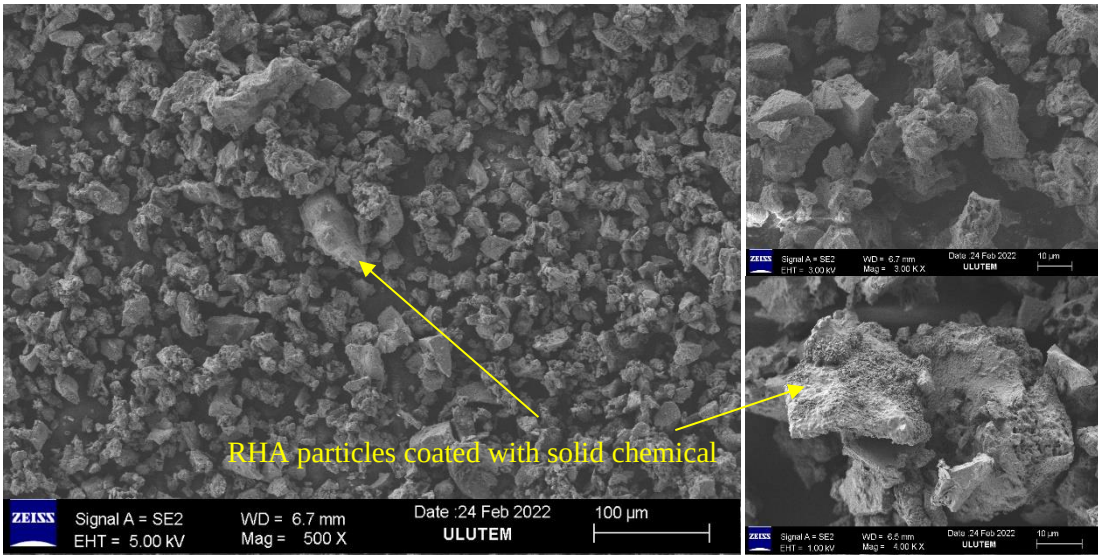

(d) RHA- MSG

Figure 4.2 SEM micrographs of (a) raw slag, (b) raw RHA, (c) slag -MSG, and (d) RHA- MSG.

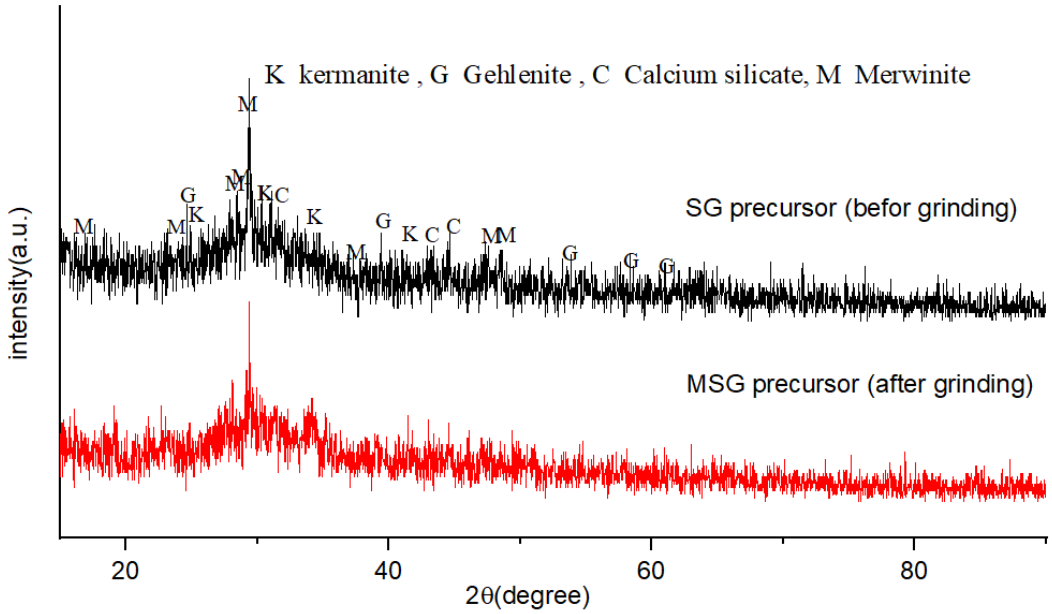

Figure 4.3 XRD patterns of geopolymeric precursors before and after mechanochemical activation.

4.3 Rheological Behavior and Responses

The flow curves of grout mixes are shown in Figure 4.4. Also, the dilatant index values (i.e. coefficient C) are summarized in Table 4.2. All the grout mixtures exhibited a shear thickening behavior (C > 0). In other words, apparent viscosity increased with the rise in the shear rate of grout.

The experimental results showed that the substitution of slag with RHA considerably affected the rheological behavior of MSG grout. As shown in Figure 4.4, the shear stress and apparent viscosity of MSG grout reduced as the RHA content increased. This behavior is most likely caused by the presence of active silicon oxide particles and the loose layer structure of RHA (Zhu, Liang, Zhang, et al., 2019). The SiO_2 particles were dissolved from the layered pore channels in RHA at the alkali activator environment, resulting in more SiO_2 micro-particles and empty pore channels emerging. The pore channels provided a space for the occupation and hydration of fine slag particles and the dissolved SiO_2 micro-particles acted as a filler for the whole pastes while participating in the reaction. The mutual-penetration effect sustained under the combined action of the pore channel and the secondary filling effect was the

primary cause for the refinement of pore structure, resulting in a decrease in cumulative pore volume in the geopolymer grout (S. S. Hossain et al., 2021; Zhu, Liang, Zhang, et al., 2019). As a result, a greater amount of water is available for lubrication, which reduces the viscosity of the MSG mix. Meanwhile, the addition of RHA dramatically affected the rheological behavior by increasing the SiO_2/Al_2O_3 ratio. According to Dadsetan et al. (2021), increased SiO_2/Al_2O_3 ratios led to a reduction in shear stress and apparent viscosity of geopolymer pastes. It might be due to the slower dissolution of Si and Al monomers at ambient temperature (Patel & Shah, 2018). Accordingly, Chouhan et al. (2018) used RHA to develop a novel superplasticizer to address the workability issue and reduce the viscosity of the geopolymeric binder.

In terms of geopolymer activation mechanism, the apparent viscosity and shear stress of CSG grout were higher than MSG grout; it can be concluded that CSG grout mixtures mostly appear to produce higher magnitudes of apparent viscosity and shear stress in comparison to MSG grout due to the high dissolution and ionization degree of MSG grout (D. W. Zhang et al., 2018). Hamid Abed, Sabbar Abbas, et al. (2022) obtained similar findings and reported that when mechanochemically activated geopolymer precursors were mixed with water, the mobility of ions and electrical conductivity of the mechanochemically activated geopolymer grout increased, leading to an increase in the degree of dissolution in the solution followed by a decrease in the solution's viscosity and degree of ion hydration. Also, the magnitudes of shear stress and apparent viscosity of the MSG grout were higher than those of the OPC grout, as illustrated in Figure 4.4. This could be due to the fact that the mechanochemical process alters the surface area and particle size of the powder; as a result, additional water is required to cover the surface of the particles, resulting in a notable reduction in the amount of excess water in fresh grout and an increase in responses (shear stress and apparent viscosity) (Marjanović et al., 2014).

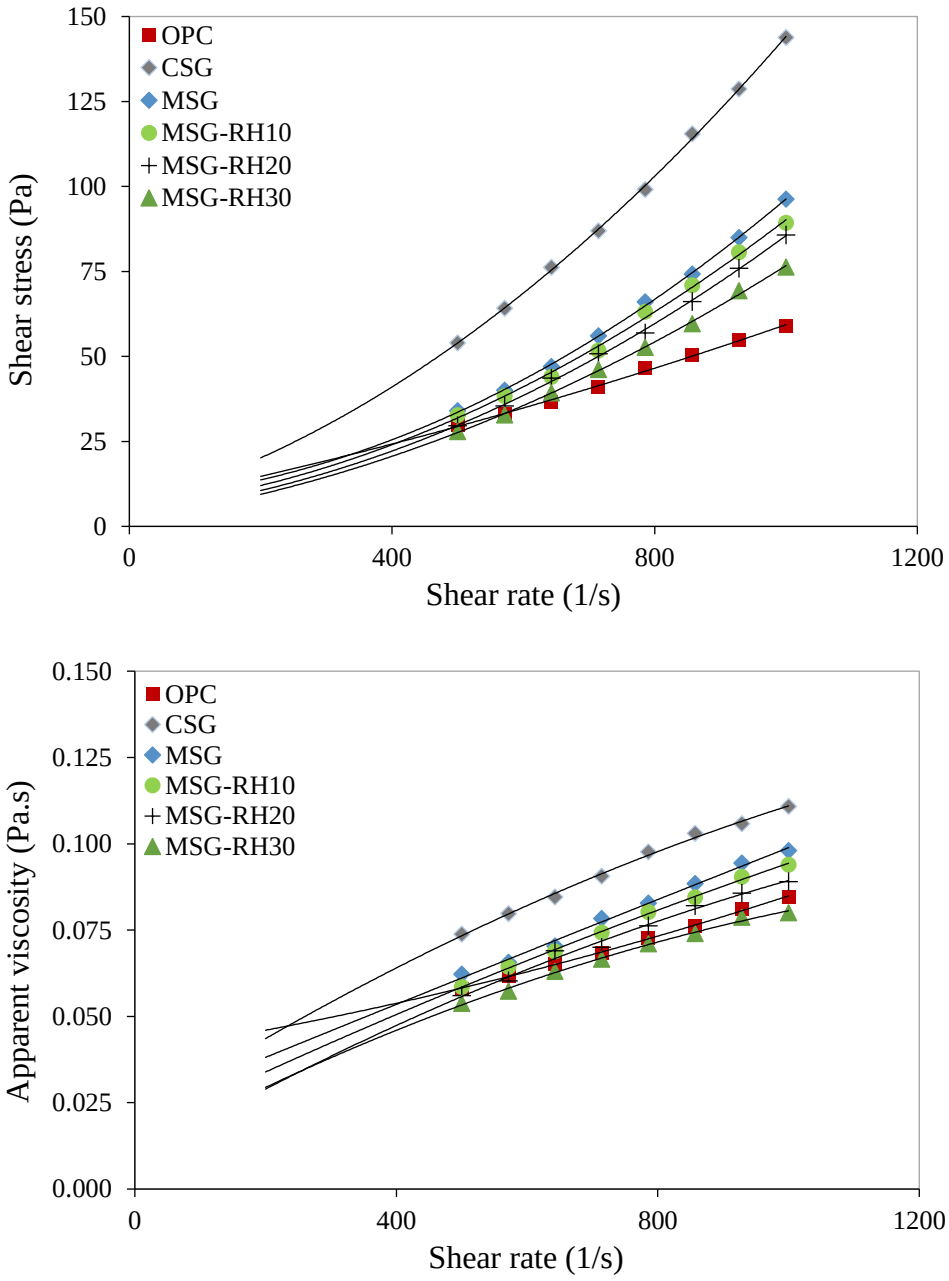

Figure 4.4 Shear stress and apparent viscosity versus shear rate curves of OPC, CSG, and MSG grout.

4.4 Yield Stress and Plastic Viscosity

The yield stress (YS) and plastic viscosity (PV) of grout types were estimated using the modified Bingham model during rheological experiments. The YS and PV of the MSG grout gradually decreased with increasing RHA content (Table 4.2). The results showed that mixtures with 100% slag (MSG) have higher YS and PV of 5.8 pa and

0.038 p.as, respectively (Figure 4.5). The high values of both YS and PV of MSG are attributable to the influence of particle shape and size, which control the rheological properties of the material (Bentz et al., 2012; Yang et al., 2018) as well as the accelerated chemical reaction caused by the high slag level, resulting in the creation of sodium aluminate -silicate-hydrate alongside calcium aluminate-silicate-hydrate gels at an early stage (Sanjay Kumar et al., 2010). Furthermore, the increased solidification rate could arise from the accelerated formation of specific reactions in the mixed materials due to the release of the Ca^{2+} ions from the slag reacting with silicates and aluminates (P. Nath & Sarker, 2014; Samantasinghar & Singh, 2019). Also, the incorporation of RHA into MSG grout dramatically alters the reaction products and physicochemical interactions. The YS of MSG-RH10, MSG-RH20, and MSG-RH30 grouts was reduced by 5%, 22%, and 38%, and the PV was reduced by 9%, 27%, and 41% when compared to MSG, respectively. The presence of RHA promotes the filling of micropores and the formation of more amorphous gel phases, resulting in a dense structure with a low water absorption value (S. S. Hossain et al., 2021). Consequently, more water is available for lubrication, which decreases the MSG mix's viscosity.

The results also demonstrated that the YS and PV of the OPC grout were higher than those of the MSG and CSG grout, as shown in Table 4.2. The YS and PV of MSG grout are 5.8 Pa and 0.038 Pa. s, respectively. In contrast, OPC grout has a YS and PV of 6.4 Pa and 0.06 Pa. s (Figure 4.5) because cement particles begin to dissolve and hydrate upon contact with water, creating positive and negative charges on the cement surface and inducing electrostatic attraction between the cement particles, which causes grouping or flocculation of the particles (Y. Zhang et al., 2018). In the synthetic pore solution (liquid phase of hydrating cement suspension), the hydration product ettringite was negatively charged, whereas the calcium silicate hydrates and tricalcium silicate were positively charged (Zingg et al., 2008). Liang, Li, et al. (2021) reported that part of the water is wrapped in cement particles; therefore, a decrease in the amount of free water would be observed, increasing the effective solids volume fraction. However, in the MSG grout, the silicate anions are absorbed on the surface of precursor particles like slag, generating negative charges on the particles' surfaces and resulting in electrostatic repulsion between them (Kashani et al., 2014). In other

words, it had a reduced effective solid volume fraction, which resulted in lower YS and PV.

From the perspective of the activation method, the MSG grout unveiled a lower YS and PV than the CSG grout (Table 4.2). The YS and PV of MSG grout are 4% and 27% less than the CSG grout. This could be because the alkali activator solution dissolves rapidly at an early stage when blended with the raw materials that are rich in alumina and silica to produce a conventional geopolymerization reaction, one which is significantly more viscous than the required water to form MSG grout, resulting in a greater YS and PV of the CSG grout (Hamid Abed, Sabbar Abbas, et al., 2022). It is well known that a suspension's viscosity increases in direct proportion to the viscosity of the suspending solution (Konijn et al., 2014). It can be concluded that the higher YS and PV values are disadvantageous for grout when used as a soil injection material, as the materials would be difficult to pump through the pipe if the slurry was overly viscous. Hence, MSG grout is more suitable for soil injection applications than CSG and OPC grout.

Table 4.2 Rheological characteristics of the grout.

Mix ID	coefficient C	YS(Pa)	PV (Pa. s)
MSG	0.00004	5.8	0.038
MSG-RH10	0.00004	5.54	0.035
MSG-RH20	0.00004	4.76	0.03
MSG-RH30	0.00004	4.2	0.027
CSG	0.00008	6.04	0.052
OPC	0.00003	6.4	0.06

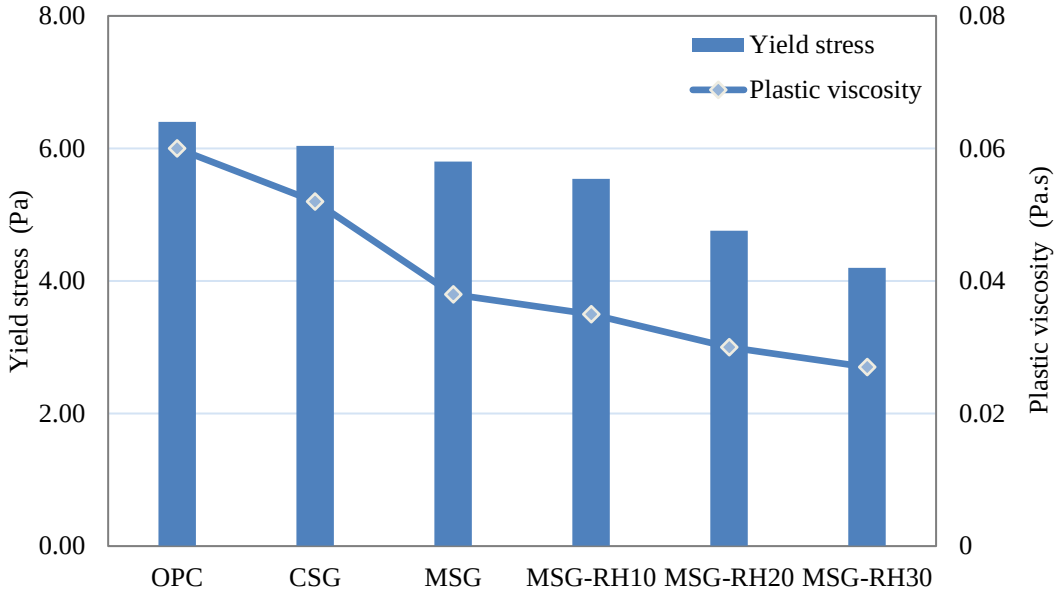

Figure 4.5 YS and PV of OPC, CSG, and MSG grout.

4.5 Fresh Properties

Grouting is one of the important civil engineering applications. The setting time is an essential factor for grouting applications, where a short setting time might cause damage to the grouting machine but a long setting time often leads to a slow construction schedule (Hamid Abed, Sabbar Abbas, et al., 2022). The effect of RHA content on the setting times of MSG grouts is depicted in Figure 4.6a. In general, the incorporation of RHA into the geopolymer composition prolonged the setting time. The initial setting time of MSG-RH10, MSG-RH20, and MSG-RH30 increased by 14%, 27%, and 44%, respectively. Similarly, the final setting time increased by 6%, 16%, and 42%, respectively, compared to the control mix (MSG). This is probably due to the combined effect of biogenic active silicon oxide particles and loose-layer structure of RHA; the dissolution of silicon oxide particles from the layer structure is slow, which delays the hydration of the geopolymer (Zhu, Liang, Zhang, et al., 2019). Furthermore, the rate of condensation between aluminosilicate species is faster than the condensation rate between silicate-silicate species (Chindaprasirt et al., 2012). Meanwhile, the inclusion of RHA increased the SiO_2/Al_2O_3 ratio, delaying the setting time. According to Billong et al. (2018), the RHA in pastes acted as a setting retarder due to the high SiO_2/Al_2O_3 ratio in the mixture, and this contributed to the inhibition of the geopolymerization reaction by the precipitation of Si-Al phases which prevented

contact between the reactive material and the activation solution. Liang, et al. (2021) observed that the addition of RHA to the metakaolin-based geopolymer significantly prolonged the setting time, but this effect was likely attributable to the increased time required for silicon oxide to dissolve from RHA.

On the other hand, the results demonstrated that the setting time of the MSG grout was shorter than that of the OPC and CSG grouts. The initial setting time of MSG, CSG, and OPC was 3.3h, 4h, and 8h, and the final setting time was 4.5h, 6.3h, and 12h, respectively, as seen in Figure 4.6a. The shorter setting time of MSG grout might be related to mechanochemical mechanisms that create electronic charges on the surface of mechanochemically activated particles, resulting in a rise in surface energy and the transition from the crystalline to amorphous phase (Hosseini et al., 2021). Furthermore, the mechanochemical process disintegrates large alumina and silica particles, increasing their surface area and resulting in a more uniform distribution of particles in the mixture, and this contributed to a higher proportion of additional aluminosilicate being formed from slag and RHA, allowing for participation and dissolution in the formation of geopolymer gels (Hamid Abed, Sabbar Abbas, et al., 2022; Marjanović et al., 2014). Thus, increased aluminosilicate availability accelerated the polymerization process, resulting in a shorter setting time for MSG grout (H. Li et al., 2014; Marjanović et al., 2014).

In addition, bleeding capacity testing was carried out in this work to assess the influence of RHA content on the stability of MSG grout, as shown in Figure 4.6b. The results revealed that the bleeding capacity of MSG grout rose along with the increase in RHA level; hence, it can be clearly observed that the mixes with 100% slag content had the lowest bleeding capability. For example, the bleeding capacity of MSG grout rises from 0.025% to 0.1% when RHA content is increased from 0 to 30%. Because of the high demand for water in the geopolymerization of slag particles (Liang, Zhu, Zhang, Wu, et al., 2019; Zhu, Liang, et al., 2021), dissolution heat flow climbed as slag amount increased since slag possesses a faster dissolution rate than RHA , leading to rapid growth synthesis of reaction products to create a rigid network (Abbas et al., 2022). The heightened bleeding capacity of geopolymer grout containing RHA can be attributed to its low water demand and its filling effect compared to slag. Furthermore,

the porous and reactive silica-containing RHA enhances ion transport mobility early on and precipitates the dissolving process of aluminosilicate precursors, leading to polycondensation reactions. The RHA contributes to the filling of micropores through its filling effect and imparts more amorphous gel phases, resulting in a dense structure and a lower water absorption value. The results also showed that the MSG grout (MSG) had significantly less bleeding capacity than the OPC and CSG grouts, as seen in Figure 4.6b. Due to the increased surface area and reduced particle size of the mechanochemically activated powder, additional water is required to cover the surfaces of the particles (Marjanović et al., 2014). Overall, the results of this research indicated that the bleeding of MSG and CSG grouts is more stable than OPC grout.

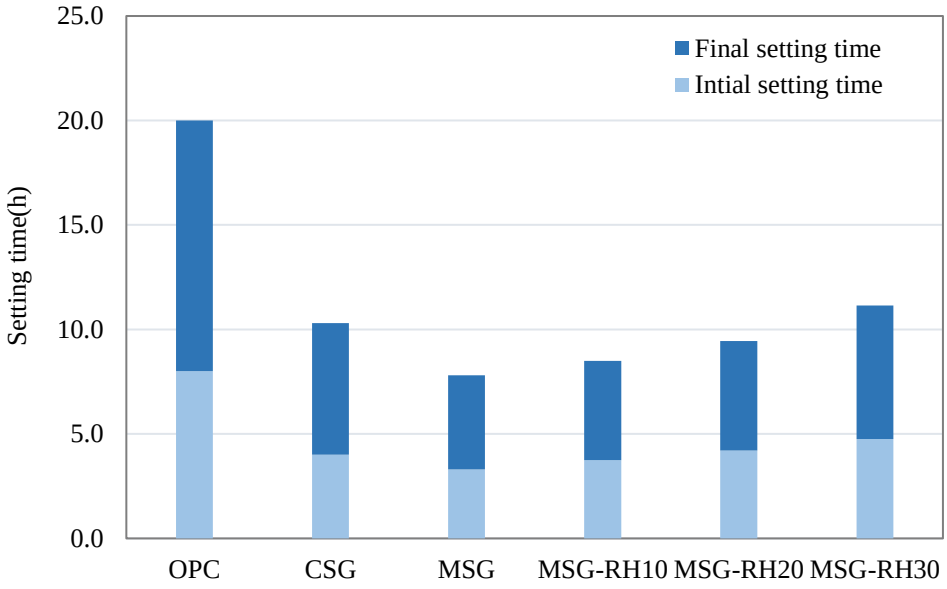

(a) Setting time

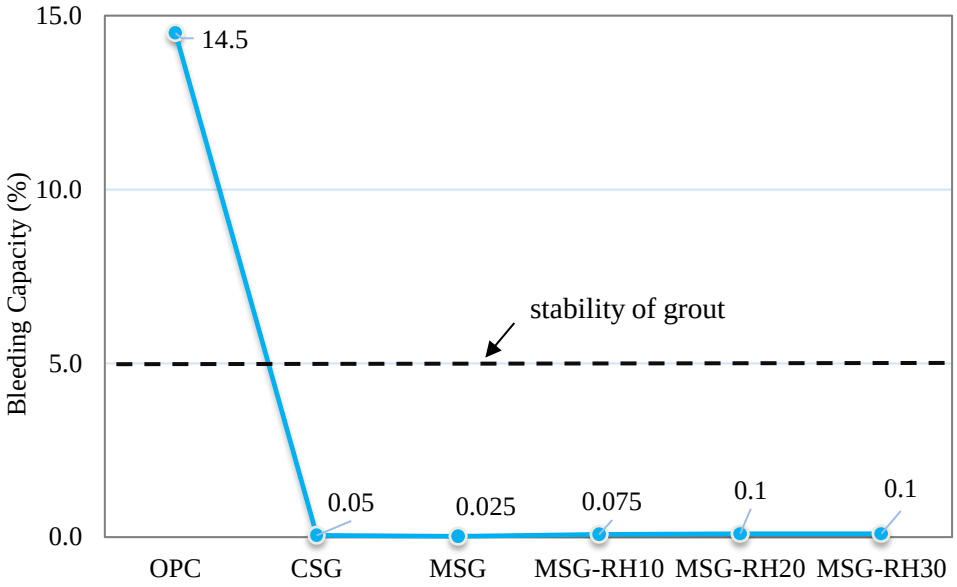

(b) Bleeding capacity

Figure 4.6 Fresh properties of MSG, CSG, and OPC grout.

4.6 Mechanical Properties

4.6.1 Unconfined Compressive Strength

The UCS results of mechanochemically activated slag-based geopolymer (MSG) grout incorporating RHA were obtained at 7 and 28 days, as shown in Figure 4.7. The UCS values of all studied mixtures improved as the age increased from 7 to 28 days due to the completion of the polymerization process and densification of the microstructure at longer ages (Athira et al., 2021; Liang, Zhu, Zhang, Wu, et al., 2019; Tho-In et al., 2016). On the other hand, the UCS results for MSG grout samples containing RHA revealed that the UCS rises in conjunction with curing time, and less cracks on the surface of the specimens were observed when compared to the MSG sample. However, the UCS test results of the MSG grout reduced with increasing RHA replacement content at 7 days then rises as RHA content expands at 28 days, as shown in Figure 4.7. For instance, at 7 days, the reductions of UCS were 4%, 12%, and 29% for the RHA contents of 10%, 20%, and 30%, respectively. Similar results were reported in previous research (Khan et al., 2021a; Tho-In et al., 2016). The increase in UCS of RH-MSG grout over time is related to the dissolution of a considerable amount of

silica from RHA in an alkaline environment (Fernández-Jiménez et al., 2017). From the perspective of geopolymers containing varying amounts of RHA, RHA contributed favorably to the development of strength. The UCS of MSG grout rose with increased partial replacement of slag with RHA up to 20% and declined beyond that. For instance, the addition of RHA as slag replacement at 10 and 20% elevated UCS values by 4.5% and 41%, respectively, compared to the control mix (MSG) at 28 days. The increased UCS with the addition of RHA is due to the relatively higher SiO_2/Al_2O_3 ratio, as well as the porous and reactive silica-containing RHA, which accelerates ion transport mobility and quickens the dissolution process of aluminosilicate precursors, resulting in polycondensation reactions and increased UCS of MSG grout (Kusbiantoro et al., 2012). The presence of RHA contributes to the filling of micropores through its filling effect and ascribes more amorphous gel phases, resulting in a dense and strengthened structure. Additionally, the RHA-active biogenic silica promotes the creation of additional calcium silicate hydrate phases in the calcium oxide-retaining geopolymer system, as RHA exhibits pozzolanic activity in the presence of Ca^{2+}ions (S. S. Hossain et al., 2021). Mehta & Siddique (2018) observed that compressive strength increased by RHA with slag substitution up to 15 wt%. It is attributed to the higher SiO_2/Al_2O_3 ratio and increased the system's reactivity, resulting in secondary calcium silicate hydrate production with sodium alumina-sulfate hydrate. However, the presence of excessive RHA (>30 wt %) decreased the UCS by 13% compared to a 20% RHA presence. The higher content of RHA leads to a high percentage of unreacted or partially reacted RHA particles in the geopolymer matrix in the course of which weaker and less ductile geopolymer gel is produced (Patel & Shah, 2018). The higher amount of SiO_2 delays the reaction of Si and Al ions and produces a lower density geopolymer binder resulting in lower compressive strength (Tho-In et al., 2016). Silva et al. (2007) reported that the Si/Al ratio had a substantial impact on the mechanical features of the geopolymer. After this, using a high Si/Al ratio, low-crosslinked aluminosilicate materials with reduced strengths were developed. Furthermore, (Kusbiantoro et al. (2012) reported that the difference in the degree of solubility between slag and RHA reduces the rate of dissolution and polycondensation of aluminosilicate compounds, hence the decrease in the strength at higher RHA content.

From the perspective of the activation method, the mechanochemical mechanism significantly impacted the strength performance of MSG grout specimens. The UCS values of CSG grout were lower than its counterpart MSG (Figure 4.7); the UCS was reduced by 18% compared to MSG due to the higher cracks observed at 28 days, as shown in Figure 4.8. Notably, the strength performance of the mixes containing 100% slag activated conventionally was reduced at a longer curing period. The UCS of the CSG grout sample was 8.7 MPa and 8 MPa at 7 days and 28 days, respectively. Moreover, the shape of the CSG grout sample at 28 days revealed apparent micro-cracks on the surface of the specimen, as seen in Figure 4.8. These cracks can be attributed to the fact that there is more apparent shrinkage after 28 days compared to days (Hamid Abed, Sabbar Abbas, et al., 2022; N. K. Lee & Lee, 2013). Additionally, mechanochemical activation presses increased the surface area and reaction rate of slag; as a result, an extra gel was generated as a consequence of the main reaction, which then accumulated and filled the pore system. The formation of a large proportion of gel in the geopolymer mixture improved the overall pore volume and porosity of the geopolymer grout, resulting in enhanced immobilization (Hamid Abed, Sabbar Abbas, et al., 2022). Similar MSG grout behaviour was reported reported in (Adesanya et al., 2020; Fernández-Jiménez et al., 2019; Hosseini et al., 2021). On the other hand, the results revealed that the USC of the OPC sample was a little higher than that of the MSG and CSG mixes due to the high shrinkage of slag and lower calcium content compared to OPC at 28 days. For example, the UCS of OPC is 1.4%, 19% higher than MSG and CSG, and 28% lower than MSG-RH20, respectively (Figure 4.7). It can be concluded that the UCS of MSG-RH20≥ OPC ≥ CSG grouts; therefore, the RHA can be effectively used in mechanochemical geopolymer grout up to 20% replacement.

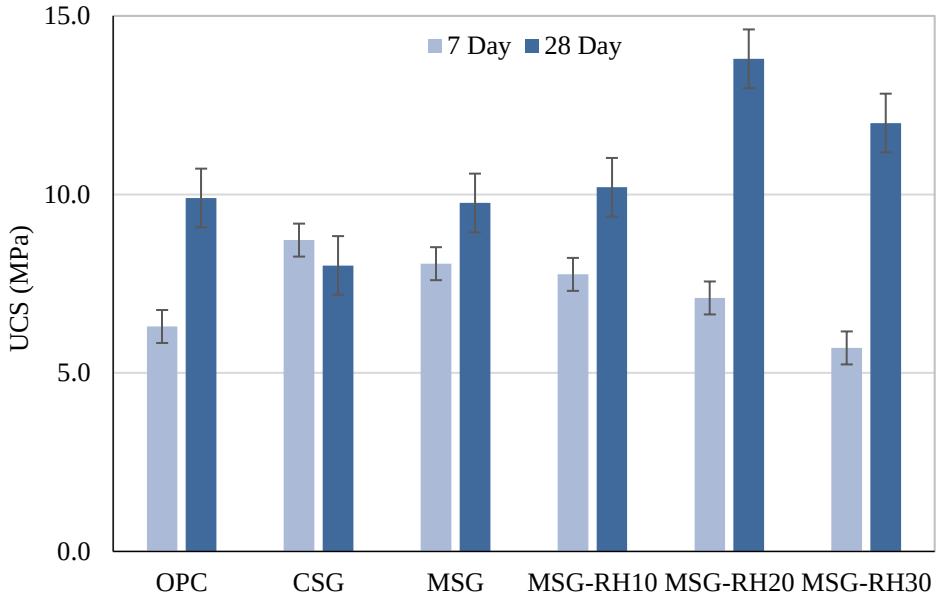

Figure 4.7 UCS of OPC, CSG, and MSG grout.

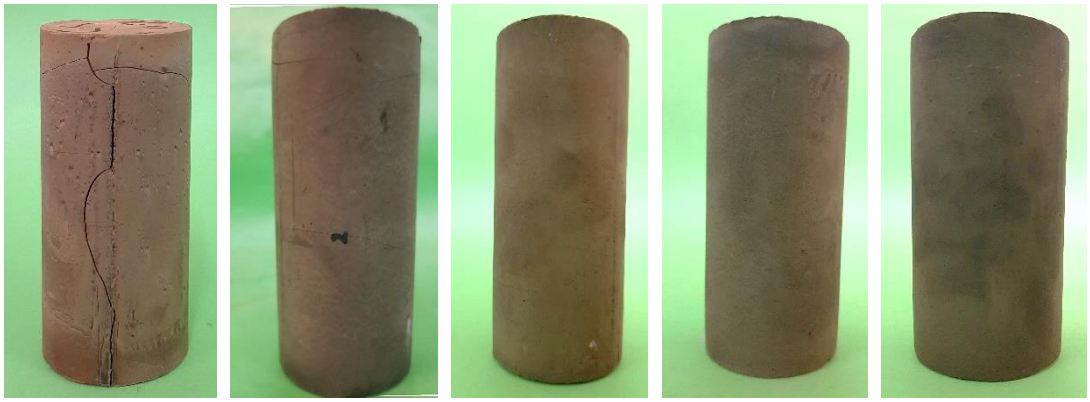

Figure 4.8 The visual appearance of CSG and MSG grout.

4.6.2 Ultrasonic Pulse Velocity and Bulk Density

Figure 4.9 presents the influence of RHA contents on ultrasonic pulse velocity (UPV) and bulk density tests of grouts. It can be seen from Figure 4.9 that the UPV values of MSG grout were enhanced significantly at curing ages of 7 and 28 days. Based on the UPV classification presented in Table 3.8, all obtained specimens' hardened states ranged from low velocity to very low velocity (Anon, 1979). It is obvious that specimens with varying levels of RHA incorporation enhance UPV after 28 days

compared to 7 days (Figure 4.9), owing to the combined strengthening effect of the bond reaction and the filling effect of the dissolved SiO_2 particles at later ages (Liang, Zhu, Zhang, Wu, et al., 2019).

The UPV of MSG grout increased with increasing partial substitution of slag with RHA up to 20 %, and declined thereafter (Figure 4.9). The UPV of the MSG grout improved by 3% and 7% when RHA content increased from 10% to 20%. The improvement in UPV performance can be ascribed to introducing more silicon ions into the aluminosilicate network produced by RHA (Samarakoon et al., 2020). Istuque et al. (2022) observed that the dissolution of RHA increased the strength and sustainability of alkali-activated mortars. Furthermore, an optimal balance between the filling effect and gel phase formation is achieved. It implies that the addition of RHA plays an important role in the refinement of pore structure. In the alkali activator environment, the silicon oxide particles were dissolved from the layered pore channels in RHA, resulting in additional silicon oxide micro-particles that acted as fillers for the whole pastes while participating in the reaction (Zhu, Liang, Zhang, et al., 2019).

However, the UPV of MSG-RH30 decreased by 1.5% when slag was replaced with 30% compared to the MSG-RH20 mix. This decrease is probably attributable to changes in elemental composition (Samarakoon et al., 2020). Based on the chemical composition of raw materials, the inclusion of RHA into a slag-based mechanochemical geopolymer increases the SiO_2 content while decreasing the Al_2O_3 and CaO content in the reaction systems. Chemical component variations in the initial systems will affect the hydrated products and thus the material characteristics (Xiao et al., 2021). Meanwhile, excessive RHA creates a looser structure resulting from incomplete chemical reactions, as well as an increase in the number of unreacted components in the system. This unfilled honeycomb hole produces a non-homogeneous microstructure, which increases water absorption (Zhu, Liang, Xu, et al., 2019).

Additionally, the results reveal that the activation mechanism of geopolymer grout significantly affected the UPV values (Figure 4.9). The UPV values of MSG samples were higher than those of CSG samples due to the fact that grinding the precursor increased the surface area and decreased the particle size of the slag and RHA particles,

hence reducing the porosity and raising the density of the geopolymer grout. In addition, the grinding process considerably expedited the polymerization process by generating extra aluminosilicate gel in the mixture, thereby increasing the density of MSG grout (Sanjay Kumar & Kumar, 2011).

A bulk density test was conducted for grout to validate ultrasonic pulse velocity results, as displayed in Figure 4.9. The bulk density follows a similar trend to the ultrasonic pulse velocity results regarding the RHA replacement. The highest bulk density of MSG grout was achieved at 20% RHA replacement among all MSG grouts after 28 days. In other words, the optimal replacement amount of slag by RHA was 20%, at which point the reaction extent of geopolymerization deepened, accompanied by a beneficial strength development and refinement of pore structure. However, it shows a slight decrease in bulk density values when the RHA addition dosage is increased to 30%. The decreased bulk density was primarily attributable to a reduced rate of aluminosilicate dissolution produced by the solubility difference between slag and RHA (Kusbiantoro et al., 2012). Furthermore, the higher concentration of unreactive silica due to increased slag replacement levels inhibited the polymerization process, resulting in reduced bulk density. As shown in Figure 4.9, mechanochemical activation of slag-based geopolymer grout altered the bulk density values. The results demonstrated that MSG samples were denser than CSG and OPC samples since the density of MSG samples was 3% and 2% higher than that of CSG and OPC, respectively. The high density of MSG specimens resulted from the ball-milling of slag/RHA and chemical precursors, which raised the surface area and reactivity of the geopolymeric precursors. The higher reactivity of the source materials resulted in the development of more gel as the principal reaction product, decreasing the porosity and increasing the density of MSG grout (Nikolić et al., 2014).

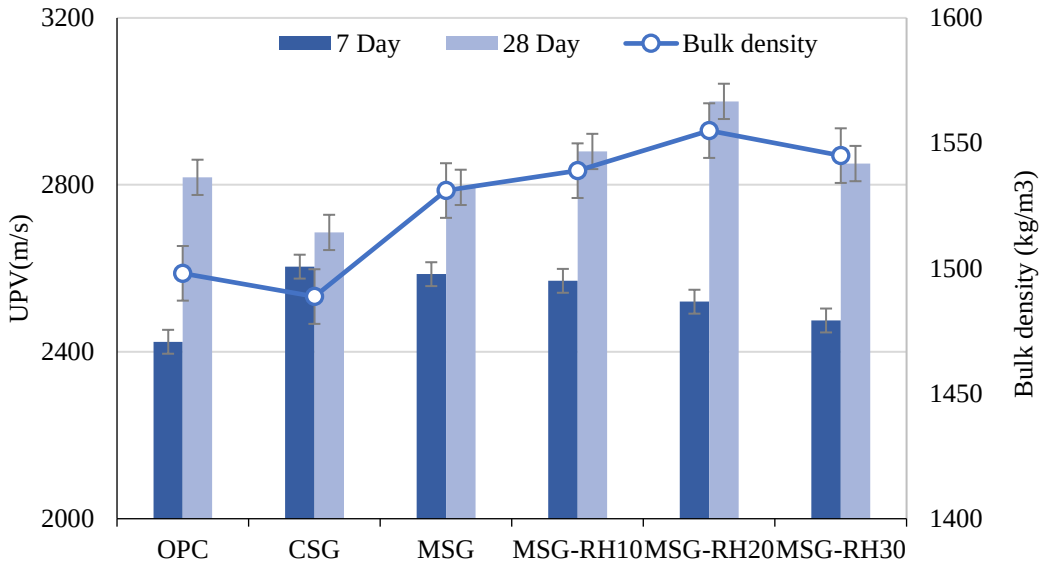

Figure. 4.9 UPV of OPC, CSG, and MSG grout.

4.7 Microstructural Analysis

XRD patterns were utilized to analyze the influence of the activation mechanism of geopolymer grout, as depicted in Figure 4.10. The XRD patterns of hardened CSG and MSG reveal the existence of the geopolymeric phases sodium aluminum silicate hydrate and sodium silicate hydrate in addition to the crystalline phase peaks observed in the raw powder (Gupta, Bhardwaj, Mishra, Mudgal, et al., 2017). These phases were much more intense in MSG than in CSG as a result of the mechanochemical grinding of slag and chemical powder. The (halo) amorphous phase and some sharp peaks of crystalline phases in the XRD traces indicated that both CSG and MSG were semi-crystalline with a substantial quantity of amorphous gel. This amorphous shape illustrates that the geopolymer contains a highly disordered glassy silicoaluminous phase.

Figure 11 shows the effect activation method on the microstructure characterization of MSG and CSG grouts. Notably, the activation method had a considerable effect on the microstructure of geopolymer grout. As seen in Figure 4.11a and b, many unreactive slag particles can be observed in CSG grout as compared to its counterpart MSG, which includes limited unreactive slag particles due to the beneficial effect of mechanochemically activated mechanism that increased surface area and reduced the particle size of slag, resulting in lower porosity and higher density in comparison with

CSG grout. Additionally, significant cracks can be seen in CSG grout (Figure 4.11a) because of the poor connectivity of the reaction products (Hamid Abed, Sabbar Abbas, et al., 2022). It can be concluded that the mechanochemically activated method is more beneficial than the conventionally activated method in densifying the compactness of grout's microstructure, and thus, the mechanical properties of MSG grout have been greatly enhanced. Furthermore, the geopolymerization reaction of MSG grout was dramatically enhanced during the grinding process due to the creation of additional aluminosilicate gel in the mix (Figure 4.11b); the produced gel has a more homogeneous microstructure which decreased the porosity and enhanced the reaction rate of slag particles.

Figure 4.12 presents the influence of RHA amount on the microstructure characterization of MSG grout. As seen in Figure 12b, a 20% RHA replacement results in a compact structure and acts more homogeneously with formed gels and less unreacted particles than the microstructures of MSG (Figure 4.11b) and MSG-RH30 (Figure 4.12b). In other words, the microstructure of the MSG-RH20 is denser with less pores or visible cracks. The incorporation of 20% RHA contributes to the filling effect or interpenetrating action between the presence of other components in the geopolymer, leading to a decrease in average pore diameters and a more compact structure (Dadsetan et al., 2021; Zhu, Liang, Xu, et al., 2019). This decreases the geopolymer's permeation properties, such as its external ion penetration rate (such as chloride ion permeability) and low sorptivity. (Zhu, Liang, Xu, et al., 2019). As a result, a 20% replacement of slag by RHA improved the mechanical performance of MSG grout, and this observation aligns well with previous studies (Liang, Zhu, Zhang, Wu, et al., 2019; A. Mehta & Siddique, 2018; Zhu, Zhai, et al., 2021).

At 30% RHA, the microstructure of the MSG-RH30 is still denser and more compact than MSG; however, it continued to allow a significant number of unreacted RHA particles with many microcracks (Figure 4.12b). These microcracks could have been caused by an excess of RHA, which inhibits the synthesis of reaction products with crosslinking structures.

Due to the excessive amount of RHA, the interface between the RHA particles and the MSG matrix was reduced. Therefore, the low mechanical interlocking and the formed

microcracks resulted in lower densification and lower mechanical performance of MSG-RH30 samples compared to MSG-RH20 samples, as shown in Figure 4.12b (Vásquez et al., 2016). This effect is due to the considerable decrease in alumina with increasing RHA content, since alumina content is important in the production of a stable polymer network (Novais et al., 2016). Meanwhile, the elevated level of RHA brings about a looser structure caused by inadequate chemical reactions and increased unreacted components in the system (Zhu, Liang, Xu, et al., 2019). As a result, partial slag replacement by 30 % RHA reduces the UCS of the mechanochemical activation geopolymer grout.

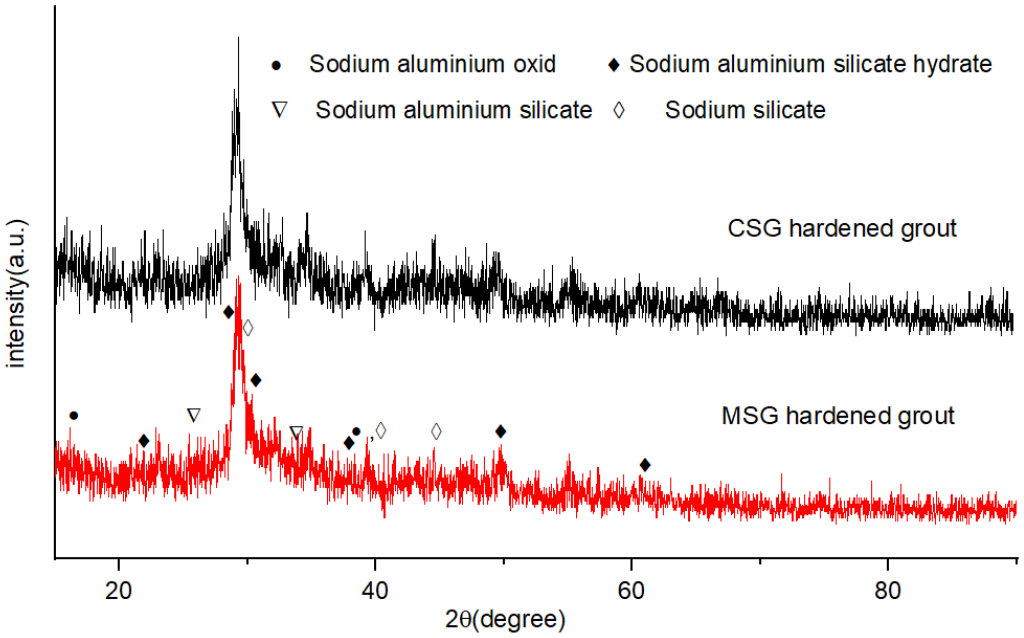

Figure 4.10 XRD patterns of CSG and MSG hardened grout.

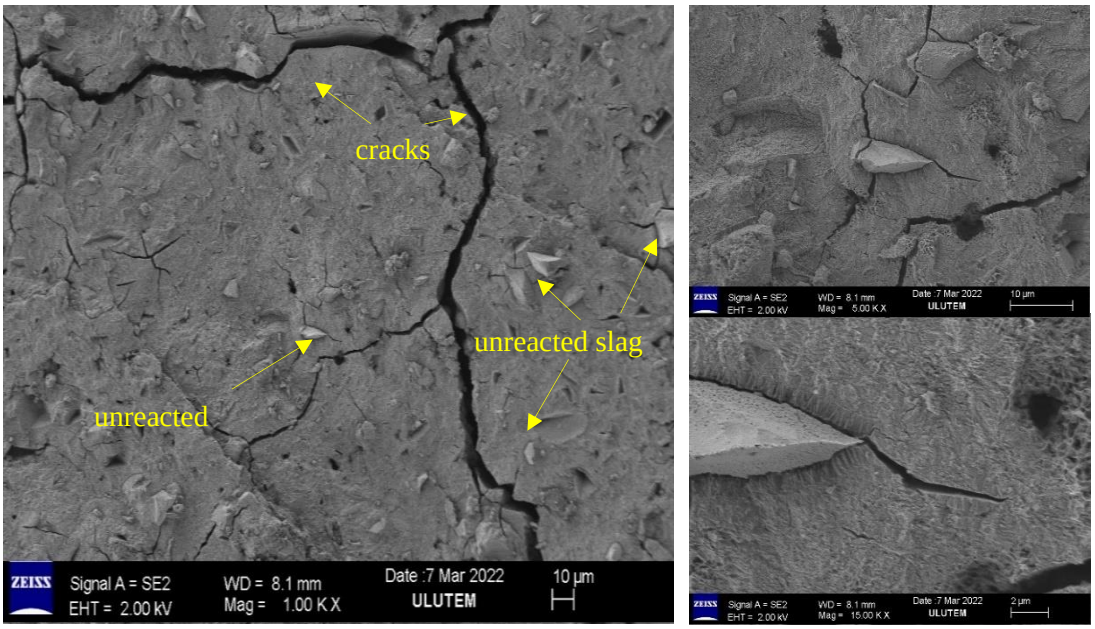

(a)

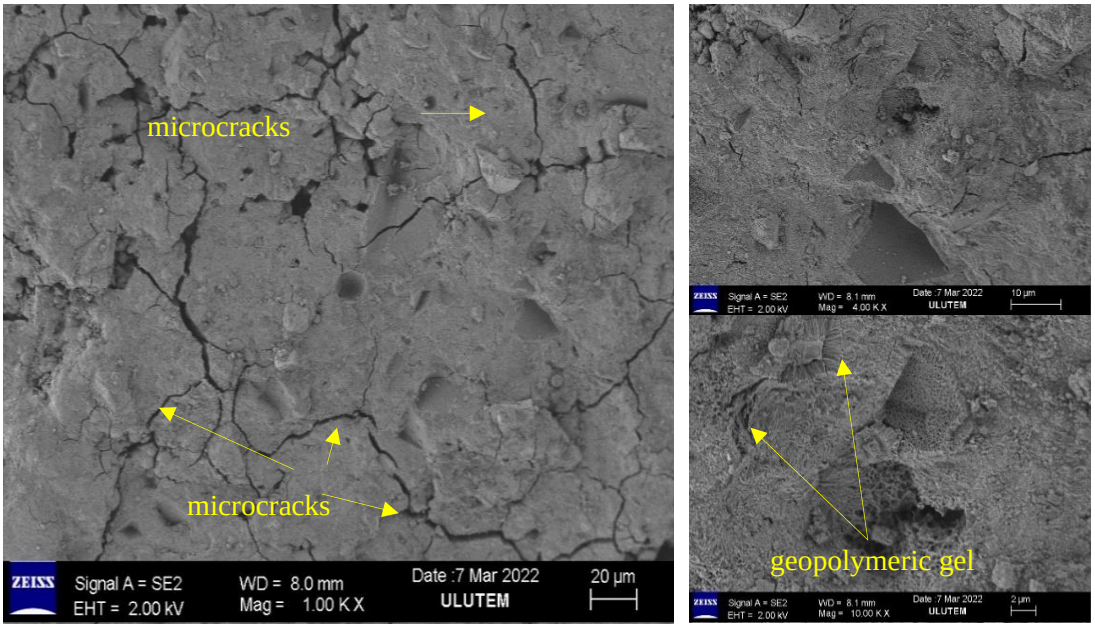

(b)

Figure 4.11 SEM images of the hardened (a) CSG and (b) MSG grout.

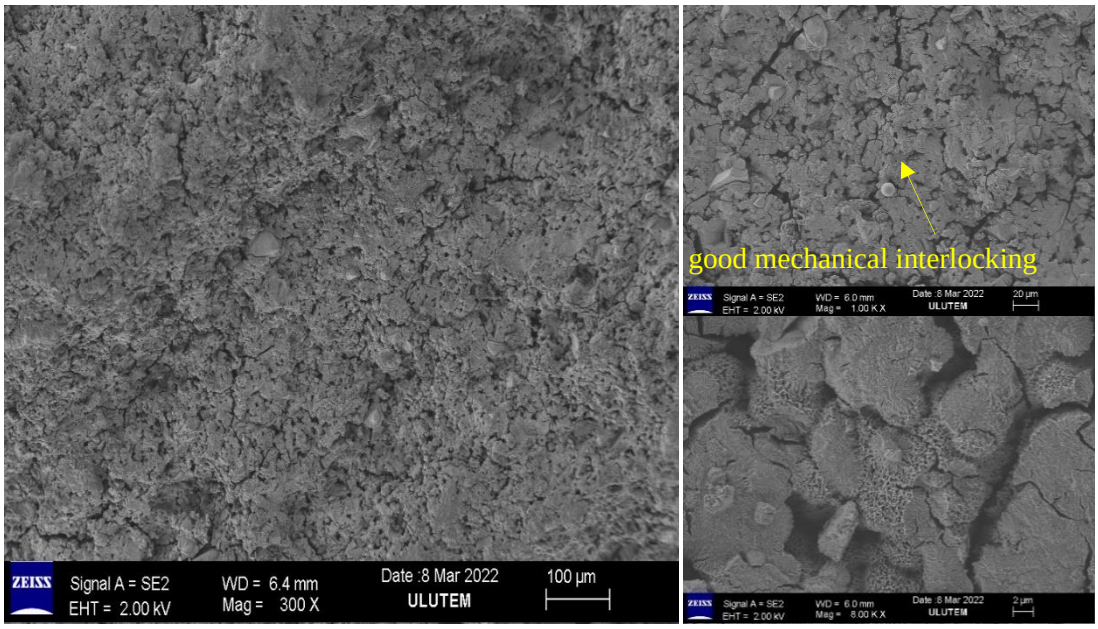

(a)

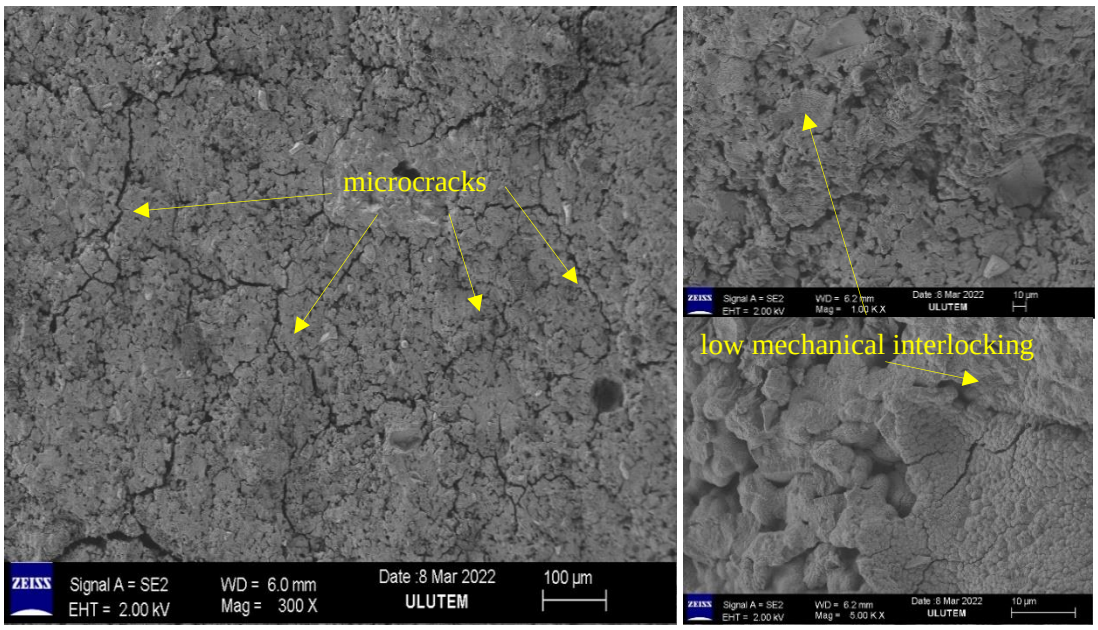

(b)

Figure 4.12 SEM images of the hardened (a) MSG-RH20 and (b) MSG-RH30 grout.

4.8 Conclusions

This research aimed to develop mechanochemically activated geopolymeric grout with an environmentally and more user-friendly approach. Current geopolymer synthesis methods address the limitations of conventional geopolymerization techniques. In addition, the feasibility of incorporating RHA as a partial precursor in slag-based mechanochemically activated geopolymer grout was investigated. Pointedly, a conventionally activated geopolymer-based grout and an ordinary Portland cement grout were investigated for comparison. All studied groups were examined for their rheological, fresh, mechanical, and microstructural performances. The following conclusions are derived from the results of the study:

- The presence of RHA as a partial substitution for slag in MSG grout has a noticeable effect with a beneficial consequence on the improvement of the rheological responses of the grout as evidenced by the decrease in apparent viscosity and shear stress of RHA-containing mixes. In addition, the mechanochemical activation approach positively affected the rheological properties of geopolymer grout.

- The yield stress and plastic viscosity values of the MSG grout were reduced by 5-38% and 9-41% when slag was substituted with 0- 30% RHA, respectively. Regarding the effect of the activation mechanism, the MSG grout exhibited between a 4% and 27% lower yield stress and plastic viscosity than the CSG grout. In addition, the results indicated that the yield stress and plastic viscosity of OPC grout were higher than those of MSG and CSG grout.

- The activation method and RHA replacement substantially impacted the setting time. Utilizing 0-30% RHA prolonged the initial and final setting times of MSG grout by 14-44% and 6-42%, respectively. In contrast, mechanochemical activation significantly accelerated the setting process. Initial setting times for MSG, CSG, and OPC were 3,3 h, 4 h, and 8 hours, respectively, whereas final setting times were 4.5 h, 6.3 h, and 12 h, respectively.

- The bleeding capacity of MSG grout increased from 0.025% to 0.1% as RHA content increased from 0 to 30 % due to its low water demand and filling impact

compared to slag. In addition, the results demonstrated that the MSG grout had a substantially lower capacity for bleeding than the CSG and OPC grout. It was found that as a result of the reduction in particle size and the rise in the powder's surface area caused by the grinding process, a greater quantity of water is required to adequately cover the surface of the particles.

- The substitution of 10–20% slag with rice husk ash enhanced the UCS of MSG grouts by 4.5–41.0% due to the introduction of more active silicon into the geopolymerization reaction process by rice husk ash, hence promoting the formation of additional gel phases. In addition, the mechanochemical technique increased the strength of geopolymer grout by 18% compared to its conventional counterpart.

- The microstructure analysis confirmed that the activation method significantly impacted the microstructure of geopolymer grout because the grinding process increased slag surface area while decreasing particle size, resulting in geopolymer grout samples with lower porosity and higher density than conventionally activated samples. Inclusive of this, the SEM images revealed that the microstructure of MSG grout at 20% RHA was densely compacted with fewer pores or no apparent cracks as a result of the incorporation of more active silicon into the geopolymerization reaction process, which promoted the generation of additional gel phases, which was also the strong support for the UCS development of MSG grout.

CHAPTER V

EFFECT OF GLASS POWDER ON THE EHEOLOGICAL AND MECAHNICAL PROPERTIES OF SLAG-BASED MECHANOCHEMICAL ACTIVATIION GEOPOLEMER GROUT

5.1 Overview

This chapter discusses the effects of glass powder (GP) replacements and sodium hydroxide (NaOH) molarity on the rheological, fresh, mechanical, and microstructure characteristics of mechanochemically activated slag-based geopolymer (MSG) grout. A conventionally activated slag-based geopolymer (CSG) and an ordinary Portland cement (OPC) grout were also investigated for comparison. Four glass powder replacement ratios were used (0%, 10%, 20%, and 30% by the total precursor weight) to prepare slag-based mechanochemical geopolymer at three NaOH concentrations (1.25, 2.5, and 3.75 molars). Table 5.1 presents all the mixture proportions of grouts.

Table 5.1 Mix proportions of grout.

		Weight %						
Molarity	Mix ID	Slag	GP	NaOH	Na_2SiO_3	OPC	Grinding duration:h	w/b
1.25	MSG	85	0	10	5	-	2	1.25
	MSG-GP10	75	10	10	5	-	2	1.25
	MSG-GP20	65	20	10	5	-	2	1.25
	MSG-GP30	55	30	10	5	-	2	1.25
2.5	MSG	85	0	10	5	-	2	1
	MSG-GP10	75	10	10	5	-	2	1
	MSG-GP20	65	20	10	5	-	2	1
	MSG-GP30	55	30	10	5	-	2	1
3.75	MSG	85	0	10	5	-	2	0.75
	MSG-GP10	75	10	10	5	-	2	0.75
	MSG-GP20	65	20	10	5	-	2	0.75
	MSG-GP30	55	30	10	5	-	2	0.75
3.75	CSG	85	0	10	5	-	-	0.75
-	OPC	-	-	-	-	100	-	0.75

5.2 Analysis of Microstructure

The particle size is the primary factor controlling rheological and mechanical characteristics variance. The particle size distribution of GP and slag before and after mechanochemical activation is displayed in Figure 5.1. The d50 (mean size) of raw GP and slag was 209 µm and 22 µm, respectively, whereas the mean size of GP and slag was reduced to 66 µm and 15 µm, respectively, after 2 hours of grinding in a ball mill with sodium hydroxide and sodium metasilicate.

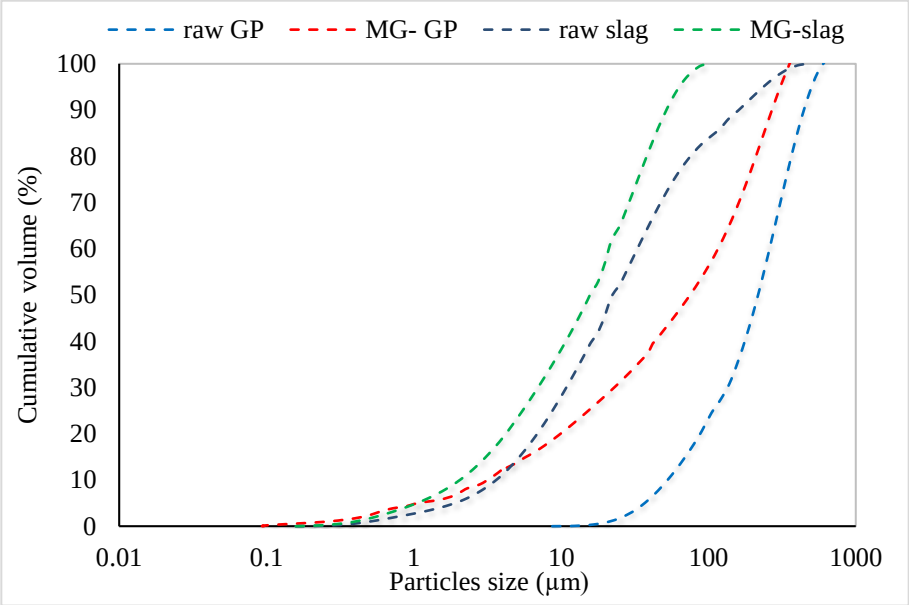

Figure 5.1 Particle size distribution of GP and slag before and after mechanochemical activation.

Scanning electron microscopy analysis (SEM) shows the microstructural characterization of slag and GP precursors before and after mechanochemical activation (Figure 5.2). As shown in Figure 5.2a, the raw slag particles are non-uniform and heterogeneous, with sub-rounded to angular forms. The roughness and edges were observed in both the angular and bulk particles (Baalamurugan et al., 2021). As seen in Figure 5.2b, most raw GP particles have irregular and angular shapes with smooth surface textures.

Figure 5.2c, d shows the microstructural analysis of slag and GP precursors obtained after 2 h of ball milling in the presence of chemical powder (NaOH and sodium

metasilicate). After grinding, the slag and GP particles were coated with solid chemical powder (NaOH and Na_2SiO_3), which decreased the average size of the precursors and solid chemicals. Nonetheless, the slag and GP particles still have angular and slightly deformed shape after the mechanochemical grinding. Furthermore, the surface area of the particles increased obviously during mechanochemical activation and resulted in a higher reaction rate of the geopolymeric precursors. Additionally, initial bonding between the particles was observed (Figure 5.2 d) due to the addition of NaOH and sodium metasilicate, which may reflect the MSG powder's adhesive nature. However, the effect of ball milling of all raw materials resulted in increased amorphousness and formation of the geopolymeric precursor (Gupta, Bhardwaj, Mishra, Mudgal, et al., 2017). Hamid Abed, Sabbar Abbas, et al. (2022) reported that grinding of fly ash and slag with NaOH and sodium metasilicate for 2 h resulted in the formation of cracks and defects, which enhanced the surface roughness of the surface the particles and increased reactivity to the geopolymeric precursors.

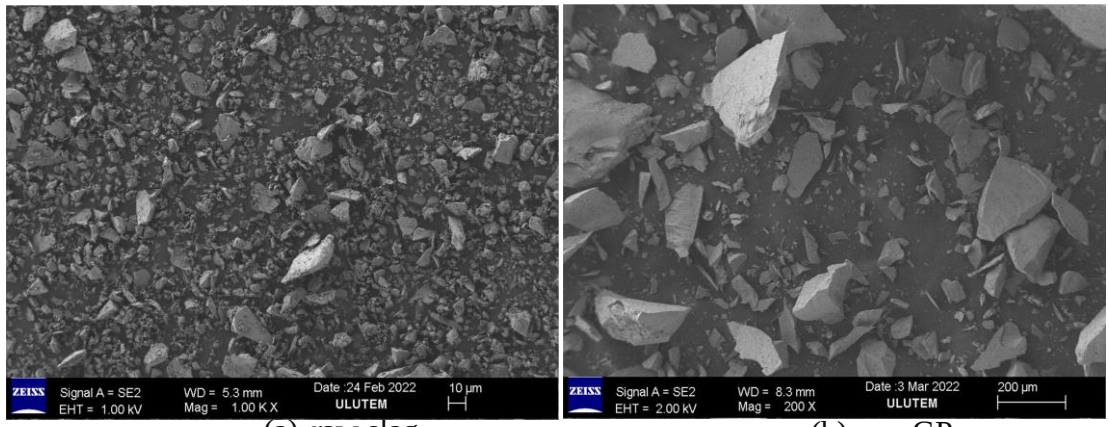

(a) raw slag (b) raw GP

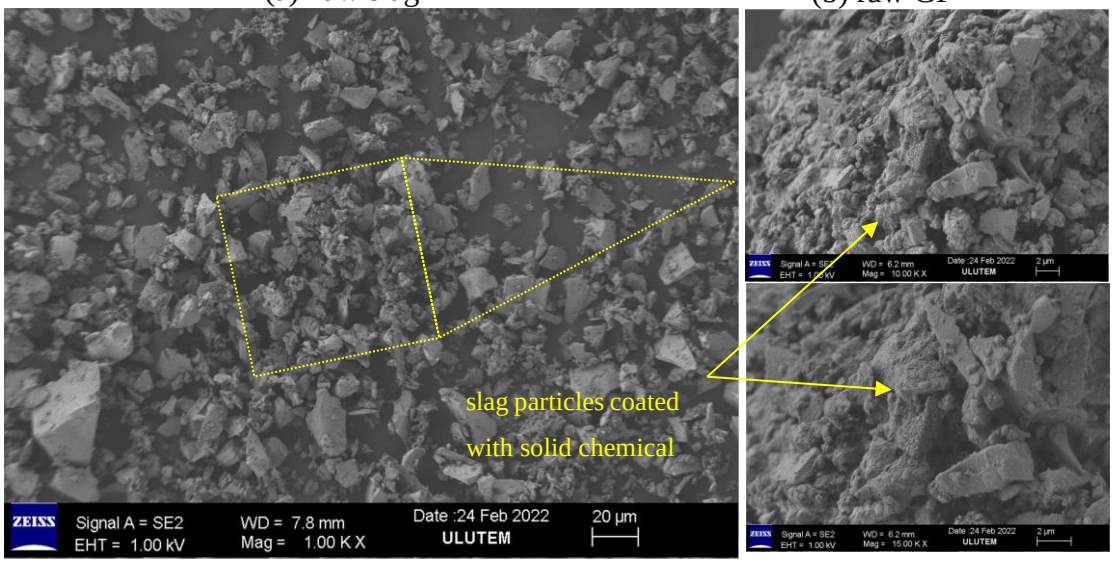

(c) MSG-Slag

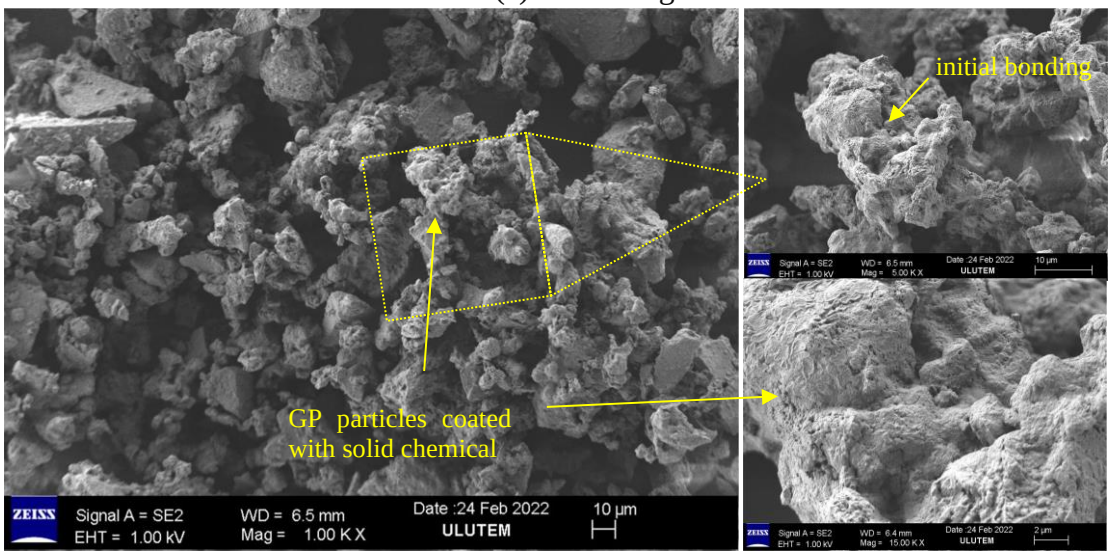

(d) MSG -GP

Figure 5.2 SEM micrographs of raw materials before and after mechanochemical process.

5.3 Rheological Behavior and Responses

The flow curves of geopolymer grouts activated by mechanochemical activation at varied NaOH concentrations are shown in Figure 5.3. Also, the dilatant index values (i.e., coefficient C) are presented in Table 5.2. All the MSG grouts exhibited a shear thickening behavior (C > 0). In other words, apparent viscosity increased as shear rate of grout increased, as illustrated in Figure 5.3. The experimental results demonstrate that the magnitudes of apparent viscosity and shear stress increased as the molarity of NaOH increased in all MSG grouts. This behavior is primarily attributed to the increase in the viscosity of the activation solution with NaOH concentration (Vance et al., 2014). Furthermore, low molarity negatively influenced the apparent viscosity due to the slow leaching rate of Al^{3+} and Si^{4+} (M. Palacios et al., 2019; Vance et al., 2014). Zhang et al. (J. Zhang et al., 2019) also reported that increasing the sodium hydroxide content (0.5 to 4 M) increased the viscosity of geopolymer-based grouts. This is due to the high reactivity of soluble aluminosilicate components, which accelerates polymerization and hydration reactions, resulting in a rapid increase in viscosity of geopolymer mixture. On the other hand, the effect of GP content on the rheological responses of the fresh MSG grout is presented in Figure 5.4. The flow curve showed that the MSG grout containing 100% slag (MSG) had the highest shear stress and apparent viscosity. In other words, a high slag amount increased the viscosity of the MSG grout mixture due to the high reactivity of the slag binder, which results in the development of primary C-S-H gel during the initial stages of the reaction (Palacios et al., 2008a). Additionally, the apparent viscosity and shear stress of the flow curves decreased dramatically as the GP content increased. This may be due to the comparatively smooth surface of GP particles, thereby reducing the water absorption, which is advantageous to reducing viscosity performance (Terro, 2006). According to Liang et al. (Liang, Li, et al., 2021), workability (flowability) is associated with clusters in liquid suspensions. It has been shown that adding GP to geopolymer grout can reduce the formation of clusters (X. Jiang et al., 2020; Vafaei & Allahverdi, 2017), resulting in a decrease in the apparent viscosity of MSG grout. Overall, the utilization of glass powder is beneficial in terms of the rheological performance of geopolymer grouts.

In terms of geopolymer activation mechanism, the apparent viscosity and shear stress of CSG grout were higher than MSG grout, it can be concluded that CSG grout mixtures mostly appear to produce higher magnitudes of apparent viscosity and shear stress in comparison to MSG grout due to the high dissolution and ionization degree of MSG grout (D. W. Zhang et al., 2018). Also, the magnitudes of shear stress and apparent viscosity of the MSG grout were higher than those of the OPC grout, as illustrated in Figure 5.4. This could be due to the fact that the mechanochemical process alters the surface area and particle size of the powder; as a result, additional water is required to cover the surface of the particles, resulting in a remarkable reduction in free water in fresh grouts and an increase in the responses (shear stress and apparent viscosity) (Marjanović et al., 2014).

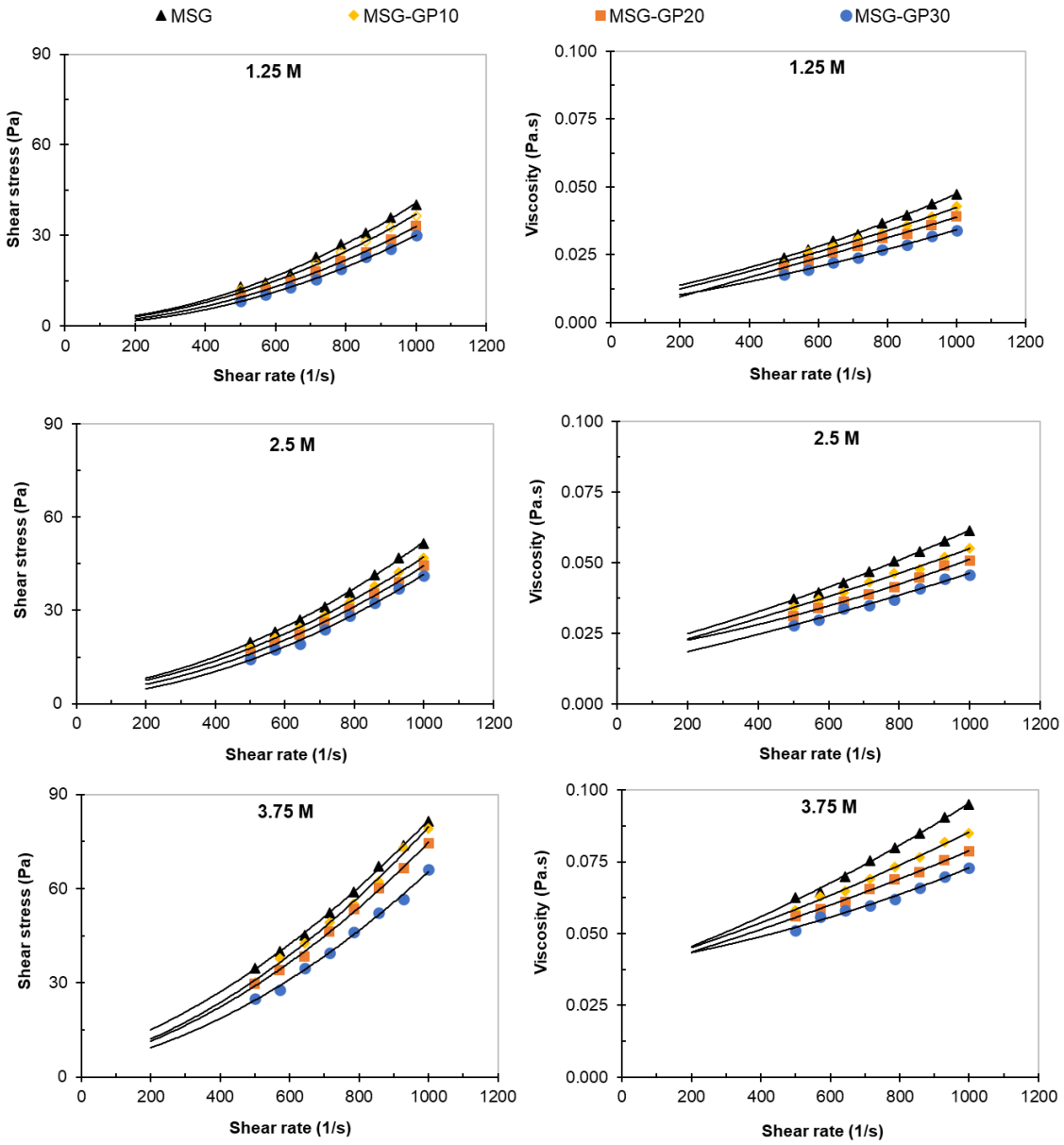

Figure 5.3 Flow responses curves of MSG grout.

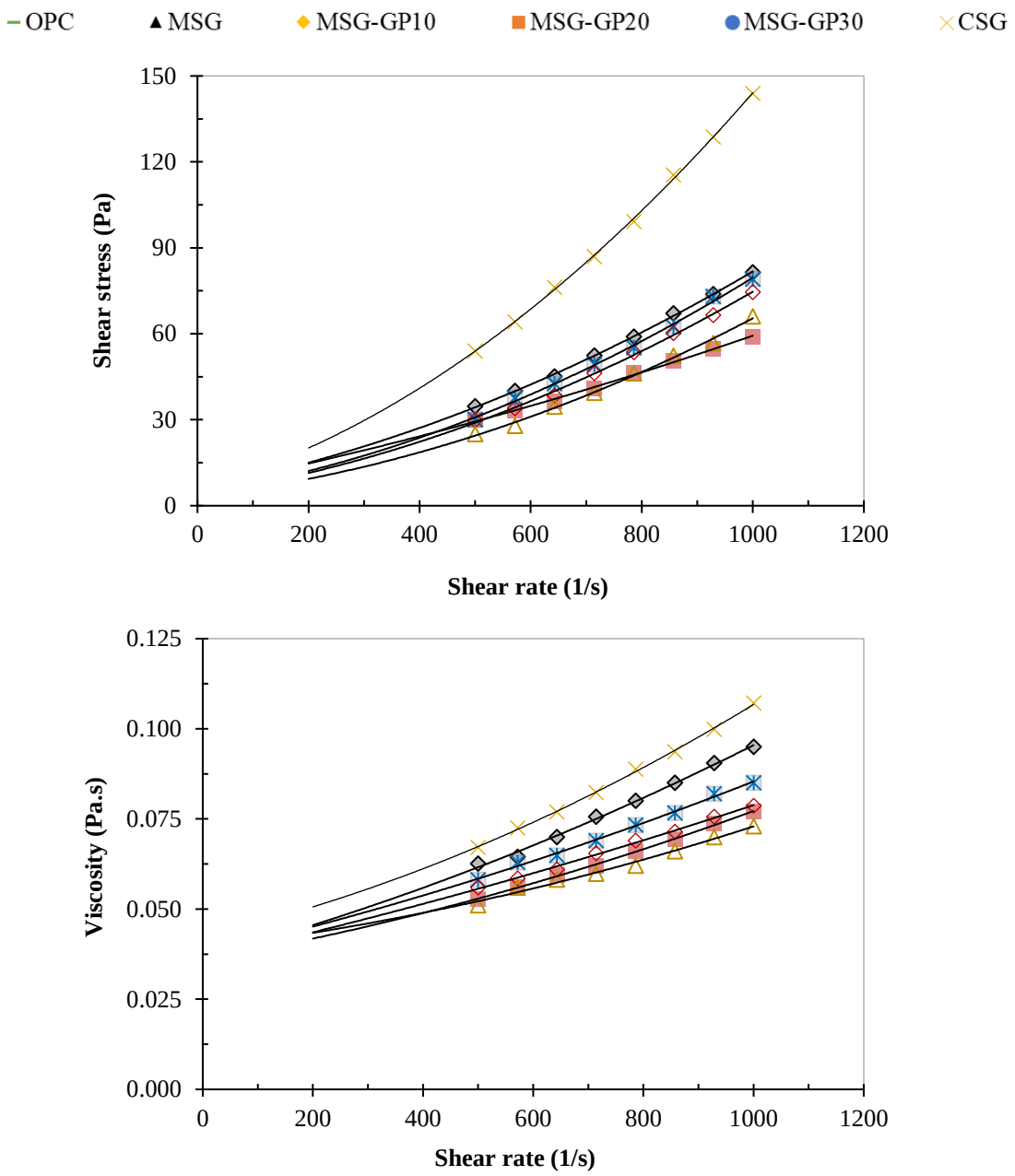

Figure 5.4 Flow responses curves of OPC, CSG, and MSG grouts.

5.4 Yield Stress and Plastic Viscosity

The yield stress (YS) and plastic viscosity (PV) of grouts were estimated using the modified Bingham model during rheological experiments. In general, both YS and PV increased with the increasing of NaOH concentration. As can be seen in Figure

5.5, the YS and PV values of MSG grout were in the range of 1.1- 0.35 Pa and 0.005-0.0014 Pa.s at 1.25 molarity and between 5.8 - 3.3 Pa and 0.038-0.023 Pa.s at 3.75 molarity, respectively, the increase in YS and PV has been mainly attributed to the use of a high concentration of sodium hydroxide resulting in higher storage modulus which indicates the presence of a rigid structure that leads to higher geopolymerization kinetics (Lu et al., 2021). Similar findings were obtained by Rifaai et al. (2019) who indicated that the increase in NaOH concentration from 2 to 7 M increased the yield stress of alkali-activated slag pastes.

On the other hand, the YS and PV of the MSG grout gradually decrease with increasing GP content (Table 5.2). The results showed that mixtures with 100% slag (MSG -GP0) have higher YS and PV of 5.8 pa and 0.038 p.as, respectively (Figure 5.6). According Marta Palacios et al. (2008) the higher yield stress of high slag content mixtures may be explained by the mechanism governing the reaction; the slag particles are surrounded by a thin layer of primary C-S-H generated by the interaction of the silicate ions and the Ca^{2+} ions in the slag immediately after contact with the alkali activator. Under these conditions, colloidal forces attracted slag particles to one another, resulting in the formation of flocs. These flocs are partially separated during mixing and treatment before rheological testing; however, the rapid precipitation of massive amounts of primary C-S-H gel continues, generating larger flocs. As a result, the higher yield stress is required to initiate flow.

Also, incorporating GP in MSG grout dramatically alters the reaction products and physicochemical interactions. The YS of MSG-GP10, MSG-GP20, and MSG-GP30 grouts reduced by 16%, 34%, and 43%, and the PV reduced by 13%, 21%, and 39% when compared to MSG, respectively. Glass powder has a lower surface area, a larger mean particle size, and a comparatively smooth surface. Thus, by including glass particles into the geopolymer grout, the demand for water to wet the solid precursors was decreased, leading to an increase in the amount of available water in the mixture during the fresh stage. The additional water in the glass powder-containing binder can act as a lubricant between the geopolymeric particles, thereby reducing the viscosity of fresh grouts (Si et al., 2020). Therefore, the YS and PV of the geopolymer grout decrease as the GP proportion of MSG mixes increases.

The results also demonstrated that the YS and PV of the OPC grout were higher than those of the MSG and CSG grouts, as illustrated in Table 5.2. The YS and PV of MSG grout are 5.8 Pa and 0.038 Pa. s, respectively. In contrast, OPC grout has a YS and PV of 6.4 Pa and 0.06 Pa. s (Figure 5.6) because cement particles begin to hydrate and dissolve when they come into contact with water, creating positive and negative charges on the cement surface and inducing electrostatic attraction between the cement particles, leading to grouping or flocculation of the particles (Y. Zhang et al., 2018). The hydration product ettringite was negatively charged in the synthetic pore solution (liquid phase of hydrating cement suspension), whereas calcium silicate hydrates and tricalcium silicate were positively charged (Zingg et al., 2008). Liang et al. (2021) reported that part of the water is wrapped in cement particles; therefore, a decrease in the amount of free water would be observed, increasing the effective solids volume fraction. However, in the MSG grout, the silicate anions are absorbed on the surface of precursor particles like slag, generating negative charges on the particles' surfaces and resulting in electrostatic repulsion between them (Kashani et al., 2014). In other words, it had a reduced effective solid volume fraction, which resulted in lower YS and PV.

From the perspective of the activation method, the MSG grout unveiled a lower YS and PV than the CSG grout (Table 5.2). The YS and PV of MSG grout are 4% and 27 less than the CSG grout. This could be because the alkali activator solution dissolves rapidly at an early stage when blended with the raw materials that rich in alumina and silica to produce a conventional geopolymerization reaction, which is significantly more viscous than the required water to form MSG grout, resulting in a greater YS and PV of the CSG grout (Hamid Abed, Sabbar Abbas, et al., 2022). It is well known that a suspension's viscosity increases in direct proportion to the viscosity of the suspending solution (Konijn et al., 2014). It can be concluded that the higher YS and PV values are disadvantageous for grout when applied as a soil injection material, as the materials would be difficult to pump through the pipe if the slurry was overly viscous. Hence, MSG grout is more suitable for soil injection applications than CSG and OPC grout.

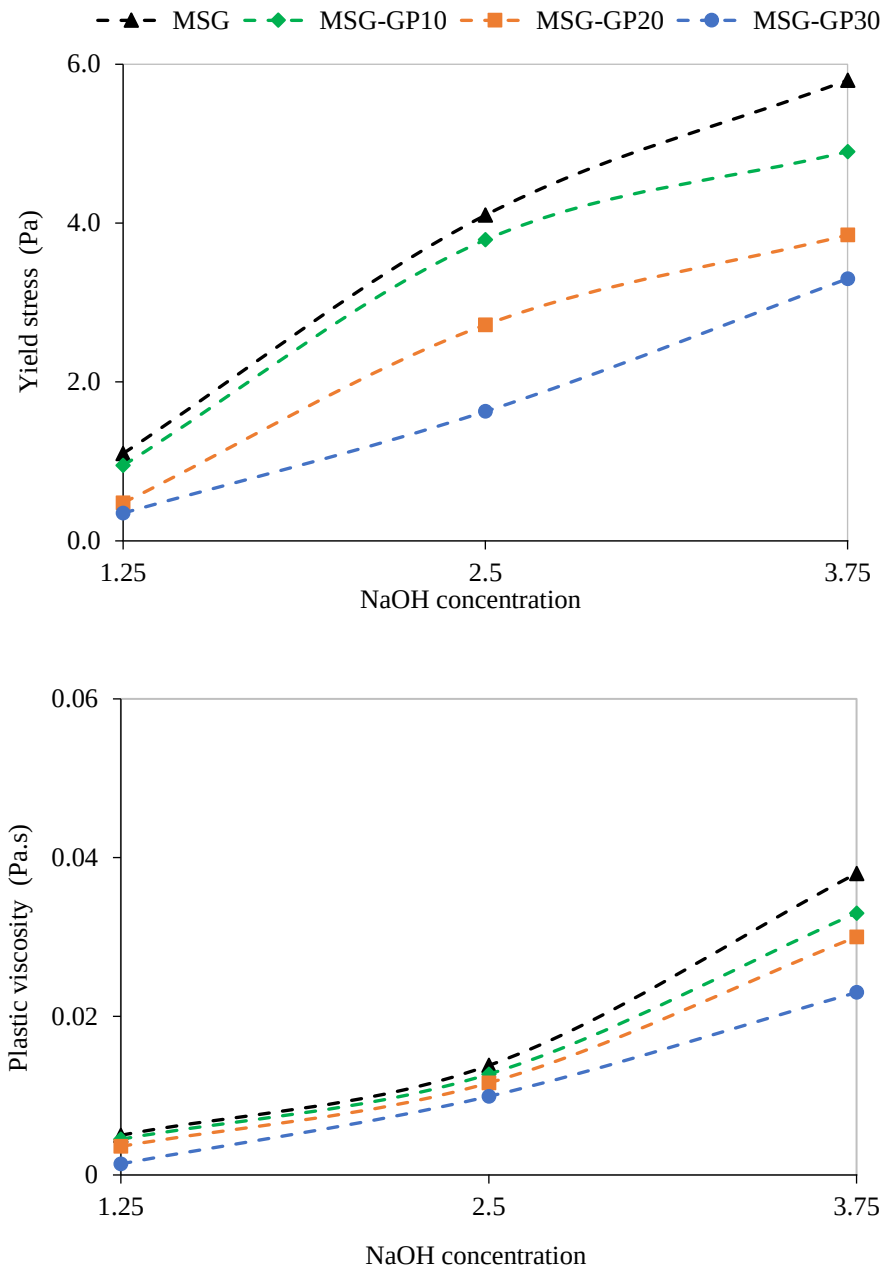

Figure 5.5 Effect of NaOH concentration on the yield stress and plastic viscosity of MSG grouts.

Table 5.2 Rheological characteristics of the grout.

Molarity	Mix ID	coefficient C	YS (Pa)	PV (Pa. s)
1.25	MSG	0.00003	1.1	0.005
	MSG-GP10	0.00003	0.95	0.0045
	MSG-GP20	0.00003	0.48	0.0036
	MSG-GP30	0.00003	0.35	0.0014
2.5	MSG	0.00003	4.1	0.0138
	MSG-GP10	0.00003	3.79	0.0127
	MSG-GP20	0.00003	2.72	0.0116
	MSG-GP30	0.00003	1.63	0.0099
3.75	MSG	0.00004	5.8	0.038
	MSG-GP10	0.00004	4.9	0.033
	MSG-GP20	0.00004	3.85	0.03
	MSG-GP30	0.00004	3.3	0.023
	CSG	0.00008	6.04	0.052
-	OPC	0.00002	6.4	0.06

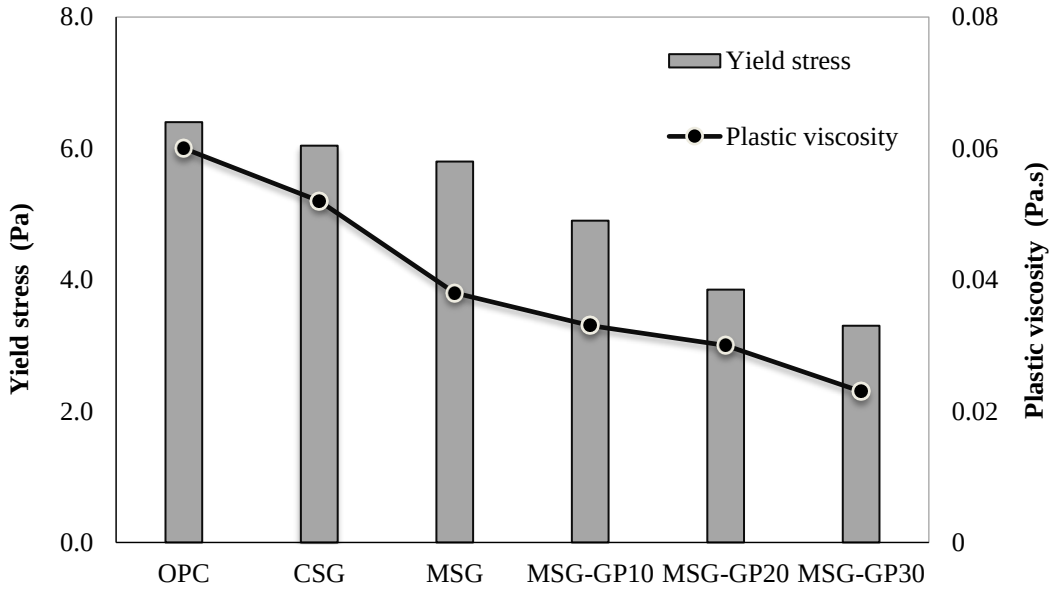

Figure 5.6 Yield stress and plastic viscosity of OPC, CSG and MSG grouts.

5.6 Fresh Properties

5.6.1 Setting Time

The setting time of MSG grouts with varying sodium hydroxide concentrations is illustrated in Figure 5.7. The results revealed that the setting time was considerably shortened with the increasing molar concentration of NaOH, the initial setting time was shortened by 28% and 64%, respectively, at 2.5 and 3.75 molarity, as compared to 1.25 molarity. This is because the alkalinity of the sodium hydroxide solution causes the release of Al^{3+}, $Ca^{2+,}$ and Si^{4+} from slag and GP, which subsequently diffuse out of the geopolymerization products that rapidly develop around unreacted particles during the leaching reaction. Alkaline conditions promote the activation reaction, whereas hydroxide accelerates slag and GP dissolution and also enhances aluminosilicate solubility (Marjanovi et al., 2014).

The effect of glass powder content on the setting times of MSG grouts is depicted in Figure 5.8. In general, the addition of GP into geopolymer grouts considerably increased the setting time duration. The initial setting time of MSG-GP10, MSG-GP20, and MSG-GP30 increased by 13%, 38%, and 50%, respectively. Similarly, the final setting time increased by 33%, 61%, and 78%, respectively, compared to MSG. This is due mainly to the higher reaction rate of slag than GP, which leads to the formation of sodium, silicon, and calcium components gels at an early stage of the reaction, accelerating the reaction process (Kumar et al., 2010). Furthermore, because the slag particles are much smaller than GP particles, the overall contact area between the solution and the solid particles decreases as the GP content in the system increases. As a result, the overall dissolving rate of the raw materials tended to be decreased during the reaction, resulting in a reduction in the polycondensation rate for samples that contain GP (Novais et al., 2016). Liang et al. (2021) reported that adding glass powder to metakaolin/fly ash-based geopolymer pastes significantly prolonged the setting time. On the other hand, the results demonstrated that the setting time of the MSG grout was shorter than that of the OPC and CSG grouts. The initial setting time of MSG, CSG, and OPC was 4 h, 6 h, and 8 h, and the final setting time was 4.5h,7.3h, and 12h, respectively, under similar conditions, as seen in Figure 5.8. The shorter setting time of MSG grout could be attributed to

mechanochemical mechanisms that create electronic charges on the surface of mechanochemically activated particles, resulting in a rise in surface energy and the transition from the crystalline to amorphous phase (Hosseini et al., 2021). Furthermore, the mechanochemical process disintegrates large alumina and silica particles, increasing their surface area and resulting in a more uniform distribution of particles in the mixture, which contributed to a higher proportion of additional alumina-silicate being formed from slag and GP, allowing for participation and dissolution in the formation of geopolymer gels (Hamid Abed, Sabbar Abbas, et al., 2022; Marjanović et al., 2014). Thus, increased alumina-silicate availability accelerated the polymerization process, resulting in creating an alumina-silicate gel network with extra alumina-silicate components. Due to the increased alumina-silicate crosslinking, the resulting gel has a more homogeneous microstructure, which results in a shorter setting time for MSG grout (H. Li et al., 2014; Marjanović et al., 2014). Li et al. (2020) noted that the setting time of the alkali activated slag/glass powder paste was much shorter than that of the OPC paste, and the time gap between the initial and the final setting was shorter. The longest setting time of the OPC mix is most likely due to the Portland cement being less reactive than the slag-based geopolymer grout, particularly in the early phases (Yi et al., 2015). The high reactivity of slag-based geopolymer tended to rapidly produce gels compared to OPC (Shang et al., 2018).

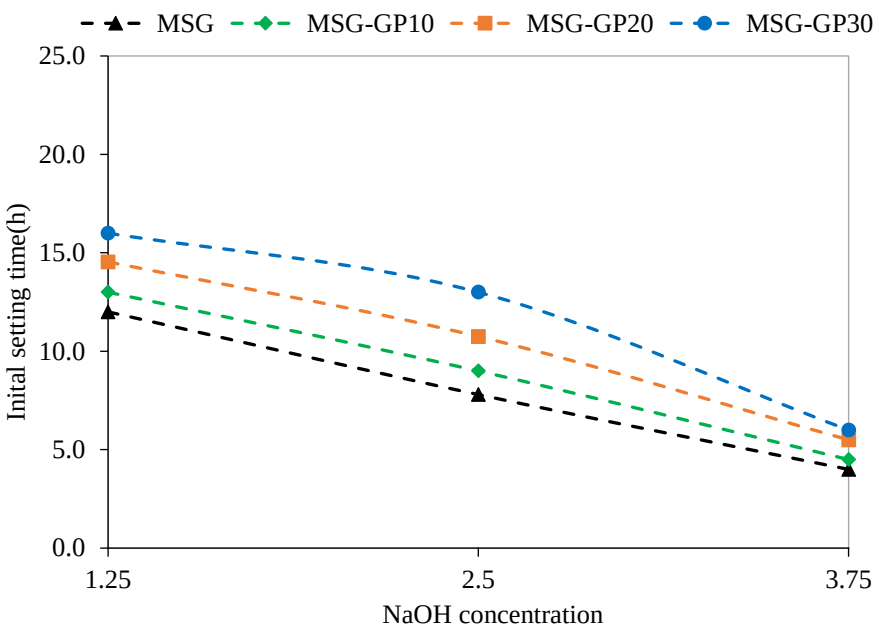

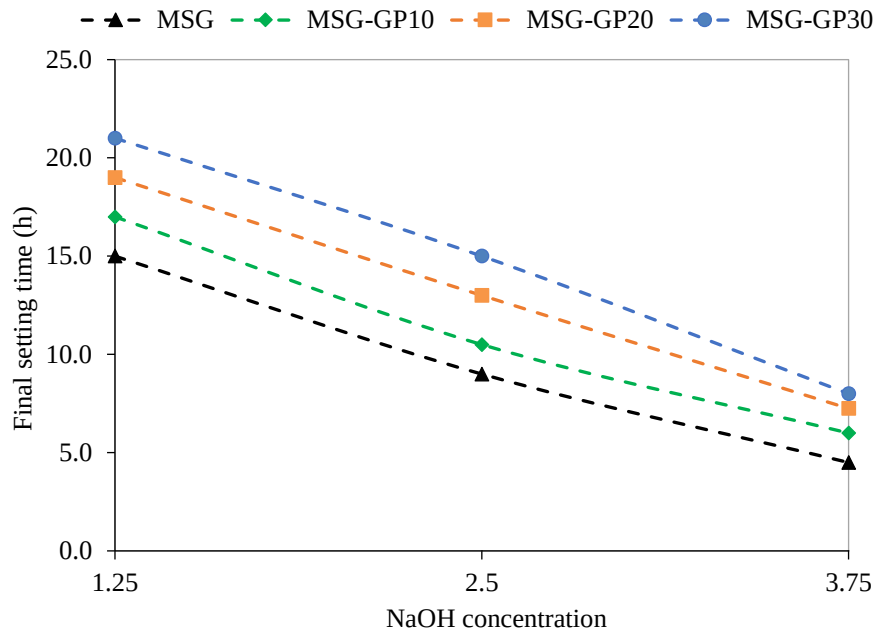

Figure 5.7 Influence of NaOH concentration on the setting time of MSG- based grouts.

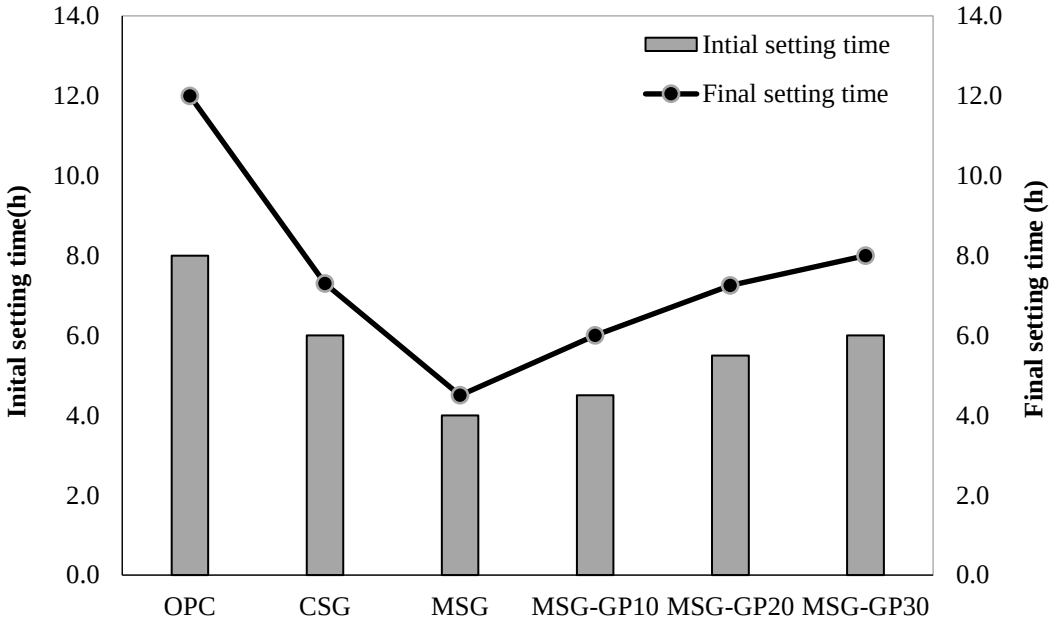

Figure 5.8 Setting time of OPC, CSG and MSG grouts.

5.6.2 Bleeding Capacity

Figure 5.9 shows the effect of the NaOH concentration on the bleeding capacity of the MSG grout. The results revealed that the bleeding capacity of MSG grouts declined steadily as the NaOH concentration increased from 1.25 M to 2.5 M; the lowest value of bleeding capacity of MSG grouts was at 3.75 molar concentration due to the fact that as the molarity increased, the leached amount of alumina-silicate enhanced, and additional water was required to form geopolymer networks (Hamid Abed, Sabbar Abbas, et al., 2022). Zhang et al. (2019) observed a similar trend for slag activated by sodium hydroxide solutions. A significant decrease in bleeding capacity was noted with an increase in the sodium hydroxide concentration in the grout mixture. This tendency clearly indicates that the sodium hydroxide concentration played a positive role in the bleeding capacity. In addition to molarity, the bleeding capacity of MSG grout increased with the increase of GP level; hence, it can be clearly observed that the bleeding capacity of MSG grout gradually increases with the increasing glass powder replacement, as illustrated in Figure 5.10. The results revealed that the mixes with 100% slag content had the lowest bleeding capability. For example, the bleeding capacity of MSG grout increased from 0.025% to 0.55% when GP content increased from 0 to 30%. Because of the high demand

for water in the geopolymerization of slag particles (Liang, Zhu, Zhang, Wu, et al., 2019; Zhu, Liang, et al., 2021), dissolution heat flow increased as slag amount increased since slag possesses a faster dissolution rate than GP (Khan et al., 2021a), leading to rapid growth synthesis of reaction products to create a rigid network. In comparison to slag, the high bleeding capacity of geopolymer grout incorporating GP can be attributed to its low water requirement and filling effect. In addition, the surface of GP particles is comparatively smooth, which reduces the amount of water absorbed (Terro, 2006). The results also showed that the MSG grout had significantly less bleeding capacity than the OPC and CSG grouts, as seen in Figure 5.10. Due to the increased surface area and reduced particle size of the mechanochemically activated powder, additional water is required to cover the particles' surfaces (Marjanović et al., 2014). In In general, the results of this research indicated that the bleeding of MSG and CSG grouts is more stable than OPC grout. The higher bleeding capacity of the OPC mix is most likely related to the fact that the Portland cement is less reactive than the slag-based geopolymer grout, particularly during these early stages (Yi et al., 2015). On the other hand, apparent viscosity played a positive role in improving the stability of grouts (Yin et al., 2021). The higher apparent viscosity of slag-based geopolymer grout represents a better reaction between water and binder and a stronger agglutination; hence, for bleeding to occur, the water needs to overcome higher friction from the grout particles (H. Xie et al., 2013).

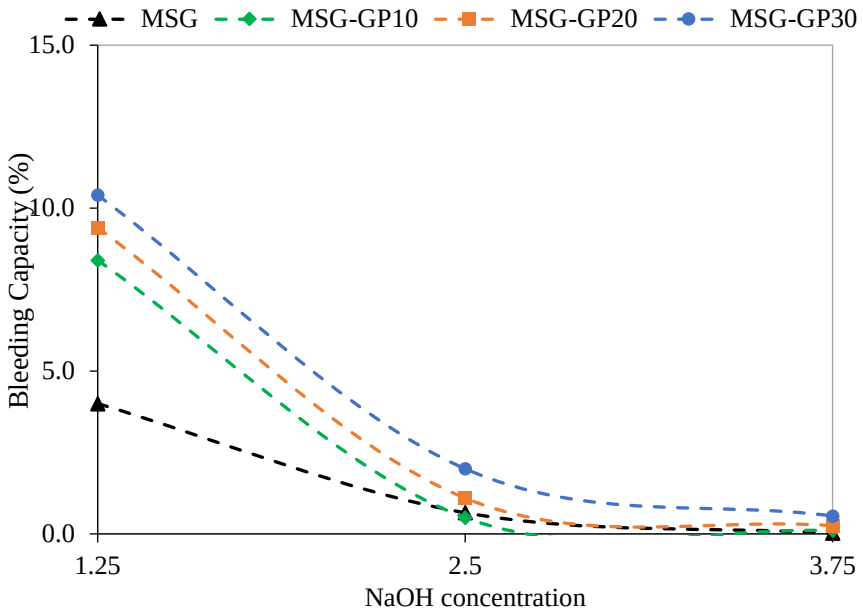

Figure 5.9 Effect of the sodium hydroxide concentration on the bleeding capacity of MSG-based grout.

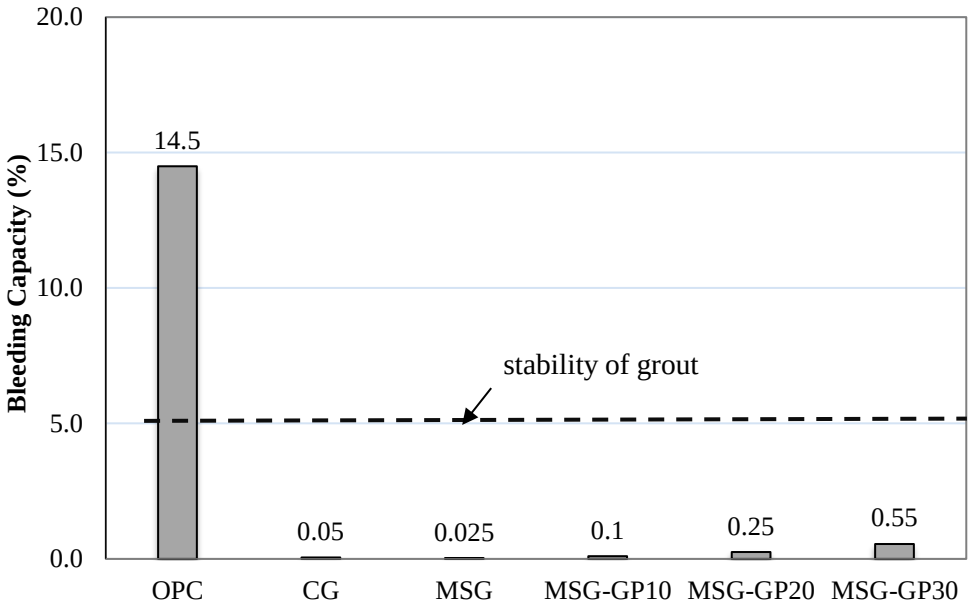

Figure 5.10 The bleeding capacity of OPC, CSG, and MSG grouts.

5.7 Mechanical Properties

5.7.1 Unconfined Compressive Strength

Figure 5.11 presents the effect of different molarities of MSG grouts on UCS at 7 days and 28 days. The results indicated that the NaOH molarity significantly influenced the UCS values of MSG specimens. In general, the UCS values of MSG grout increased as the molarity of NaOH increased. For instance, the UCS of MSG improved by 40% and 71%, respectively, whereas the UCS of MSG-GP30 improved by 39% and 90% at 2.5 and 3.75 molarity, respectively, at 28 days. It can be concluded that the optimum UCS values were seen at 3.75 molarity among all the MSG grouts. Strength enhancement is usually controlled by the amount of alumina silicate leached from the source materials; hence, increasing the molarity of NaOH results in increased Al^{3+} and Si^{4+} dissolved, resulting in a strong geopolymeric network (J. Zhang et al., 2019). Liang et al. (2021) also reported that the GP's active ions (Si^{4+}, Al^{3+}, and Ca^{2+}) are dissolved and leached efficiently in the NaOH solution. Furthermore, dissolution of NaOH at low molarity indicated that OH^- ions were insufficient to break the Al-Si link, resulting in the formation of a few alumina silicate tetrahedral monomers. Whereas, at a high molar concentration of NaOH, OH ions completely broke all silicon–aluminum bonds and generated extra alumina silicate tetrahedral monomers, completing the dissolution. As a result, the microstructure of geopolymer grout was condensed, and the mechanical properties were increased (A. Abdullah et al., 2021; Muraleedharan & Nadir, 2021).

Figure 5.12 shows the effect of GP replacements on UCS values of MSG specimens at 7 and 28 days. The UCS values of all studied mixtures improved as the age increased from 7 to 28 days; specimens cured at 28 days displayed better strength characteristics than specimens cured at 7 days due to the completion of the polymerization process and densification of the microstructure at longer ages (Athira et al., 2021; Liang, Zhu, Zhang, Wu, et al., 2019; Tho-In et al., 2016). On the other hand, the UCS results for MSG grout samples containing GP revealed that the UCS increases with increased curing time, and fewer cracks on the surface of the specimens were observed compared to the MSG sample. The UCS test results

of the MSG grout reduced with increasing GP replacement level at 7 days after that, started to increase with increasing GP content up to 20% at 28 days, as shown in Figure 5.12. For instance, after 7 days of curing, the decreases in UCS were 18%, 23%, and 37% for GP levels of 10%, 20%, and 30%, respectively. Similar results were reported in previous research (Khan et al., 2021a; Tho-In et al., 2016). The increase in UCS of MSG-GP grout over time is due to the dissolving a notable proportion of silica from GP in an alkali media (Fernández-Jiménez et al., 2017). Whereas, the UCS of MSG grout increased slightly at 10% GP, and the MSG-GP20 mix exhibited the highest UCS at 20% GP replacement among all MSG grouts after 28 days. The UCS of the MSG-GP20 grout was 13% higher than that of the control mix (MSG) because the major active ions (Si^{4+}, Al^{3+}, and Ca^{2+}) were dissolved and leached from GP in the alkaline activator, and the soluble ions contribute to the increased reactivity of solid precursors and participate further in the geopolymerization reaction, hence increasing strengths (X. Jiang et al., 2020; Liang, Li, et al., 2021; S. Zhang et al., 2017). It is important to note that replacing slag with 30% GP decreased the UCS by 4% compared to MSG. The higher amount of GP substantially impacted the silica-alumina ratio due to the high silicon concentration in GP. Silva et al. (2007) reported that the silica-alumina ratio had a substantial impact on the mechanical characteristics of the geopolymer. With a high silica-alumina ratio, low-crosslinked aluminosilicate materials with reduced strengths were developed (Tho-In et al., 2016). Furthermore, the relatively lower calcium oxide content in GP decreased the UCS because the high calcium oxide content in the geopolymer gel could create more hydrated products such as calcium silicate hydrate gel in addition to the three-dimensional matrix network (N. K. Lee & Lee, 2013), which lowered the UCS. Thus, it can be concluded that GP up to 20% can be used as a precursor for geopolymer synthesis after mechanochemical treatment (Hamid et al., 2022).

From the perspective of the activation method, the mechanochemical mechanism had a considerable influence on the strength performance of MSG grout specimens. The UCS values of CSG grout were lower than its counterpart MSG (Figure 5.13); the UCS was reduced by 18% compared to MSG due to the higher cracks observed at 28 days, as shown in Figure 5.13. Notably, the strength performance of the mixes

containing 100% slag activated conventionally was reduced at longer curing period. The UCS of the CSG grout sample was 8.7 MPa and 8 MPa at 7 days and 28 days, respectively. Moreover, the shape of the CSG grout sample at 28 days revealed apparent micro-cracks on the surface of the specimen. These cracks can be attributed to the fact that there is more apparent shrinkage after 28 days compared to 7 days; this aspect contributes to the decrease in strength of CSG samples after 28 days (Hamid Abed, Sabbar Abbas, et al., 2022; N. K. Lee & Lee, 2013). Additionally, mechanochemical activation increased the surface area and reaction rate of slag; as a result, an extra gel was generated as a consequence of the main reaction, which then accumulated and filled the pore system. The formation of a large proportion of gel in the geopolymer mixture improved the overall pore volume and porosity of the geopolymer grout, resulting in enhanced immobilization (Hamid Abed, Sabbar Abbas, et al., 2022). Similar MG grout behavior was reported in (Adesanya et al., 2020; Fernández-Jiménez et al., 2019; Hamid Abed, Abbas, et al., 2022; Hosseini et al., 2021). On the other hand, the results revealed that the USC of OPC sample was a little higher than that of the MSG and CSG mixes due to the high shrinkage of slag and lower calcium content compared to OPC. For example, the UCS of OPC is 1.4%, 19% higher than MSG and CSG, and 10% lower than MSG-GP20, respectively (Figure 5.12). It can be concluded that the UCS of MSG-GP20 $\geq$ OPC $\geq$ CSG grouts; therefore, the GP can be effectively used in mechanochemical geopolymer grout up to 20% replacement.

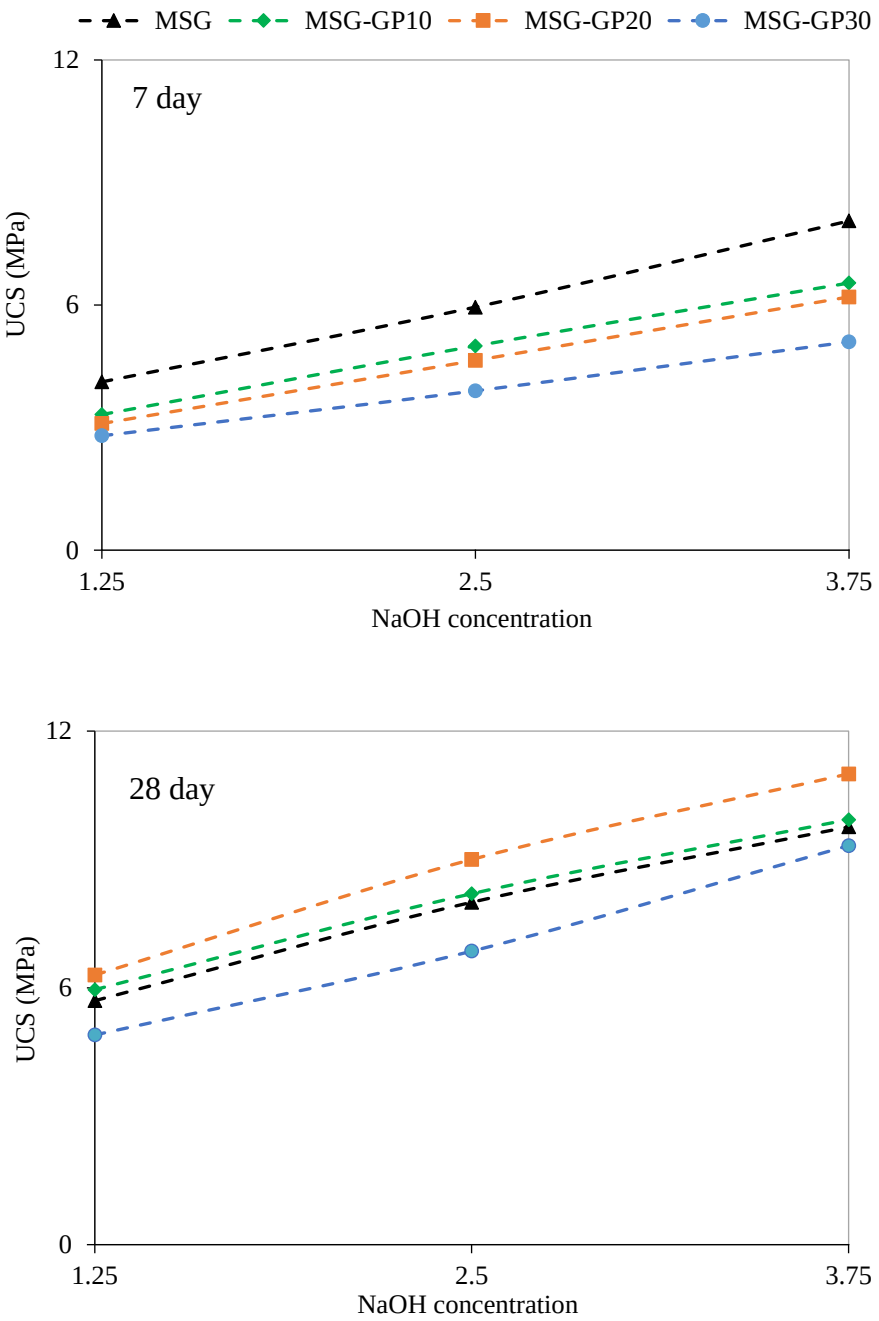

Figure 5.11 Effect of the sodium hydroxide concentration on the UCS of MSG grouts.

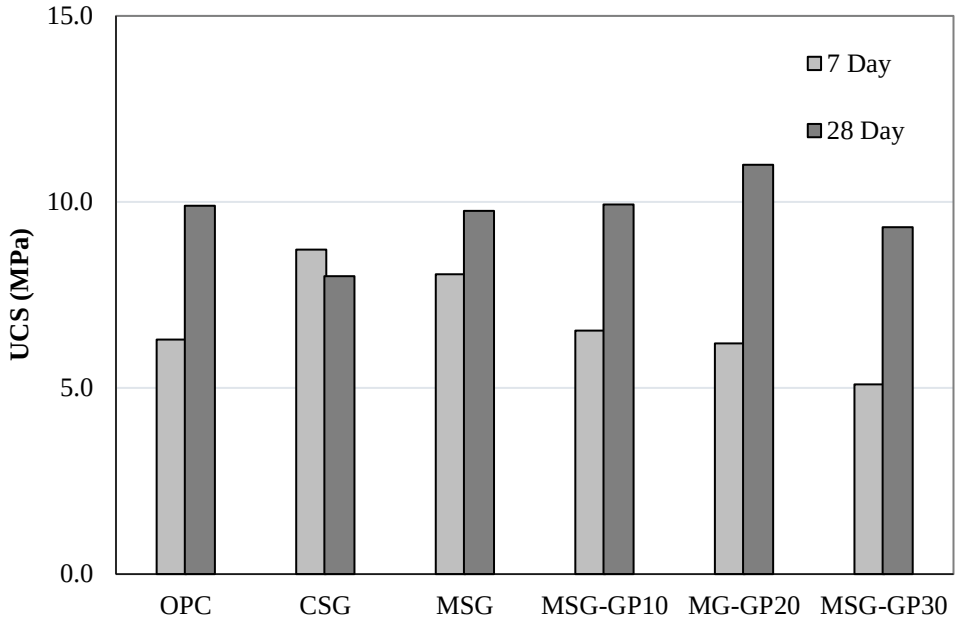

Figure 5.12 UCS of OPC, CSG, and MSG grouts.

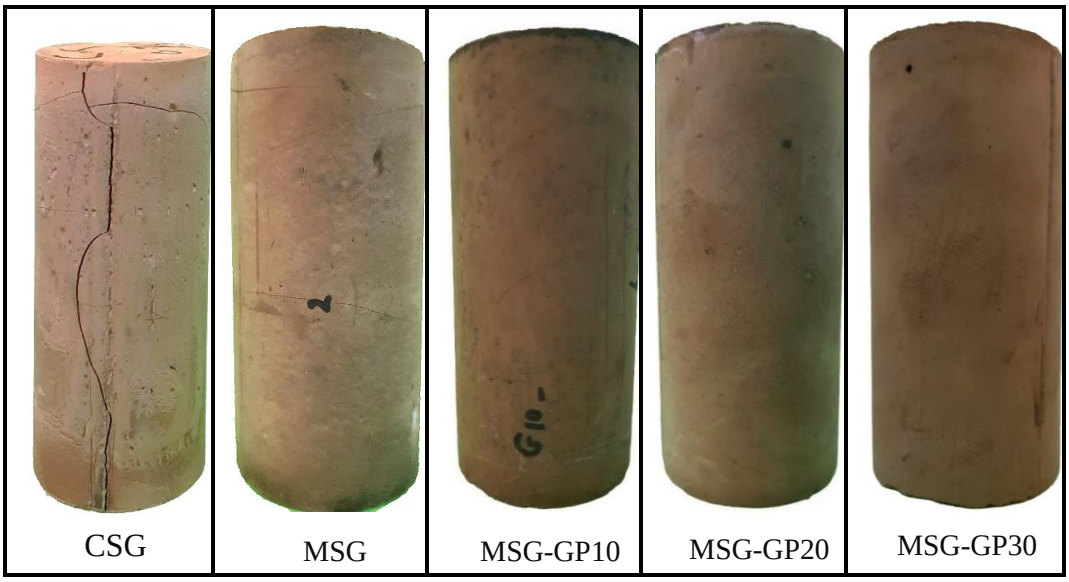

Figure 5.13 The visual appearance of CSG and MSG grouts.

5.7.2 Ultrasonic Pulse Velocity

Figure 5.14 presents the influence of molarity on UPV tests for MSG grouts at 7 and 28 days. It can be seen that the UPV values of MSG grout were enhanced significantly at the curing ages of 7 and 28 days. Based on the UPV classification presented in Table 3.8, all obtained specimens' hardened states ranged from low velocity to very low velocity (Anon, 1979). This indicates that the microstructure of hardened grout becomes denser as the curing period increases. It was observed that increasing NaOH concentration significantly influenced UPV measurements. In other words, the UPV increased as the molar concentration increased, and the highest UPV values were observed at 3.75 molarity. Moreover, the combined effect of sodium hydroxide concentration and glass powder content in geopolymer grout showed higher UPV values than those of control samples (MSG). For instance, the UPV of MSG, MSG-GP10, MSG-GP20, and MSG-GP30 increased by 31%, 44%, 50%, and 60% when the molarity of sodium hydroxide increased from 1.25 to 3.75 M, respectively due to the fact that the increasing NaOH concentration resulted in an increase in leaching conditions, including the quantity and rate of active ions (Al^{3+} and Si^{4+}), which constitute an important basis for GP as a precursor to participating in the geopolymerization reaction. Thus, the leaching environment for these active ions in GP has an effect on the reaction kinetics, mechanical characteristics, and microstructure formation of the geopolymer grout (S. Zhang et al., 2017). Besides, the UPV values of the MSG grout increased noticeably at different GP contents (Figure 5.15). The UPV of the MSG grout improved by 2 % and 6 % when GP content increased from10% to 20%. The improved performance of the UPV can be attributed to the integration of more silicon ions into the aluminosilicate network, which is provided by GP (Samarakoon et al., 2020). However, the UPV of MSG-GP30 decreased by 1.5% when slag was replaced with 30% compared to the MSG-GP20 mix. This reduction is due to in an insufficient amount of calcium and alumina in the reaction systems, reducing the amount of precipitated C-(N-) A-S-H, which may explain why MSG-GP30 had lower strengths than other mixtures (Samarakoon et al., 2020; Xiao et al., 2021). Additionally, the results reveal that the activation mechanism of geopolymer grout significantly affected the UPV values (Figure 5.15). The UPV values of MSG samples were

higher than CSG samples because the grinding of the precursor led to a reduction in particle size and increased the surface area of the slag and GP particles, lowering the porosity and raising the density of the geopolymer grout. Additionally, the polymerization process was significantly accelerated upon grinding due to the addition of aluminosilicate gel to the mixture, reducing the porosity and enhancing GP and slag particles (Sanjay Kumar & Kumar, 2011).

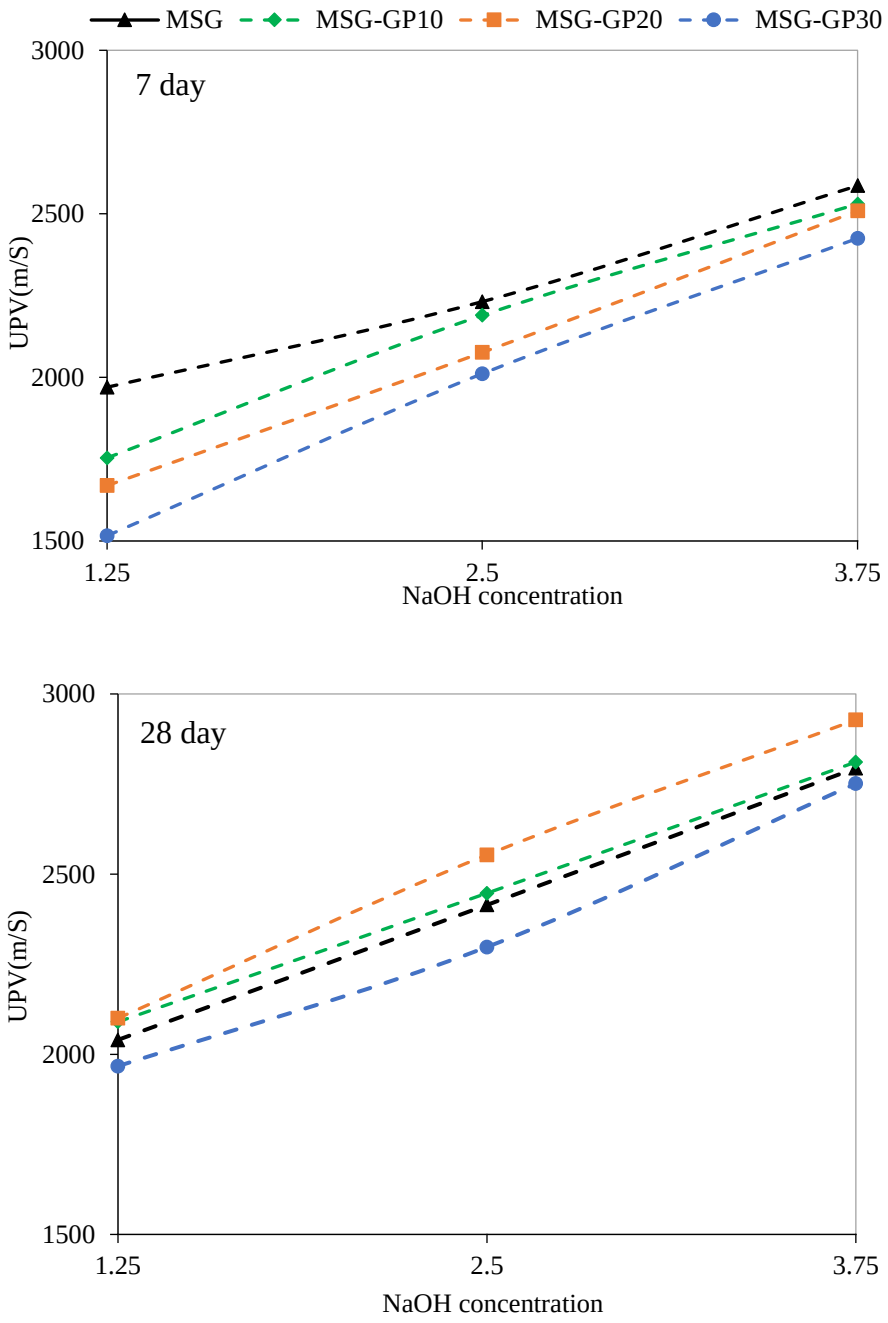

Figure 5.14 Effect of the NaOH concentration on the UPV of MSG grout.

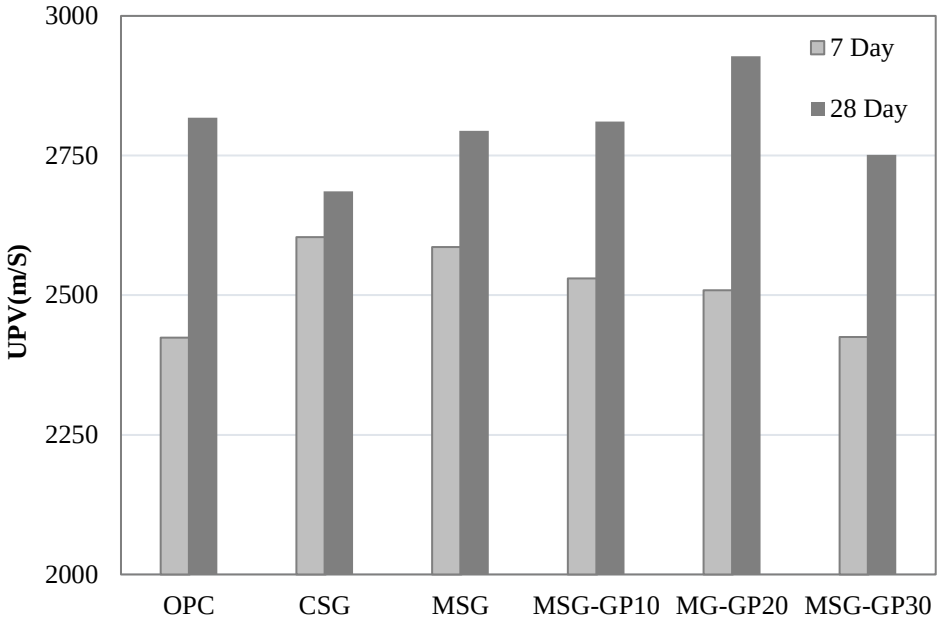

Figure 5.15 UPV of OPC, CSG, and MSG grouts.

5.8 Microstructural Analysis

Figure 5.16 shows the effect of the activation method on the microstructure characterization of MSG and CSG grouts. Notably, the activation method considerably impacts the microstructure of geopolymer grout. As seen in Figure 5.16a and b, many unreactive slag particles can be observed in CSG grout as compared to its counterpart MSG which did not include any unreactive slag particles due to the beneficial effect of mechanochemical treatment that increased surface area and reduced the particle size of slag, resulting in lower porosity and higher density in comparison with slag based-CSG grout. Additionally, significant cracks can be seen in CSG grout (Figure 5.16a) because of the poor connectivity of the reaction products (Hamid Abed, Sabbar Abbas, et al., 2022). It can be indicated that the mechanochemical activation method is more beneficial than the conventional activation method in densifying the compactness of grout's microstructure, and thus, the mechanical properties of MSG grout have been greatly enhanced. Furthermore, the geopolymerization reaction of MSG grout was dramatically enhanced during the ball milling process due to the creation of additional aluminosilicate gel in the mixture (Figure 5.16b); the produced gel has a more homogeneous microstructure which decreased the porosity and enhanced the

reaction rate of slag particles (Abbas et al., 2022). Figure 5.17 presents the influence of glass powder contents on the microstructure characterization of MSG grout. The results indicated that the MSG grout exhibited a more compact morphology with 20% GP replacements, and the reaction products became entirely completed. The number of non-reacted GP particles is limited, indicating that the inclusion of 20% GP promotes the formation of a highly dense microstructure (Figure 5.17a). In other words, the SEM micrographs of MSG-GP20 displayed a high compactness microstructure with less pores and no visible cracks in comparison with MSG micrographs (Figure 5.16b) and MSG-GP30 (Figure 5.17b). This reveals that 20% GP in MSG grout led to the production of additional aluminosilicate gels due to more reactive SiO_2 participating in the geopolymerization process (Khan et al., 2021a; Pascual et al., 2021; Samarakoon et al., 2020). Similarly, Jiang et al. (2020) observed that the geopolymer paste specimens with 20% GP had better homogeneity due to reactive SiO_2 and Al_2O_3, which contributed to the generation of hydrated sodium aluminosilicate gel (N–A–S– H). As a result, 20% slag replacement by glass powder improved the mechanical performance of slag-based MSG grout. This observation shows a good agreement with previous studies (Khan et al., 2021b; Liang, Li, et al., 2021). At 30 % GP, the microstructure of the MSG-GP30 is still denser and more compact than MSG; however, it showed a significant number of unreacted GP particles with many microcracks (Figure 5.17b). These microcracks may occur as a result of an excess of GP, which reduces the production of crosslinking structures in reaction products. Due to the excessive amount of GP, the interface between the glass powder particles and the MSG matrix was reduced. Therefore, the low mechanical interlocking and the formed microcracks resulted in lower densification and a lower mechanical performance of MSG-GP30 samples compared to MSG-GP20 samples, as shown in Figure 5.17b (Vásquez et al., 2016). This behavior is related to the considerable decrease in alumina content as the GP content increases as alumina is required for the formation of a stable polymer network (Novais et al., 2016). Therefore, partial slag replacement with 30% GP decreased the UCS of the geopolymer grout used for mechanochemical activation.

The FTIR spectra for all the geopolymer grout at age of 28 days are presented in Figure 5.18. It apparently illustrates that a band associated with the vibrations of

OH and H-OH at approximately 1640 and 2000 cm^{-1}, which was assigned to the existence of crystal or absorbed water produced during the reaction procedures. The strongest vibration of T-O-Si bonds at 900–1000 cm^{-1} (where T = tetrahedral Si or Al) could be attributed to the formation of gel phases (S. Zhang et al., 2017; Zuhua Zhang et al., 2012; Zhu, Liang, Xu, et al., 2019). This bond indicates the presence of geopolymerization resulting from the production of amorphous aluminosilicate phases; thus, this band can be used to determine the degree of polymerization (Karim et al., 2013; Sanjay Kumar et al., 2017; Tho-In et al., 2016). The FTIR spectrum reveals that the Si–O band at 940 cm^{-1} is more intense in the MSG grout than in the CSG grout, indicating that the mechanochemical activation method positively affected the geopolymerization rate of geopolymer grout (Hosseini et al., 2021). On the other hand, the intensity of the Si-O stretching bands at 950 cm^{1} becomes broader and more intense at a 20% GP replacement, owing to the formation of a more stable gel (Tho-In et al., 2016; S. Zhang et al., 2017). However, the wavenumber bands weaken in samples MSG-GP30 with the more addition of GP, which indicates that the excessive GP content plays a negative role in the procedure of reaction and is unfavorable to the formation of gel phases. This result is consistent with the change in the unconfined compressive strength. That is to say, the addition of GP dosage should not be beyond 20%.

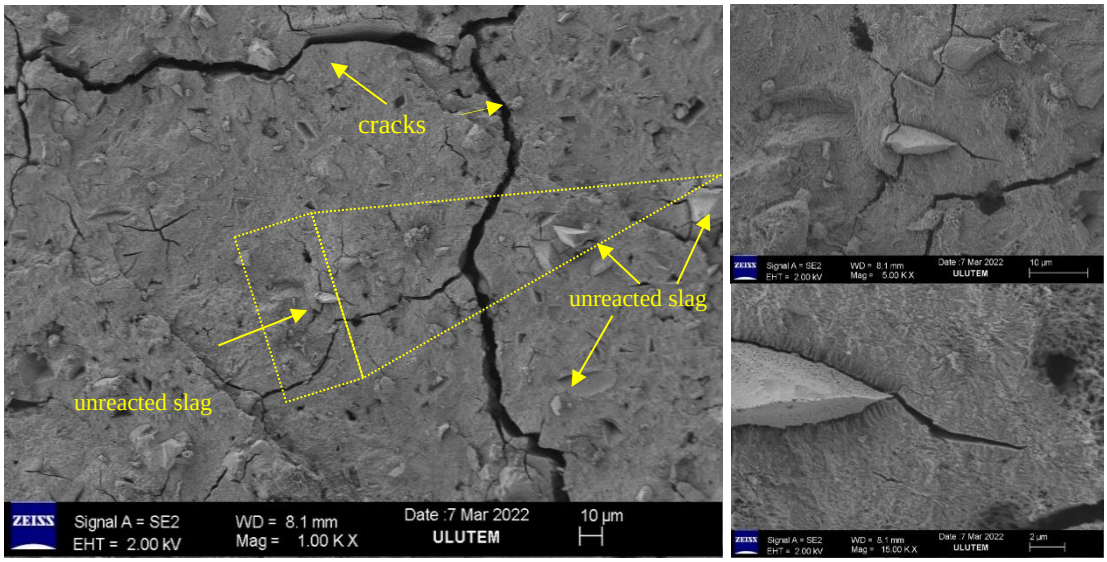

(a) CSG

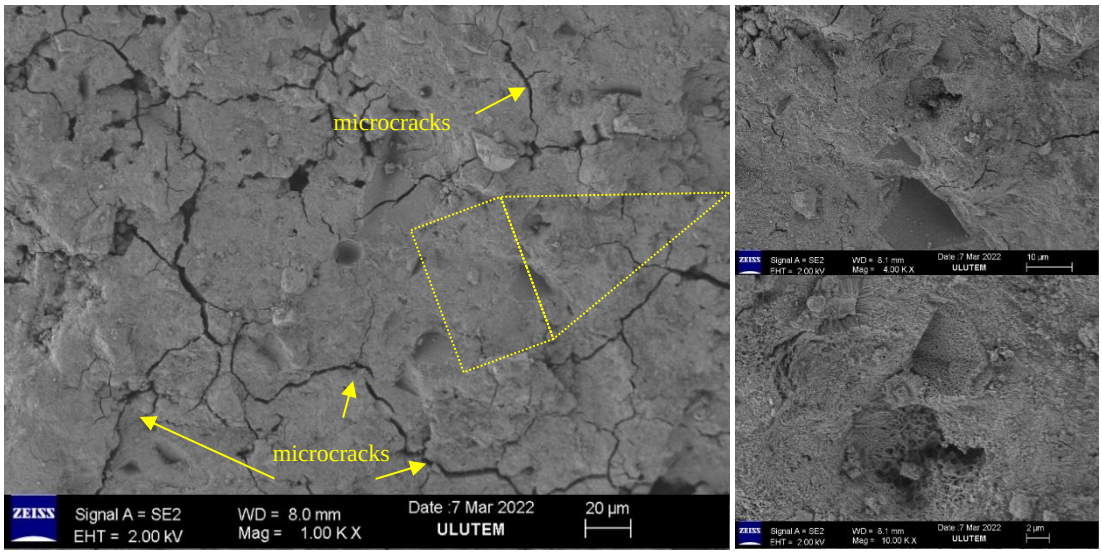

(b) MSG

Figure 5.16 SEM images of the hardened (a) CSG and (b) MSG grouts.

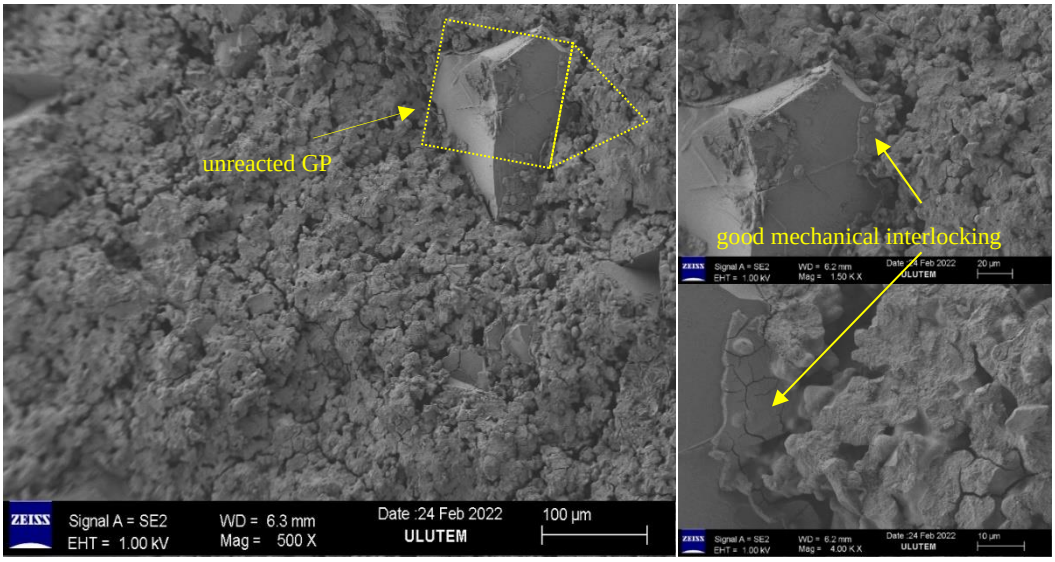

(a) MSG-GP20

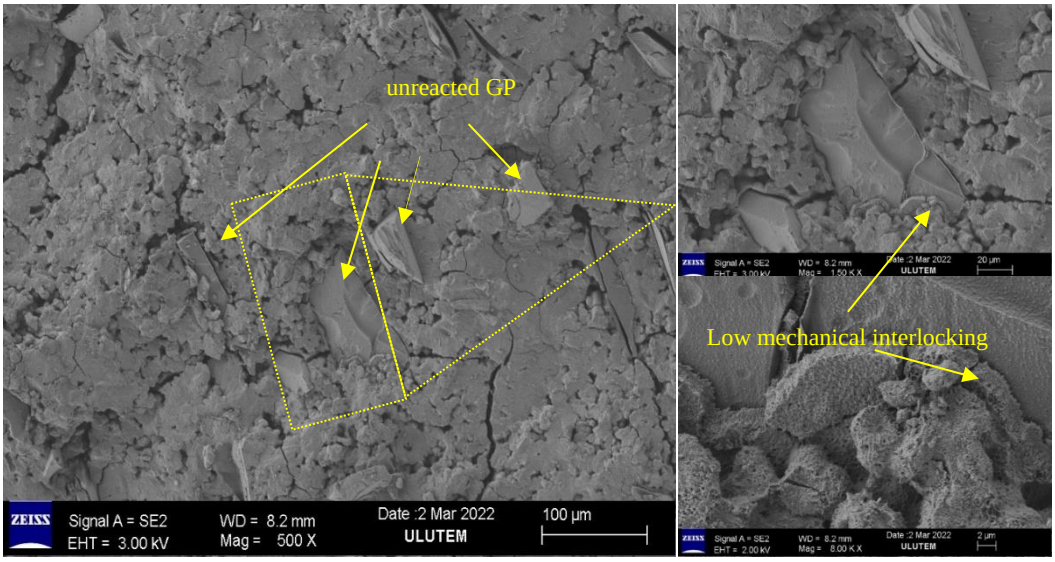

(b) MSG-GP30

Figure 5.17 SEM images of the hardened (a) MSG-GP20 and (c) MSG-GP30 grouts.

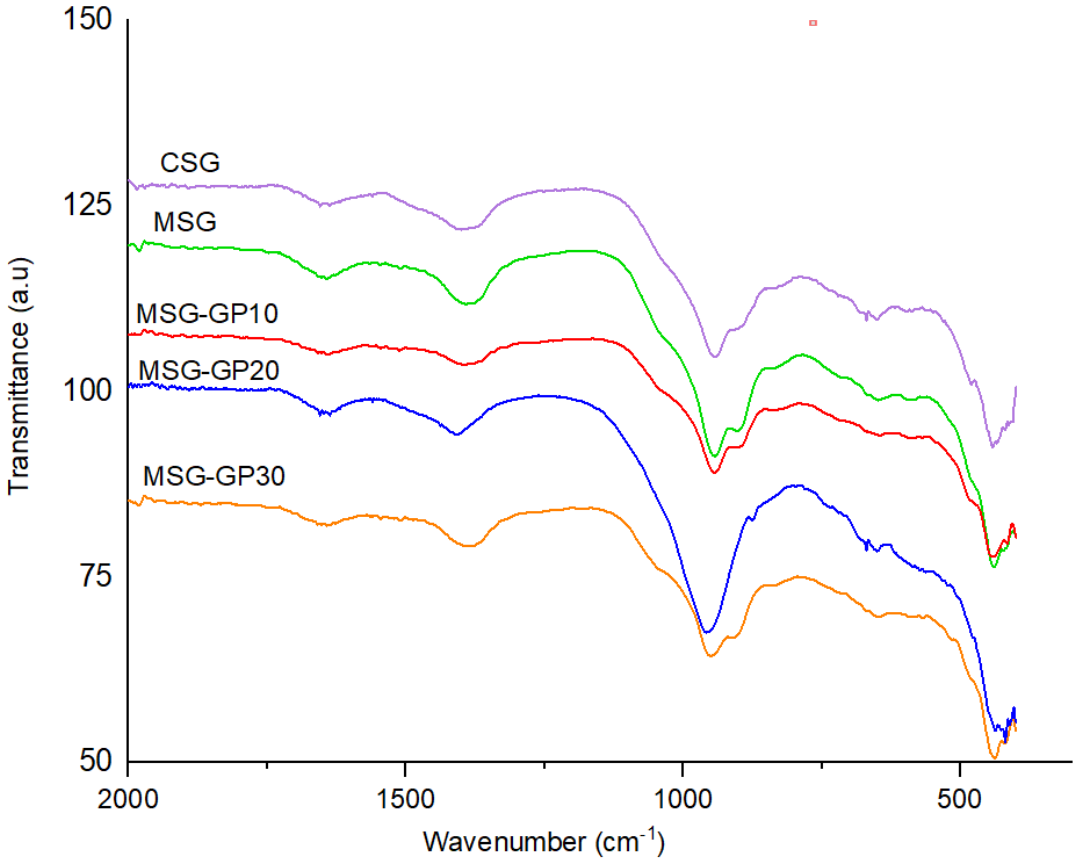

Figure 5.18 FTIR spectra of the hardened CSG, and MSG grouts.

5.9 Conclusions

In this research, the effects of glass powder and molar concentration of NaOH on the performance of mechanochemical geopolymer grout were investigated. Also, a conventionally activated geopolymer-based grout and an ordinary Portland cement (OPC) grout were also investigated for comparison. The rheological, fresh, mechanical and microstructural performances were examined for all obtained grouts. The conclusions were as follows:

- The apparent viscosity and shear stress of all MSG grouts dramatically decreased with the increasing GP content, while increasing as the molarity of NaOH increased. The yield stress and plastic viscosity values of the MSG grout were reduced by16-43% and 13-39% when slag was substituted with 0- 30% GP, respectively. Additionally, the yield stress and plastic viscosity of MSG grouts increased as NaOH concentration increased. Furthermore, the mechanochemical activation method positively affected the rheological properties of geopolymer grouts.
- The use of 0-30% glass powder increased the initial and final setting time of MSG grout between 33-50% and 33-78% as compared to the control mix (MSG), respectively. On the contrary, the setting time was considerably shortened with mechanochemical activation and a higher molar concentration of NaOH.
- The bleeding capacity of MSG grout increased from 0.025% to 0.55% when GP content increased from 0 to 30% due to its low water demand and filling impact compared to slag. Whereas the bleeding capacity of geopolymer grouts reduced as NaOH concentration increased. Moreover, the results also showed that the MSG grout had significantly less bleeding capacity than the CSG and OPC grouts.
- The substitution of 10–20% slag with glass powder enhanced the UCS of MSG grouts by 2–13% due to introducing more active silicon into the geopolymerization reaction process by glass powder, hence promoting the formation of additional gel phases. In addition, the UCS values of MSG grouts increased in the range of 40-90% as the NaOH concentration

increased from 1.25 to 3.75 M. Regarding the effect of the activation mechanism, the mechanochemical technique increased the strength of geopolymer grout by 18% in comparison to its conventional counterpart.

- The ultrasonic pulse velocity increased as GP content and sodium hydroxide molarity increased. The highest UPV was 2928 m/s for MSG grout with 20% GP content and 3.75 M, at 28 days. Besides, the results revealed that the UPV of MSG-GP20 ≥ OPC ≥ CSG grouts; hence, it can be inferred that GP can be used efficiently in mechanochemically activated geopolymer grout up to 20% replacement.
- The microstructural analysis confirmed that the activation method had a measurable effect on the microstructure of geopolymer grout because of the grinding process increased the surface area and reduced the particle size of slag, resulting in lower porosity and higher density than conventionally activated geopolymer grout samples. Furthermore, the SEM images demonstrated that the microstructure of MSG grout at 20% GP was densely compacted with less pores due to the enhanced polymerization of reaction products inside the structure, which contributed to the formation of additional aluminosilicate gels.

CHAPTER VI

ASSESSING THE MECHANICAL AND DURABILITY PROPERTIES OF ECO- AND USER-FRIENDLY MECHANOCHEMICALLY ACTIVATED SLAG/RHA GEOPOLYMER STABILIZERS FOR DEEP SOIL MIXING

6.1 Overview

This chapter investigates the potential application of mechanochemically activated geopolymer (MSG) stabilizers for deep soil mixing (DSM). This study investigated conventionally activated geopolymer-stabilized soil and ordinary Portland cement (OPC) stabilized soil for comparative purposes. The feasibility of utilizing rice husk ash (RHA) as a partial precursor in mechanochemically activated slag-based geopolymer (MSG) stabilized soil was examined using four RHA replacement ratios (0%, 10%, 20%, and 30% by the total precursor weight). The samples of deep soil mixing (OPC, MSG, and CSG) were immersed in a 1% magnesium sulfate ($MgSO_4$) solution for 60 and 120 days. A series of tests were conducted to assess the sulfate erosion resistance of the DSM specimens, including visual examination of appearance, measurement of mass changes, UPV, UCS, and FTIR. Table 6.1 displays the mixture proportions of OPC, MSG- and CSG-stabilized soils.

Table 6.1 Mix proportions deep mixing soil.

Mix ID	OPC grout %	geopolymer grout						Soil	
		Slag %	RHA %	NaOH %	Na_2SiO_3 %	Grinding duration: h	w/b	s/b	Wc
MSG	-	85	0	10	5	2	1	30	36
MSG-RH10	-	75	10	10	5	2	1	30	36
MSG-RH20	-	65	20	10	5	2	1	30	36
MSG-RH30	-	55	30	10	5	2	1	30	36
CSG	-	85	0	10	5	-	1	30	36
OPC	100	-	-	-	-	-	1	30	36

6.2 Strength Performance of DSM

Figure 6.1 depicts the UCS results of the geopolymer (MSG and CSG) and OPC-stabilized soil samples after 28 days of curing. Puppala et al. (2008) suggested a minimum 28-day UCS value of 1.034 MPa for ground improvement under embankments and earth constructions using the DSM technique utilizing cement as the binder, as shown in Figure 6.1 for comparison. It is obvious that MSG-stabilized soil attained the highest UCS, followed by CSG and OPC stabilizers; the UCS of MSG, CSG and OPC were 6.4, 5.5, and 4.9 MPa, respectively. Similar findings were reported by Arulrajah et al. (2018), Luo et al. (2022), and Ghadir & Ranjbar (2018), who used geopolymer in the deep ground improvement of soft soils and reported that the geopolymer performed better than OPC-stabilized mixtures; it can be due to the fact that both geopolymerization and pozzolanic reactions occur in geopolymer-stabilized mixtures (P. Nath & Sarker, 2017). Du et al. (2017) found that geopolymer-stabilized soil had a higher pozzolanic reaction and hence higher UCS values than cement-stabilized soil.

However, the findings from the conducted experiments have unveiled that the mechanical properties of DSM samples are significantly influenced by the activation method (mechanochemical activation) of the geopolymer binder. Specifically, the UCS values of MSG were 16 % higher than its counterpart CSG (Figure 6.1). According to Hamid Abed, et al., (2022) and Abbas et al., (2022) the mechanochemical activation process enhanced the surface area and reactivity of geopolymer binders, resulting in the formation of more gel within the geopolymer-stabilized matrix, and the total pore volume and porosity decreased, thereby strengthening the bond between soil particles and leading to an increase in the strength of the stabilized soil sample.

In addition, the UCS trend of MSG-stabilized soil increased with increasing partial substitution of slag with RHA up to 20%, and afterwards declined. Figure 6.1 illustrates that the UCS of the MSG improved by 4.3% and 12.5% for RHA levels of 10% and 20%, respectively, while it decreased by 4.7% for RHA levels of 30% compared to the mix without RHA after 28 days. The similar results have been found in previous studies (Liang, et al., 2019; Zhu, et al., 2019).The fine RHA particles include biogenic reactive silica, which accelerates the geopolymer polycondensation reaction and improves the dissolution of aluminosilicate components. Abbas et al. (2022) have reported that adding RHA increases the SiO_2/Al_2O_3 ratio, which in turn

increases the number of Si-O-Si bonds within the system. This leads to a change in the composition of the gel produced, which has a direct impact on the microstructure of the MSG-RHA stabilizer. The formation of tetrahedral aluminosilicate networks as a result of this process is responsible for the improvement in the unconfined compressive strength of the stabilizer (S. S. Hossain et al., 2021; A. Mehta & Siddique, 2018). However, the presence of excessive RHA (>30 wt%) in the MSG stabilizer adversely affects the UCS. The decreased strength values beyond 30% RHA were mainly due to the decreased alumina-silica dissolution caused by the theolubility difference between GGBS and RHA (A. Mehta & Siddique, 2018). In addition, the increase in the content of unreactive silica with the increased replacement levels of slag also hindered the polymerization process, resulting in decreased UCS values (Abbas et al., 2022).

As shown in Figure 6.1, an UPV test was conducted on MSG, CSG, and OPC-stabilized soil for the purpose of validating the results of the unconfined compressive strength test. The UPV values fall within the range of 2090 to 2475 m/s, corresponding to the very low-velocity degree described in previous work (Anon, 1979) (Table 3.8). This low strength and UPV quality may be attributable to the soil type employed in this investigation (clay) (Güllü et al., 2017). The results suggest that the UPV values follow a pattern comparable to the UCS findings. It is obvious that MSG-stabilized soil attained the highest UPV (2300 m/s), followed by CSG (2200 m/s) and OPC stabilizers (2090 m/s). In other words, the UCS of DSM samples with geopolymer stabilizer (MSG and CSG) was greater than that of cement-stabilized soil samples. Nath & Sarker (2017) noted that geopolymer possesses both enhanced pozzolanic and geopolymerization reactions.

Moreover, the activation method of the geopolymer binder had an effect on the UPV values; as shown in Figure 6.1, the UPV of MSG-stabilized soil samples was 4.5% higher than that of CSG-stabilized soil samples. It can be indicated that the mechanochemical synthesis process exceeds the conventional activation method in terms of increasing UPV values because the grinding process of source material reduced particle size and raised the surface area of geopolymeric particles, leading to decreased porosity and increased density of geopolymer stabilized soil (Hamid Abed, Abbas, et al., 2022; Hamid Abed, Sabbar Abbas, et al., 2022). Hamid Abed et al. (2022) demonstrated that the mechanochemical treatment of geopolymer binder is more advantageous for increasing the UPV values because the geopolymerization reaction of geopolymer binder increased significantly after the grinding process due to

the formation of additional geopolymeric gel in the mixture, which decreased the porosity and increased the reactivity of slag particles.

Furthermore, incorporating RHA into MSG-stabilized soil resulted in a higher increase in the UPV value. Figure 6.1 shows that the inclusion of RHA as slag replacement at 10 and 20% increased UPV values by 3.4% and 7.6%, respectively, compared to MSG samples without RHA (MSG) after 28 days. The presence of RHA enhances the filling of micropores via its filling effect and imparts more amorphous gel phases, resulting in a dense and strengthened link between soil particles and, consequently, a rise in the UPV of the MSG-stabilized soil (Abbas et al., 2022). Nonetheless, when 30% of the slag was substituted with RHA, the UPV trend decreased by 2% compared to the pure slag-based MSG-stabilized soil. The substitution with 30% RHA dramatically altered the Si/Al ratio due to the high silicon content in RHA (Long, 2021)(Liang, Zhu, Zhang, & Wu, 2019)(R. Chen et al., 2021). Silva et al. (2007) revealed that the Si/Al ratio significantly affected the mechanical properties of geopolymers. A very high Si/Al ratio produced aluminosilicate materials with limited crosslinking and diminished strength. Moreover, the relatively lower CaO level in RHA decreased the strength because the higher CaO amount in the geopolymer gel could create more hydrated products, such as C-A-S-H gel, in conjunction with the three-dimensional matrix network (X. Jiang et al., 2020; N. K. Lee & Lee, 2013).

In conclusion, the UPV of the DSM mixes was consistent with the strength rate change, with an increasing order at OPC < CSG < MSG-RH30<MSG <MSG-RH10< MSG-RH20. Therefore, the RHA can be effectively used in mechanochemical geopolymer stabilizers up to 20% replacement.

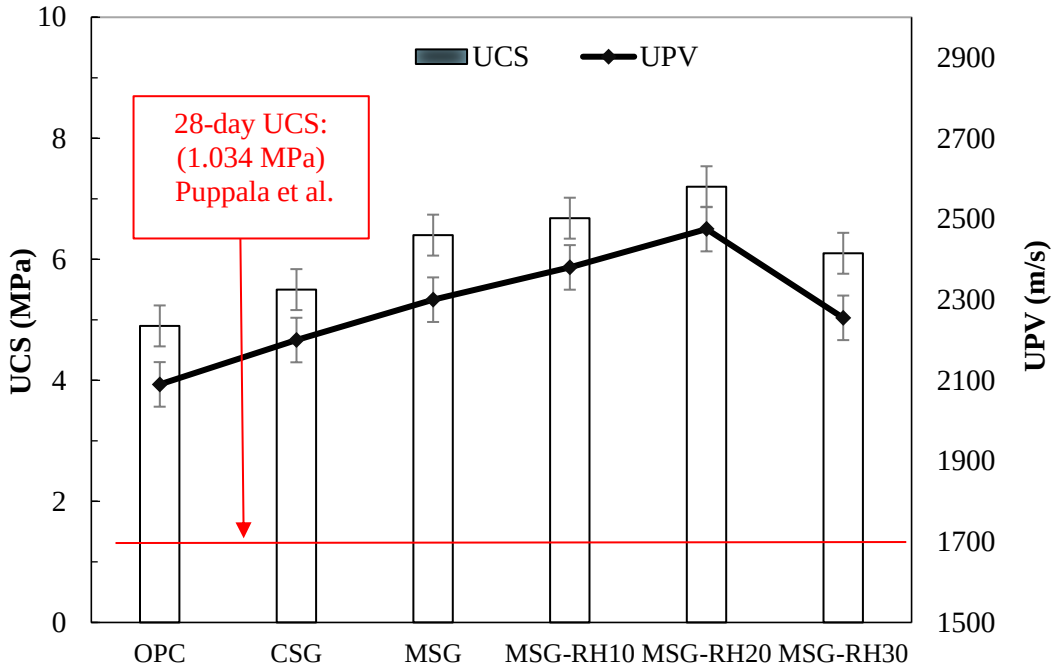

Figure 6.1 UCS and UPV of OPC, MSG and CSG- stabilized soil specimens.

6.3 Microstructure Analysis of Geopolymeric Precursor

Figure 6.2 depicts the effect of the activation method and slag substitution on the microstructure characterization of stabilized soils. Figures 6.2(a and b) show that the MSG-stabilized soil is denser and more compact than the CSG-stabilized soil. Furthermore, unreacted particles are more evident in CSG-stabilized soil, which developed less geopolymeric gels and resulted in a loose microstructure, in contrast to MSG-stabilized soil, which appeared to be well-connected by a gel-like network. This is due to the fact that the mechanochemical activation process increases the reactivity of the source materials, resulting in the development of additional gel as the primary reaction product and a gel-like network with greater interconnectivity (Hamid Abed, Abbas, et al., 2022; Hamid Abed, Sabbar Abbas, et al., 2022). In the microstructure of the soil samples, the gels overlapped and formed a high level of compactness. It may be concluded that the mechanochemical synthesis of raw materials would form hydrated gels that would increase the UCS values of MSG -stabilized soil.

The FTIR spectra of the DSM samples at 28 days are presented in Figure 6.3. The absorption bands at about 2500 cm^{-1} and the weak band at 1650 cm^{-1} relate to the stretching vibrations of O–H bonds and bending vibrations of H–O–H bonds in the absorbed water molecules. These bands indicate that water, present during geopolymerization, was absorbed on the surface or entrapped in the pores of the

geopolymer product (Fernández-Jiménez & Palomo, 2005; Swanepoel & Strydom, 2002) , the carbonate in the system was characterized by absorption at 1425 cm^{-1}, which was consistent with the presence of anorthite and calcite particularly in OPC samples (Farmer, 1976). The main binder gel band appeared at 1010 cm^{1}, assigned to the asymmetric stretching mode of the C–S–H structure formed in OPC samples, whereas the position at 1040 cm^{1} is consistent with N–A–S–H gels formed in geopolymer binder systems derived from solid precursor (Farmer, 1976; A. Mehta & Siddique, 2017a) In geopolymer stabilizers only based on slag or RHA, this vibration band had usually been identified between 950 and 1100 cm^{-1}, and it was typically associated with the binding gels (C–(A)–S–H for slag and N–A–S–H for RHA), with a lower wavenumber indicating a depolymerized or more highly substituted silicate gel, and higher wavenumbers being due to more crosslinked and highly siliceous gels (C. Li et al., 2010; Shi et al., 2011). According to Gao et al. (2013) and Karim et al. (2013),this band can be used to determine the degree of polymerization.

According to Figure 6.3, the vibrational component bands of the MSG and CSG stabilized soils in the FTIR spectrum differed. The change in the intensity of peaks was associated with the structural reorganization due to the activation mechanism (Hosseini et al., 2021). It should be noted that the main difference appeared in the low-frequency range (1000–500 cm^{-1}), where a high number of bands were observed; this is a region characteristic of amorphous Si–Al bonds. In the DSM samples prepared using mechanochemically activated geopolymer binder, there is an increase in the intensity of IR peaks indicating greater polymerization (Sanjay Kumar & Kumar, 2011). In addition, the appearance of these bands suggests the creation of three-dimensional ring interconnections associated with the higher strength performance of the MSG-stabilized soil (Gupta, Bhardwaj, Mishra, Mudgal, et al., 2017).

In addition, the intensity of the Si-O stretching bands at 1000 cm^{1} becomes broader and more intense with a 20% RHA replacement due to creating a more stable gel, which indicates a higher rate of geopolymerization than in the DSM samples (Tho-In et al., 2016; S. Zhang et al., 2017). However, the wavenumber bands weaken in samples MSG-RH30 with the more addition of RHA, which indicates that the excessive RHA content plays a negative role in the procedure of reaction and is unfavorable to the formation of gel phases. This result is consistent with the change in the unconfined compressive strength.

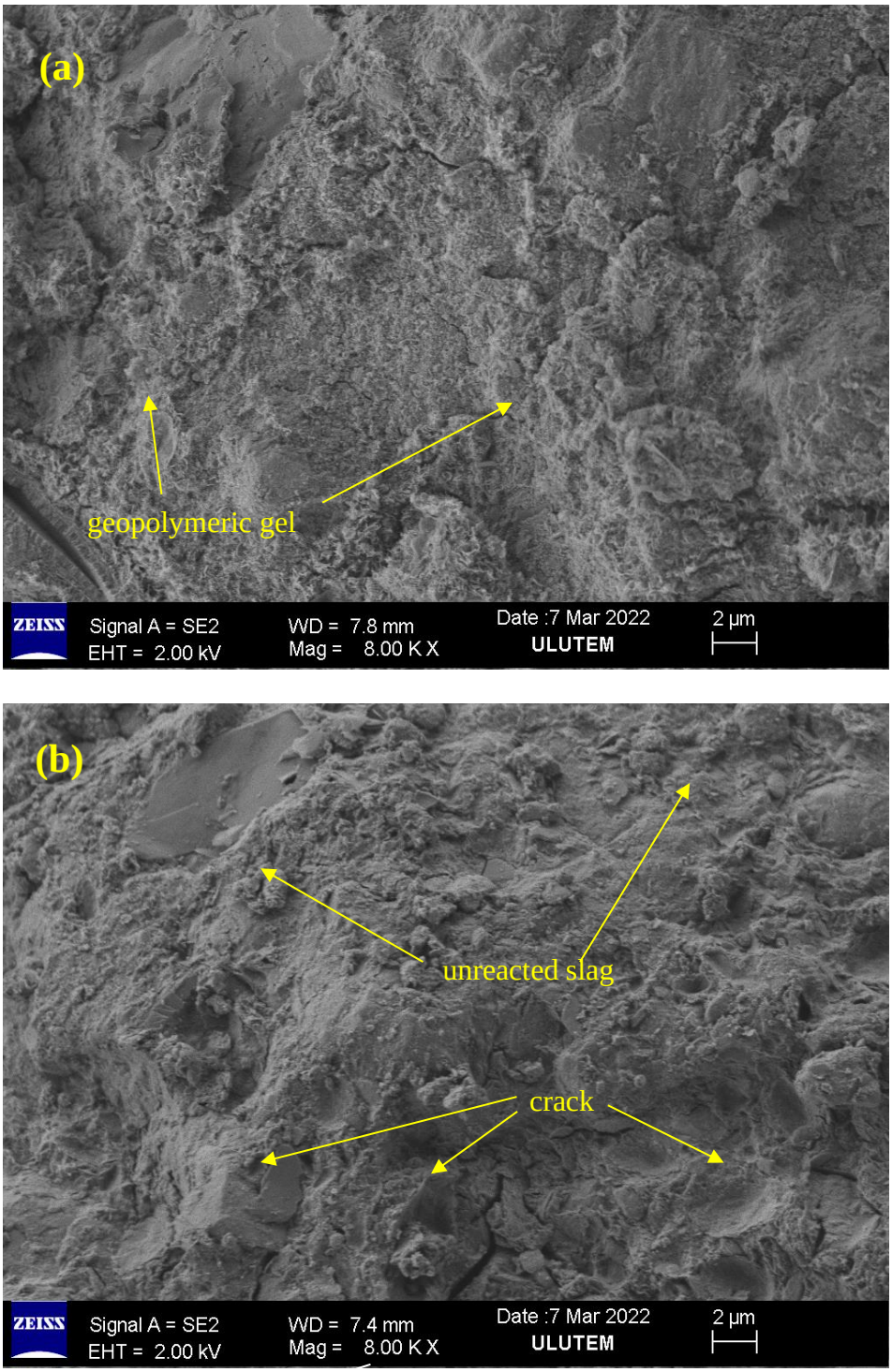

Figure 6.2 SEM images of geopolymer-stabilized soil ;(a) MSG; (b) CSG.

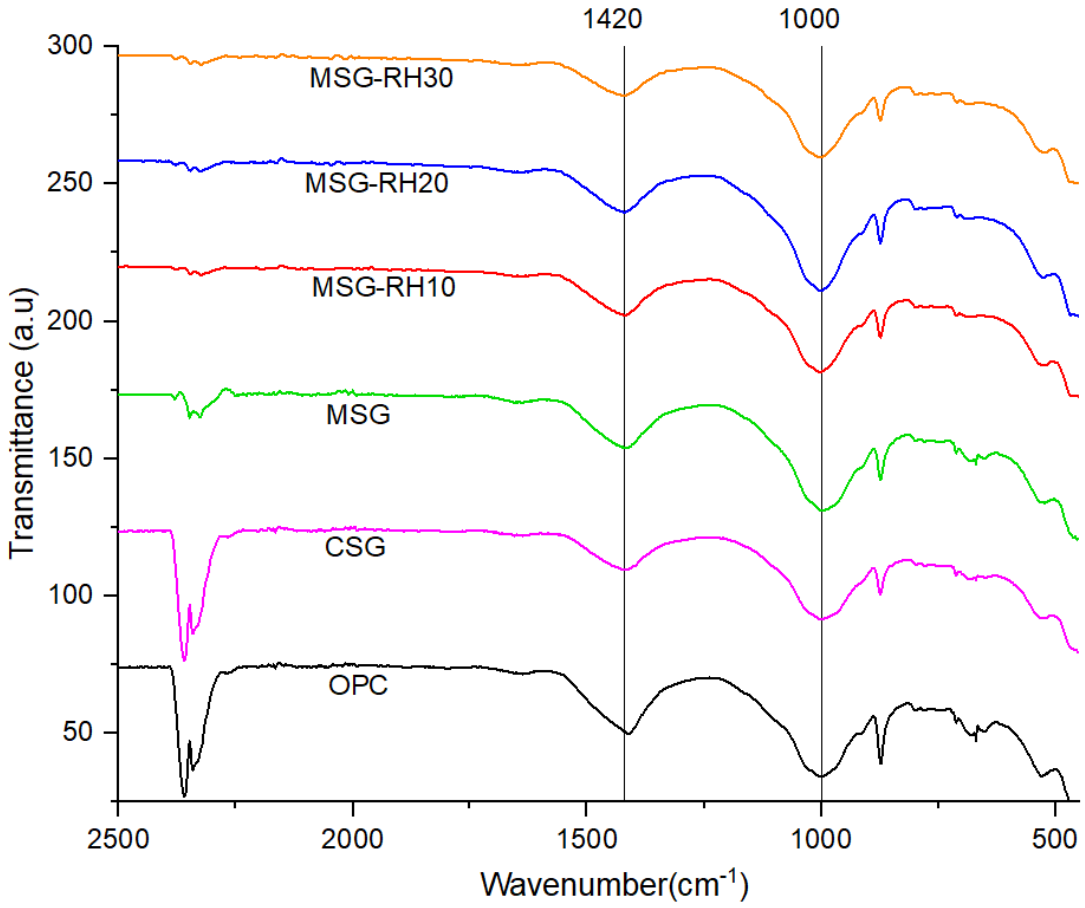

Figure 6.3 The FTIR spectra of OPC, MSG and CSG- stabilized soil.

6.4 Durability Studies

6.4.1 Resistance to Sulfate Sttack

6.4.1.1 Visual Sppearance

Figure 6.4 depicts images of DSM (OPC, CSG, and MSG) samples subjected to 1% magnesium sulfate solutions for 0, 60, and 120 days, respectively. It can be seen that the DSM samples immersed in $MgSO_4$ solution for 60 days exhibited minor deterioration, and their surfaces were slightly rough and coated with a layer of white precipitates, which was mainly ascribed to the formation of magnesium sulfate hydrate. The degree of deterioration of all DSM specimens increased with the risen in the exposure time to the magnesium sulfate solutions (Kwasny et al., 2018). However, as the immersion age increases, the deterioration of OPC appears to be more severe than that of geopolymer (MSG, CSG)-stabilized soils. The OPC surface shows many visible corrosions layers spalling observed, and varying degrees of falling off and

peeling appeared along the edges and corners at 120 days of immersion. This occurs because SO_4^{2-} in the sulfate solution enters the specimen via capillary adsorption to neutralize C-A-H, and Ca $(OH)_2$ chemically reacts to form expanding ettringite crystals (Rollings et al., 1999). The Increased ettringite caused expansion stress, which destroyed the soil's internal structure, increased porosity, and the number of connected pores (Luo, Zhang, et al., 2022). Saavedra et al. (2016) demonstrate that the OPC samples exhibit significant physical deterioration; delamination at the edges and a highly rough appearance were observed due to the greater dissolution and material loss, whereas for the geopolymer specimens, only slight surface deterioration was observed after 270 days of exposure.

Figure 6.4 reveals that the mechanochemically activated geopolymer stabilizer is more efficient in MSG-stabilized soil than the conventional (CSG) stabilizer. It was observed that the CSG-stabilized soil degraded considerably more than the MSG-stabilized soil; as immersion age increases, the surface of CSG exhibits a larger supply of corrosion layer flaking. In contrast, the MSG-stabilized soil specimens exposed to the same conditions exhibit limited physical deterioration; only salt deposits were observed on their surface, which does not compromise the mechanical integrity of the samples. The superior performance of MSG samples was attributed to the mechanochemical synthesis of the source material, which increased the surface area and reactivity of the geopolymeric binder, resulting in the production of more gel as the major reaction product; this gel filled the pore system, thereby preventing magnesium sulfate attack penetration (Abbas et al., 2022; Hamid Abed, Sabbar Abbas, et al., 2022). Furthermore, the presence of RHA particles causes a noticeable variation in the appearance of MSG specimens. Figure 6.4 demonstrates that MSG samples with 20% RHA exhibit less visual deterioration, discoloration, expansion, and cracking than other samples. According to Abbas et al. (2022) the addition of 20% RHA contributes to the filling effect or interpenetrating activity of other components in the geopolymer, resulting in a reduction in average pore diameters and a more compact structure. This reduces the permeation characteristics of the geopolymer, such as its external ion penetration rate and low sorptivity.

Nonetheless, at 30% RHA, MSG-RH30 degrades more rapidly than other MSG-stabilized soils. As the immersion age of MSG-RH30 increased, the surface gradually began to peel, and a visible corrosion layer and flaking occurred around the edges and corners. The substitution of 20% slag with RAHA resulted in modifying the CaO

content and matrix composition (in terms of SiO_2/Al_2O_3). According to According to Chen et al. (2021) the Ca^{2+} in (C, N)-A-S-H gel can be exchanged by external cations during a sulfate attack. Therefore, the high content of Ca has a certain negative effect on sulfate resistance. Therefore, the sulfate resistance of geopolymer is primarily dependent on the calcium concentration of the system, and it is preferable to select raw materials with a low calcium content in order to resist sulfate attack (A. Wang et al., 2020). Nonetheless, at 30% RHA, MSG-RH30 degrades more rapidly than other MSG-stabilized soils. As the immersion age of MSG-RH30 increased, the surface gradually began to peel, and a visible corrosion layer and flaking occurred around the edges and corners.

These results suggested that substituting 20% RHA for slag could reduce the deterioration potential of MSG, which may be due to the higher CaO content in slag compared to RHA (X. Jiang et al., 2020; Qu et al., 2021).

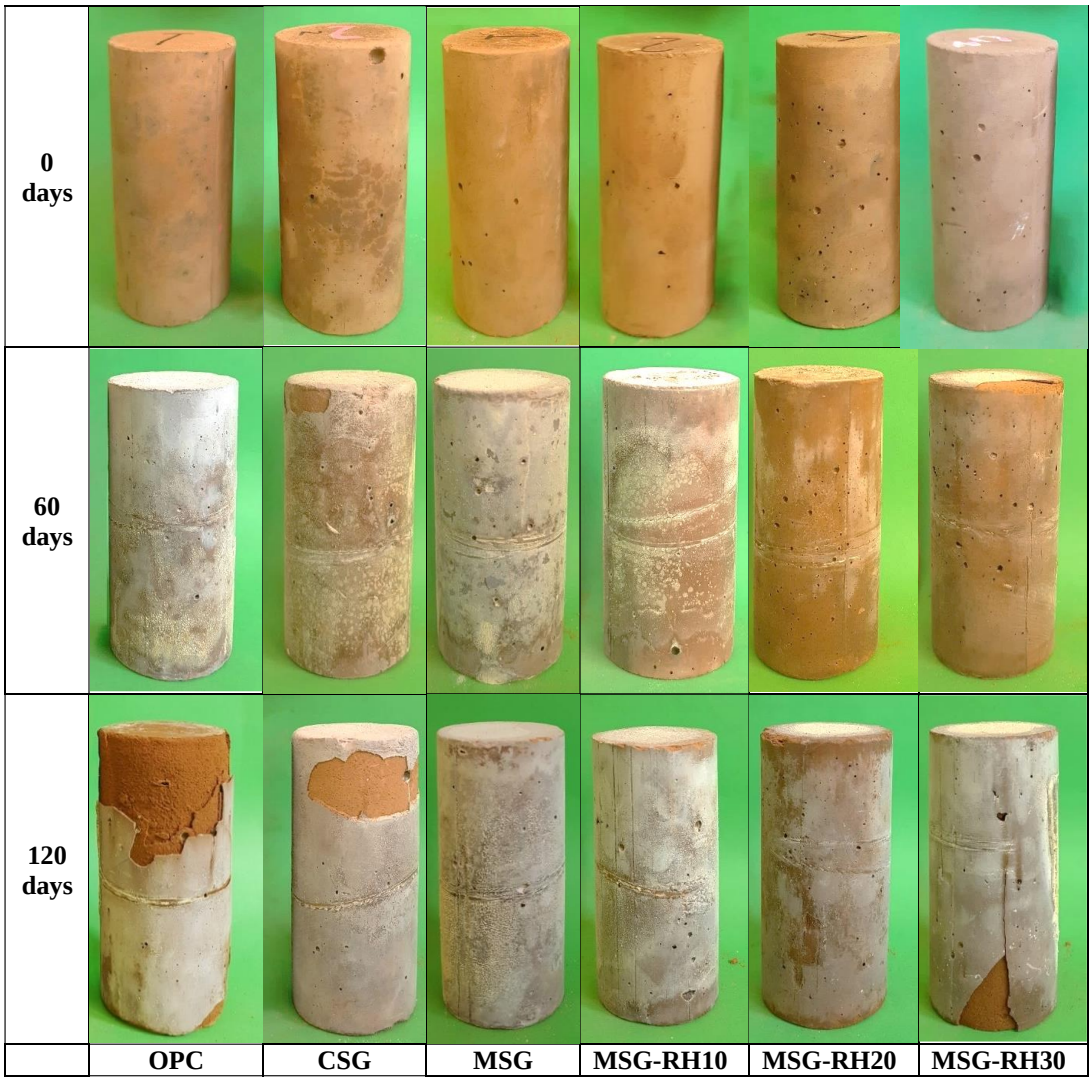

Figure 6.4 The visual appearance of OPC, MSG and CSG- stabilized soil samples exposed to sulfate solution.

6.4.1.2 Mass change

Figure 6.5 depicts the mass change of DSM samples stored at room temperature. The results showed that all DSM samples exhibited mass loss when stored at ambient temperature for up to 120 days. The mass loss of MSG samples was less than that of OPC and CSG samples stored at ambient temperature for up to 120 days; the mass loss of MSG, CSG and OPC stabilized soil samples after 120 days were -5.22%, -6.96 and -6.47%, respectively. The geopolymer-stabilized soil loses weight over time due to the evaporation of water contained in the sample during curing at ambient temperature. The geopolymer-stabilized soil loses weight over time due to the evaporation of water contained in the sample during curing at ambient temperature. For OPC samples, the weight loss is attributable to the ongoing hydration processes that occurred during

prolonged curing durations. On the other hand, the mass loss rate of MSG samples reduces as the partial substitution of slag with RHA reaches 20%. The lowest weight loss occurs in MSG-RH20 samples, which after 120 days loses -4.92%, followed by MSG-RH10 and MSG-RH30 samples with losses of -5.11% and -6.76%, respectively (Figure 6.5).

Figure 6.6 presents the mass loss of the DSM specimens after exposure to magnesium sulfate solution. The mass losses after various exposure durations were computed relative to the initial mass before exposure. In the same immersion period, the OPC-stabilized soil demonstrated a higher mass change than the geopolymer (MSG- and CSG) stabilized soils. The mass of the OPC specimens increased slightly (to a maximum of +1.1% of their mass at 30 days), and then rapidly declined, reaching a maximum decreasing of -5.47% at 120 days of exposure to the magnesium sulfate solutions. The early increase in the mass of OPC is due to the formation of expanding crystalline substances, such as ettringite inside the specimens (Ismail et al., 2013) and the absorption of the solution into the sample's microstructure (N. J. Jiang et al., 2018). Nevertheless, a period of 60 days of immersion, a significant reduction in mass was observed in the OPC sample. This could be attributed to erosion of the specimen by the ettringite crystal, resulting in severe surface peeling.

Kwasny et al. (2018) reported that the mass of geopolymer samples changed little after 90 and 120 days of exposure to a magnesium sulfate solution, which is superior to OPC samples. Similarly, Luo et al. (2022) indicate that the mass of geopolymer samples increased gradually with increasing immersion age, whereas the mass of OPC-stabilized so tended to increase and then decline with increasing immersion age. In general, these weight decreases correlate with the greater observed strength loss.

In addition, the activation mechanism of the geopolymer stabilizer had a significant effect on the mass change rate of DSM samples exposed to $MgSO_4$. The results show that the CSG and MSG specimens gained weight after 30, 60, and 90 days of chemical exposure; the weight gains of the MSG specimens were +0.67%, +1.14, and +1.55%, respectively, and +0.81%, +1.66, and +0.25% for the CSG samples. This was attributable to the fact that when subjected to the sulfate solution, the pores in the DSM samples absorbed the solution and thus increased the resultant mass at an early age. The previous studies also reported similar results (Ariffin et al., 2013; Çevik et al., 2018; Degirmenci, 2017; Ren et al., 2022). Also, Mehta & Siddique, (2017a) indicated that the increase in volume due to the absorbed solution was the primary reason for the

early-age mass increase of exposed geopolymer specimens. After 120 days of exposure, mass losses were recorded for CSG specimens (-0.59%), whereas a slight mass increase or constant mass was observed for MSG (+1.46%). The mass loss of CSG samples after 120 days of exposure was due to peeling and falling from samples surface layers in a sulfate environment (Çevik et al., 2018; Salami et al., 2017). According to Kwasny et al. (2018), the mass loss resulted from progressive surface layer degradation caused by pressure exerted by expansive crystals of the salts generated inside the pore structure. Meanwhile, the good behavior of the MSG samples is because mechanochemical activation increased the surface area and reactivity of the geopolymer binder, resulting in a greater amount of gel as the primary reaction product. This gel plugged the pore system and hindered sulfate from accessing the sample, leading in less weight change of MSG samples (Hamid Abed, Sabbar Abbas, et al., 2022)(Hamid Abed, Abbas, et al., 2022).

Moreover, the rate of mass change of MSG-stabilized soil decreased when partial substitution of slag with RHA increased up to 20%. The results showed the gain in mass in the 30 days of sulfate exposure by +0.67%, +0.7%, +0.64% & +1% for the MSG specimens with 0, 10, 20 & 30% RHA, respectively. Previous research Mehta & Siddique (2017b) identified the increase volume caused by the absorbed solution as the primary reason for the increased mass of geopolymer specimens after 28 days.

However, as exposure time increased, only the MSG-RH30 samples lost mass, whereas other MSG-stabilized soil samples gained mass. For instance, at 60 days, the mass change was +1.14%, +1.18%, +0.95%, and -0.4%, and at 120 days, it was +1.46, +1%, +0.76%, and -3.1% for specimens with 0, 10, 20, and 30% RHA, respectively (Figure 6.6). It can be observed that the MSG samples with 20% RHA have a lower mass change rate when compared to the other DSM samples. The less mass loss of the 20% RHA samples is ascribed to the low calcium content of MSG and more stable sodium aluminosilicate hydrate (N-A-S-H) gels (Abbas et al., 2022). The substitution of 20% slag with RAHA resulted in modifying the CaO content and matrix composition (in terms of SiO_2/Al_2O_3). According to Chen et al. (2021) the Ca^{2+} in (C, N)-A-S-H gel can be exchanged by external cations during a sulfate attack. Therefore, the high content of Ca has a certain negative effect on sulfate resistance. Therefore, the sulfate resistance of geopolymer primarily depends on the system's calcium concentration, and it is preferable to select raw materials with a low calcium content to resist sulfate attack (A. Wang et al., 2020). Nana et al. (2021) showed that 20%

RHA inclusion increases the release of SO_4^{-2}, hence enhancing the formation of gel and decreasing the open pores and absorption capacity of the samples.

Nonetheless, at 30% RHA, MSG-RH30 degrades more rapidly than other MSG-stabilized soils. As the immersion age of MSG-RH30 increased, the surface gradually began to peel, and spalling occurred in the surface layers which leads to reduce the mass of the sample.

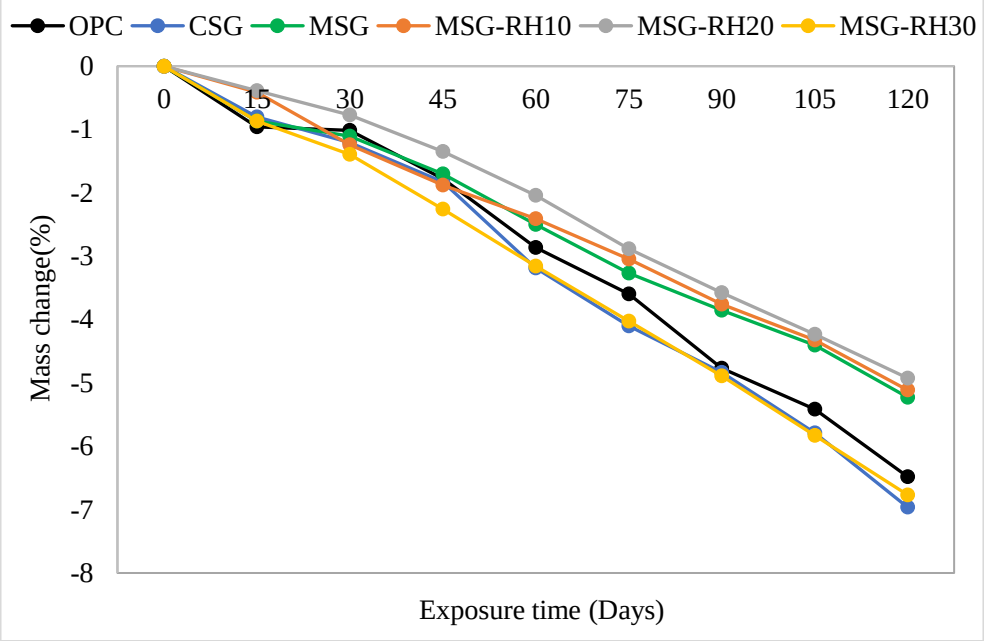

Figure 6.5 Mass change of OPC, MSG and CSG- stabilized soil specimens stored at ambient temperature.

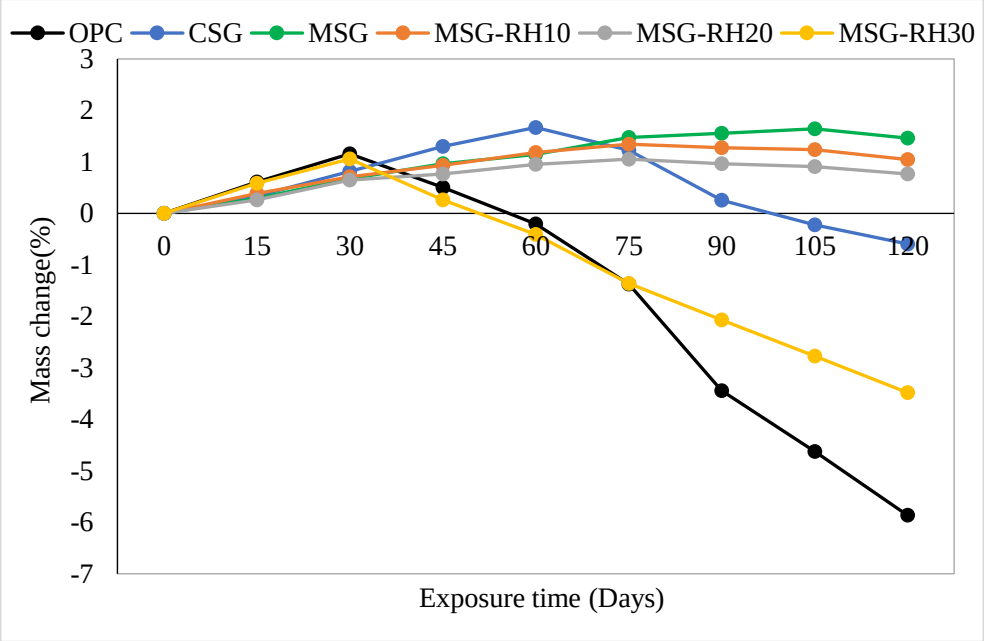

Figure 6.6 Mass change of OPC, MSG and CSG- stabilized soil specimens exposed to 1% $MgSO_4$ solution.

6.4.1.3 Strength loss

The unconfined compressive strength (UCS) of DSM specimens subjected to $MgSO_4$ solution for 0, 60, and 120 days is shown in Figure 6.7. Control samples (unexposed) were also displayed for comparison purposes (Figure 6.7a) . The UCS of OPC, CSG, and MSG samples maintained at room temperature climbed as curing time increased, with maximum UCS (9.2 MPa) recorded in MSG containing 20% RHA (MSG-RH20). Nonetheless, it is essential to note that the UCS responses (4.9 MPa-9.2 MPa) from all DSM samples satisfied the strength quality requirements (i.e., >0.4 MPa;(Coduto et al., 1999)) for the bearing capacity regarding ground improvement (Güllü & Ali Agha, 2021).

The residual unconfined compressive strength (%) of DSM sample specimens exposed to 1% $MgSO_4$ solution at different ages were also given in Table 6.2 and Figure 6.7b. The results revealed that the residual UCS of DSM samples dropped when exposed to $MgSO_4$ solution, and the rate of reduction increased as exposure time increased. The residual UCS for OPC, CSG and MSG samples were 65%, 71% and 75% for 60 days, whereas more declined to 47%, 58% and 63 %, respectively, after 120 days of immersion. However, the experimental results shows that the maximum strength loss was seen in the case of OPC specimens, while geopolymer stabilized soil (MSG and

CSG) specimens exhibited minimal strength loss. According to Luo et al. (2022), a similar observation was made where geopolymer stabilized soil exhibited better resistance to sulfate erosion as compared to soil stabilized with cement. Likewise, Saavedra et al. (2016) reported that OPC samples exhibited greater deterioration following sulfate exposure due to chemical reactions between calcium hydroxide and calcium monosulfoaluminates, which resulted in the formation of gypsum and ettringite. These reactions led to decreased mechanical resistance, heightened volumetric expansions, and ultimately, the detachment of sample surface layers and the development of cracks. The superior performance of geopolymer samples subjected to $MgSO_4$ solution compared to OPC samples was also consistent with what has been observed in previous research (K. Chen et al., 2021; Elyamany et al., 2018).

On the other hand, the activation mechanism of the geopolymeric stabilizer has an appreciable effect on the residual unconfined compressive strength of DSM samples after exposure to magnesium sulfate solution. The residual UCS of MSG was 8% higher than the counterparts of CSG-stabilized soil samples (Figure 6.7b). It can be revealed that MSG samples performed better than CSG samples under magnesium sulfate attack due to the mechanochemical synthesis process of the geopolymeric binder, which reduced the particle size and increased the surface area of geopolymeric particles, thereby decreasing the porosity and raised the density of the geopolymeric binder. The low porosity of the MSG samples makes ionic species migration via the pore structure difficult and results in the least amount of deterioration during the test period. Also, the geopolymerization reaction rate of the MSG binder rose dramatically after grinding due to the development of more aluminosilicate gel in the mixture, which led to the creation of a more resistant structure against sulfate attack (Hamid Abed, Abbas, et al., 2022).

Notably, the mechanism underlying geopolymer deterioration in a sulfate environment varies depending on the calcium content, as reported by Chen et al. (2021). Specifically, an increase in the calcium content within the solution indicates that calcium-containing hydrates, such as C-S-H gel and C-(A)-S-H gel, exhibit less resistance to sulfate attack during the formation of gypsum and ettringite, as compared to N-A-S-H gels (Alcamand et al., 2018; Yan et al., 2019). Therefore, substituting slag with RHA altered the CaO content, and matrix composition (in terms of SiO_2/Al_2O_3) (see Table 3.2 and Table 3.4), which affected the residual strength values of MSG-RHA stabilized soil specimens. Table 6.2 shows partial replacement of slag with RHA

up to 10-20% recorded as the highest residual UCS and then decreased beyond that level; The residual strength ratio was 63%, 73%, 78% and 60% for the RHA contents of 0, 10%, 20%, and 30%, respectively, after 120 days of exposure. The reaction between calcium from slag and magnesium sulfate results in the decalcification of calcium silicate hydrate (C-S-H) gel, primarily due to the constant formation of gypsum, which explains why MSG specimens with 0 RHA (100 slag%) lost more strength compared to 10-20% RHA when exposed to sulfate attack (A. Wang et al., 2020).While in case, 10 and 20% RHA geopolymeric binders were the strength contributing products with strong Al-O and Si-O linkages that were less impacted by sulfate exposure (A. Mehta & Siddique, 2017b). Mehta & Siddique (2018) reveal that the increase in strength caused by the incorporation of RHA was due to the relatively greater SiO_2/Al_2O_3 ratio of RHA compared to slag; the presence of adequate silica strengthened the N-A-S-H gels, resulting in higher strength values.

At 30 % RHA, the residual UCS of the MSG-RH30 decreased by 3% compared to MSG after 120 days of exposure. The excessive RHA in the geopolymer mixture increased the silica content, inhibited the creation of strong N-(A)-S-H gels and negatively affected the structural intactnessv(Oyekan & Kamiyo, 2011). This also resulted in a weakened matrix and increased ion transport into the MSG-RH30 stabilized soil.

Table 6.2 Residual unconfined compressive strength (%) of DSM specimens exposed to 1% magnesium sulfate solution.

Exposure time (days)	**OPC**	**CSG**	**MSG**	**MSG-RH10**	**MSG-RH20**	**MSG-RH30**
0	100	100	100	100	100	100
60	65	71	75	79	85	77
120	47	58	63	73	78	60

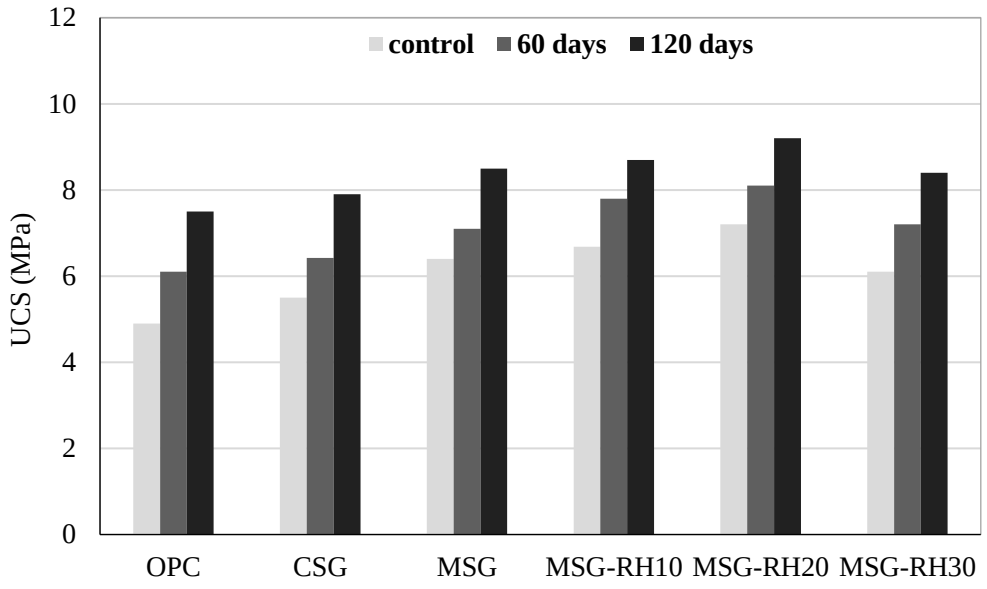

(a) UCS of DSM specimens stored at ambient temperature.

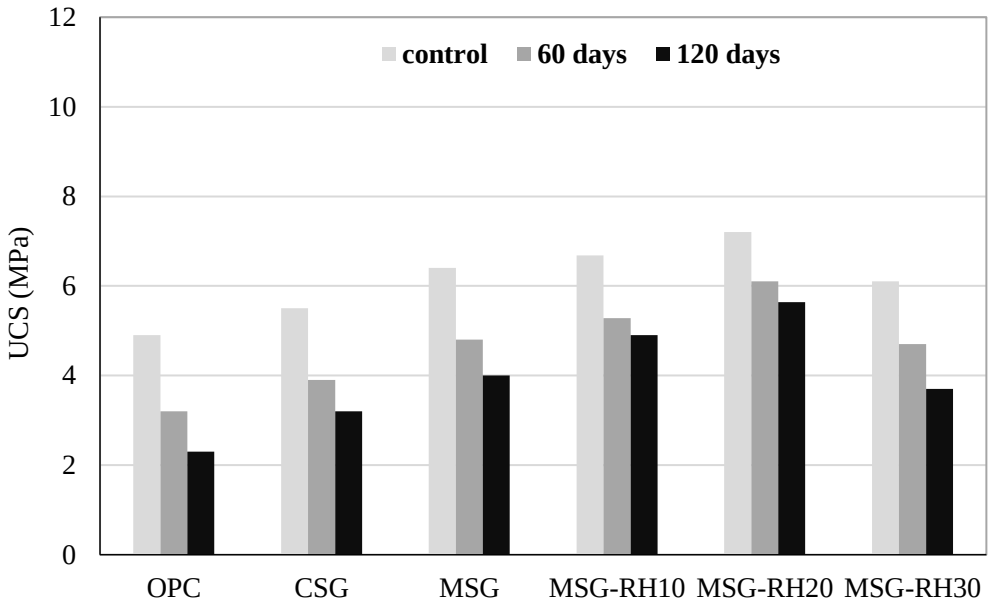

(b) UCS of DSM specimens exposed to $MgSO_4$ solution.

Figure 6.7 Unconfined compressive strength of unexposed and exposed OPC and CSG-stabilized soil, compared to samples of MSG with varying slag/RHA ratios.

6.4.1.4 Ultrasonic pulse velocity changes

Figure 6.8 shows the variation in UPV for OPC, MSG and CSG - stabilized soil specimens after 0, 60, and 120 days of exposure to magnesium sulfate. The results revealed that the UPV measurements decreased with increasing exposure time; The residual UPV values of OPC, CSG and MSG-stabilized soil samples were 81% , 84% and 87% after 60 days of immersion in a sulfate solution and were 67% 75, and 78% after 120 days compared to the control samples. (Elyamany et al., 2018). This behaviour is comparable to that observed in previous (Bakharev, 2005; Thokchom et al., 2010). It can be observed that DSM stabilized with geopolymer (MSG and CSG) showed lower losses of UPV than the OPC. In OPC systems, $MgSO_4$ are diffused through various channels into OPC-stabilized soil, followed by a reaction with cement hydration products. The main reaction products are ettringite, gypsum, and thaumasite, which result in expansion and crack spalling of OPC-stabilized soil. The breakdown of C–S–H also causes disintegration (K. Chen et al., 2021)(Taylor & Gollop, 1997).

Regarding the effect of the activation method of the geopolymer binder on the resistance of DSM samples to sulfate attack. The exposed MSG-stabilized soil samples exhibited a lesser drop in UPV values than their CSG-stabilized counterparts; the UPV values of CSG were 4% lower than the MSG-stabilized soil after 120 days (Figure 6.8). The lesser drop in UPV values of MSG-stabilized soil samples was attributable to the mechanochemical activation of the geopolymer binder. According to Hamid Abed, et al. (2022), the mechanochemical activation process increased the surface area and reactivity of geopolymer binders, which led to the production of additional gel within the geopolymer-stabilized matrix and a reduction in the overall pore volume and porosity. The reduced porosity of MSG samples makes it harder for ionic species to migrate through the pore structure, resulting in a structure that is more resistant to sulfate attack.

In addition, the UPV values of DSM samples with mechanochemically activated geopolymer stabilizers containing various amounts of RHA, which contributed favorably to the decrease of UPV loss, were higher than those of samples without RHA. The UPV values of MSG-stabilized soil declined by 87%, 88%, 91%, and 84% for samples containing 0,10,20 and 30% RHA, respectively, for 60 days and by 78%, 80%, 83%, and 77% after120 days of exposure (Figure 6.8). Accordingly, the MSG samples displayed the highest UPV loss rate, whilst the MSG-RH20 samples

demonstrated the lowest rate of UPV loss. However, the higher reduction in UPV of MSG samples with 100% slag (MSG) was caused by the development of cracks within the sample due to the diffusion of Ca^{2+} into the $MgSO_4$ solution (Bakharev, 2005). This finding was further supported by the studies of Jiang et al. (2018) and Luo et al., (2022), who attributed the decline in the strength of high-calcium geopolymer-stabilized soil immersed in sulfate solution to the formation of microcracks in the sample. In contrast, the lowest UPV reduction of MSG samples with 20% RHA substitution was attributable to the decreased Ca-content of the binder and the integration of additional silicon ions into the aluminosilicate network provided by RHA (Abbas et al., 2022; Long, 2021; Zabihi & Tavakoli, 2018). Similarly , Liang et al. (2019) and Zhu et al . (2019) observed that the geopolymer paste specimens with 20% RHA had better homogeneity due to reactive SiO_2 and Al_2O_3, which contributed to the generation of hydrated sodium aluminosilicate gel (N–A–S– H). As a result, 20% slag replacement by RHA showed a significant superiority for the generation of compact microstructure and reduction of connectivity between inner spaces of the sample, which restricted the entry of sulfate into the geopolymer matrix, thereby improving its resistance to sulfate attack (Abbas et al., 2022).

Notably, the 30% RHA of the MSG sample had a slightly lower UPV reduction than the 20% RHA sample. The higher amount of RHA substantially impacted the silica-alumina ratio due to the high silicon concentration in RHA. Silva et al. (2007) reported that the silica-alumina ratio had a substantial impact on the mechanical characteristics of the geopolymer. With a high silica-alumina ratio, low-crosslinked aluminosilicate materials with reduced strengths were developed (Tho-In et al., 2016). Furthermore, excessive RHA creates a looser structure resulting from incomplete chemical reactions, as well as an increase in the number of unreacted components in the system (X. Jiang et al., 2020; Khan et al., 2021b), and this unfilled honeycomb-hole creates an inhomogeneous microstructure and enhances sulfate absorption (Zhu, Liang, Xu, et al., 2019) . Thus, it can be concluded that RHA up to 20% can be used as a precursor for geopolymer synthesis after mechanochemical treatment.

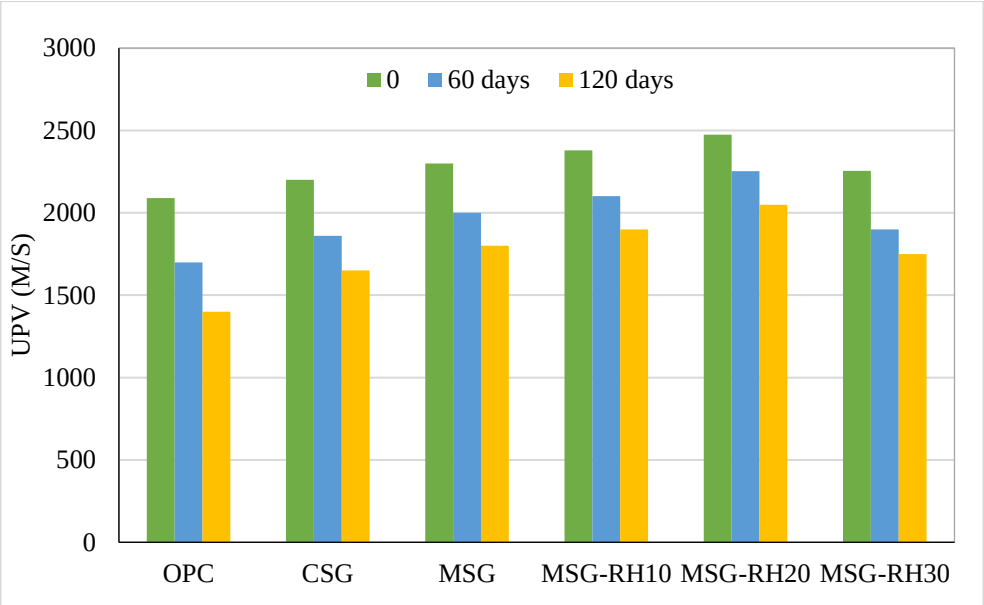

Figure 6.8 Ultrasonic pulse velocity of OPC, MSG and CSG- stabilized soil specimens exposed to 1% sulfate solution.

6.4.1.5 FTIR spectroscopy

Figure 6.9 illustrates the FTIR spectra acquired from the outermost surface layer of OPC, MSG, and CSG-stabilized soil specimens that underwent exposure to $MgSO_4$ solutions for a duration of 120 days. These spectra are compared to those obtained from the inner sections of control (unexposed) specimens stored under ambient temperature conditions. The unexposed DSM specimen featured a distinct and sharp band centered around 1000 cm^{-1}, which is attributed to asymmetric T-O stretching (T = Si or Al). Furthermore, a shoulder at approximately 860-880 cm^{-1} was observed, which is associated with M-O vibrations (M = K) (Gao et al., 2013; Kwasny et al., 2018). The band at 1420 cm^{-1} is assigned to the asymmetric modes of the calcite O–C–O bonds (Bernal et al., 2012). Lastly, the vibration band located at 2400 cm^{-1} is linked to the bending modes of the H–OH bonds of water molecules bonded to the hydration products (Gao et al., 2013).

In an experimental study conducted by Kwasny et al. (2018), the impact of sulfate solutions on OPC-stabilized soil was investigated. The study revealed that exposure to sulfate solutions decreased the intensity of a band observed at 985 cm^{-1}, which can be attributed to the asymmetric Si-O stretching vibrations in C-S-H. Furthermore, it was observed that the band at 2400 cm^{-1}, which is typically associated with O-H stretching vibrations in calcium hydroxide, was absent in samples exposed to sulfate solutions.

Conversely, the intensity of a broad shoulder corresponding to the asymmetric stretching vibrations of SO_4^{2-} in ettringite increased in samples immersed in sulfate solutions (Kwasny et al., 2018; Peyvandi et al., 2015). These findings suggest that exposure to sulfate solutions can significantly impact the chemical composition and structural integrity of OPC-stabilized soil and should be considered when designing and constructing infrastructure in areas with high sulfate concentrations.

In the case of soil stabilized with geopolymer (MSG, CSG), the spectra varied relatively little, with the exception of an increase in the intensity, but not the position, of the principal band centered approximately 1000 cm^1, and the band at 2400 cm^{-1} was significantly diminished in CSG stabilized soil samples. Meanwhile, the MSG-stabilized soil exhibited less spectral change than their CSG counterparts after exposed to the $MgSO_4$ environment, indicating that the mechanochemical activation approach positively influenced the improved resistance of the geopolymer stabilizer against the sulfate attack. Furthermore, the MSG-stabilized soil with 20% RHA exhibited no noticeable change in the spectra before and after exposure to the $MgSO_4$ attack, which suggested that the original structure of the MSG-RH20 samples was not affected after exposure. The incorporation of 20% RHA contributes to the filling effect or interpenetrating action between the presence of other components in the geopolymer, leading to a decrease in average pore diameters and a more compact structure (Abbas et al., 2022). This decreases the geopolymer's permeation properties, such as its external ion penetration rate (such as sulfate ion permeability) and low sorptivity (Zhu, Liang, Xu, et al., 2019). As a result, a 20% replacement of slag by RHA improved the sulfate attack of MSG-stabilized soil.

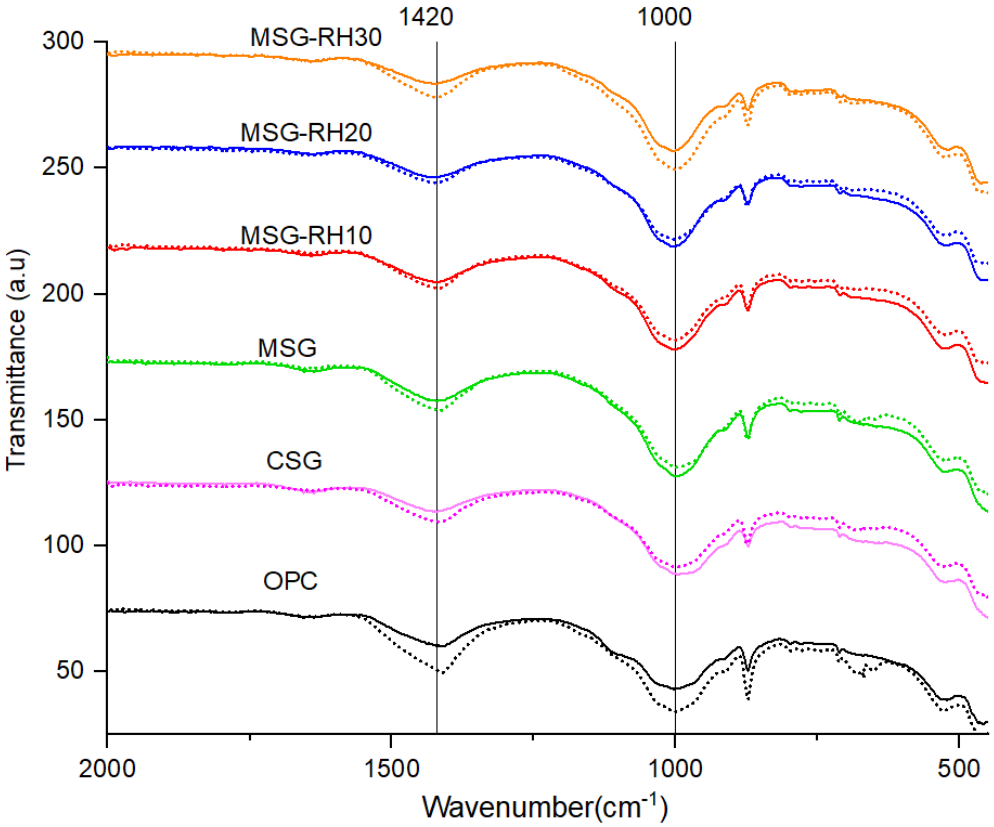

Figure 6.9 FTIR spectra of unexposed and exposed OPC and CSG-stabilized soil, compared to samples of MSG with varying slag/RHA ratios.

6.5 Conclusions

- The results show that MSG-stabilized soil attained the highest UCS, followed by CSG and OPC stabilizers; the UCS of MSG, CSG and OPC were 6.4, 5.5, and 4.9 MPa, respectively
- The UCS trend of MSG-stabilized soil increased with increasing partial substitution of slag with RHA up to 20% and afterward declined.
- The MSG-stabilized soil is denser and more compact than the CSG-stabilized soil. Furthermore, unreacted particles are more evident in CSG-stabilized soil, which developed less geopolymeric gels and resulted in a loose microstructure, in contrast to MSG-stabilized soil, which appeared to be well-connected by a gel-like network.
- The surface of the OPC exhibited numerous visible corrosion layers, and there were varying degrees of spalling, falling off, and peeling along the edges and corners at 120 days of immersion.
- The surface of CSG exhibits a larger supply of corrosion layer flaking. In contrast, the MSG-stabilized soil specimens exposed to the same conditions exhibited limited physical deterioration; only salt deposits were observed on their surface.
- The MSG samples with 20% RHA exhibit less visual deterioration, discoloration, expansion, and cracking than other DSM samples.
- The experimental results show that the maximum strength loss was seen in the case of OPC specimens, while geopolymer-stabilized soil (MSG and CSG) specimens exhibited minimal strength loss. In addition, the residual UCS of MSG was 8% higher than the counterparts of CSG-stabilized soil samples. It can be revealed that MSG samples performed better than CSG samples under a magnesium sulfate attack.
- Partial replacement of slag with RHA up to 10-20% was recorded as the highest residual UCS due to the relatively greater SiO_2/Al_2O_3 ratio of RHA compared to slag; the presence of adequate silica strengthened the N-(A)-S-H gels.

CHAPTER VII

EVALUATION OF THE MECHANICAL AND DURABILITY PROPERTIES OF ECO- AND USER-FRIENDLY MECHANOCHEMICALLY ACTIVATED SLAG/GLASS POWDER GEOPOLYMER STABILIZERS FOR DEEP SOIL MIXING

7.1 Overview

This chapter examines the possibility of using slag-based mechanochemically activated geopolymer (MSG) stabilizers for deep soil mixing (DSM), along with conventionally activated geopolymer (CSG) and ordinary Portland cement (OPC) stabilizers for comparison. The study investigates the feasibility of using glass powder (GP) as a partial precursor in MSG stabilizers at different replacement ratios (0%, 10%, 20%, and 30% by the total precursor weight). The DSM specimens were subjected to immersion in a 1% sulfate ($MgSO_4$) solution for 60 and 120 days to evaluate their sulfate erosion resistance, with testing including appearance, mass changes, (UPV), (UCS), and FTIR spectra. The study results provide insights into the potential application of MSG stabilizers in DSM projects. Table 7.1 displays the mixture proportions of OPC, MSG- and CSG-stabilized soils.

Table 7.1 Mix proportions deep mixing soil.

Mix ID	OPC grout %	geopolymer grout						Soil	
		Slag %	GP %	NaOH %	Na_2SiO_3 %	Grinding duration: h	w/b	s/b	Wc %
MSG	-	85	0	10	5	2	1	30	36
MSG-GP10	-	75	10	10	5	2	1	30	36
MSG-GP20	-	65	20	10	5	2	1	30	36
MSG-GP30	-	55	30	10	5	2	1	30	36
CSG	-	85	0	10	5	-	1	30	36
OPC	100	-	-	-	-	-	1	30	36

7.2 Strength Performance of DSM

Figure 7.1 depicts the UCS values of the geopolymer and OPC-stabilized soil samples after 28 days of curing. The UCS of geopolymer (MSG, CSG) stabilized soil samples was clearly greater than that of OPC stabilized soil specimens; the UCS of MSG, CSG, and OPC were 6.4, 5.5, and 4.9 MPa, respectively. Similar findings were reported by Arulrajah et al. (2018), Luo et al., (2022), and Ghadir and Ranjbar, (2018b), who used geopolymer in the deep ground improvement of soft soils and reported that the geopolymer performed better than OPC-stabilized mixtures. The increased strength of geopolymer-stabilized soil specimens is attributable to the disintegration of additional Si^{4+} and Al^{3+} ions from the slag, which contributes to the creation of both geopolymeric gel and hydration products (P. Nath & Sarker, 2017; Sahoo & Prasad Singh, 2022). Geopolymer-stabilized mixtures exhibit geopolymerization and pozzolanic reactions, according to Du et al. (2017).

Regarding the activation mechanism of the geopolymer binder, the experimental results indicated that the mechanochemical activation of the geopolymer binder significantly impacts the mechanical characteristics of DSM samples; the UCS values of MSG were 16 % higher than its counterpart CSG (Figure 7.1). According to Hamid Abed et al. (2022) and Abbas et al., (2022) the mechanochemical activation process enhanced the surface area and reactivity of geopolymer binders, resulting in the formation of more gel within the geopolymer-stabilized matrix and the total pore volume and porosity decreased, thereby strengthening the bond between soil particles and leading to an increase in the strength of the stabilized soil sample.

Furthermore, concerning the feasibility of utilizing GP as a partial precursor in MSG stabilizers, Figure 7.1 demonstrates that the UCS of soil stabilized with MSG increased the most at a GP content of 10%, followed by 20%, then declined after this proportion. The UCS of MSG increased by 9.4% and 4.6% for GP contents of 10% and 20%, respectively, while it decreased by 1.6% for GP content of 30% compared to the mixture without GP. The low development of UCS in geopolymer-stabilized soil samples containing 100% slag can be attributed to the rapid solidification rate and coagulation of the geopolymer slurry, resulting in poor fluidity and difficulty in achieving uniform spreading of the slurry in the soil. This reduces the effective contact area between the slurry and soil particles, as reported by Wang and Scrivener, (1995)

and Shi and Day, (1996). The higher UCS value observed in the MSG-stabilized soil with 10% GP content is attributed to the presence of active silica and alumina mineral components in GP.

The hydration reactions between the components and the Ca^{2+} produced from the decomposition of slag produce several colloidal flocculation products such as C-S-H) and C-(A)-S-H, which significantly improve the soil strength (Jun et al., 2021; Samantasinghar & Singh, 2021). This observation is consistent with previous studies (Khan et al., 2021b; Liang, Li, et al., 2021). However, the presence of excessive GP (>30 wt %) decreased the UCS because the higher content of GP leads to not participating in the hydration reaction and only act as a mineral additive, hence increasing porosity (Luo, Luo, et al., 2022; Palomo et al., 1999).In addition, the higher amount of GP substantially impacted the silica-alumina ratio due to the high silicon concentration in GP (Tho-In et al., 2016).

As shown in Figure 7.1, the UPV test was conducted on MSG, CSG, and OPC-stabilized soil for the purpose of validating the results of the unconfined compressive strength test. The UPV values fall within the range of 2090 to 2500 m/s, corresponding to the very low-velocity degree described in previous work (Anon, 1979) (Table 3.8). This low strength and UPV quality may be attributable to the soil type employed in this investigation (clay) (Güllü et al., 2017). The results suggest that the UPV values follow a pattern comparable to the UCS findings. It is obvious that MSG-stabilized soil attained the highest UPV (2500 m/s), followed by CSG (2200 m/s) and OPC stabilizers (2090 m/s). In other words, the UCS of geopolymer stabilized soil samples (MSG and CSG) was greater than that of OPC-stabilized soil samples. Nath and Sarker, (2017) noted that geopolymer possesses both enhanced pozzolanic and geopolymerization reactions.

Moreover, the activation method of the geopolymer binder had an effect on the UPV values; as shown in Figure 7.1, the UPV of MSG-stabilized soil samples was 4.5% higher than that of CSG-stabilized soil samples. It can be indicated that the mechanochemical synthesis process exceeds the conventional activation method in terms of increasing UPV values because the grinding process of source material reduced particle size and raised the surface area of geopolymeric particles, leading to decreased porosity and increased density of geopolymer stabilized soil (Hamid Abed, Abbas, et al., 2022; Hamid Abed, Sabbar Abbas, et al., 2022). Hamid Abed et al., (2022a) showed that the mechanochemical treatment of geopolymer binder is more

beneficial for raising UPV values because the geopolymerization reaction of geopolymer binder increased significantly after the grinding process due to the formation of additional geopolymeric gel in the mixture, which decreased the porosity and increased the reactivity of slag particles.

The incorporation of GP into MSG-stabilized soil by 10% resulted in a higher increase in the UPV value. As shown in Figure 7.1, the inclusion of GP as slag replacement at 10 and 20% increased UPV values by 8.7% and 7.4%, respectively, compared to MSG samples without GP (MSG) after 28 days. The reason for the optimal ultrasonic pulse velocity UPV in MSG-GP10 could be due to the presence of a balanced quantity of SiO_2 and Al_2O_3. This balanced composition may provide sufficient Si and Al, which are necessary for the polymerization process that forms the gel structure, thereby optimizing the UPV. Nonetheless, when 30% of the slag was substituted with GP, the UPV trend decreased to 3.2 and 2% compared to the compared to MSG samples with 10% and 20% GP. This decrease is attributed to insufficient calcium and alumina in the reaction systems, which decreased the amount of precipitated C-(N-) A-S-H, which may explain why MSG-GP30 had lower strengths than other mixtures (Samarakoon et al., 2020; Xiao et al., 2021).

It can be concluded, the UPV of the DSM mixes was consistent with the strength rate change, with an increasing order at OPC < CSG < MSG <MSG-GP30<MSG-GP20<MSG-GP10. Therefore, the GP can be effectively used in mechanochemical geopolymer stabilizers up to 20% replacement.

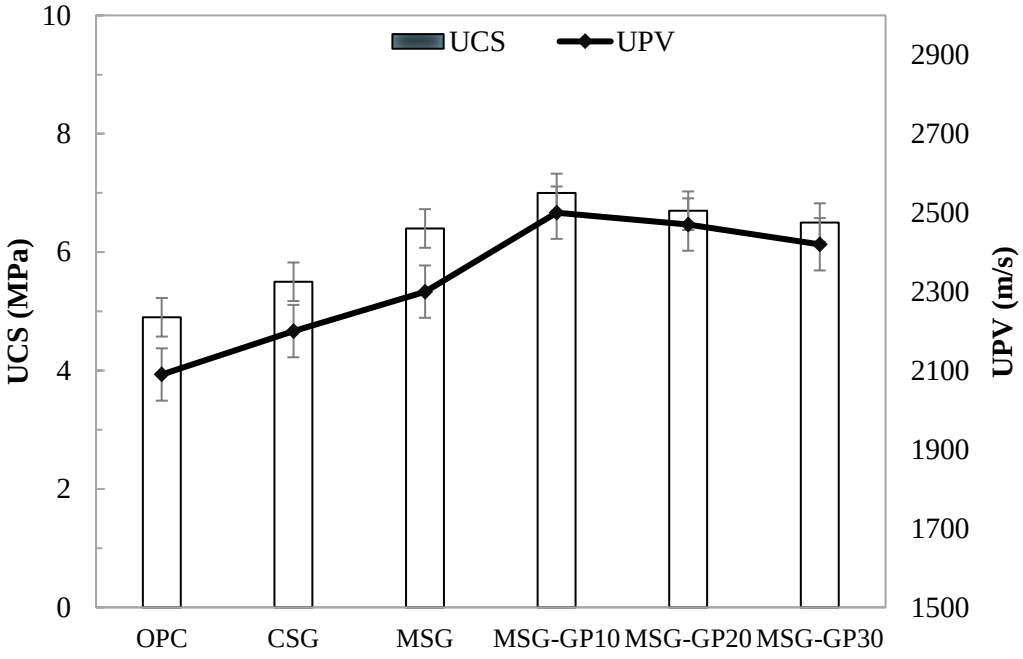

Figure 7.1 UCS and UPV of OPC, MSG and CSG- stabilized soil specimens.

7.3 Durability Studies

7.3.1 Resistance to Sulfate Sttack

7.3.1.1 Visual Appearance

Figure 7.2 depicts the appearances of DSM (OPC, CSG, and MSG) samples before and after immersion in 1% $MgSO_4$ solution for 60 and 120 days, respectively. The visual appearance results indicate that DSM specimens, which were subjected to immersion in $MgSO_4$ solution for a period of 60 days, showed only slight deterioration. The surfaces of these specimens appeared slightly rough, and a layer of white precipitates was observed, primarily attributed to the formation of magnesium sulfate hydrate. Notably, no significant visual degradation, such as surface erosion or cracking, was observed in any specimens. The results of the study suggest that there was only a slight modification in the visual characteristics of the samples following exposure, indicating that there was minimal alteration in their appearance when compared to their original condition. The extent of degradation of all DSM specimens increased as exposure time to magnesium sulfate solutions increased (Kwasny et al., 2018). However, with an increase in immersion age to 120 days, the degradation of OPC seems to be more severe than that of geopolymer (MSG, CSG)-stabilized soils. OPC deterioration is generally attributed because it contains hydration products of Ca

$(OH)_2$ and C-A-H, which leads to the formation of expansive products within specimens exposed to sulfate sources such as ettringite and gypsum which causes expansion, spalling, and cracking in the specimens. This occurs because SO_4^{2-} in the sulfate solution enters the specimen via capillary adsorption to neutralize Ca $(OH)_2$ and C-A-H and chemically reacts to form expanding ettringite crystals (Rollings et al., 1999). The Increased ettringite caused expansion stress, which led to the destruction of the soil's internal structure, increased porosity, and the number of connected pores (Luo, Zhang, et al., 2022). Valencia Saavedra et al. (2016) conducted a study that demonstrated the substantial physical deterioration of OPC samples, characterized by delamination at the edges and a markedly rough appearance, attributed to greater dissolution and material loss, whereas the geopolymer specimens exhibited only minimal surface deterioration even after 270 days of exposure.

The impact of the activation mechanism on the visual inspection of MSG and CSG-stabilized soil samples exposed to magnesium sulfates was analyzed and presented in Figure 7.2. The CSG samples demonstrated minimal visible damage and remained structurally sound, with only minor erosions observed at the corners and edges after 60 days of exposure. However, the CSG specimens exhibited color changes due to the formation of a white covering approximately 1 mm thick on their surfaces, consistent with the findings of Salami et al. (2017). According to Ye et al. (2019), the production of gypsum and ettringite is principally responsible for the white color of the samples. As the duration of exposure increased, the appearance of the CSG-stabilized soil samples displayed significant degradation against sulfate attack, manifested as surface erosion, expansion, and surface cracking after 120 days of exposure, compared to the control specimens. In other words, the extent of erosion increased with an increase in the exposure duration. This chemical change is commonly attributed to the crystallization pressures generated by the development of salts, such as gypsum and ettringite, which increase with the duration of exposure, as noted by Helson et al. (2018). In contrast, the MSG-stabilized soil specimens exposed to the same conditions exhibit limited physical deterioration; only salt deposits were observed on their surface, which does not compromise the mechanical integrity of the samples. The superior performance of MSG specimens was attributed to the mechanochemical synthesis of the source material, which increased the surface area and reactivity of the geopolymeric binder, resulting in the production of more gel as the major reaction

product; this gel filled the pore system, thereby preventing magnesium sulfate attack penetration (Abbas et al., 2022; Hamid Abed, Sabbar Abbas, et al., 2022).

Figure 7.2 shows that MSG specimens with 20% glass powder exhibit less visual deterioration than other specimens. These results suggested that substituting 20% GP for slag could reduce the deterioration potential of MSG, which may be due to the higher CaO content in slag compared to GP, the high CaO content in 100% slag content specimens considerably increases the possibility of ettringite and gypsum formation during exposure to sulfate solution (X. Jiang et al., 2020; Qu et al., 2021).

Figure 7.2 The visual appearance of OPC, MSG and CSG- stabilized soil samples exposed to sulfate solution.

7.3.1.2 Mass change

Figure 7.3 depicts the change in the mass of DSM samples stored at room temperature. The results showed that all DSM samples exhibited mass loss during a storage period of up to 120 days at ambient temperature. The mass loss of MSG samples was less than that of OPC and CSG samples stored at ambient temperature for up to 120 days; the mass loss of MSG, CSG and OPC stabilized soil samples after 120 days were -5.22%, -6.96 and -6.47%, respectively. The geopolymer-stabilized soil loses weight over time due to the evaporation of water contained in the sample during curing at ambient temperature. The geopolymer-stabilized soil loses weight over time due to the evaporation of water contained in the sample during curing at ambient temperature. For OPC samples, the weight loss is attributable to the ongoing hydration processes that occurred during protracted curing durations. On the other hand, the mass loss rate of MSG samples reduces as the partial substitution of slag with GP reaches 20%. The lowest weight loss occurs in MSG-GP10 samples, which after 120 days loses -4.46%, followed by MSG-GP20 and MSG-GP30 samples with losses of -6.3% and -8.3%, respectively (Figure 7.3).

Specimen mass change percentages of OPC, CSG and MSG stabilized soils at the same soaking time in the 1% $MgSO_4$ solution are shown in Figure 7.4. In the early soaking, the OPC-stabilized soil exhibited a greater mass change than the geopolymer (MSG and CSG) stabilized soils. The OPC samples gained a negligible amount of mass (up to +1.1% of their initial mass after 30 days). The initial increase in OPC mass was due to the development of expanding crystalline compounds, such as ettringite, within the sample (Ismail et al., 2013) and the absorption of the solution into the sample's microstructure (N. J. Jiang et al., 2018). Nevertheless, after 60, 90, and 120 days of immersion, a substantial decrease in the mass of the sample was observed, ultimately reaching a minimum value of -5.86%. This may be attributed to the erosion of the OPC specimen by the ettringite crystal, which may have led to a significant degree of surface peeling. Kwasny et al. (2018) reported that the mass of geopolymer samples changed little after 90 and 120 days of being subjected to a sulfate solution, which is superior to OPC samples. Similarly, Luo et al. (2022b) reported that the mass of geopolymer (MSG and CSG)-stabilized soil exhibited a gradual increase with an increase in immersion age, whereas the mass of OPC-stabilized soil demonstrated an initial increase followed by a subsequent decline with an increase in immersion age.

These observations are generally consistent with the greater strength loss observed in the samples.

In addition, the activation mechanism of the geopolymer stabilizer had a significant effect on the mass change rate of DSM samples exposed to $MgSO_4$. The results show that the CSG and MSG specimens gained weight after 30, 60, and 90 days of chemical exposure; the weight gains of the MSG specimens were 0.67%, 1.1, and 1.55%, respectively, and 0.81%, 1.66, and 0.25% for the CSG samples. This was attributable to the fact that upon exposure to the sulfate solution, the pores within the DSM samples absorbed the solution, thereby leading to an early-age increase in the resulting mass. The previous studies have reported similar results to the current study being discussed (Ariffin et al., 2013; Çevik et al., 2018; Degirmenci, 2017; Ren et al., 2022). Also, Mehta and Siddique, (2017b) have indicated that the primary cause of the early-age mass increase of exposed geopolymer specimens is the increase in volume resulting from the absorbed solution. After 120 days of exposure, mass losses were recorded for CSG specimens (-0.59%), whereas a slight mass increase or constant mass was observed for MSG (+1.46%). The mass loss of CSG samples after 120 days of exposure was due to peeling and falling from samples surface layers in a chemical environment (Çevik et al., 2018; Salami et al., 2017). According to Kwasny et al. (2018) , the mass loss was caused by the increasing surface layer deterioration due to the pressure applied by expanding salt crystals formed within the pore structure. Meanwhile, the good behavior of the MSG samples is because mechanochemical activation increased the surface area and reactivity of the geopolymer binder, resulting in a greater amount of gel as the primary reaction product. This gel plugged the pore system and hindered the sulfate from accessing the sample, leading in less weight change of MSG samples (Hamid Abed, Abbas, et al., 2022).

It can be observed that the MSG samples with 20% GP have a lower mass change rate when compared to the other DSM samples. The less mass loss of the 20% MSG samples is ascribed to the low calcium content of MSG and more stable sodium aluminosilicate hydrate (N-A-S-H) gels (Abbas et al., 2022). The substitution of 20% slag with GP resulted in modifying the CaO content and matrix composition (in terms of SiO_2/Al_2O_3). Chen et al. (2021) have highlighted that external cations can displace the Ca^{2+} present in (C, N)-A-S-H gel during sulfate attack. As a result, the high concentration of Ca has an adverse impact on sulfate resistance (Hamid et al., 2022).

Therefore, the resistance of geopolymer to sulfate attack is determined mainly by the calcium concentration in the system, and it is recommended to select raw materials with a low calcium content to enhance sulfate resistance (A. Wang et al., 2020).

However, it should be noted that the degradation rate of MSG30-GP was found to be higher than that of other MSG-stabilized soils when the GP content exceeded 30%. During the immersion period, the surface of the MSG-GP30 gradually began to peel, and spalling was observed in the surface layers, resulting in a reduction in the sample's mass. This trend implies that incorporating GP beyond the 20% threshold in MSG-stabilized soil increases porosity, which in turn allows for greater sulfate ingress into the matrix, thus decreasing its resistance.

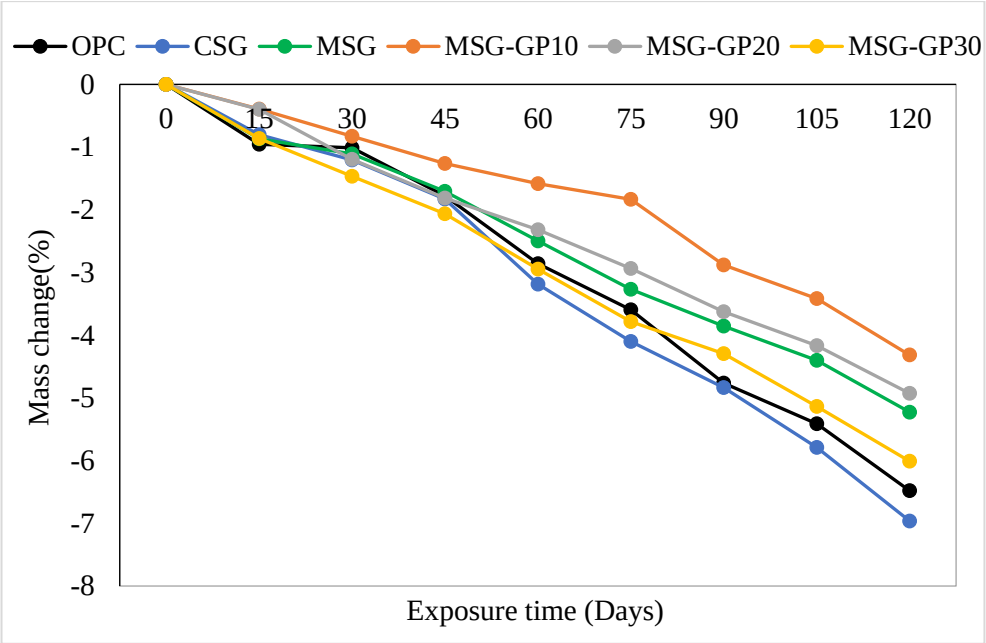

Figure 7.3 Mass change of OPC, MSG and CSG- stabilized soil specimens stored at ambient temperature.

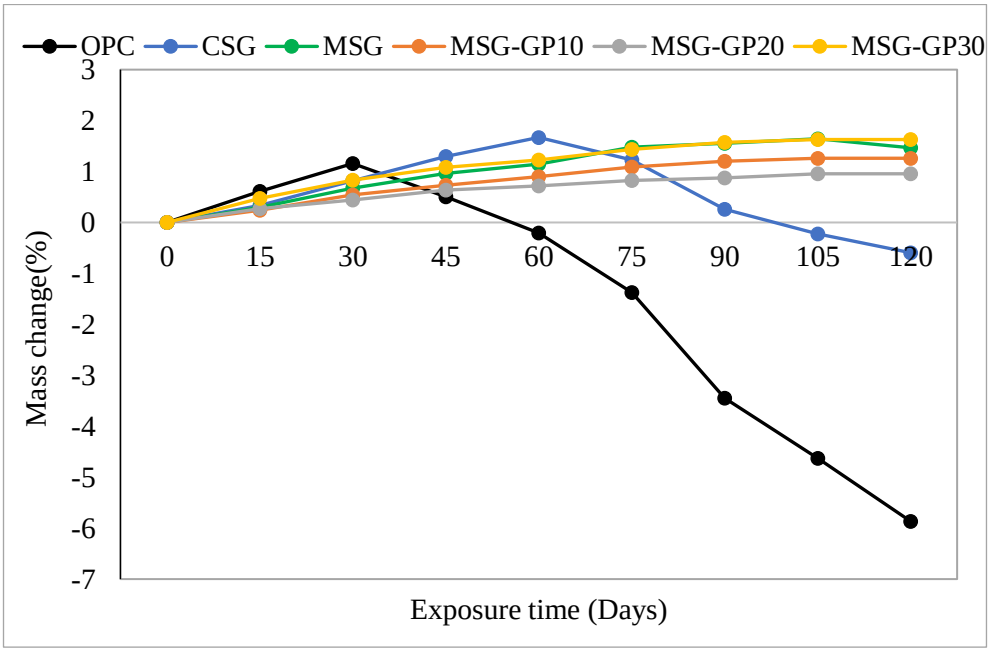

Figure 7.4 Mass change of OPC, MSG and CSG- stabilized soil specimens exposed to 1% $MgSO_4$ solution.

7.3.1.3 Strength loss

The UCS of DSM specimens that were exposed to $MgSO_4$ solution for varying durations of 0, 60, and 120 days is presented in Figure 7.5. Control samples that were not exposed to the solution were included for comparative purposes as shown in Figure 7.5b. The UCS of OPC, CSG, and MSG stabilized soil at room temperature progressively increased with curing time, with the highest UCS (8.9 MPa) recorded in MSG that contained 10% GP (MSG-GP10). However, it is worth noting that the UCS values (4.9 MPa-8.9 MPa) of all DSM samples were found to satisfy the prescribed strength quality requirements (i.e., >0.4 MPa; (Coduto et al., 1999)) concerning bearing capacity for ground improvement (Güllü & Ali Agha, 2021). Table 7.2 shows the residual unconfined compressive strength (%) of specimens immersed in magnesium sulfate solutions. The findings of this study indicate that the residual UCS of DSM specimens decreased when exposed to $MgSO_4$ solution, with the rate of reduction increasing as exposure time increased. After 60 days of immersion, the residual UCS values for OPC, CSG, and MSG specimens were found to be 65%, 71%, and 75%, respectively. However, these values further declined to 47%, 58%, and 63%, respectively, after 120 days of exposure. Notably, the results revealed that OPC specimens experienced the highest level of strength loss, while geopolymer stabilized soil (MSG and CSG) specimens exhibited minimal strength loss. This observation is consistent with the findings of a prior study conducted by Luo et al. (2022b), which reported that geopolymer-stabilized soil exhibits superior resistance to sulfate erosion when compared to cement-stabilized soil. Additionally, Valencia Saavedra et al. (2016) found that the higher deterioration rate of OPC specimens after sulfate exposure was due to reactions with calcium hydroxide and calcium monosulfoaluminates that led to the creation of gypsum and ettringite. This reaction resulted in a loss of mechanical resistance, higher volumetric expansions, and ultimately led to the detachment of surface layers and the development of cracks. Meanwhile, Sata et al. (2012) demonstrated that the primary products of geopolymerization products differ from OPC hydration products and are more resistant to sulfate attack than normal cement hydration products. Moreover, it was found that the geopolymer samples showed excellent performance in sodium and magnesium sulfate solutions, which was attributed to having a more stable crosslinked aluminosilicate polymer structure. The superior performance of geopolymer samples in sulfate corrosion resistance compared

to OPC samples is consistent with the results of previous research (K. Chen et al., 2021; Elyamany et al., 2018).

On the other hand, the activation mechanism of the geopolymeric stabilizer has an appreciable effect on the residual unconfined compressive strength of DSM samples after exposure to magnesium sulfate solution. The residual UCS of MSG was 8% higher than the counterparts of CSG-stabilized soil samples (Figure 7.5b) due to the mechanochemical synthesis process of the geopolymeric binder, which reduced the particle size and increased the surface area of geopolymeric particles, thereby decreasing the porosity and raised the density of the geopolymeric binder, which led to the creation of a more resistant structure against sulfate attack (Hamid Abed, Abbas, et al., 2022).

However, the erosion mechanism of geopolymer deterioration in a sulfate environment is varied depending on the calcium content (K. Chen et al., 2021).Fernández-Jiménez et al. (2007) stated that the low Ca content in the geopolymer is an essential characteristic of the durability of geopolymer binding materials. In the case of samples containing 100% slag, their resistance was found to be lower compared to samples containing 10% and 20% glass. This can be attributed to the increased calcium content in the matrix, which suggests that calcium-containing hydrates such as C-S-H gel and C-(A)-S-H gel have a lower resistance to sulfate attack during the creation of ettringite and gypsum compared to N-A-S-H gels (Alcamand et al., 2018; Yan et al., 2019). Therefore, substituting slag with GP altered the CaO content, and matrix composition (in terms of SiO_2/Al_2O_3) (see Table 3.2 and 3.4), which affected the residual strength values of MSG-GP stabilized soil specimens. Table 7.2 shows partial replacement of slag with GP up to 10-20% recorded as the highest residual UCS and then decreased beyond that level; the residual strength ratio was 63%, 69%, 84% and 51% for the GP contents of 0, 10%, 20%, and 30%, respectively, after 120 days of exposure. Meanwhile, the reduction in slag led to a rise in N-A-S-H gels and a decrease in C-(A)-S-H gels. As a result, the less dense matrix caused a greater sulfate penetration depth in the MSG-GP30 sample binder, hence less resistance. According to Trochez et al. (2015) and Wang et al. (2005), the primary factors contributing to the reduction in strength were the alkali dissolution from the geopolymer matrix into the sulfate solution, the leaching of Si into the sulfate solution, and the creation of gypsum within the geopolymer matrix. These mechanisms result in an increase in porosity (Wang et al., 2005) and possibly the formation of micro-

cracks (Trochez et al., 2015), both of which lead to a reduction in mechanical characteristics.

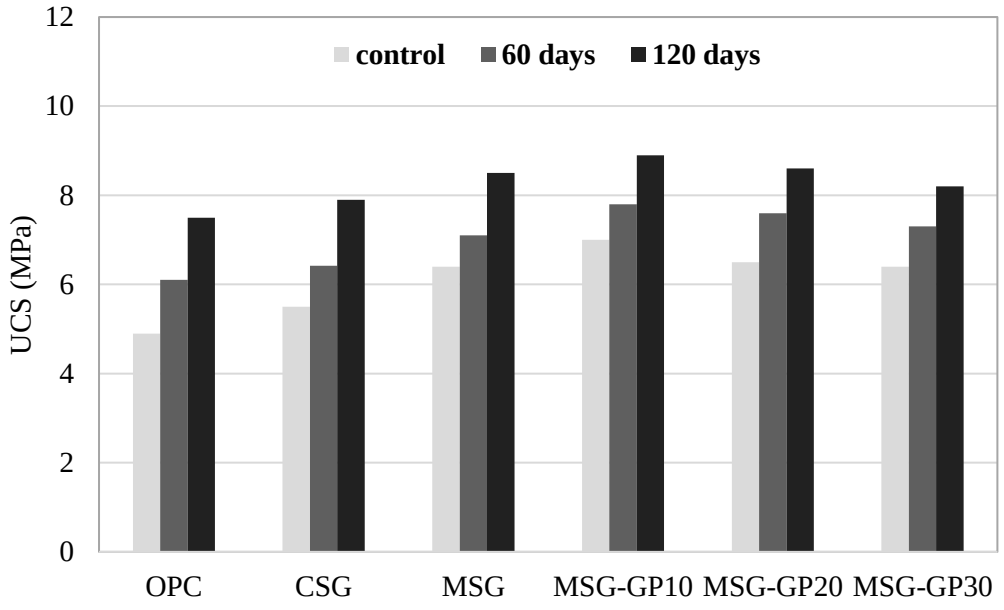

(a) UCS of DSM specimens stored at ambient temperature.

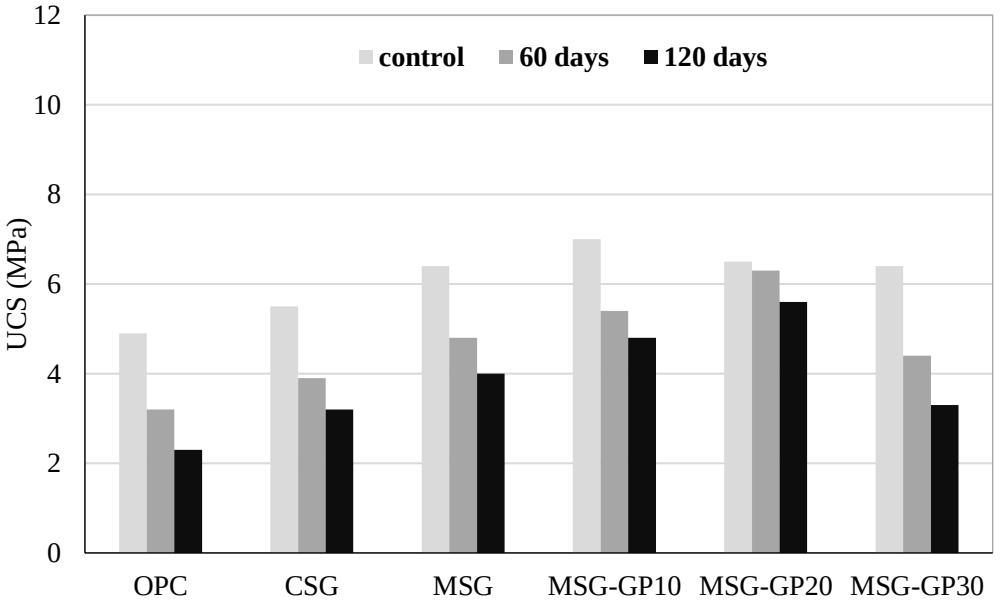

(b) UCS of DSM specimens exposed to magnesium sulfate solution.

Figure 7.5 Unconfined compressive strength of unexposed and exposed OPC and CSG-stabilized soil, compared to samples of MSG with varying slag/glass powder ratios.

Table 7.2 Residual unconfined compressive strength (%) of DSM specimens exposed to 1% magnesium sulfate solution.

Exposure time (days)	OPC	CSG	MSG	MSG-GP10	MSG-GP20	MSG-GP30
0	100	100	100	100	100	100
60	65	71	75	77	94	68
120	47	58	63	69	84	51

7.3.1.4 Ultrasonic pulse velocity changes

Figure 7.6 illustrates the variation in ultrasonic pulse velocity (UPV) for stabilized soil specimens composed of OPC, CSG, and MSG after exposure to magnesium sulfate for 0, 60, and 120 days. The findings demonstrate a decline in UPV measurements with increasing exposure time. The UPV values of OPC, CSG, and MSG-stabilized soil samples were lowered by 19%, 15%, and 13%, respectively, after 60 days of immersion in a sulfate solution, and by 33%, 25%, and 21%, respectively, after 120 days of immersion, compared to the control samples. This trend is consistent with prior studies (Bakharev, 2005; Elyamany et al., 2018; Thokchom et al., 2010). Notably, the MSG and CSG-stabilized soil samples demonstrated lower UPV losses compared to the OPC-stabilized soil samples. In OPC systems, $MgSO_4$ penetrates through various channels into the OPC-stabilized soil and reacts with cement hydration products, resulting in the formation of ettringite, gypsum, and thaumasite. This reaction causes expansion and crack spalling of the OPC-stabilized soil. Furthermore, the breakdown of C-S-H also leads to disintegration (K. Chen et al., 2021; Taylor & Gollop, 1997).

In relation to the impact of the activation method of the geopolymer binder on the resistance of deep cement mixing (DSM) samples to sulfate attack, it was observed that the MSG-stabilized soil samples exhibited a lower decline in UPV values compared to their CSG-stabilized soil counterparts. After 120 days, the UPV values of CSG-stabilized soil were 4% lower than those of MSG-stabilized soil, as shown in Figure 7.6. The improved resistance of MSG-stabilized soil samples to sulfate attack can be attributed to the mechanochemical activation of the geopolymer binder. According to Hamid Abed et al. (2022a), the mechanochemical activation process enhances the surface area and reactivity of geopolymer binders, leading to the

generation of additional gel within the geopolymer-stabilized matrix and a decrease in the overall pore volume and porosity. The reduced porosity of MSG samples creates a more challenging path for ionic species to penetrate through the pore structure, thereby resulting in a structure that exhibits greater resistance to sulfate attack.

Furthermore, adding GP to mechanochemically activated geopolymer stabilizers further enhanced the resistance of DSM samples to sulfate attack. The UPV values of MSG-stabilized soil specimens containing different percentages of GP were higher than those of samples without geopolymer binder. The UPV values of MSG-stabilized soil specimens with 0%, 10%, 20%, and 30% GP declined by 13%, 7%, 8%, and 17%, respectively, after 60 days of exposure to sulfate solution, and by 21%, 19%, 16%, and 23% after 120 days (Figure.7.6). Among these samples, MSG showed the highest rate of UPV loss, while MSG-GP10 showed the lowest rate. However, the higher reduction of UPV values in MSG samples was attributed to the formation of cracks inside the sample caused by Ca^{2+} diffusion into the $MgSO_4$ solution (Bakharev, 2005). This phenomenon was also reported in previous studies Jiang et al. (2018) and Luo et al. (2022b), which attributed the loss of strength in high-calcium geopolymer-stabilized soil to the formation of microcracks in the sample. In contrast, the lowest reduction in UPV values in MSG samples with 20% GP substitution was attributed to the decreased Ca-content of the binder and the integration of additional silicon ions into the aluminosilicate network provided by GP (Abbas et al., 2022)(Long, 2021)(Zabihi & Tavakoli, 2018). Previous studies by Liang et al.(2019) and Zhu et al. (2019a) also observed that geopolymer specimens with 20% GP had better homogeneity due to reactive SiO_2 and Al_2O_3, which contributed to the generation of hydrated sodium aluminosilicate gel (N–A–S–H). The 20% slag replacement by GP showed a significant advantage in generating a compact microstructure and reducing the connectivity between the inner spaces of the sample, which restricted the entry of sulfate into the geopolymer matrix and improved its resistance to sulfate attack

Notably, it seems that adding a higher amount of GP (30%) resulted in a lower UPV reduction compared to the 20% GP sample, which suggests that an excessive amount of GP may negatively impact the properties of the geopolymer (Hamid et al., 2022). The high concentration of silicon in GP affected the silica-alumina ratio, which has a substantial impact on the mechanical characteristics of the geopolymer (Silva et al., 2007). A high silica-alumina ratio can result in the development of low-crosslinked aluminosilicate materials with reduced strengths. In addition, excessive GP can lead

to incomplete chemical reactions, resulting in a looser structure and an increase in the number of unreacted components in the system (X. Jiang et al., 2020; Khan et al., 2021b).

Based on these findings, it is suggested that GP up to 20% can be used as a precursor for geopolymer synthesis after mechanochemical treatment. Beyond this amount, the excessive GP may negatively impact the properties of the geopolymer (Hamid et al., 2022).

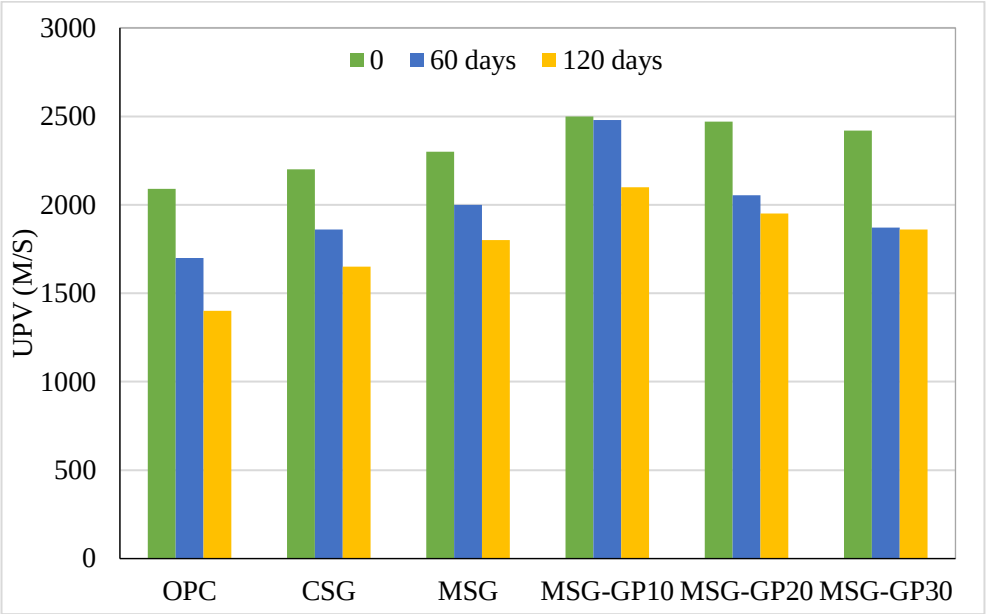

Figure 7.6 Ultrasonic pulse velocity of OPC, MSG and CSG- stabilized soil specimens exposed to 1% sulfate solution.

7.3.1.5 FTIR spectroscopy

The FTIR spectra of OPC, MSG, and CSG stabilized soil specimens were examined after being subjected to $MgSO_4$ solutions for a period of 120 days, were depicted in Figure 7.7. The spectra were compared with those of unexposed control specimens stored at ambient temperature. The unexposed DSM specimen exhibited a characteristic sharp band at approximately 1000 cm^{-1}, which is commonly associated with asymmetric T-O stretching (T representing Si or Al). Additionally, a shoulder at around 860-880 cm^{-1} was observed, which is typically associated with M-O vibrations according to previous studies (Gao et al., 2013; Kwasny et al., 2018). Another vibration band at 1420 cm^{-1} was assigned to the asymmetric modes of the O-C-O bonds in calcite (Bernal et al., 2012).

The OPC stabilized soil intensity of a band observed at 985 cm^{-1} and ascribed to asymmetric Si-O stretching vibrations in C-S-H decreased when exposed to sulfate solutions (Kwasny et al., 2018). The intensity of a broad shoulder corresponding to the asymmetric stretching vibrations of SO_4^{2-} in ettringite increased when samples were immersed in sulfate solutions (Kwasny et al., 2018; Peyvandi et al., 2015)

The FTIR spectra of geopolymer stabilized soil exhibited minimal variation, except for an increase in the intensity of the principal band centered around 1000 cm^{-1}, without any significant shift in position. Conversely, MSG stabilized soil showed less spectral changes than CSG stabilized soil when exposed to the $MgSO_4$ environment, suggesting that the mechanochemical activation approach positively influenced the improved resistance of the geopolymer stabilizer against sulfate attack. Notably, MSG-stabilized soil with 20% GP exhibited no significant changes in spectra before and after exposure to $MgSO_4$, suggesting that the original structure of MSG-GP20 samples was not affected by the exposure. This improvement in stability can be attributed to the incorporation of 20% GP, which contributes to a filling effect or interpenetrating action between the geopolymer's various components, resulting in a more compact structure and a decrease in average pore diameters (Abbas et al., 2022). Consequently, the geopolymer's permeation properties, such as external ion penetration rate (e.g., sulfate ion permeability) and low sorptivity, are reduced (Zhu, Liang, Xu, et al., 2019). Thus, the replacement of 20% slag with GP led to an improvement in the sulfate attack resistance of MSG-stabilized soil.

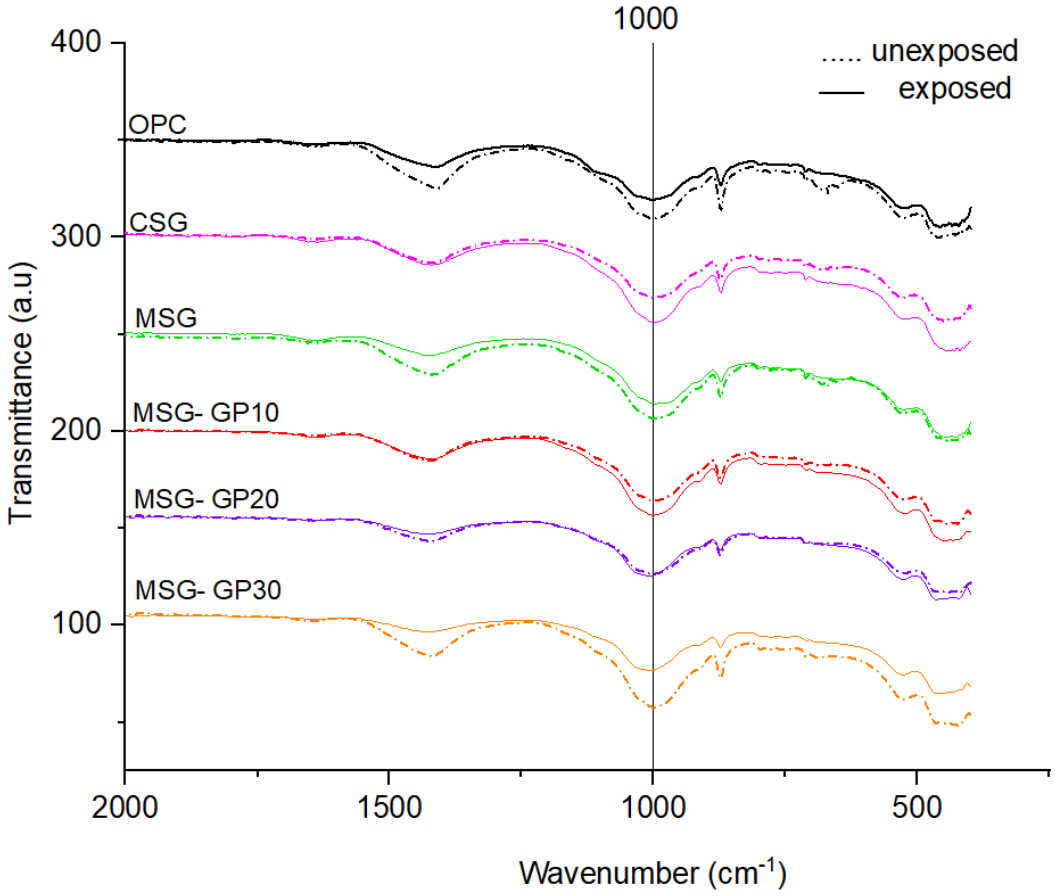

Figure 7.7 FTIR spectra of unexposed and exposed OPC and CSG-stabilized soil, compared to samples of MSG with varying slag/glass powder ratios.

7.4 Conclusions

- The results show that the UCS of the geopolymer-stabilized soil was higher than OPC stabilizers; due to the fact that both geopolymerization and pozzolanic reactions occur in geopolymer-stabilized mixtures.
- The UCS values of MSG were 16 % higher than its counterpart CSG because the mechanochemical activation process enhanced the reactivity of geopolymer binders, resulting in the formation of more gel within the geopolymer-stabilized matrix, thereby strengthening the bond between soil particles and leading to an increase in the strength of the stabilized soil sample.
- The UCS of geopolymer stabilized soil reached the highest when the amount of GP was 10% of the geopolymer stabilizer (MSG-GP10). The experimental findings indicated that the UCS of soil stabilized with MSG displayed an initial increase at a GP content of 10%, followed by a subsequent decline beyond this proportion; the UCS of MSG increased by 9.4% and 1.6% for GP contents of 10% and 20%, respectively, while it decreased by 3.13% for GP content of 30% compared to the mixture without GP.
- The deterioration of OPC appears to be more severe than that of geopolymer-stabilized soils. OPC deterioration is generally attributed because it contains hydration products of calcium silicates hydrate (CSH) and lime (Ca(OH)2). which leads to the formation of expansive products within specimens exposed to sulfate sources such as gypsum and ettringite.
- The CSG-stabilized soil degraded considerably more than the MSG-stabilized soil; as immersion age increases, the surface of CSG exhibits a larger supply of corrosion layer flaking.
- The MSG samples with 20% GP exhibit less visual deterioration, discoloration, expansion, and cracking than other DSM samples.
- The minimum decrease in compressive strength was seen in MSG-GP20 with 22%, approximately. It can be said that MSG-GP20 samples show lower compressive strength loss after magnesium sulfate attacks compared to GAG and OPC samples.
- The residual UCS of MSG were 8% higher than the counterparts of CSG-stabilized soil samples due to the mechanochemical synthesis process of the geopolymeric binder, which reduced the particle size and increased the surface

area of geopolymeric particles, thereby decreasing the porosity and raising the density of the geopolymeric binder, which led to the creation of a more resistant structure against sulfate attack.

CHAPTER VIII

CONCLUSIONS AND RECOMMENDATIONS

8.1 General Conclusions

- The yield stress and plastic viscosity values of the MSG grout were reduced when slag was substituted with 0- 30% RHA and GP. In addition, the results indicated that the yield stress and plastic viscosity of OPC grout were higher than those of MSG and CSG grout.
- Utilizing 0-30% RHA and GP prolonged the initial and final setting times of MSG grout. In contrast, mechanochemical activation significantly accelerated the setting process. Initial setting times for MSG, CSG, and OPC were 3,3 h, 4 h, and 8 hours, respectively, whereas final setting times were 4.5 h, 6.3 h, and 12 h, respectively.
- The bleeding capacity of MSG grout increased as RHA and GP content increased. In addition, the results demonstrated that the MSG grout had a substantially lower capacity for bleeding than the CG and OPC grout.
- The substitution of 10–20% slag with rice husk ash enhanced the UCS of MSG grouts by 4.5–41.0%. Meanwhile, the substitution of 10–20% slag with glass powder enhanced the UCS of MG grouts by 2–13%. In addition, the mechanochemical technique increased the strength of geopolymer grout by 18% compared to its conventional counterpart.
- The SEM images demonstrated that the microstructure of MG grout at 20% RHA and GP was densely compacted with less pores due to the enhanced polymerization of reaction products inside the structure, which contributed to the formation of additional aluminosilicate gels.

- The results show that MSG-stabilized soil attained the highest UCS, followed by CSG and OPC stabilizers; The UCS of MSG, CSG, and OPC were 6.4, 5.5, and 4.9 MPa, respectively.
- The UCS trend of MSG-stabilized soil increased with increasing partial substitution of slag with RHA up to 20% and afterward declined. Meanwhile, the UCS reached the highest when the amount of GP was 10% of the geopolymer stabilizer (MSG-GP10).
- The OPC surface shows many visible corrosions layers spalling observed and varying degrees of peeling and falling off appeared along the edges and corners at 120 days of immersion.
- The surface of CSG exhibits a larger supply of corrosion layer flaking. In contrast, the MSG-stabilized soil specimens exposed to the same conditions exhibited limited physical deterioration; only salt deposits were observed on their surface.
- The MSG samples with 20% RHA and GP exhibit less visual deterioration, discoloration, expansion, and cracking than other DSM samples.
- The experimental results show that the maximum strength loss was seen in the case of OPC specimens, while geopolymer-stabilized soil (MSG and CSG) specimens exhibited minimal strength loss. In addition, the residual UCS of MSG was 8% higher than the counterparts of CSG-stabilized soil samples. It can be revealed that MSG samples performed better than CSG samples under a magnesium sulfate attack.
- Partial replacement of slag with RHA up to 10-20% was recorded as the highest residual UCS due to the relatively greater SiO_2/Al_2O_3 ratio of RHA compared to slag; the presence of adequate silica strengthened the N-A-S-H gels.
- The minimum decrease in compressive strength was seen in MSG-GP20 with 22%, approximately. It can be said that MSG-GP20 samples show lower compressive strength loss after magnesium sulfate attacks compared to GSG and OPC samples.
-

8.2 Recommendation for Future Work

Based on the results of the current study, many investigations are recommended to provide a broader view of the behavior of mechanochemically activated geopolymeric binders, and the results suggest that further investigations are needed to understand its behavior and potential applications better. Here are some potential investigations that could be conducted:

- Durability testing: It would be useful to investigate the long-term durability of the geopolymeric binder under different environmental conditions, such as exposure to water, heat, wetting–drying or freeze-thaw cycles. This would help determine whether the binder is suitable for use in various construction applications.
- Strength testing: The strength of the geopolymeric binder should be investigated under different curing conditions, such as temperature and humidity, to determine the optimal curing conditions for the binder to achieve maximum strength.
- Cost-benefit analysis: A cost-benefit analysis could be conducted to determine the economic feasibility of using the geopolymeric binder compared to traditional binders such as Portland cement. This would help determine whether the geopolymeric binder is a viable alternative to traditional binders.
- Chemical analysis: A detailed chemical analysis of the geopolymeric binder could be conducted better to understand the mechanisms of its activation and hardening. This would help refine the production process and optimize the binder's properties.
- Applications testing: The binder could be tested in various construction applications, such as concrete, mortar, and grout, to determine its effectiveness in these applications. This would help determine the potential for wider adoption of the geopolymeric binder in the construction industry.

Overall, these investigations would help provide a more comprehensive understanding of mechanochemically activated geopolymeric binder behavior and its potential applications in the construction industry.

REFERENCES

Abbas, I. S., Abed, M. H., Canakci, H. (2022). Development and characterization of eco-and user-friendly grout production via mechanochemical activation of geopolymer. *Journal of Building Engineering*, 105336.

Abbey, S. J., Ngambi, S., Ngekpe, B. E. (2015). Understanding the performance of deep mixed column improved soils-a review. *International Journal of Civil Engineering and Technology (IJCIET)*, **6(3)**, 97–117.

Abdullah, A., Hussin, K., Abdullah, M. M. A. B., Yahya, Z., Sochacki, W., Razak, R. A., Błoch, K., Fansuri, H. (2021). Article the effects of various concentrations of naoh on the inter-particle gelation of a fly ash geopolymer aggregate. *Materials*, **14(5)**, 1–11.

Abdullah, H. H., Shahin, M. A., Sarker, P. (2017). Stabilisation of clay with fly-ash geopolymer incorporating GGBFS. *Proceedings of the Second Proceedings of the Second World Congress on Civil, Structural and Environmental Engineering (CSEE'17)*, 1–8.

Abdullah, H. H., Shahin, M. A., Walske, M. L. (2019). Geo-mechanical behavior of clay soils stabilized at ambient temperature with fly-ash geopolymer-incorporated granulated slag. *Soils and Foundations*, **59(6)**, 1906–1920.

Aboulayt, A., Jaafri, R., Samouh, H., El Idrissi, A. C., Roziere, E., Moussa, R., Loukili, A. (2018). Stability of a new geopolymer grout: Rheological and mechanical performances of metakaolin-fly ash binary mixtures. *Construction and Building Materials*, **181**, 420–436.

Adesanya, E., Ohenoja, K., Yliniemi, J., Illikainen, M. (2020). Mechanical transformation of phyllite mineralogy toward its use as alkali-activated binder precursor. *Minerals Engineering*, **145,** 106093.

Aghaeipour, A., Madhkhan, M., Ashrafian, A., Taheri Amiri, (2017). Improved Management of RCC Pavement Technology. In *Construction and Building*

Materials **21 (3)**.

Ahn, Y. B., Jang, J. G., Lee, H. K. (2016). Mechanical properties of lightweight concrete made with coal ashes after exposure to elevated temperatures. *Cement and Concrete Composites*, ***72***, 27–38.

Alcamand, H. A., Borges, P. H. R., Silva, F. A., Trindade, A. C. C. (2018). The effect of matrix composition and calcium content on the sulfate durability of metakaolin and metakaolin/slag alkali-activated mortars. *Ceramics International*, **44(5)**, 5037–5044.

Alonso, S., Palomo, A. (2001). Alkaline activation of metakaolin and calcium hydroxide mixtures: influence of temperature, activator concentration and solids ratio. *Materials Letters*, **47(1–2)**, 55–62.

American Society for Testing Mater. (1987). *Standard test methods for felt*. 1–8.

Anagnostopoulos, C. A., Chatziangelou, M. (2008). Compressive strength of cement stabilized soils. A new statistical model. *Electronic Journal of Geotechnical Engineering*, **13**, 1–10.

Anon, O. H. (1979). Classification of rocks and soils for engineering geological mapping. Part 1: rock and soil materials. *Bull Int Assoc Eng Geol*, **19**, 355–371.

Ariffin, M. A. M., Bhutta, M. A. R., Hussin, M. W., Mohd Tahir, M., Aziah, N. (2013). Sulfuric acid resistance of blended ash geopolymer concrete. *Construction and Building Materials*, **43**, 80–86.

Arulrajah, A., Yaghoubi, M., Disfani, M. M., Horpibulsuk, S., Bo, M. W., Leong, M. (2018). Evaluation of fly ash-and slag-based geopolymers for the improvement of a soft marine clay by deep soil mixing. *Soils and Foundations*, **58(6)**, 1358–1370.

ASTM:C940-10a. (2010). Standard Test Method for Expansion and Bleeding of Freshly Mixed Grouts for Preplaced-Aggregate Concrete in the Laboratory. *ASTM International*, **i(c)**, 1–3.

ASTM. (2009). *Standard test method for unconfined compressive strength of compacted soil-lime mixtures*. ASTM D5102, West Conshohocken, PA.

ASTM, C. (2009). Standard test method for pulse velocity through concrete. *ASTM*

International, West Conshohocken, PA.

ASTM C618. (2015). C618-15 Standard Specification for Coal Fly Ash and Raw or Calcined Natural Pozzolan for use in Concrete. *West Conshohocken, PA, USA: ASTM International*.

ASTM C989-99. (1999). Standard Specification for Ground Granulated Blast-Furnace Slag for Use in Concrete and Mortars. *ASTM International*, **2004**, 1–7.

ASTM, D. (2006). Standard test method for unconfined compressive strength of cohesive soil. *ASTM Standard D, 2166*.

Athira, V. S., Bahurudeen, A., Saljas, M., Jayachandran, K. (2021). Influence of different curing methods on mechanical and durability properties of alkali activated binders. *Construction and Building Materials*, **299**.

Baalamurugan, J., Ganesh Kumar, V., Stalin Dhas, T., Taran, S., Nalini, S., Karthick, V., Ravi, M., Govindaraju, K. (2021). Utilization of induction furnace steel slag based iron oxide nanocomposites for antibacterial studies. *SN Applied Sciences*, **3(3)**, 1–8.

Bai, T., Liu, B., Wu, Y., Huang, W., Wang, H., Xia, Z. (2020). Mechanical properties of metakaolin-based geopolymer with glass fiber reinforcement and vibration preparation. *Journal of Non-Crystalline Solids*, **544(206)**, 120173.

Bakharev, T. (2005). Durability of geopolymer materials in sodium and magnesium sulfate solutions. *Cement and Concrete Research*, **35(6)**, 1233–1246.

Baláž, P., Choi, W. S., Fabián, M., Godoč\'\iková, E. (2006). Mechanochemistry in the preparation of advanced materials. *Acta Montanistica Slovaca*, **11(2),** 122–129.

Banerjee, A., Patil, U. D., Puppala, A. J., Hoyos, L. R. (2018). Evaluation of liquefaction resistance in silty sand via suction controlled cyclic triaxial tests. In *PanAm Unsaturated Soils 2017*. 543–552.

Barbosa, V. F. F., MacKenzie, K. J. D. (2003). Thermal behaviour of inorganic geopolymers and composites derived from sodium polysialate. *Materials Research Bulletin*, **38(2)**, 319–331.

Barbosa, V. F. F., MacKenzie, K. J. D., Thaumaturgo, C. (2000). Synthesis and

characterisation of materials based on inorganic polymers of alumina and silica: Sodium polysialate polymers. *International Journal of Inorganic Materials*, **2(4)**, 309–317.

Barrdahl, A. (2022). *Geomechanical testing of non-hardening grout Geomechanical testing of non-hardening grout*.

Bell, F. (1993). *Engineering treatment of soils*. CRC Press.

Bell, J. L., Driemeyer, P. E., Kriven, W. M. (2009). Formation of ceramics from metakaolin-based geopolymers: Part I—Cs-based geopolymer. *Journal of the American Ceramic Society*, **92(1)**, 1–8.

Bellato, D., Dalle Coste, A., Gerressen, F. W., Simonini, P. (2012). Long-term performance of CSM walls in slightly overconsolidated clays. *ISSMGE-TC 211 International Symposium on Ground Improvement IS-GI*.

Bentz, D. P., Ferraris, C. F., Galler, M. A., Hansen, A. S., Guynn, J. M. (2012). Influence of particle size distributions on yield stress and viscosity of cement-fly ash pastes. *Cement and Concrete Research*, **42(2)**, 404–409.

Bernal, S. A., Rodr\'\iguez, E. D., de Gutiérrez, R., Provis, J. L. (2012). Performance of alkali-activated slag mortars exposed to acids. *Journal of Sustainable Cement-Based Materials*, **1(3)**, 138–151.

Bhadriraju, V., Puppala, A. J., Madhyannapu, R. S., Williammee, R. (2008). Laboratory procedure to obtain well-mixed soil binder samples of medium stiff to stiff expansive clayey soil for deep soil mixing simulation. *Geotechnical Testing Journal*, **31(3)**, 225–238.

Bhardwaj, P., Gupta, R., Mishra, D., Sanghi, S. K., Verma, S., Amritphale, S. S. (2020). Corrosion and Fire Protective Behavior of Advanced Phosphatic Geopolymeric Coating on Mild Steel Substrate. *Silicon*, **12(3)**, 487–500.

Bhat, G., Kandagor, V. (2014). Synthetic polymer fibers and their processing requirements. In *Advances in filament yarn spinning of textiles and polymers* (pp. 3–30). Elsevier.

Billong, N., Kinuthia, J., Oti, J., Melo, U. C. (2018). Performance of sodium silicate free geopolymers from metakaolin (MK) and Rice Husk Ash (RHA): Effect on tensile strength and microstructure. *Construction and Building Materials*, **189**,

307–313.

Bilondi, M. P., Toufigh, M. M., Toufigh, V. (2018). Experimental investigation of using a recycled glass powder-based geopolymer to improve the mechanical behavior of clay soils. *Construction and Building Materials*, **170**, 302–313.

Biswas, N., Ghosh, P. (2018). Interaction of adjacent strip footings on reinforced soil using upper-bound limit analysis. *Geosynthetics International*, *25*(6), 599–611.

Biswas, N., Ghosh, P. (2019). *Bearing capacity factors for isolated surface strip footing resting on multi-layered reinforced soil bed. Indian Geotech J 49 (1): 37--49*.

Bobiric\ua, C., Shim, J.-H., Pyeon, J.-H., Park, J.-Y. (2015). Influence of waste glass on the microstructure and strength of inorganic polymers. *Ceramics International*, **41(10)**, 13638–13649.

Boehm, D. W. (2004). The utilization of jet grouting and soil mixing methods to repair and support bulkhead structures. In *Ports 2004: Port Development in the Changing World* (pp. 1–10).

Boldyrev, V. V. (2004). Mechanochemical modification and synthesis of drugs. *Journal of Materials Science*, **39(16–17)**, 5117–5120.

Bouzón, N., Payá, J., Borrachero, M. V., Soriano, L., Tashima, M. M., Monzó, J. (2014). Refluxed rice husk ash/NaOH suspension for preparing alkali activated binders. *Materials Letters*, **115**, 72–74.

Boynton, R. (n.d.). *S., 1980;"Chemistry and Technology of Lime and Limestone."* John Wiley and Sons, Inc., New York.

Bredenberg, H., Broms, B. B., Holm, G. (1999). *Dry mix methods for deep soil stabilization*. CRC Press.

Brown, D. R., Warner, J. (1973). Compaction grouting. *Journal of the Soil Mechanics and Foundations Division*, **99(8)**, 589–601.

Bruce, D. A., Geosystems, E. C. O. (2000). *An introduction to the deep soil mixing methods as used in geotechnical applications*.

Buchwald, A., Hilbig, H., Kaps, C. (2007). Alkali-activated metakaolin-slag blends—performance and structure in dependence of their composition. *Journal of*

Materials Science, **42**, 3024–3032.

Caballero, S., Acharya, R., Banerjee, A., Bheemasetti, T. V, Puppala, A., Patil, U. (2016). Sustainable slope stabilization using biopolymer-reinforced soil. In *Geo-Chicago 2016* (pp. 116–126).

Canakci, H., Güllü, H., Alhashemy, A. (2019). Performances of Using Geopolymers Made with Various Stabilizers for Deep Mixing. *Materials*, **12(16)**, 2542.

Canakci, H., Güllü, H., Dwle, M. I. K. (2018). Effect of glass powder added grout for deep mixing of marginal sand with clay. *Arabian Journal for Science and Engineering*, **43(4)**, 1583–1595.

Çevik, A., Alzeebaree, R., Humur, G., Niş, A., Gülşan, M. E. (2018). Effect of nano-silica on the chemical durability and mechanical performance of fly ash based geopolymer concrete. *Ceramics International*, **44(11)**, 12253–12264.

Chen, F. H. (2012). *Foundations on expansive soils* (**12**). Elsevier.

Chen, K., Wu, D., Xia, L., Cai, Q., Zhang, Z. (2021). Geopolymer concrete durability subjected to aggressive environments – A review of influence factors and comparison with ordinary Portland cement. *Construction and Building Materials*, **279**, 122496.

Chen, R., Congress, S. S. C., Cai, G., Duan, W., Liu, S. (2021). Sustainable utilization of biomass waste-rice husk ash as a new solidified material of soil in geotechnical engineering: A review. *Construction and Building Materials*, **292**, 123219.

Cheng, T.-W., Chiu, J. P. (2003). Fire-resistant geopolymer produced by granulated blast furnace slag. *Minerals Engineering*, **16(3)**, 205–210.

Chew, S. H., Kamruzzaman, A. H. M., Lee, F. H. (2004). Physicochemical and Engineering Behavior of Cement Treated Clays. *Journal of Geotechnical and Geoenvironmental Engineering*, **130(7)**, 696–706.

Chindaprasirt, P., De Silva, P., Sagoe-Crentsil, K., Hanjitsuwan, S. (2012). Effect of SiO 2 and Al 2O 3on the setting and hardening of high calcium fly ash-based geopolymer systems. *Journal of Materials Science*, **47(12)**, 4876–4883.

Chouhan, R. K., Mudgal, M., Bisarya, A., Srivastava, A. K. (2018). Rice-husk-based superplasticizer to increase performance of fly ash geopolymer concrete.

Emerging Materials Research, **7(3)**, 169–177.

Christensen, A. P. (1969). Cement modification of clay soils. *Portland Cement Assoc R \& D Lab Bull*.

Coduto, D. P., Abbey, S. J., Ngambi, S., Ngekpe, B. E. (1999). Geotechnical engineering: principles and practices. In *International Journal of Civil Engineering and Technology (IJCIET)* **6(3).**

Criado, M., Fernández-Jiménez, A., De La Torre, A. G., Aranda, M. A. G., Palomo, A. (2007). An XRD study of the effect of the SiO2/Na2O ratio on the alkali activation of fly ash. *Cement and Concrete Research*, **37(5)**, 671–679.

Cristelo, N., Glendinning, S., Miranda, T., Oliveira, D., Silva, R. (2012). Soil stabilisation using alkaline activation of fly ash for self compacting rammed earth construction. *Construction and Building Materials*, **36**, 727–735.

Cristelo, N., Soares, E., Rosa, I., Miranda, T., Oliveira, D. V, Silva, R. A., Chaves, A. (2013). Rheological properties of alkaline activated fly ash used in jet grouting applications. *Construction and Building Materials*, **48**, 925–933.

D1557-12, A. (2009). *Standard Test Methods for Laboratory Compaction Characteristics of Soil Using Modified Effort (56,000 Ft-Lbf/Ft3 (2,700 KN-M/M3)) 1*. ASTM international.

Dadsetan, S., Siad, H., Lachemi, M., Sahmaran, M. (2021). Extensive evaluation on the effect of glass powder on the rheology, strength, and microstructure of metakaolin-based geopolymer binders. *Construction and Building Materials*, **268**, 121168.

Davidovits, J. (1991). Geopolymers. *Journal of Thermal Analysis*, **37(8)**, 1633–1656.

Davidovits, J. (1988). Structural characterization of geopolymeric materials with X-Ray diffractometry and MAS-NMR spectroscopy. *Geopolymer*, **88**, 149–166.

Davidovits, Joseph. (1991). Geopolymers: inorganic polymeric new materials. *Journal of Thermal Analysis and Calorimetry*, **37(8)**, 1633–1656.

Davidovits, Joseph. (1994). Properties of geopolymer cements. *First International Conference on Alkaline Cements and Concretes*, **1**, 131–149.

Deere, D. U. (1982). Cement-bentonite grouting for dams. *Mine Induced Subsidence:*

Effects on Engineered Structures, 279–300.

Degirmenci, F. N. (2017). Effect of sodium silicate to sodium hydroxide ratios on durability of geopolymer mortars containing natural and artificial pozzolans. *Ceramics - Silikaty*, **61(4)**, 340–350.

Denies, N., Huybrechts, N., De Cock, F., Lameire, B., Maertens, J., Vervoort, A., Guimond-Barrett, A. (2015). *Thoughts on the durability of the soil mix material*.

Diniz, D. H., de Carvalho, J. M. F., Mendes, J. C., Peixoto, R. A. F. (2017). Blast oxygen furnace slag as chemical soil stabilizer for use in roads. *Journal of Materials in Civil Engineering*, **29(9)**, 4017118.

Du, Y. J., Yu, B. W., Liu, K., Jiang, N. J., Liu, M. D. (2017). Physical, hydraulic, and mechanical properties of clayey soil stabilized by lightweight alkali-activated slag geopolymer. *Journal of Materials in Civil Engineering*, **29(2)**.

Duan, P., Yan, C., Zhou, W. (2017). Compressive strength and microstructure of fly ash based geopolymer blended with silica fume under thermal cycle. *Cement and Concrete Composites*, **78**, 108–119.

Dungca, J. R., Codilla II, E. E. T. (2018). Fly-ash-based geopolymer as stabilizer for silty sand embankment materials. *GEOMATE Journal*, **14(46)**, 143–149.

Duxson, P., Fernández-Jiménez, A., Provis, J. L., Lukey, G. C., Palomo, A., Van Deventer, J. S. J. (2007). Geopolymer technology: The current state of the art. *Journal of Materials Science*, **42(9)**, 2917–2933.

Duxson, P. (2009). Geopolymer precursor design. In *Geopolymers* (pp. 37–49). Elsevier.

Duxson, Peter, Provis, J. L. (2008). Designing precursors for geopolymer cements. *Journal of the American Ceramic Society*, **91(12)**, 3864–3869.

El-Didamony, H., Amer, A. A., Abd Ela-Ziz, H. (2012). Properties and durability of alkali-activated slag pastes immersed in sea water. *Ceramics International*, **38(5)**, 3773–3780.

El-Kelesh, A. M., Matsui, T., Hayashi, K., Tsuboi, H., Fukada, H. (2002). Compaction grouting and ground surface upheave. *Proc., 4th Int. Conf. on Ground Improvement Techniques*, **1**, 323–330.

Elyamany, H. E., Abd Elmoaty, A. E. M., Elshaboury, A. M. (2018). Magnesium sulfate resistance of geopolymer mortar. *Construction and Building Materials*, *184*, 111–127.

Emin, A., Alzeebaree, R., Aljumaili, O., Niş, A., Eren, M., Humur, G., Abdulkadir, Ç. (2018). *Mechanical and durability properties of fly ash and slag based geopolymer concrete*. **4**, 345–362.

Fangtian, W., Cun, Z., Shuaifeng, W., Xiaogang, Z., Shenghua, G. (2016). Whole section anchor--grouting reinforcement technology and its application in underground roadways with loose and fractured surrounding rock. *Tunnelling and Underground Space Technology*, **51**, 133–143.

Fapohunda, C., Akinbile, B., Shittu, A. (2017). Structure and properties of mortar and concrete with rice husk ash as partial replacement of ordinary Portland cement--A review. *International Journal of Sustainable Built Environment*, **6(2)**, 675–692.

Farmer, V. C. (1976). Gadsden. The infrared spectra of minerals and related inorganic compounds. London (Butterworths), 1975. 277 pp. Price£15.00. *Mineralogical Magazine*, **40(313)**, 540.

Feng, L., Huang, F., Wang, G., Huang, T., Qian, Z. (2023). Experimental investigation on pneumatic pre-fracturing grouting in low-permeability soil. *Tunnelling and Underground Space Technology*, **131**, 104798.

Fernández-Jiménez, A., Cristelo, N., Miranda, T., Palomo, Á. (2017). Sustainable alkali activated materials: Precursor and activator derived from industrial wastes. *Journal of Cleaner Production*, **162**, 1200–1209.

Fernández-Jiménez, A., Garc\'\ia-Lodeiro, I., Palomo, A. (2007). Durability of alkali-activated fly ash cementitious materials. *Journal of Materials Science*, **42(9)**, 3055–3065.

Fernández-Jiménez, A., Garcia-Lodeiro, I., Maltseva, O., Palomo, A. (2019). Mechanical-chemical activation of coal fly ashes: An effective way for recycling and make cementitious materials. *Frontiers in Materials*, **6, 51**.

Fernandez-Jimenez, A. M., Palomo, A., Lopez-Hombrados, C. (2006). Engineering properties of alkali-activated fly ash concrete. *ACI Materials Journal*, **103(2)**, 106.

Fernández-Jiménez, A., Palomo, A. (2005). Composition and microstructure of alkali activated fly ash binder: Effect of the activator. *Cement and Concrete Research*, **35(10)**, 1984–1992.

Firoozi, A. A., Guney Olgun, C., Firoozi, A. A., Baghini, M. S. (2017). Fundamentals of soil stabilization. *International Journal of Geo-Engineering*, **8,** 1–16.

Fletcher, R. A., MacKenzie, K. J. D., Nicholson, C. L., Shimada, S. (2005). The composition range of aluminosilicate geopolymers. *Journal of the European Ceramic Society*, **25(9)**, 1471–1477.

Fluids, C. (2003). Standard Test Method for Viscosity of Chemical Grouts by Brookfield Viscometer. *Annual Book of ASTM Standards*, **04**, 8–10.

Gao, X. X., Michaud, P., Joussein, E., Rossignol, S. (2013). Behavior of metakaolin-based potassium geopolymers in acidic solutions. *Journal of Non-Crystalline Solids*, **380**, 95–102.

George, A M, Banerjee, A., Puppala, A. J., Praticò, F. (2019). An integrated LCA-LCCA framework for the selection of sustainable pavement design. *Transportation Research Board, 98th Annual Meeting. Washington, DC*.

George, Anu M, Banerjee, A., Taylor, T., Puppala, A. J. (2019). Large-scale experimental studies to evaluate the resilient modulus of geocell-reinforced reclaimed asphalt pavement bases. *Geosynthetics Conference*, 10–13.

Georgea, A. M., Banerjeeb, A., Puppala, A. J., Saladhia, M. (2019). *Performance evaluation of geocell-reinforced reclaimed asphalt pavement (RAP) bases in flexible pavements*.

Ghadir, P., Ranjbar, N. (2018a). Clayey soil stabilization using geopolymer and Portland cement. *Construction and Building Materials*, **188**, 361–371.

Goncalves, J., El-Bakkari, M., Boluk, Y., Bindiganavile, V. (2019). Cellulose nanofibres (CNF) for sulphate resistance in cement based systems. *Cement and Concrete Composites*, **99**, 100–111.

Gordon, M., Bell, J., Kriven, W. M. (2005). Comparison of naturally and synthetically-derived potassium-based geopolymers. *Ceramic Transactions Series*, **165**, 95–106.

Güllü, H. (2016). Comparison of rheological models for jet grout cement mixtures with various stabilizers. *Construction and Building Materials*, **127**, 220–236.

Güllü, H., Al Nuaimi, M. M. D., Aytek, A. (2021). Rheological and strength performances of cold-bonded geopolymer made from limestone dust and bottom ash for grouting and deep mixing. *Bulletin of Engineering Geology and the Environment*, **80(2)**, 1103–1123.

Güllü, H., Ali Agha, A. (2021). The rheological, fresh and strength effects of cold-bonded geopolymer made with metakaolin and slag for grouting. *Construction and Building Materials*, **274**, 122091.

Güllü, H., Canakci, H., Al Zangana, I. F. (2017). Use of cement based grout with glass powder for deep mixing. *Construction and Building Materials*, **137**, 12–20.

Güllü, H., Cevik, A., Al-Ezzi, K. M. A., Gülsan, M. E. (2019). On the rheology of using geopolymer for grouting: A comparative study with cement-based grout included fly ash and cold bonded fly ash. *Construction and Building Materials*, **196**, 594–610.

Güneyisi, E., Gesoglu, M., Naji, N., Ipek, S. (2016). Evaluation of the rheological behavior of fresh self-compacting rubberized concrete by using the Herschel-Bulkley and modified Bingham models. *Archives of Civil and Mechanical Engineering*, **16(1)**, 9–19.

Guo, X., Xiang, D., Duan, G., Mou, P. (2010). A review of mechanochemistry applications in waste management. *Waste Management*, **30(1)**, 4–10.

Gupta, R., Bhardwaj, P., Mishra, D., Mudgal, M., Chouhan, R. K., Prasad, M., Amritphale, S. S. (2017). Evolution of advanced geopolymeric cementitious material via a novel process. *Advances in Cement Research*, **29(3)**, 125–134.

Gupta, R., Bhardwaj, P., Mishra, D., Prasad, M., Amritphale, S. S. (2017). Formulation of mechanochemically evolved fly ash based hybrid inorganic--organic geopolymers with multilevel characterization. *Journal of Inorganic and Organometallic Polymers and Materials*, **27(2)**, 385–398.

Gupta, R., Tomar, A. S., Mishra, D., Sanghi, S. K. (2020). Multinuclear MAS NMR Characterization of Fly-Ash-Based Advanced Sodium Aluminosilicate Geopolymer: Exploring Solid-State Reactions. *ChemistrySelect*, **5(16)**, 4920–

4927.

Hadi, P., Ning, C., Kubicki, J. D., Mueller, K., Fagan, J. W., Luo, Z., Weng, L., McKay, G. (2016). Sustainable development of a surface-functionalized mesoporous aluminosilicate with ultra-high ion exchange efficiency. *Inorganic Chemistry Frontiers*, **3(4)**, 502–513.

Hamid Abed, M., Abbas, I. S., Canakci, H. (2022). Influence of mechanochemical activation on the rheological, fresh, and mechanical properties of one-part geopolymer grout. *Advances in Cement Research*, 1–38.

Hamid Abed, M., Sabbar Abbas, I., Hamed, M., Canakci, H. (2022). Rheological, fresh, and mechanical properties of mechanochemically activated geopolymer grout: A comparative study with conventionally activated geopolymer grout. *Construction and Building Materials*, **322**, 126338.

Hamid, M., Abbas, I. S., Canakci, H. (2022). Effect of glass powder on the rheological and mechanical properties of slag-based mechanochemical activation geopolymer grout. *European Journal of Environmental and Civil Engineering*, **0(0)**, 1–25.

Hashim, R, Islam, S. (2008). Stabilized peat by deep mixing method: a critical review of the state of practice. *The Electronic Journal of Geotechnical Engineering (EJGE Journal)*, **13**.

Hashim, Roslan, Islam, M. S. (2008). Properties of stabilized peat by soil-cement column method. *Electronic Journal of Geotechnical Engineering*, **13**, 1–9.

He, J., Jie, Y., Zhang, J., Yu, Y., Zhang, G. (2013). Synthesis and characterization of red mud and rice husk ash-based geopolymer composites. *Cement and Concrete Composites*, **37**, 108–118.

He, S., Yu, X., Banerjee, A., Puppala, A. J. (2018). Expansive soil treatment with liquid ionic soil stabilizer. *Transportation Research Record*, **2672(52)**, 185–194.

Heidrich, C., Feuerborn, H., Weir, A. (2013). Coal Combustion Products : a Global Perspective. *World of Coal Ash*, **17**.

Helson, O., Eslami, J., Beaucour, A. L., Noumowe, A., Gotteland, P. (2018). Durability of soil mix material subjected to wetting/drying cycles and external sulfate attacks. *Construction and Building Materials*, **192,** 416–428.

Higgins, D. (2007). *Briefing: GGBS and sustainability*. Thomas Telford Ltd.

Hojati, M., Radlińska, A. (2017). Shrinkage and strength development of alkali-activated fly ash-slag binary cements. *Construction and Building Materials*, **150**, 808–816.

Holtz, W. G. (1969). Volume change in expansive clay soils and control by lime treatment. *Proceedings of 2nd International Research and Engineering Conference on Expansive Clay Soils*, 157–174.

Hossain, S. K. S., Mathur, L., Roy, P. K., Hossain, S. K. S., Mathur, L. (n.d.). R.(2018).“Rice husk/rice husk ash as an alternative source of silica in ceramics: A review,.” *Journal of Asian Ceramic Societies*, **6(4)**, 299–313.

Hossain, S. S., Roy, P. K., Bae, C. J. (2021). Utilization of waste rice husk ash for sustainable geopolymer: A review. *Construction and Building Materials*, **310**, 125218.

Hosseini, S., Brake, N. A., Nikookar, M., Günaydın-Şen, Ö., Snyder, H. A. (2021). Mechanochemically activated bottom ash-fly ash geopolymer. *Cement and Concrete Composites*, **118.**

Humur, G., Çevik, A. (2022). Mechanical characterization of lightweight engineered geopolymer composites exposed to elevated temperatures. *Ceramics International*.

Hussain, M., Varley, R. J., Cheng, Y. B., Simon, G. P. (2004). Investigation of thermal and fire performance of novel hybrid geopolymer composites. *Journal of Materials Science*, **39(14)**, 4721–4726.

Ikegami, M., Ichiba, T., Ohishi, K., Terashi, M. (2003). Long-term strength change of cement treated soil at Daikoku Pier. In *Soft Ground Engineering in Coastal Areas* (pp. 241–246). AA Balkema The Netherlands.

Islam, A., Alengaram, U. J., Jumaat, M. Z., Bashar, I. I., Kabir, S. M. A. (2015). Engineering properties and carbon footprint of ground granulated blast-furnace slag-palm oil fuel ash-based structural geopolymer concrete. *Construction and Building Materials*, **101**, 503–521.

Ismail, I., Bernal, S. A., Provis, J. L., Hamdan, S., Van Deventer, J. S. J. (2013). Microstructural changes in alkali activated fly ash/slag geopolymers with sulfate

exposure. *Materials and Structures/Materiaux et Constructions*, **46(3)**, 361–373.

Istuque, D. B., Payá, J., Soriano, L., Borrachero, M. V., Monzó, J., Tashima, M. M. (2022). The role of dissolved rice husk ash in the development of binary blast furnace slag-sewage sludge ash alkali-activated mortars. *Journal of Building Engineering*, ***52*(April)**.

Jiang, N. J., Du, Y. J., Liu, K. (2018). Durability of lightweight alkali-activated ground granulated blast furnace slag (GGBS) stabilized clayey soils subjected to sulfate attack. *Applied Clay Science*, **161(April)**, 70–75.

Jiang, X., Xiao, R., Ma, Y., Zhang, M., Bai, Y., Huang, B. (2020). Influence of waste glass powder on the physico-mechanical properties and microstructures of fly ash-based geopolymer paste after exposure to high temperatures. *Construction and Building Materials*, **262**, 120579.

Jittin, V., Bahurudeen, A., Ajinkya, S. D. (2020). Utilisation of rice husk ash for cleaner production of different construction products. *Journal of Cleaner Production*, **263**, 121578.

Jun, W. U., Xiyao, Z., Aiwu, Y. (2021). Experimental study on the compressive strength of muddy clay solidified by the one-part slag-fly ash based geopolymer. *Rock Soil Mech*, **42**, 647–655.

Kamon, M., Nontananandh, S., Katsumi, T. (1993). Utilization of stainless-steel slag by cement hardening. *Soils and Foundations*, **33(3)**, 118–129.

Kamseu, E., Ceron, B., Tobias, H., Leonelli, E., Bignozzi, M. C., Muscio, A., Libbra, A. (2012). Insulating behavior of metakaolin-based geopolymer materials assess with heat flux meter and laser flash techniques. *Journal of Thermal Analysis and Calorimetry*, **108(3)**, 1189–1199.

Kani, E. N., Allahverdi, A., Provis, J. L. (2012). Efflorescence control in geopolymer binders based on natural pozzolan. *Cement and Concrete Composites*, **34(1)**, 25–33.

Karatai, T. R., Kaluli, J. W., Kabubo, C., Thiong'o, G. (2017). Soil stabilization using rice husk ash and natural lime as an alternative to cutting and filling in road construction. *Journal of Construction Engineering and Management*, **143(5)**, 4016127.

Karim, M. R., Zain, M. F. M., Jamil, M., Lai, F. C. (2013). Fabrication of a non-cement binder using slag, palm oil fuel ash and rice husk ash with sodium hydroxide. *Construction and Building Materials*, **49**, 894–902.

Kashani, A., Provis, J. L., Qiao, G. G., Van Deventer, J. S. J. (2014). The interrelationship between surface chemistry and rheology in alkali activated slag paste. *Construction and Building Materials*, **65**, 583–591.

Kazemain, S., Barghchi, M. (2012). Review of soft soils stabilization by grouting and. *Scientific Research and Essays*, **7(24)**, 2104–2111.

Kazemian, S., Huat, B. B. K. (2010). Assessment of stabilization methods for soft soils by admixtures. *2010 International Conference on Science and Social Research* **(2010)**, 118–121.

Kazemian, S., Prasad, A., Huat, B. B. K. (2012). Review of Newtonian and non-Newtonian fluids behaviour in the context of grouts. *Geotechnical Aspects of Underground Construction in Soft Ground*, 321–326.

Ke, X., Bernal, S. A., Ye, N., Provis, J. L., Yang, J. (2015). One-part geopolymers based on thermally treated red mud/NaOH blends. *Journal of the American Ceramic Society*, **98(1)**, 5–11.

Kézdi, A. (1979). *Soil physics-selected topics-developments in geotechnical engineering*-**25**.

Khadka, S. D., Jayawickrama, P. W., Senadheera, S. (2018). Strength and shrink/swell behavior of highly plastic clay treated with geopolymer. *Transportation Research Record*, **2672(52)**, 174–184.

Khan, M. N. N., Kuri, J. C., Sarker, P. K. (2021a). Effect of waste glass powder as a partial precursor in ambient cured alkali activated fly ash and fly ash-GGBFS mortars. *Journal of Building Engineering*, **34(April 2020)**, 101934.

Khan, M. N. N., Kuri, J. C., Sarker, P. K. (2021b). Effect of waste glass powder as a partial precursor in ambient cured alkali activated fly ash and fly ash-GGBFS mortars. *Journal of Building Engineering*, **34(June 2020)**, 101934.

Khatami, H., O'Kelly, B. C. (2018). Prevention of bleeding of particulate grouts using biopolymers. *Construction and Building Materials*, **192**, 202–209.

Khater, H. M. (2013). *Effect of silica fume on the characterization of the geopolymer materials*. 1–10.

Khoury, N., Brooks, R., Boeni, S. Y., Yada, D. (2013). Variation of resilient modulus, strength, and modulus of elasticity of stabilized soils with postcompaction moisture contents. *Journal of Materials in Civil Engineering*, **25(2)**, 160–166.

Kim, Y. Y., Lee, B., Saraswathy, V., Kwon, S. (2014). *Strength and Durability Performance of Alkali-Activated Rice Husk Ash Geopolymer Mortar*. *2014*.

Kirsch, K., Bell, A. (2012). *Ground improvement*. CRC Press.

Kitazume, M., Terashi, M. (2013). *The deep mixing method*. CRC press.

Kleinlugtenbelt, R., Bezuijen, A., Van Tol, A. F. (2006). Model tests on compensation grouting. *Tunnelling and Underground Space Technology*, **21(3–4)**.

Kong, D. L. Y., Sanjayan, J. G., Sagoe-Crentsil, K. (2007). Comparative performance of geopolymers made with metakaolin and fly ash after exposure to elevated temperatures. *Cement and Concrete Research*, **37(12)**, 1583–1589.

Konijn, B. J., Sanderink, O. B. J., Kruyt, N. P. (2014). Experimental study of the viscosity of suspensions: Effect of solid fraction, particle size and suspending liquid. *Powder Technology*, **266**, 61–69.

Kumar, P., Singh, S. P. (2008). Fiber-reinforced fly ash subbases in rural roads. *Journal of Transportation Engineering*, **134(4)**, 171–180.

Kumar, Sanjay, Kumar, R. (2011). Mechanical activation of fly ash: Effect on reaction, structure and properties of resulting geopolymer. *Ceramics International*, **37(2)**, 533–541.

Kumar, Sanjay, Kumar, R., Mehrotra, S. P. (2010). Influence of granulated blast furnace slag on the reaction, structure and properties of fly ash based geopolymer. *Journal of Materials Science*, **45(3)**, 607–615.

Kumar, Sanjay, Mucsi, G., Kristály, F., Pekker, P. (2017). Mechanical activation of fly ash and its influence on micro and nano-structural behaviour of resulting geopolymers. *Advanced Powder Technology*, **28(3)**, 805–813.

Kumar, Sundar, Ash, F. (2013). *Development and Determination of Mechanical properties of fly ash and slag blended geo polymer concrete Compound*. **4(8)**.

Kurtoğlu, A. E., Alzeebaree, R., Aljumaili, O., Niş, A., Gülşan, M. E., Humur, G., Çevik, A. (2018). Mechanical and durability properties of fly ash and slag based geopolymer concrete. *Advances in Concrete Construction*, **6(4)**, 345–362.

Kusbiantoro, A., Nuruddin, M. F., Shafiq, N., Qazi, S. A. (2012). The effect of microwave incinerated rice husk ash on the compressive and bond strength of fly ash based geopolymer concrete. *Construction and Building Materials*, **36**, 695–703.

Kutzner, C. (2020). *Grouting of rock and soil*. CRC Press.

Kwasny, J., Aiken, T. A., Soutsos, M. N., McIntosh, J. A., Cleland, D. J. (2018). Sulfate and acid resistance of lithomarge-based geopolymer mortars. *Construction and Building Materials*, **166**, 537–553.

Lagerlund, J. (2009). *Remedial injection grouting of embankment dams with non-hardening grouts*. KTH.

Lee, N. K., Kim, E. M., Lee, H. K. (2016). Mechanical properties and setting characteristics of geopolymer mortar using styrene-butadiene (SB) latex. *Construction and Building Materials*, **113**, 264–272.

Lee, N. K., Lee, H. K. (2013). Setting and mechanical properties of alkali-activated fly ash/slag concrete manufactured at room temperature. *Construction and Building Materials*, **47**, 1201–1209.

Lee, W. K. W., J, J. S. (2002). *Structural reorganisation of class F fly ash in alkaline silicate solutions*. **211**, 49–66.

Lee, W. K. W., Van Deventer, J. S. J. (2003). Use of Infrared Spectroscopy to Study Geopolymerization of Heterogeneous Amorphous Aluminosilicates. *Langmuir*, **19(21)**, 8726–8734.

Li, C., Sun, H., Li, L. (2010). A review: The comparison between alkali-activated slag (Si+ Ca) and metakaolin (Si+ Al) cements. *Cement and Concrete Research*, **40(9)**, 1341–1349.

Li, H., Xu, D., Feng, S., Shang, B. (2014). Microstructure and performance of fly ash micro-beads in cementitious material system. *Construction and Building Materials*, **52**, 422–427.

Li, L., Lu, J. X., Zhang, B., Poon, C. S. (2020). Rheology behavior of one-part alkali activated slag/glass powder (AASG) pastes. *Construction and Building Materials*, **258**, 120381.

Li, Y., Jia, S., Liu, J. (2018). The solidification mechanism of cement and fly ash towards contaminated soil. *Chemical Engineering Transactions*, **67**, 571–576.

Li, Z., You, H., Gao, Y., Wang, C., Zhang, J. (2021). Effect of ultrafine red mud on the workability and microstructure of blast furnace slag-red mud based geopolymeric grouts. *Powder Technology*, **392**, 610–618.

Liang, G., Li, H., Zhu, H., Liu, T., Chen, Q., Guo, H. (2021). Reuse of waste glass powder in alkali-activated metakaolin/fly ash pastes: Physical properties, reaction kinetics and microstructure. *Resources, Conservation and Recycling*, **173(February),** 105721.

Liang, G., Zhu, H., Li, H., Liu, T., Guo, H. (2021). Comparative study on the effects of rice husk ash and silica fume on the freezing resistance of metakaolin-based geopolymer. *Construction and Building Materials*, **293**, 123486.

Liang, G., Zhu, H., Zhang, Z., Wu, Q. (2019). Effect of rice husk ash addition on the compressive strength and thermal stability of metakaolin based geopolymer. *Construction and Building Materials*, **222**, 872–881.

Liang, G., Zhu, H., Zhang, Z., Wu, Q., Du, J. (2019). Investigation of the waterproof property of alkali-activated metakaolin geopolymer added with rice husk ash. *Journal of Cleaner Production*, **230**, 603–612.

Ling, T.-C., Poon, C. S. (2017). Spent fluorescent lamp glass as a substitute for fine aggregate in cement mortar. *Journal of Cleaner Production*, **161**, 646–654.

Little, D N. (1996). Evaluation of resilient and strength properties of lime-stabilized soils for the Denver, Colorado area. *Report for the Chemical Lime Company*.

Little, Dallas N. (1995). *Stabilization of pavement subgrades and base courses with lime*.

Little, Dallas N, Nair, S. (2009). *Recommended practice for stabilization of subgrade soils and base materials*.

Liu, Y., Shi, C., Zhang, Z., Li, N. (2019). An overview on the reuse of waste glasses

in alkali-activated materials. *Resources, Conservation and Recycling*, **144**, 297–309.

Liu, Z., Cai, C. S., Liu, F., Fan, F. (2016). Feasibility study of loess stabilization with fly ash--based geopolymer. *Journal of Materials in Civil Engineering*, **28(5)**, 4016003.

Lizcano, M., Gonzalez, A., Basu, S., Lozano, K., Radovic, M. (2012). Effects of water content and chemical composition on structural properties of alkaline activated metakaolin-based geopolymers. *Journal of the American Ceramic Society*, **95(7)**, 2169–2177.

Long, H. V. (2021). Optimizing mixtures of alkali aluminosilicate cement based on ternary by-products. *Civil Engineering Journal (Iran)*, ***7(7)***, 1264–1274.

Lu, C., Zhang, Z., Shi, C., Li, N., Jiao, D., Yuan, Q. (2021). Rheology of alkali-activated materials: A review. *Cement and Concrete Composites*, **121**, 104061.

Luo, Z., Luo, B., Zhao, Y., Li, X., Su, Y., Huang, H., Wang, Q. (2022). Experimental Investigation of Unconfined Compression Strength and Microstructure Characteristics of Slag and Fly Ash-Based Geopolymer Stabilized Riverside Soft Soil. *Polymers*, **14(2)**, 307.

Luo, Z., Zhang, B., Zou, J., Luo, B. (2022). Case Studies in Construction Materials Sulfate erosion resistance of slag-fly ash based geopolymer stabilized soft soil under semi-immersion condition. *Case Studies in Construction Materials*, **17(June)**, e01506.

Malhotra, V. M., Carino, N. J. (1991). NDT E International October 1991 NDT & E International October 1991. *NDT & E International*, **25(12)**, 267–268.

Manish, M., Kumar, C. R., Deepti, M., Application, F., Data, P. (2016). *(12) United States Patent*. **2(12)**.

Maraghechi, H., Salwocki, S., Rajabipour, F. (2017). Utilisation of alkali activated glass powder in binary mixtures with Portland cement, slag, fly ash and hydrated lime. *Materials and Structures/Materiaux et Constructions*, **50(1)**, 1–14.

Marathe, S., Mithanthaya, I. R., Rao, N. B. S. (2016). *A Review on Strength and Durability Studies on Geopolymer Concrete*. **2008**, 119–124.

Marjanovi, N., Komljenovi, M., Ba, Z., Nikoli, V., Petrovi, R. (2014). *Physical – mechanical and microstructural properties of alkali-activated fl y ash – blast furnace slag blends.*

Marjanović, N., Komljenović, M., Baščarević, Z., Nikolić, V. (2014). Improving reactivity of fly ash and properties of ensuing geopolymers through mechanical activation. *Construction and Building Materials*, **57**, 151–162.

Marjanović, N., Komljenović, M., Baščarević, Z., Nikolić, V., Petrović, R. (2015). Physical-mechanical and microstructural properties of alkali-activated fly ash-blast furnace slag blends. *Ceramics International*, **41(1)**, 1421–1435.

Masi, G., Filipponi, A., Bignozzi, M. C. (2021). Fly ash-based one-part alkali activated mortars cured at room temperature: effect of precursor pre-treatments. *Open Ceramics*, **8**, 100178.

Matalkah, F., Xu, L., Wu, W., Soroushian, P. (2017). Mechanochemical synthesis of one-part alkali aluminosilicate hydraulic cement. *Materials and Structures/Materiaux et Constructions*, **50(1)**, 1–12.

Mateos, M., Davidson, D. T. (1962). Lime and fly ash proportions in soil, lime and fly ash mixtures, and some aspects of soil lime stabilization. *Highway Research Board Bulletin*, **335**.

Medri, V., Fabbri, S., Dedecek, J., Sobalik, Z., Tvaruzkova, Z., Vaccari, A. (2010). Role of the morphology and the dehydroxylation of metakaolins on geopolymerization. *Applied Clay Science*, ***50(4)***, 538–545.

Mehta, A., Siddique, R. (2017a). Sulfuric acid resistance of fly ash based geopolymer concrete. *Construction and Building Materials*, **146,** 136–143.

Mehta, A., Siddique, R. (2017b). Sulfuric acid resistance of fly ash based geopolymer concrete. *Construction and Building Materials*, **146**, 136–143.

Mehta, A., Siddique, R. (2018). Sustainable geopolymer concrete using ground granulated blast furnace slag and rice husk ash: Strength and permeability properties. *Journal of Cleaner Production*, **205**, 49–57.

Mehta, P. K. (1999). Concrete technology for sustainable development. *Concrete International*, **21(11)**, 47–53.

Mehta, P. K., Monteiro, P. J. M. (2014). *Concrete: microstructure, properties, and materials*. McGraw-Hill Education.

Miao, S., Shen, Z., Wang, X., Luo, F., Huang, X., Wei, C. (2017). Stabilization of highly expansive black cotton soils by means of geopolymerization. *Journal of Materials in Civil Engineering*, **29(10)**, 4017170.

Mitchell, J. M., Jardine, F. M. (2002). *A guide to ground treatment* (Vol. 573). CIRIA London.

Mohammadinia, A., Arulrajah, A., Sanjayan, J., Disfani, M. M., Win Bo, M., Darmawan, S. (2016). Stabilization of demolition materials for pavement base/subbase applications using fly ash and slag geopolymers. *Journal of Materials in Civil Engineering*, **28(7)**, 4016033.

Mudgal, M., Chouhan, R. K., Kushwah, S., Srivastava, A. K. (2019). Enhancing reactivity and properties of fly-ash-based solid-form geopolymer via ball-milling. *Emerging Materials Research*, **9(1)**, 2–9.

Muraleedharan, M., Nadir, Y. (2021). Factors affecting the mechanical properties and microstructure of geopolymers from red mud and granite waste powder: A review. *Ceramics International*, **47(10)**, 13257–13279.

Murdoch, L. C. (1990). A field test of hydraulic fracturing in glacial till. *Proceedings of the 15th Annual Reservoir Symposium*, 164–174.

Muthukrishnan, S., Ramakrishnan, S., Sanjayan, J. (2021). Effect of alkali reactions on the rheology of one-part 3D printable geopolymer concrete. *Cement and Concrete Composites*, **116**, 103899.

Nair, D. G., Fraaij, A., Klaassen, A. A. K., Kentgens, A. P. M. (2008). A structural investigation relating to the pozzolanic activity of rice husk ashes. *Cement and Concrete Research*, **38(6)**, 861–869.

Nana, A., Epey, N., Rodrique, K. C., Deutou, J. G. N., Djobo, J. N. Y., Tomé, S., Alomayri, T. S., Ngouné, J., Kamseu, E., Leonelli, C. (2021). Mechanical strength and microstructure of metakaolin/volcanic ash-based geopolymer composites reinforced with reactive silica from rice husk ash (RHA). *Materialia*, **16.**

Nath, P., Sarker, P. K. (2014). Effect of GGBFS on setting, workability and early

strength properties of fly ash geopolymer concrete cured in ambient condition. *Construction and Building Materials*, **66**, 163–171.

Nath, P., Sarker, P. K. (2017). Flexural strength and elastic modulus of ambient-cured blended low-calcium fly ash geopolymer concrete. *Construction and Building Materials*, **130**, 22–31.

Nath, S. K., Kumar, S. (2013). Influence of iron making slags on strength and microstructure of fly ash geopolymer. *Construction and Building Materials*, **38**, 924–930.

Nazarian, S., Mazari, M., Abdallah, I. N., Puppala, A. J., Mohammad, L. N., Abu-Farsakh, M. Y. (2015). *Modulus-based construction specification for compaction of earthwork and unbound aggregate*. Transportation Research Board Washington, DC.

Nematollahi, B., Sanjayan, J., Ahmed Shaikh, F. U. (2015). Tensile Strain Hardening Behavior of PVA Fiber-Reinforced Engineered Geopolymer Composite. *Journal of Materials in Civil Engineering*, **27(10)**, 04015001.

Nematollahi, B., Sanjayan, J., Shaikh, F. U. A. (2015). Synthesis of heat and ambient cured one-part geopolymer mixes with different grades of sodium silicate. *Ceramics International*, **41(4)**, 5696–5704.

Newman, J., Choo, B. S. (2003). *Advanced concrete technology 3: processes*. Butterworth-Heinemann.

Ng, T. S. (2011). An investigation into the development of high performance geopolymer concrete. In *School of Civil and Environmental Engineering*. University of New South Wales Australia.

Nguyen, V.-H., Remond, S., Gallias, J.-L. (2011). Influence of cement grouts composition on the rheological behaviour. *Cement and Concrete Research*, **41(3)**, 292–300.

Nicholson, P. G. (2014). *Soil improvement and ground modification methods*. Butterworth-Heinemann.

Nikbakhtan, B., Osanloo, M. (2009). Effect of grout pressure and grout flow on soil physical and mechanical properties in jet grouting operations. *International Journal of Rock Mechanics and Mining Sciences*, **46(3)**, 498–505.

Nikolić, V., Komljenović, M., Marjanović, N., Baščarević, Z., Petrović, R. (2014). Lead immobilization by geopolymers based on mechanically activated fly ash. *Ceramics International*, **40(6)**, 8479–8488.

Novais, R. M., Ascensão, G., Seabra, M. P., Labrincha, J. A. (2016). Waste glass from end-of-life fluorescent lamps as raw material in geopolymers. *Waste Management*, **52**, 245–255.

Odeh, N. A., Al-Rkaby, A. H. J. (2022). Strength, Durability, and Microstructures characterization of sustainable geopolymer improved clayey soil. *Case Studies in Construction Materials*, **16**, e00988.

Oh, J. E., Monteiro, P. J. M., Jun, S. S., Choi, S., Clark, S. M. (2010). The evolution of strength and crystalline phases for alkali-activated ground blast furnace slag and fly ash-based geopolymers. *Cement and Concrete Research*, ***40(2)***, 189–196.

Oyekan, G. L., Kamiyo, O. M. (2011). A study on the engineering properties of sandcrete blocks produced with rice husk ash blended cement. *Journal of Engineering and Technology Research*, **3(3)**, 88–98.

Pakbaz, M. S., Farzi, M. (2015). Comparison of the effect of mixing methods (dry vs. wet) on mechanical and hydraulic properties of treated soil with cement or lime. *Applied Clay Science*, **105**, 156–169.

Palacios, M., Alonso, M. M., Varga, C., Puertas, F. (2019). Influence of the alkaline solution and temperature on the rheology and reactivity of alkali-activated fly ash pastes. *Cement and Concrete Composites*, **95**, 277–284.

Palacios, M., Gismera, S., Alonso, M. M., d'Espinose de Lacaillerie, J. B., Lothenbach, B., Favier, A., Brumaud, C., Puertas, F. (2021). Early reactivity of sodium silicate-activated slag pastes and its impact on rheological properties. *Cement and Concrete Research*, **14**, 106302.

Palacios, Marta, Banfill, P. F. G., Puertas, F. (2008). Rheology and setting of alkali-activated slag pastes and mortars: Effect of organic admixture. *ACI Materials Journal*, **105(2)**, 140.

Palomo, A., Grutzeck, M. W., Blanco, M. T. (1999). Alkali-activated fly ashes: A cement for the future. *Cement and Concrete Research*, **29(8)**, 1323–1329.

Park, C. K., Noh, M. H., Park, T. H. (2005). Rheological properties of cementitious

materials containing mineral admixtures. *Cement and Concrete Research*, **35(5)**, 842–849.

Parsons, R. L. (2002). Subgrade improvement through fly ash stabilization. *Miscellaneous Report*.

Partha, S. D., Pradip, N., Prabir, K. S. (2013). Strength and Permeation Properties of Slag Blended Fly Ash Based Geopolymer Concrete. *Advanced Materials Research*, **651**, 168–173.

Pascual, A. B., Tognonvi, T. M., Tagnit-Hamou, A. (2021). Optimization study of waste glass powder-based alkali activated materials incorporating metakaolin: Activation and curing conditions. *Journal of Cleaner Production*, **308**, 127435.

Paso, E. L. (n.d.). *Special Specifi cation for Deep Soil Mixing*.

Patel, Y. J., Shah, N. (2018). Enhancement of the properties of ground granulated blast furnace slag based self compacting geopolymer concrete by incorporating rice husk ash. *Construction and Building Materials*, **171**, 654–662.

Petry, T. M., Little, D. N. (2002). Review of stabilization of clays and expansive soils in pavements and lightly loaded structures—history, practice, and future. *Journal of Materials in Civil Engineering*, **14(6)**, 447–460.

Petry, T. M., Wohlgemuth, S. K. (1988). *Effects of pulverization on the strength and durability of highly active clay soils stabilized with lime and Portland cement* **119**.

Peyvandi, A., Holmes, D., Soroushian, P., Balachandra, A. M. (2015). Monitoring of Sulfate Attack in Concrete by Al27 and Si29 MAS NMR Spectroscopy. *Journal of Materials in Civil Engineering*, **27(8)**, 1–10.

Phetchuay, C., Horpibulsuk, S., Arulrajah, A., Suksiripattanapong, C., Udomchai, A. (2016). Strength development in soft marine clay stabilized by fly ash and calcium carbide residue based geopolymer. *Applied Clay Science*, **127**, 134–142.

Phetchuay, C., Horpibulsuk, S., Suksiripattanapong, C., Chinkulkijniwat, A., Arulrajah, A., Disfani, M. M. (2014). Calcium carbide residue: Alkaline activator for clay--fly ash geopolymer. *Construction and Building Materials*, **69**, 285–294.

Phummiphan, I., Horpibulsuk, S., Phoo-ngernkham, T., Arulrajah, A., Shen, S.-L.

(2017). Marginal lateritic soil stabilized with calcium carbide residue and fly ash geopolymers as a sustainable pavement base material. *Journal of Materials in Civil Engineering*, **29(2)**, 4016195.

Pourakbar, S., Huat, B. B. K., Asadi, A., Fasihnikoutalab, M. H. (2016). Model Study of Alkali-Activated Waste Binder for Soil Stabilization. *International Journal of Geosynthetics and Ground Engineering*, **2(4)**.

Provis, J. L. (2009). Activating solution chemistry for geopolymers. *Geopolymers: Structures, Processing, Properties and Industrial Applications*, 50–71.

Provis, John L, Bernal, S. A. (2014). Geopolymers and related alkali-activated materials. *Annual Review of Materials Research*, **44**, 299–327.

Provis, John L, Duxson, P., van Deventer, J. S. J. (2010). The role of particle technology in developing sustainable construction materials. *Advanced Powder Technology*, **21(1)**, 2–7.

Provis, John LVan Deventer, J. S. J. (2009). *Geopolymers: structures, processing, properties and industrial applications*. Elsevier.

Provis, John L, Van Deventer, J. S. J. (2013). *Alkali activated materials: state-of-the-art report, RILEM TC 224-AAM* (Vol. 13). Springer Science Business Media.

Prusinski, J. R., Bhattacharja, S. (1999). Effectiveness of Portland cement and lime in stabilizing clay soils. *Transportation Research Record*, **1652(1)**, 215–227.

Puppala, A. J., Congress, S. S. C., Talluri, N., Wattanasanthicharoen, E. (2019). Sulfate-heaving studies on chemically treated sulfate-rich geomaterials. *Journal of Materials in Civil Engineering*, **31(6)**, 4019076.

Puppala, A. J., Mohammad, L. N., Allen, A. (1996). Engineering behavior of lime-treated Louisiana subgrade soil. *Transportation Research Record*, **1546(1)**, 24–31.

Puppala, A. J., Wattanasanticharoen, E., Hoyos, L. R. (2003). Ranking of four chemical and mechanical stabilization methods to treat low-volume road subgrades in Texas. *Transportation Research Record*, **1819(1)**, 63–71.

Purdon, A. O. (1940). The action of alkalis on blast-furnace slag. *Journal of the Society of Chemical Industry*, **59(9)**, 191–202.

Qu, F., Li, W., Wang, K., Zhang, S., Sheng, D. (2021). Performance deterioration of fly ash/slag-based geopolymer composites subjected to coupled cyclic preloading and sulfuric acid attack. *Journal of Cleaner Production*, **321**, 128942.

Raja, S., Anand, J. (2014). *Design and Construction Guidelines for Deep Soil Mixing to Stabilize Expansive Soils*.

Rakhimova, N. R. (2020). A review of calcined clays and ceramic wastes as sources for alkali-activated materials. *Geosystem Engineering*, **23(5)**, 287–298.

Rashad, A. M. (2019). Insulating and fire-resistant behaviour of metakaolin and fly ash geopolymer mortars. *Proceedings of Institution of Civil Engineers: Construction Materials*, **172(1)**, 37–44.

Ren, J., Sun, H., Li, Q., Li, Z., Ling, L., Zhang, X., Wang, Y., Xing, F. (2021). Experimental comparisons between one-part and normal (two-part) alkali-activated slag binders. *Construction and Building Materials*, **309**, 125177.

Ren, J., Zhang, L., Walkley, B., Black, J. R., San Nicolas, R. (2022). Degradation resistance of different cementitious materials to phosphoric acid attack at early stage. *Cement and Concrete Research*, **151**, 106606.

Rifaai, Y., Yahia, A., Mostafa, A., Aggoun, S., Kadri, E. H. (2019). Rheology of fly ash-based geopolymer: Effect of NaOH concentration. *Construction and Building Materials*, **223**, 583–594.

Rios, S., Ramos, C., da Fonseca, A. V., Cruz, N., Rodrigues, C. (2016). Colombian soil stabilized with geopolymers for low cost roads. *Procedia Engineering*, **143**, 1392–1400.

Rios, S., Ramos, C., Viana da Fonseca, A., Cruz, N., Rodrigues, C. (2019). Mechanical and durability properties of a soil stabilised with an alkali-activated cement. *European Journal of Environmental and Civil Engineering*, **23(2)**, 245–267.

Rollings, R. S., Burkes, J. P., Rollings, M. P. (1999). Sulfate attack on cement-stabilized sand. *Journal of Geotechnical and Geoenvironmental Engineering*, *125*(5), 364–372.

Rowles, M., O'connor, B. (2003). Chemical optimisation of the compressive strength of aluminosilicate geopolymers synthesised by sodium silicate activation of metakaolinite. *Journal of Materials Chemistry*, **13(5)**, 1161–1165.

Saberian, M., Li, J., Cameron, D. (2019). Effect of crushed glass on behavior of crushed recycled pavement materials together with crumb rubber for making a clean green base and subbase. *Journal of Materials in Civil Engineering*, **31(7)**, 4019108.

Şahmaran, M. (2008). The effect of replacement rate and fineness of natural zeolite on the rheological properties of cement-based grouts. *Canadian Journal of Civil Engineering*, **35(8)**, 796–806.

Sahoo, S., Prasad Singh, S. (2022). Strength and durability properties of expansive soil treated with geopolymer and conventional stabilizers. *Construction and Building Materials*, **328**, 127078.

Sakir, S., Raman, S. N., Kaish, A. B. M. A. (2020). *Utilization of By-Products and Wastes as Supplementary Cementitious Materials in Structural Mortar for Sustainable Construction*.

Salami, B. A., Megat Johari, M. A., Ahmad, Z. A., Maslehuddin, M. (2017). Durability performance of Palm Oil Fuel Ash-based Engineered Alkaline-activated Cementitious Composite (POFA-EACC) mortar in sulfate environment. *Construction and Building Materials*, **131**, 229–244.

Samantasinghar, S., Singh, S. P. (2019). Fresh and Hardened Properties of Fly Ash–Slag Blended Geopolymer Paste and Mortar. *International Journal of Concrete Structures and Materials*, **13(1)**, 1–12.

Samantasinghar, S., Singh, S. P. (2021). Strength and durability of granular soil stabilized with FA-GGBS geopolymer. *Journal of Materials in Civil Engineering*, **33(6)**, 6021003.

Samarakoon, M. H., Ranjith, P. G., De Silva, V. R. S. (2020). Effect of soda-lime glass powder on alkali-activated binders: Rheology, strength and microstructure characterization. *Construction and Building Materials*, **241**, 118013.

Sata, V., Sathonsaowaphak, A., Chindaprasirt, P. (2012). Resistance of lignite bottom ash geopolymer mortar to sulfate and sulfuric acid attack. *Cement and Concrete Composites*, **34(5)**, 700–708.

Scharff, H. (2014). Landfill reduction experience in The Netherlands. *Waste Management*, *34*(11), 2218–2224.

Shang, J., Dai, J., Zhao, T., Guo, S., Zhang, P., Mu, B. (2018). Alternation of traditional cement mortars using fl y ash-based geopolymer mortars modi fi ed by slag. *Journal of Cleaner Production*, **203**, 746–756.

Sharma, A. K., Sivapullaiah, P. V. (2016). Ground granulated blast furnace slag amended fly ash as an expansive soil stabilizer. *Soils and Foundations*, **56(2)**, 205–212.

Shen, S.-L., Wang, Z.-F., Yang, J., Ho, C.-E. (2013). Generalized approach for prediction of jet grout column diameter. *Journal of Geotechnical and Geoenvironmental Engineering*, **139(12)**, 2060–2069.

Shi, C., Day, R. L. (1996). Some factors affecting early hydration of alkali-slag cements. *Cement and Concrete Research*, *26*(3), 439–447.

Shi, C., Jiménez, A. F., Palomo, A. (2011). New cements for the 21st century: The pursuit of an alternative to Portland cement. *Cement and Concrete Research*, **41(7)**, 750–763.

Si, R., Guo, S., Dai, Q., Wang, J. (2020). Atomic-structure, microstructure and mechanical properties of glass powder modified metakaolin-based geopolymer. *Construction and Building Materials*, **254**, 119303.

Silva, P. De, Sagoe-Crenstil, K., Sirivivatnanon, V. (2007). Kinetics of geopolymerization: Role of Al2O3 and SiO2. *Cement and Concrete Research*, **37(4)**, 512–518.

Singhi, B., Laskar, A. I., Ahmed, M. A. (2017). Mechanical behavior and sulfate resistance of alkali activated stabilized clayey soil. *Geotechnical and Geological Engineering*, **35(5)**, 1907–1920.

Soroushian, P., Plasencia, J., Ravanbakhsh, S. (2003). Assessment of reinforcing effects of recycled plastic and paper in concrete. *Materials Journal*, **100(3)**, 203–207.

Suresh, D., Nagaraju, K. (2015). Ground granulated blast slag (GGBS) in concrete--a review. *IOSR Journal of Mechanical and Civil Engineering*, **12(4)**, 76–82.

Swanepoel, J. C., Strydom, C. A. (2002). Utilisation of fly ash in a geopolymeric material. *Applied Geochemistry*, **17(8)**, 1143–1148.

Taylor, H. F. W., Gollop, R. S. (1997). 21 SOME CHEMICAL AND MICROSTRUCTURAL ASPECTS OF CONCRETE DURABILITY. *Mechanisms of Chemical Degradation of Cement-Based Systems*, ***177***.

Tchakouté, H. K., Rüscher, C. H., Kong, S., Kamseu, E., Leonelli, C. (2016). Comparison of metakaolin-based geopolymer cements from commercial sodium waterglass and sodium waterglass from rice husk ash. *Journal of Sol-Gel Science and Technology*, **78,** 492–506.

Teerawattanasuk, C., Voottipruex, P. (2019). Comparison between cement and fly ash geopolymer for stabilized marginal lateritic soil as road material. *International Journal of Pavement Engineering*, **20(11)**, 1264–1274.

Temuujin, J, Williams, R. P., Van Riessen, A. (2009). Effect of mechanical activation of fly ash on the properties of geopolymer cured at ambient temperature. *Journal of Materials Processing Technology*, **209(12–13)**, 5276–5280.

Temuujin, Jadambaa, Minjigmaa, A., Rickard, W., Lee, M., Williams, I., Van Riessen, A. (2009). Preparation of metakaolin based geopolymer coatings on metal substrates as thermal barriers. *Applied Clay Science*, **46(3)**, 265–270.

Temuujin, Jadambaa, Rickard, W., Lee, M., van Riessen, A. (2011). Preparation and thermal properties of fire resistant metakaolin-based geopolymer-type coatings. *Journal of Non-Crystalline Solids*, **357(5)**, 1399–1404.

Terro, M. J. (2006). Properties of concrete made with recycled crushed glass at elevated temperatures. *Building and Environment*, **41(5)**, 633–639.

Their, J. M., Özakça, M. (2018). Developing geopolymer concrete by using cold-bonded fly ash aggregate , nano-silica , and steel fiber. *Construction and Building Materials*, **180**, 12–22.

Thiedeitz, M., Schmidt, W., Härder, M., Kränkel, T. (2020). Performance of rice husk ash as supplementary cementitious material after production in the field and in the lab. *Materials*, **13(19)**, 4319.

Tho-In, T., Sata, V., Boonserm, K., Chindaprasirt, P. (2016). Compressive strength and microstructure analysis of geopolymer paste using waste glass powder and fly ash. *Journal of Cleaner Production*, **172**, 2892–2898.

Tho-In, T., Sata, V., Chindaprasirt, P., Jaturapitakkul, C. (2012). Pervious high-

calcium fly ash geopolymer concrete. *Construction and Building Materials*, **30**, 366–371.

Thokchom, S., Ghosh, P., Ghosh, S. (2010). Performance of fly ash based geopolymer mortars in sulphate solution. *Journal of Engineering Science and Technology Review*, **3(1)**, 36–40.

Thompson, M R. (1970). Soil stabilization of pavement systems—State of the art. *Technical Rep. Prepared for Construction Engineering Research Laboratory*.

Thompson, Marshall R. (1966). Lime reactivity of Illinois soils. *Journal of the Soil Mechanics and Foundations Division*, ***92(5)***, 67–92.

Thompson, Marshall R. (1969). *Engineering properties of lime-soil mixtures*.

Tikalsky, P. J., Huffman, M. V., Barger, G. M. (2001). Use of Raw or Processed Natural Pozzolans in Concrete. *American Concrete Institute*, 1–24.

Tingle, J. S., Newman, J. K., Larson, S. L., Weiss, C. A., Rushing, J. F. (2007). Stabilization mechanisms of nontraditional additives. *Transportation Research Record*, **1989(1)**, 59–67.

Tingle, J. S., Santoni, R. L. (2003). Stabilization of clay soils with nontraditional additives. *Transportation Research Record*, **1819(1)**, 72–84.

Tironi, A., Trezza, M. A., Scian, A. N., Irassar, E. F. (2012). Kaolinitic calcined clays: Factors affecting its performance as pozzolans. *Construction and Building Materials*, **28(1)**, 276–281.

Trochez, J. J., de Gutiérrez, R., Rivera, J., Bernal, S. A. (2015). Synthesis of geopolymer from spent FCC: Effect of SiO2/Al2O3 and Na2O/SiO2 molar ratios. *Materiales de Construcción*, **65(317)**, e046.

Ushaa, T. G., Anuradha, R., Venkatasubramani, G. S. (2015). *Performance of self-compacting geopolymer concrete containing different mineral admixtures*. **22**, 473–481.

Usmen, M. A., Bowders Jr, J. J. (1990). Stabilization characteristics of class F fly ash. *Transportation Research Record, 1288*.

Vafaei, M., Allahverdi, A. (2017). High strength geopolymer binder based on waste-glass powder. *Advanced Powder Technology*, ***28(1)***, 215–222.

Valencia Saavedra, W. G., Angulo, D. E., Mejía de Gutiérrez, R. (2016). Fly Ash Slag Geopolymer Concrete: Resistance to Sodium and Magnesium Sulfate Attack. *Journal of Materials in Civil Engineering*, **28(12)**, 1–9.

van Deventer, J. S. J., Provis, J. L., Duxson, P., Brice, D. G. (2010). Chemical research and climate change as drivers in the commercial adoption of alkali activated materials. *Waste and Biomass Valorization*, **1**, 145–155.

Van Jaarsveld, J. G. S., Van Deventer, J. S. J., Lukey, G. C. (2002). The effect of composition and temperature on the properties of fly ash-and kaolinite-based geopolymers. *Chemical Engineering Journal*, **89(1–3)**, 63–73.

Van Jaarsveld, J. G. S., Van Deventer, J. S. J., Lukey, G. C. (2003). The characterisation of source materials in fly ash-based geopolymers. *Materials Letters*, **57(7)**, 1272–1280.

Van Jaarsveld, J. G. S., Van Deventer, J. S. J., Schwartzman, A. (1999). The potential use of geopolymeric materials to immobilise toxic metals: Part II. Material and leaching characteristics. *Minerals Engineering*, **12(1)**, 75–91.

Vance, K., Dakhane, A., Sant, G., Neithalath, N. (2014). Observations on the rheological response of alkali activated fly ash suspensions: the role of activator type and concentration. *Rheologica Acta*, **53(10–11)**, 843–855.

Vásquez, A., Cárdenas, V., Robayo, R. A., de Gutiérrez, R. M. (2016). Geopolymer based on concrete demolition waste. *Advanced Powder Technology*, **27(4)**, 1173–1179.

Wallah, S. E., Hardjito, D., Sumajouw, D. M. J., Rangan, B. V. (2005). Performance of Geopolymer Concrete Under Sulfate Exposure. *Ed Nawy Symposium*, *April*.

Wang, A., Zheng, Y., Zhang, Z., Liu, K., Li, Y., Shi, L., Sun, D. (2020). The Durability of Alkali-Activated Materials in Comparison with Ordinary Portland Cements and Concretes: A Review. *Engineering*, **6(6)**, 695–706.

Wang, C., Wen, P., Wang, M., Fan, Q., Wang, X. (2018). Preparation and characterization of road alkali-activated blast furnace slag paste. *Construction and Building Materials*, **181**, 175–184.

Wang, H., Li, H., Yan, F. (2005). Synthesis and mechanical properties of metakaolinite-based geopolymer. *Colloids and Surfaces A: Physicochemical and*

Engineering Aspects, **268(1–3)**, 1–6.

Wang, Q., Gao, H., Jiang, B., Li, S., He, M., Qin, Q. (2021). In-situ test and bolt-grouting design evaluation method of underground engineering based on digital drilling. *International Journal of Rock Mechanics and Mining Sciences*, **138**, 104575.

Wang, S.-D., Scrivener, K. L. (1995). Hydration products of alkali activated slag cement. *Cement and Concrete Research*, **25(3)**, 561–571.

Wang, S., Xue, Q., Zhu, Y., Li, G., Wu, Z., Zhao, K. (2021). Experimental study on material ratio and strength performance of geopolymer-improved soil. *Construction and Building Materials*, **267**, 120469.

Wansom, S., Janjaturaphan, S., Sinthupinyo, S. (2010). Characterizing pozzolanic activity of rice husk ash by impedance spectroscopy. *Cement and Concrete Research*, **40(12)**, 1714–1722.

Warner, J. (2004). *Practical handbook of grouting: soil, rock, and structures*. John Wiley Sons.

Widjaja, B., Lee, S. H.-H. (2013). Flow box test for viscosity of soil in plastic and viscous liquid states. *Soils and Foundations*, **53(1)**, 35–46.

Xiao, R., Ma, Y., Jiang, X., Zhang, M., Zhang, Y., Wang, Y., Huang, B., He, Q. (2020). Strength, microstructure, efflorescence behavior and environmental impacts of waste glass geopolymers cured at ambient temperature. *Journal of Cleaner Production*, *252*, 119610.

Xiao, R., Polaczyk, P., Zhang, M., Jiang, X., Zhang, Y., Huang, B., Hu, W. (2020). Evaluation of Glass Powder-Based Geopolymer Stabilized Road Bases Containing Recycled Waste Glass Aggregate. *Transportation Research Record*, **2674(1)**, 22–32.

Xiao, R., Zhang, Y., Jiang, X., Polaczyk, P., Ma, Y., Huang, B. (2021). Alkali-activated slag supplemented with waste glass powder: Laboratory characterization, thermodynamic modelling and sustainability analysis. *Journal of Cleaner Production*, **286**, 125554.

Xie, H., Liu, F., Fan, Y., Yang, H., Chen, J., Zhang, J., Zuo, C. (2013). Workability and proportion design of pumping concrete based on rheological parameters.

Construction and Building Materials, **44**, 267–275.

Xie, Z., Xi, Y. (2001). Hardening mechanisms of an alkaline-activated class F fly ash. *Cement and Concrete Research*, **31(9)**, 1245–1249.

Xu, H., Van Deventer, J. S. J. (2000). The geopolymerisation of alumino-silicate minerals. *International Journal of Mineral Processing*, **59(3)**, 247–266.

Yaghoubi, M., Arulrajah, A., Disfani, M. M., Horpibulsuk, S., Darmawan, S., Wang, J. (2019). Impact of field conditions on the strength development of a geopolymer stabilized marine clay. *Applied Clay Science*, **167**, 33–42.

Yahia, A, Mantellato, S., Flatt, R. J. (2016). Concrete rheology: a basis for understanding chemical admixtures. In *Science and Technology of Concrete Admixtures* (pp. 97–127). Elsevier.

Yahia, Ammar, Khayat, K. H. (2001). Analytical models for estimating yield stress of high-performance pseudoplastic grout. *Cement and Concrete Research*, **31(5)**, 731–738.

Yahya, Z., Abdullah, M. M. A. B., Hussin, K., Ismail, K. N., Razak, R. A., Sandu, A. V. (2015). Effect of solids-to-liquids, Na2SiO3-to-NaOH and curing temperature on the palm oil boiler ash (Si + Ca) geopolymerisation system. *Materials*, **8(5)**, 2227–2242.

Yan, X., Jiang, L., Guo, M., Chen, Y., Song, Z., Bian, R. (2019). Evaluation of sulfate resistance of slag contained concrete under steam curing. *Construction and Building Materials*, **195**, 231–237.

Yang, T., Zhu, H., Zhang, Z., Gao, X., Zhang, C., Wu, Q. (2018). Effect of fly ash microsphere on the rheology and microstructure of alkali-activated fly ash/slag pastes. *Cement and Concrete Research*, **109,** 198–207.

Ye, H., Chen, Z., Huang, L. (2019). Mechanism of sulfate attack on alkali-activated slag: The role of activator composition. *Cement and Concrete Research*, **125(May)**, 105868.

Ye, H., Radlińska, A. (2016). Shrinkage mechanisms of alkali-activated slag. *Cement and Concrete Research*, **88**, 126–135.

Ye, H., Radlińska, A. (2017). Shrinkage mitigation strategies in alkali-activated slag.

Cement and Concrete Research, **101**, 131–143.

Yi, Y., Zheng, X., Liu, S., Al-Tabbaa, A. (2015). Comparison of reactive magnesia- and carbide slag-activated ground granulated blastfurnace slag and Portland cement for stabilisation of a natural soil. *Applied Clay Science*, **111**, 21–26.

Yin, W., Li, X., Sun, T., Chen, Y., Xu, F., Yan, G., Xu, M., Tian, K. (2021). Utilization of waste glass powder as partial replacement of cement for the cementitious grouts with superplasticizer and viscosity modifying agent binary mixtures: Rheological and mechanical performances. *Construction and Building Materials*, **286**, 122953.

Yusuf, M. O., Johari, M. A. M., Ahmad, Z. A., Maslehuddin, M. (2014). Effects of addition of Al(OH)3 on the strength of alkaline activated ground blast furnace slag-ultrafine palm oil fuel ash (AAGU) based binder. *Construction and Building Materials*, **50**, 361–367.

Yuyou, Y., Zengdi, C., Xiangqian, L., Haijun, D. (2016). Development and materials characteristics of fly ash- slag-based grout for use in sulfate-rich environments. *Clean Technologies and Environmental Policy*, **18(3)**, 949–956.

Zabihi, S. M., Tavakoli, H. R. (2018). Mechanical and microstructural properties of GGBFS-RHA geopolymer concrete. *Emerging Materials Research*, **7(4)**, 233–241.

Zhang, D. W., Wang, D. min, Liu, Z., Xie, F. zhu. (2018). Rheology, agglomerate structure, and particle shape of fresh geopolymer pastes with different NaOH activators content. *Construction and Building Materials*, **187**, 674–680.

Zhang, H. Y., Kodur, V., Wu, B., Cao, L., Wang, F. (2016). Thermal behavior and mechanical properties of geopolymer mortar after exposure to elevated temperatures. *Construction and Building Materials*, *109*, 17–24.

Zhang, J., Li, S., Li, Z., Zhang, Q., Li, H., Du, J., Qi, Y. (2019). Properties of fresh and hardened geopolymer-based grouts. *Ceramics - Silikaty*, **63(2)**, 164–173.

Zhang, M., Guo, H., El-Korchi, T., Zhang, G., Tao, M. (2013). Experimental feasibility study of geopolymer as the next-generation soil stabilizer. *Construction and Building Materials*, **47**, 1468–1478.

Zhang, M., Zhao, M., Zhang, G., Nowak, P., Coen, A., Tao, M. (2015). Calcium-free

geopolymer as a stabilizer for sulfate-rich soils. *Applied Clay Science*, **108**, 199–207.

Zhang, P., Zheng, Y., Wang, K., Zhang, J. (2018). A review on properties of fresh and hardened geopolymer mortar. *Composites Part B: Engineering*, **152**, 79–95.

Zhang, S., Keulen, A., Arbi, K., Ye, G. (2017). Waste glass as partial mineral precursor in alkali-activated slag/fly ash system. *Cement and Concrete Research*, **102**, 29–40.

Zhang, W., Li, S., Wei, J., Zhang, Q., Liu, R., Zhang, X., Yin, H. (2018). Grouting rock fractures with cement and sodium silicate grout. *Carbonates and Evaporites*, **33**, 211–222.

Zhang, Y. J., Zhao, Y. L., Li, H. H., Xu, D. L. (2008). Structure characterization of hydration products generated by alkaline activation of granulated blast furnace slag. *Journal of Materials Science*, **43(22)**, 7141–7147.

Zhang, Y., Luo, X., Kong, X., Wang, F., Gao, L. (2018). Rheological properties and microstructure of fresh cement pastes with varied dispersion media and superplasticizers. *Powder Technology*, **330**, 219–227.

Zhang, Zhigang, Liu, J. C., Xu, X., Yuan, L. (2020). Effect of sub-elevated temperature on mechanical properties of ECC with different fly ash contents. *Construction and Building Materials*, **262**, 120096.

Zhang, Zuhua, Wang, H., Provis, J. L. (2012). Quantitative study of the reactivity of fly ash in geopolymerization by ftir. *Journal of Sustainable Cement-Based Materials*, **1(4)**, 154–166.

Zhu, H., Liang, G., Li, H., Wu, Q., Zhang, C., Yin, Z., Hua, S. (2021). Insights to the sulfate resistance and microstructures of alkali-activated metakaolin/slag pastes. *Applied Clay Science*, **202**, 105968.

Zhu, H., Liang, G., Xu, J., Wu, Q., Zhai, M. (2019). Influence of rice husk ash on the waterproof properties of ultrafine fly ash based geopolymer. *Construction and Building Materials*, **208**, 394–401.

Zhu, H., Liang, G., Zhang, Z., Wu, Q., Du, J. (2019). Partial replacement of metakaolin with thermally treated rice husk ash in metakaolin-based geopolymer. *Construction and Building Materials*, **221**, 527–538.

Zhu, H., Zhai, M., Liang, G., Li, H., Wu, Q., Zhang, C., Hua, S. (2021). Experimental study on the freezing resistance and microstructure of alkali-activated slag in the presence of rice husk ash. *Journal of Building Engineering*, **38**, 102173.

Zingg, A., Winnefeld, F., Holzer, L., Pakusch, J., Becker, S., Gauckler, L. (2008). Adsorption of polyelectrolytes and its influence on the rheology, zeta potential, and microstructure of various cement and hydrate phases. *Journal of Colloid and Interface Science*, 323(2), 301–312.

Zulkifley, M. T. M., Ng, T. F., Raj, J. K., Hashim, R., Bakar, A. F. A., Paramanthan, S., Ashraf, M. A. (2014). A review of the stabilization of tropical lowland peats. *Bulletin of Engineering Geology and the Environment*, **73**, 733–746.

CURRICULUM VITAE

Israa Sabbar ABBAS

Education:

- **Ph. D. Civil Engineering, Graduated 2023**

  University of Gaziantep College of Engineering. Civil Engineering. Dept. Gaziantep/Turkey.

- **M.Sc. Civil Engineering, Graduated 2017**

  University of Gaziantep College of Engineering. Civil Engineering. Dept. Gaziantep/Turkey.

- **BSc. Civil Engineering, Graduated 2014**

  University of Kirkuk /College of Engineering/ Civil Engineering / Kirkuk / Iraq.

- **Secondary school education, Graduated 2008**

  Al-Baydaa High-school for Girls / Kirkuk / Iraq.

Publication:

1. Abbas, I. S., Abed, M. H., Canakci, H. (2022). Development and characterization of eco-and user-friendly grout production via mechanochemical activation of geopolymer. Journal of Building Engineering, 105336.
2. Hamid Abed, M., Sabbar Abbas, I., Hamed, M., Canakci, H. (2022). Rheological, fresh, and mechanical properties of mechanochemically activated geopolymer grout: A comparative study with conventionally activated geopolymer grout. *Construction and Building Materials*, *322*, 126338.

3. Abed, M. H., Abbas, I. S., Canakci, H. (2022). Effect of glass powder on the rheological and mechanical properties of slag-based mechanochemical activation geopolymer grout. European Journal of Environmental and Civil Engineering, 0(0), 1–25.

4. Hamid Abed, M., Abbas, I. S., Canakci, H. (2022). Influence of mechanochemical activation on the rheological, fresh, and mechanical properties of one-part geopolymer grout. *Advances in Cement Research*, 1–38.